Understanding and Exploiting the DNA Cleavage and Resealing Reactions of Bacterial Type II Topoisomerases

Victoria M Baskerville

John Innes Centre
Department of Biochemistry and Metabolism
February 2023

A thesis submitted in fulfilment of the
requirements for the degree of
Doctor of Philosophy

This work was supported by the Biotechnology and Biological Sciences Research Council

Statement

The word submitted in this thesis is my own work, except where due reference is made to other authors, and has not been submitted to this or any other University for any degree.

"You can never get a cup of tea large enough or a book long enough to suit me." — C. S. Lewis

Please enjoy this thesis with a good cup of tea <3

Acknowledgements

The first in my very long list of thank yous to the people who have helped me in the last four or so years of my PhD studies has to belong to my supervisor, Prof. Tony Maxwell. My PhD endeavors would not have been possible without you sharing your knowledge and advice. Thank you for your enthusiasm and encouragements throughout my project, and providing the most supportive and friendly environment for me to be in. You have made my PhD journey enjoyable, and one I will deeply miss. I have huge gratitude towards the other members of my supervisory team, Prof. Dave Lawson, Dr. Thomas Germe and Prof. Nick le Brun. Their guidance and ideas are greatly appreciated. I have huge gratitude towards the mentorship that Dr. Thomas Germe gave me throughout my PhD. He was pivotal in the direction my PhD and I cannot express my thanks enough.

Thank you to the current and previous members of the biophysical and crystallography platform team - Prof. Dave Lawson, Dr. Clare Stevenson and Julia Mundy, for your generous advice and technical help during my studies.

My thanks extend to my collaborators at the University of Uppsala, for providing me the opportunity to work on their exciting antibiotic project, with a special mention to Dr. Luke Odell and Marcus Söderström.

Thank you to Dr. Dmitry Ghilarov for supplying me with gyrase mutant plasmids and proteins, and the advice on their purification.

The Maxwell lab - past and present members - thanks for being the most lovely people (and the Ghilarov lab too!). Thank you to the student office tea station and users for feeding my tea obsession and providing the coziest office ever. A special thank you has to go to Adam and Harriet who were with me since day one of the PhD - the experience would not have been as memorable or enjoyable without them.

My computer skills started off questionable, so thank you to Dr. A. Hughes for teaching my python, modelling, latex and an appreciation for computational skills that I will take with me in life. Additional thanks extend to Gurpinder for helping me fix my latex woes.

I have been extremely fortunate to carry out my studies at the John Innes Centre. JIC is a lovely environment to work in, and thank you to the people who make it great, and for lending your knowledge throughout my time here. I am extremely grateful for the lab support team, administrator team and anyone else who has helped me behind the scenes.

Thank you to the friends I have made during my time in Norwich, I would not have had as much fun without you all. Thank you to Norwich, you are a fine city to call home for 4 years. And finally, thank you to my lovely family, who have always supported my love of science since day one.

Abstract

Bacterial type II DNA topoisomerases resolve DNA topological problems by a DNA strand passage mechanism. Transient double-stranded covalent phosphotyrosine linkages form between the enzyme and DNA that are subsequently resealed are critical to the reaction. Exploitation of the reaction by antibiotics leads to accumulation of lethal double-stranded DNA breaks. However, antibiotic resistance is a problem. To address this, a novel series of antibiotics has been developed by Uppsala University: the quinazoliniums. Here, the compounds have been found to target DNA gyrase and DNA topoisomerase IV. The potency of the quinazoliniums has been assessed, and the binding site on DNA gyrase has been characterised using X-ray crystallography, which shows that the compounds bind at the DNA cleavage site without a water-metal ion bridge. The quinazoliniums have some cross-resistance to fluoroquinolone-resistant gyrase mutations, however, the lead quinazolinium is more active than ciprofloxacin at inhibiting DNA supercoiling in the quinolone-resistant mutant *E. coli* gyrase GyrA S83L.

Due to the importance of the DNA cleavage/resealing reaction to antibiotic action, this equilibrium has been investigated. A lysine residue the conserved YKGLG motif, and the Greek Key domain have been suggested to be involved in DNA resealing. Mutations in the lysine and Greek Key domain of *Escherichia coli* and *Staphylococcus aureus* gyrase leads to a reduced rate of reaction. Experiments investigating how the concentration of free metal ions influence the equilibrium between gyrase-DNA cleavage complexes and free DNA show the catalytic metal ions to be very dynamic. The DNA resealing and cleavage reactions have different metal ion concentration requirements. An adapted model for the metal-ion mechanism to catalyse the reaction, which takes into consideration the dynamic nature of the catalytic metal ion, is proposed.

Contents

List of Figures

List of Tables

Chapter 1

General introduction

1.1 DNA topology

1.1.1 DNA supercoiling

The DNA helix is formed of two inter-twined DNA strands which contains genetic instructions that require manipulation and maintenance for cellular function [1]. Strand separation and DNA processes create inter- and intra-DNA duplex entanglements, which must be resolved and regulated. Topological control is maintained by the DNA topoisomerases, enzymes which were first discovered in 1971 by James Wang, who observed an *Escherichia coli* (*E. coli*) protein capable of introducing a "swivel" reversibly into DNA [2].

The DNA helix in conventionally described in the relaxed state, forming a right-handed coil. When the DNA helix is over-wounded, the DNA is positively supercoiled. Under-winding of the DNA helix is described as negatively supercoiled DNA. Therefore, supercoiling is influenced by the twist of the DNA helix. The twist (Tw) describes the number of helical turns along an axis. The supercoiling state of DNA is also determined by the bending or contortion of the DNA helix, also known as writhe (Wr). Wr is a measure of the coiling of the DNA duplex along an axis in space. Tw and Wr are mathematical parameters and can be summed to calculate the linking number (Lk), where Lk = Tw + Wr [3]. The linking number describes how the DNA strands are linked together within a topological domain. Without strand breakage, manipulation of DNA topology will alter the Tw and Wr, whereas the Lk would be invarient. Topoisomerases act by changing the Lk by breaking the DNA strands. Topoisomerases are specialised to relax supercoiled DNA, introduce negative supercoils, and remove catenated DNA [4] [fig. 1.1].

DNA can be modelled as a linear topological domain, where sections of DNA are constrained by a physical barrier. Constrained DNA domains in a cell arise from chromosomal loops anchored to the nuclear matrix and large protein complexes, preventing free rotation of DNA ends [5]. The viscous cellular environment also contributes to the inhibition DNA end

rotation [6]. Therefore, constrained DNA ends cannot rotate to resolve the positive or negative supercoiling, or catenation, which arise during DNA processes [7].

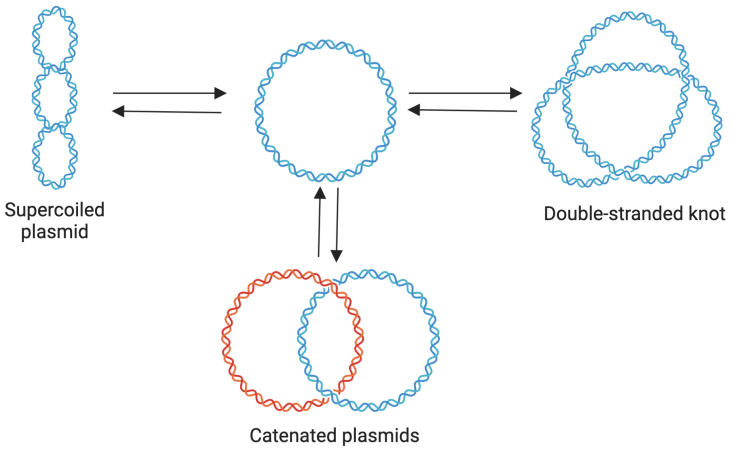

(a)

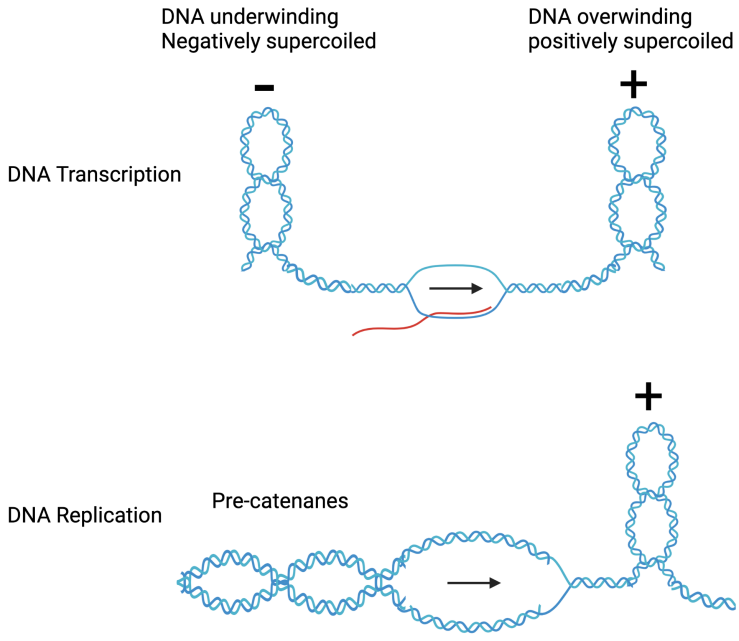

(b)

Figure 1.1: Topological problems resolved by type II topoisomerases. **(a)** Type II topoisomerases can relax supercoiled DNA, decatenate DNA, undo knots, and negatively supercoil DNA. **(b)** During DNA transcription, ahead of the RNA polymerase, DNA can be over-wound, and behind of the RNA polymerase, the DNA can be under-wound. During DNA replication, the replication bubble progression can lead to over-wound positively supercoiled DNA. Behind the replication fork, the daughter DNA strands intertwine due to fork rotation, which leads to pre-catenanes, and catenated DNA on chromosome segregation.

1.1.2 DNA topology resolved by topoisomerases

DNA is very dynamic, and continually metabolised, transcribed and manipulated, which alters the supercoiled state and DNA topology [fig. 1.1]. During the elongation phase of DNA replication and transcription, the DNA strands are separated and a DNA fork is formed. During DNA transcription, the under-winding of DNA behind the DNA bubble leads to negative supercoiling, and positive supercoiling ahead of the DNA bubble. The oppositely supercoiled states formed during DNA transcription coined the twinned supercoiled domain model, which was proposed in 1987 [8]. On progression of the replication fork, the resulting positive supercoils ahead of the replication fork are relieved by the rotation of the two, newly synthesised DNA helixes which intertwine, forming pre-catenanes. The pre-catenanes are removed by topoisomerases, to prevent catenation during cell division on chromosome segregation [9]. Topoisomerases relieve the torsional stress from supercoiled DNA, so the cell can maintain high speeds of DNA processes. The initiation of bacterial replication is efficient if the DNA is maintained in a negatively supercoiled state, to reduce the strain from overwindind DNA ahead of DNA/RNA polymerases. Resolving topological elements are vital for cell survival, making the topoisomerases essential enzymes which have been identified in the three domains of life, eukarya, archaea and bacteria [10].

1.2 DNA topoisomerases

DNA topoisomerases are responsible for the maintenance of DNA topology [2], [11]. The enzymes are split into two distinct groups, the type I and type II topoisomerases which are distinguished by their structure and catalytic mechanisms. The topoisomerases alter the linking number of DNA by transient strand scission. Conserved catalytic tyrosines attack the DNA phosphate by nucleophilic attack, forming covalent phosphotyrosine bonds which are resealed following linking number alteration. The type I topoisomerases form single-stranded DNA breaks and are monomeric, reduce the linking number by units or multiples of one after each catalytic cycle, generally not requiring the free energy from ATP. The type II topoisomerases are multimeric and change the linking number in units of two using a double-stranded DNA cleavage mechanism, which generally requires ATP [12], [13].

1.2.1 Type I DNA topoisomerases

The type I topoisomerases can be subdivided into three subfamilies: IA, 1B and 1C, based on differences in sequences and domain architecture, and the catalytic mechanism. Different type I enzymes are specialised to maintain certain topological elements, such as to relax positive and negative DNA supercoils, introduce positive supercoils, catenate/decatenated single-stranded DNA, catenate/decatenate nicked DNA, and resolve single-stranded DNA knots [14], [15].

Type IA topoisomerases bind and cleave negatively supercoiled DNA via a transient phosphotyrosine linkage with the $5'$ DNA or RNA phosphate, with a preference for single-stranded regions of DNA. The enzyme passes a strand of DNA or RNA through the break via a strand-passage mechanism. In general, these enzymes require a divalent metal ion to catalyse the DNA scission and rejoining reaction [16]. An exception to this includes topo 3β, which does not require, but are enhanced by, a divalent metal to catalyse DNA cleavage, however, resealing the broken DNA does require a divalent metal ion [17]. The type IA topoisomerases include the bacterial topoisomerase I, topoisomerase III from all domains of life, and reverse gyrase, found in hyperthermophiles [18]. These enzymes share a core domain and are diversified through variations in a C-terminal tail and proteins that they interact with [19].

Type IB topoisomerases are primarily found in eukaryotes and viruses. The enzymes form phosphotyrosine linkages with the $3'$ phosphate of positively, or negatively supercoiled DNA. The $5'$ broken end rotates in a controlled manner around the uncleaved opposite DNA strand via a swivel mechanism, which can alter the linking number in units of one for each rotation. The free energy stored in supercoiled DNA drives rotation of the broken DNA strand [20]. The type IB enzymes do not require a catalytic metal ion, however metal ions may facilitate the release of DNA from the enzyme after the catalytic cycle [20].

Topoisomerase V has only been identified in the *Methanopyrus* genus which are hyperthermophiles, and is the sole member of the type IC topoisomerases, which was originally classed as a type IB topoisomerase. The enzyme cleaves DNA via a $3'$ phosphotyrosyl linkage and the mechanism does not require metal ions or ATP to proceed [21]. Additionally, the enzyme relaxes negatively and positively supercoiled DNA, and acts via the strand-rotation mechanism. Despite the similarities to the type IB enzymes, topo V has an additional role in DNA repair and has a structural fold absent in other topoisomerases [22].

1.3 Type II topoisomerases

The type II topoisomerases are divided into two subgroups, type IIA and type IIB. Both groups transiently form double-stranded DNA breaks, the reaction is catalysed by divalent metal ions and generally requires ATP. The enzymes manipulate DNA topology via strand-passage and change the Lk in units of two per catalytic cycle. The type IIA and B enzymes are classed separately, generally based on the evolution of the enzymes which contain unique domains and structural architectures [23].

1.3.1 Type IIA topoisomerases

Type IIA topoisomerases are distributed throughout the kingdoms of life [23]. The primarily prokaryotic type IIA topoisomerases are DNA gyrase and topoisomerase IV (topo IV) [24]. The majority of bacteria have both gyrase and topo IV [23]. DNA gyrase is present in some archaea, which is thought to arise from rare horisontal gene transfer events via bacterial donors [25]. DNA gyrase is localised to chloroplasts in plants, but has not been identified in mammals [26]. DNA gyrase and topo IV are A_2B_2 heterotetramers, consisting of two GyrA and GyrB, or, ParC and ParE subunits respectively. Eukaryotic topoisomerase II (topo II) is a homodimer, which evolutionally came about by fusion of the monomeric bacterial topoisomerase subunits [10].

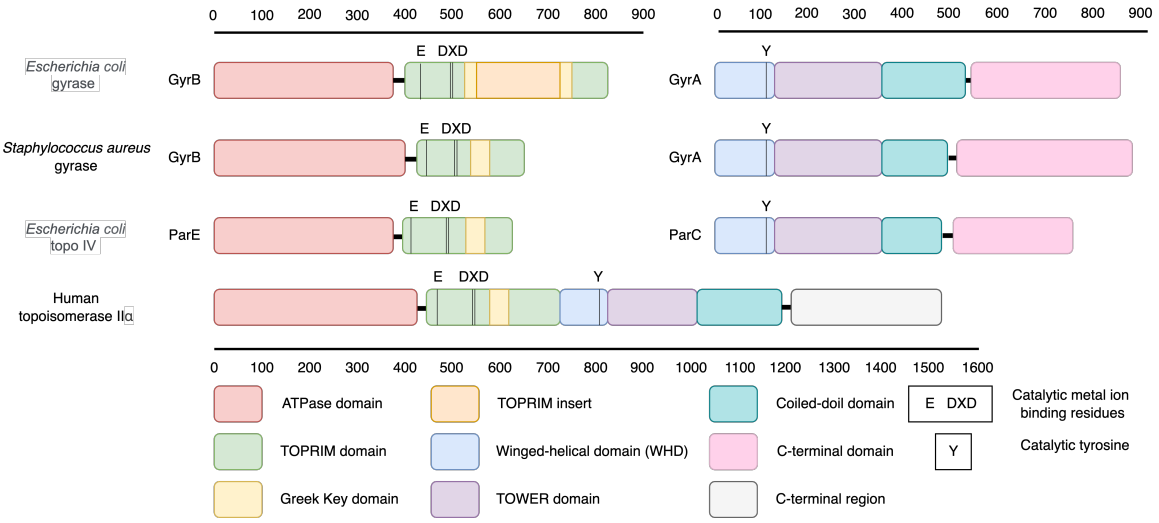

Figure 1.2: The domain architecture of type II topoisomerases. The GyrB acidic metal ion coordinating residues are indicated (E DXD), which are E424, D498 and D500 for *E. coli* gyrase, E435, D508 and D510 for *S. aureus* gyrase, E418, E492 and D494 for *E. coli* topo IV, and D543, D541 and E461 for human topoisomerase IIα. The catalytic tyrosines are labelled with a Y; Y122 for *E. coli* gyrase, Y123 for *S. aureus* gyrase, Y120 for *E. coli* topo IV and Y805 for human topoisomerase IIα.

1.3.2 The catalytic cycle of type IIA topoisomerases

Firgure 1.3 depicts the strand-passage catalytic cycle for DNA gyrase to manipulate DNA topology - the catalytic cycle of all type II topoisomerase share the basic principles of this strand-passage reaction. A gate segment (G-segment) is a double-stranded DNA duplex and is captured across a positively charged basic groove along the DNA binding domains. The G-segment is deformed by bending the DNA between 120 and 150° [27], [28], such that the DNA scission sites are positioned for attack by the catalytic tyrosines. The B-form like DNA now resembles A-form DNA, which shortens the distance between the base pairs. The topoisomerase captures an additional DNA duplex, termed the transported segment (T-segment). The T-segment moves between two open clamps that are ATP-controlled and form the N-gate. ATP binds to these ATPase domains and triggers dimerisation, closing the N-gate. The strand-passage reaction may also proceed without N-gate closing. The G-segment is cleaved by nucleophilic attack on the DNA backbone, forming two $5'$ phosphotyrosyl transient covalent linkages, which are catalysed by magnesium ions. For type IIA topoisomerases, the DNA cleavage sites are staggered by 4 bp on opposite strands of the DNA helix.

The T-segment physically pushes open the DNA gate and rotations and movements in the DNA binding domains open the DNA-gate. The opening of the DNA gate creates a funnel shaped channel that the T-segment passes through [29]. The T-segment traverses the G-segment at various angles, but most commonly at 60° [30]. The enzyme is reset by resealing the G-segment, and release of the T-segment through the exit gate, also known as the C-gate. The N-gate clamp reopens to repeat the catalytic cycle and capture a new T-segment. This process is coupled to the hydrolysis of ATP and release of the nucleotide and organic phosphates [31]. To ensure the G-segment broken ends are resealed, it is likely that only one gate can be open at a time.

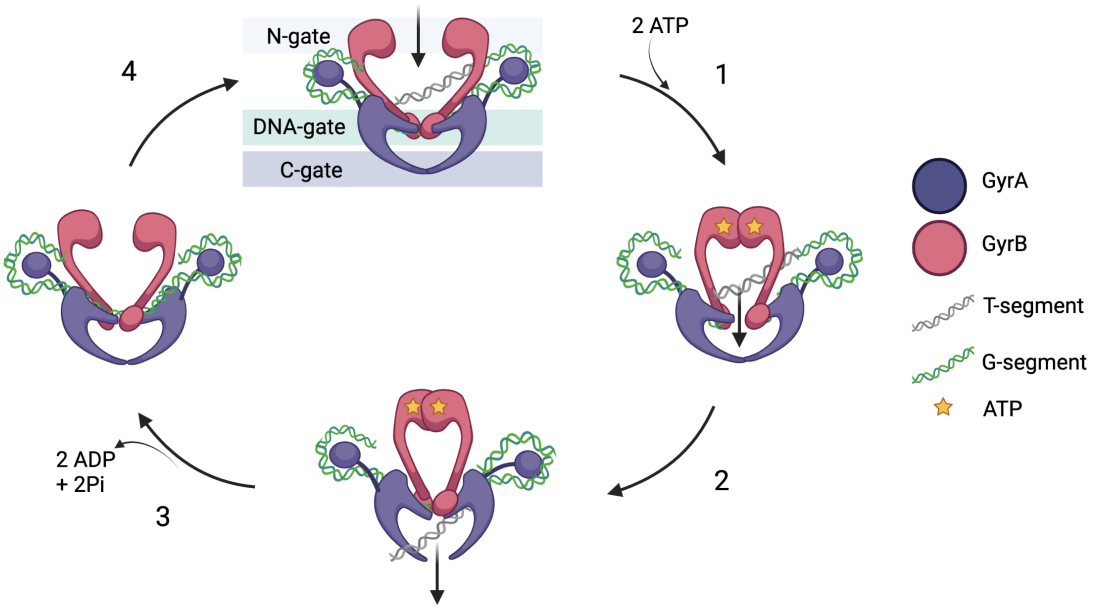

Figure 1.3: The strand passage cycle of DNA gyrase. A gyrase complex bound to the gate DNA wrapped around the C-terminal domain captures the T-segment when the N-gate is open. 1. On binding of two molecules of ATP to the GyrB ATPase domains, the N-gate closes, and the DNA gate opens, allowing passage of the T-segment DNA through the DNA gate. 2. The exit gate opens, allowing the T-segment to exit the gyrase complex. 3. Hydrolysis of ATP and dissociation of ADP and pi resets the gyrase complex to open the N-gate. 4. The gyrase-DNA complex captures a T-segment.

1.3.3 DNA gyrase

E. coli DNA gyrase is a 370 kDa A_2B_2 heterotetramer composed of two GyrA subunits and two GyrB subunits of 96 and 89 kDa respectively [fig. 1.4a] [32]. The enzyme can efficiently relax positive and negative DNA supercoils; relaxation of positive DNA supercoils is an ATP-dependent reaction, whereas relaxation of negative supercoils can occur independently of ATP, albeit less efficiently. The introduction of negative supercoils into the DNA requires ATP, and is an activity found only in DNA gyrase [33]. The primary functions of gyrase is supercoiling, the enzyme's relaxation and decatenation activity proceeds at a slower rate. DNA gyrase prefers to remove positive supercoils, and works together with type I topoisomerases, which remove negative supercoils, and topo IV, a potent decatenase to maintain the homeostasis of DNA topology [34].

The separation of the DNA helix locally and globally during DNA transcription and replication respectively increases the torsional strain ahead of the DNA bubble, introducing positive supercoils [fig. 1.1]. Therefore, gyrase maintains the genome in a negatively supercoiled

state to facilitate strand separation and chromosome condensation, and removes the accumulating positive supercoils upstream of the DNA bubble. Inhibition of the catalytic mechanism of gyrase impacts the cellular morphology and DNA metabilism. Gyrase must relieve topological constraints at a fast rate, or the mechanical strain on DNA may reduce the rate of DNA processes which may ultimately lead to fork stalling and cell death [33]. In a negatively supercoiled genome, the DNA is under-wound, which reduces the free energy required to part DNA strands at sites of transcription and at the origin of replication. Therefore, the genome is generally maintained to be underwound [35]

1.3.3.1 Structural developments to solve the DNA gyrase structure

The roles of gyrase domains in the catalytic cycle, and the structural architecture of the protein is well characterised. Figure 1.4b-c is the cryo-EM structure of *E. coli* gyrase [36], bound to a G-segment, which is wrapped around the GyrA C-terminal domain. The 3D cryo-electron microscopy (cryo-EM) structures of gyrase are the most complete structures of gyrase available in the literature. The structures of the *E. coli* GyrA and GyrB subunits were first determined by small angle X-ray crystallography [37], [38], which were followed by X-ray crystallography structures of a truncated and fused construct of *S. aureus* gyrase that lacks the GyrB ATPase domain and the GyrA C-terminal wrapping domain [39]. This *S. aureus* gyrase core fusion construct, along with gyrases from other species, are used as model systems to crystallise gyrase with drugs to aid drug discovery. Snapshots of gyrase have been captured in different conformations during the strand-passage cycle, including gyrase without DNA present, gyrase bound to a cleaved and uncleaved G-segment, various degrees of DNA gate opening, and the N-terminal ATPase clamp in an open and closed conformation [40]. There are still conformations during strand passage which have not been solved, such as a structure of gyrase with the G-segment and the T-segment, the opening of the exit gate, and transition states to the DNA cleavage and resealing reaction. The resolution of cryo-EM structures of gyrase are improving; in 2013, the full-length *Thermus thermophilus* gyrase GyrB-GyrA fusion bound to a 155 bp DNA duplex was solved to 18 Å [41]. In 2019, the cryo-EM structures of full length *E.coli* gyrase bound to a 130 bp DNA segment that was solved to 4.0 Å, with local resolution reached up to 3.0 Å.

1.3.3.2 DNA gyrase domains

Gyrase has a 2-fold symmetry axis, also termed the dyad axis. The axis lies between the three gates and arises because gyrase has an A_2B_2 format. The G-segment binds between the GyrB TOPRIM (topoisomerase primase) domains, the GyrA winged helical domains (WHD), and the GyrA TOWER domains. The WHD and the TOPRIM domains form the interface for the DNA gate. The WHD domain on GyrA contains the catalytic tyrosines which form the phosphotyrosyl linkage with the DNA backbone [33]. The domain architecture of DNA gyrase is depicted in figure 1.2.

The TOPRIM domain, identified from structural and gene alignments, is a compact alpha-beta fold consisting of 4 beta strands and 3 alpha helices, which are generally highly conserved. The domain contains a conserved E DXD motif which coordinates divalent metal ions and catalyses the DNA breakage and reunion reaction. The TOPRIM domain is found in type IA and type II topoisomerases, and also DnaG-type primases, RecR/M family proteins and OLD nucleases. These proteins all act on nucleic acids [42]. DnaG-type primases and OLD nucleases have been shown to coordinate various numbers of metal ions to perform nucleotide scission and/or joining [43], [44]. Located within the TOPRIM domain is the highly flexible Greek Key domain, which consists of three antiparallel β sheets and an α helix, and has been implicated in the control of the DNA scission and rejoining reaction [45], [46]. Located within the sequence of the Greek Key domain is an insert of around 165 amino acids, that when deleted, affects the enzyme's activity [47], [48]. This insert is not present in Gram-positive bacteria or mycoplasma, as well as eukaryotic topoisomerase II, topo IV and topo VI [49], and the insert is highly disordered.

The WHD is structurally conserved and consists of helix-turn-helix motifs with beta-sheet wings. The domain contains the catalytic tyrosine that forms the phosphotyrosyl bond with the DNA phosphate. The position of this tyrosine is not conserved across the topoisomerase enzymes, and is present on different alpha helices, beta sheets and loops on the WHD [50]. In DNA gyrase, the tyrosine is located on a loop [51]. Functionally, the WHD-containing proteins are diverse; the domain has been implicated in nucleic acid binding, sequence specificity and protein-protein interaction. The topoisomerases have evolved such that they can act on a diverse range of DNA sequences, although the enzymes are more efficient at acting on certain DNA sequences. Gyrase prefers specific DNA sequences and DNA that can be easily bent. *S. aureus* gyrase has positional preferences for bases with respect to the site of DNA cleavage: a

guanine at -4, adenine at -2 and thymine at -1 [52].

The G-segment DNA also contacts the TOWER domain, and wraps around the C-terminal GyrA β-pinwheel. The TOWER domain has a critical role in bending DNA; type IIA topoisomerases are the only topoisomerases to possess the TOWER domain and therefore have been suggested to be the only topoisomerases capable of bending DNA. The TOWER domain consists of an α/β fold, which is found in DNA- and RNA- binding proteins, and is lined with basic residues to interact with DNA via electrostatic and polar interactions [27].

Based on DNA footprinting and structural analysis, *E. coli* gyrase binds to roughly 128-150 bp of a DNA duplex [53], [36]. The DNA adjacent to the G-segment is positively wrapped around the wrapping domain, allowing the introduction of two negative supercoils into the DNA. The wrapping of DNA positions the T-segment at a 60° angle with respect to the G-segment. The wrapping domain consists of a β-pinwheel that bends DNA by an angle of 200° [54]. The DNA contacts the six blades on the outside of the β-pinwheel; the first blade of the β-pinwheel is essential for DNA wrapping and contains the highly conserved GyrA box motif (QRRGGKG), and thus is essential for supercoiling activities [55]. The GyrA box interaction with the wrapped DNA is strong, clamping the DNA in position whilst the DNA is unfavourably manipulated [36]. The C-terminal tail may contact the TOPRIM/Greek Key domain insert, to ensure directed transport of the T-segment through the gyrase complex [36]. The β-pinwheel resembles a β-propeller, which is a more common protein fold. The structures differ in their β-strand arrangement; the β-pinwheel exchanges beta strands with other blades in their propellers, which increases the domains stability [56].

The cleavage of the G-segment can be influenced by ATP. The ATPase domain of gyrase consists of the GHKL (Gyrase, Hsp90, Histidine Kinase, MutL) domain, which contains conserved residues that bind ATP and catalyse ATP hydrolysis, and the transducer domain, which is more variable. The GHKL domain contains a Bergerat ATP-binding fold, which consists of 4 β strands and 3 α helices and forms a lid structure, which completely closes on capture of an ATP molecule [31], [57]. The cavity created by the transducer domain, GHKL domain and the DNA gate captures the T-segment. The transducer domain is lined with basic residues, which has been proposed to navigate the T-segment through the cavity to the DNA gate. The transducer domain translates the allosteric binding and hydrolysis of ATP at the GHKL domain to the DNA gate [58], [36]. Although gyrase does not require ATP for relaxation of negatively supercoiled DNA, ATP makes the strand-passage reaction energetically

favourable and increases the efficiency of the reaction.

The final gate for the T-segment to pass is the C-gate. The cavity for T-segment exit is formed by a coiled-coil domain of long α helices, and a small globular dimer interface, which are highly conserved. Basic residues line the cavity to direct T-segment passage [59]. These structures are located at the C-terminus of GyrA, which is proceeded by the C-terminal wrapping domain. Following resealing of the G-segnent after T-segment passage, the C-gate opens, allowing the T-segment to exit the enzyme [60], [27].

1.3.4 Topoisomerase IV

Topo IV, like gyrase is a heterotetramer, but has two ParC subunits and two ParE subunits, which share homology with GyrA and GyrB respectively [fig. 1.2] [61], [62]. Whilst DNA gyrase acts during the initiation, elongation and termination stages of DNA replication, topo IV primarily acts during the termination stage. Topo IV acts to decatenate the daughter chromosome strands that are intertwined during replication fork rotation to aid DNA segregation, and is efficient at relaxing supercoils [9]. The decatenation and relaxation activities of topo IV are ATP-dependent [63].

Topo IV has a preference to relax positive supercoils over negative supercoils; *in vitro*, topo IV relaxes positive supercoils 20-fold faster. Topo IV has a preference for crossing angles formed in positively supercoiled catenated DNA, which is a determinant in the topo IV activity [64], [63]. Topo IV has the C-terminal β-pinwheel to aid DNA bending, however, topo IV does not constrain positive supercoils, and thus cannot introduce negative supercoils like gyrase. The β-pinwheel has 5 blades, rather than the 6 like gyrase, and lacks the conserved GyrA-box motif, which is implicated in clamping the positive wrap [65]. From footprinting analysis, *E. coli* topo IV could not protect 150 bp of a DNA duplex like with *E. coli* gyrase. Instead, topo IV could protect a 34 bp DNA duplex and therefore the topo IV G-segment is shorter than the G-segment of gyrase [66].

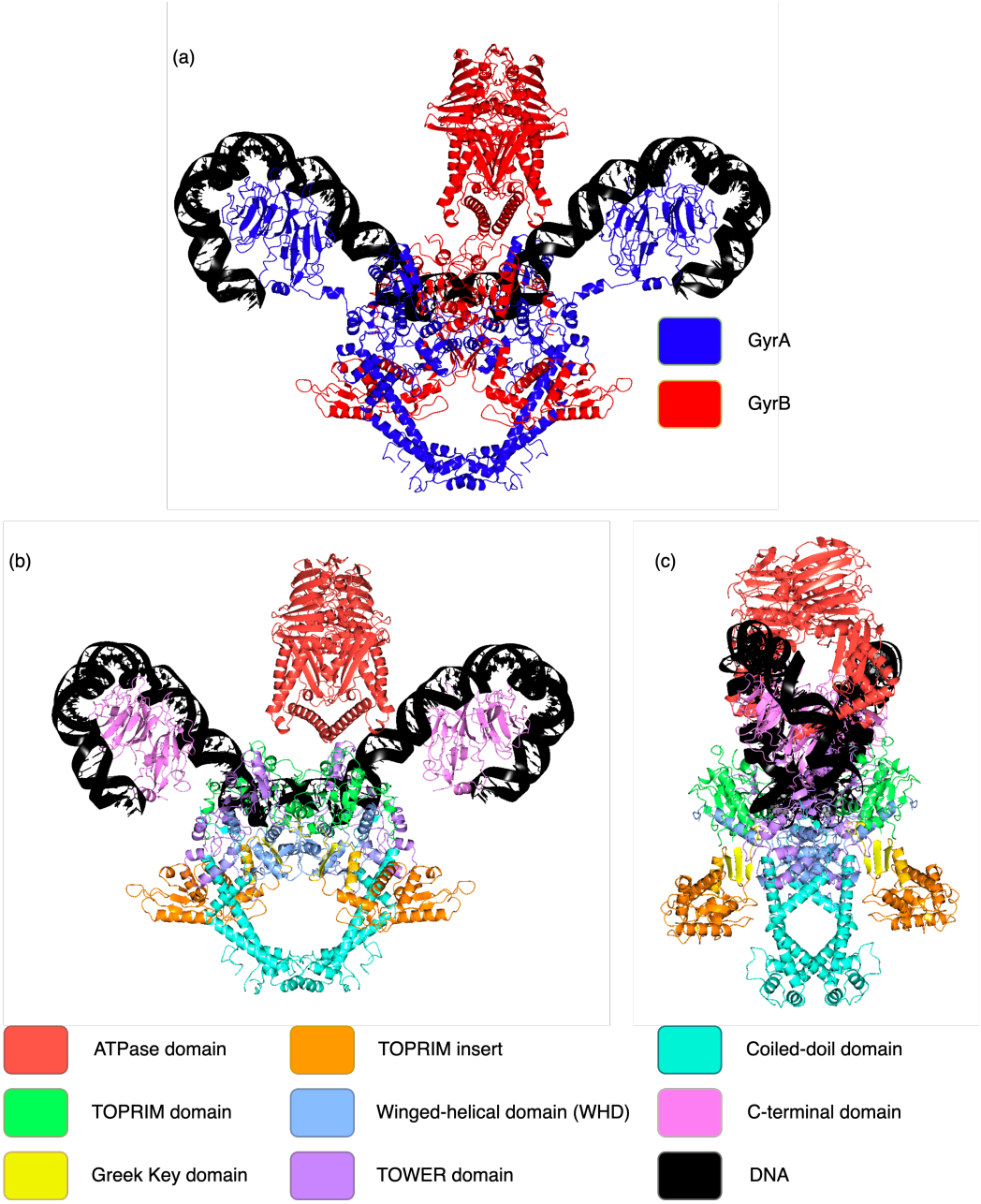

Figure 1.4: The structure of *E. coli* gyrase bound to the gate DNA. (a) *E. coli* gyrase is formed of two A subunits (blue), and two B subunits (red), forming an A_2B_2 heterotetramer. **(b-c)** The front and side view of *E. coli* gyrase with the domains coloured. The winged helical domain (WHD) where the catalytic tyrosine is located, the TOWER domain, the coiled-coil domain where the exit-gate is located, and the C-terminal domain, which contains a β-pinwheel which wraps the G-segment are located on GyrA. GyrB contains the ATPase domain, and the TOPRIM domain, where the acidic metal ion binding residues reside. Inserted within the TOPRIM domain is the Greek Key domain, which sometimes contains an insert domain. This figure was made using the cryo-EM *E. coli* gyrase model pdb 6RKW [36]

1.3.5 Eukaryotic topoisomerase II

Eukaryotic topoisomerase II (topo II) is formed of two homodimeric polypeptides (A_2) that are homologous to the prokaryotic type II topoisomerases. The N-terminal half of topo II shares homology with GyrB/ParE, and the C-terminal half is homologous to GyrA/ParC. Topo IIs are essential to condense chromosomes, resolve precatenanes following replication, and relax both positive and negative supercoils that arise during DNA processes. These activities are ATP-dependent.

In lower eukaryotes, only one topo II is present, these organisms include *Drosophila melanogaster* [67], *Saccharomyces cerevisiae* [68] and fungi, such as *Candida albicans* [69]. DNA bending of topo II can still be achieved in absence of the prokaryotic C-terminal wrapping domain; *Saccharomyces cerevisiae* topo II bends the G-segment by 150°, achieved by intercalating a conserved isoleucine residue into the G-segment between the +8 and +9 bp from the DNA cleavage site [27].

Topoisomerase II has two non-redundent isoforms, topo IIα and topo IIβ. The human topo IIα and β enzymes share 68% sequence identity, and are 77% homologous [70]; the highest variation is at the N- and C-terminus. The topo IIα isoform is highly expressed in proliferating tissues, whereas the topo IIβ isoform is more widely expressed, and the isoforms are localised to different cell tissues [71]. The expression is modulated by the cell cycle and the topo IIα isoform is highly expressed in dividing cells [72]. High levels of proliferation is a hallmark in cancerous cells; the expression of topo II is a marker for cancer and the eukaryotic topoisomerases are targets for anti-cancer therapies [73]. The β isoform does not discriminate between negative and positive supercoils. The α isoform relaxes positive supercoils over 10-fold faster than negative supercoils, which implicates the protein upstream of the progressing replication and transcription DNA bubble. Fast processing of positively supercoiled DNA ensures a low lifespan of the topoisomerase-cleaved DNA intermediates, which have the potential to stall DNA forks, leading to the accumulation of lethal double-stranded DNA breaks [74].

Topo II can protect around 25-28 bp of DNA in footprinting analysis [75], [76]. Gyrase and topo IV can bind longer regions of DNA, of 150 and 34 bp respectively [66], [53], [36]. Topo II does not have a wrapping domain, resulting in a smaller DNA binding region for the G-segment helix. The C-terminal region of human topo IIs controls the isoform functions; creating chimeras of the C-terminal domains of topo IIα and IIβ controlled the localisation of the enzymes in cells [77]. Additionally, the C-terminal domain is important in determining the

preference in supercoiling handedness of topo IIα, a cluster of positively-charged residues on the C-terminal domain controls this supercoiling discrimination [78].

1.3.6 Type IIB topoisomerases

The type IIB topoisomerase are subdivided into topoisomerase VI (topo VI) and topoisomerase VIII (topo VIII), that differ from the type IIA topoisomerases from their evolution, domain architecture and the strand-passage mechanism. The type IIB enzymes are primarily archeal enzymes, the first of which to be discovered was *Sulfolobus shibatae* topo VI [79]. Topo IIB enzymes lack the C-gate and therefore have only one cavity to navigate the T-segment. The enzymes must be tightly regulated to ensure the transient double-stranded DNA breaks are resealed following T-segment passage [80].

The topo VI enzymes have since been identified in some bacteria, red and green algae and dotted around the plant kingdom [81], [24]. Topo VI is an A_2B_2 heterodimer, which is observed with the bacterial type II topoisomerases: DNA gyrase and topo IV. However, the domain arrangements on topo VI diverge from the classical arrangements in type IIA topoisomerases. On bacterial type IIA topoisomerases, the catalytic tyrosine is present on the WHD, and the catalytic metal ion coordinating residues are present on the TOPRIM domain, the TOPRIM and WHD domains are on different subunits. On the archeal *Methanosarcina mazei*, the TOPRIM domain and the WHD are both present on the B-subunit. The A-subunit contains the GHKL and transducer domains, separated by a domain which, within the topoisomerase enzymes, is exclusive to the type IIB enzymes. The domain is a helix-two-turns-helix (H2TH) formed of 4 α helices, the function of which is not fully characterised, however may have a role in G-segment binding and translating conformational changes from the ATPase domain [82], [83]. The type IIA topoisomerases cleave the G-segment via a 4 bp staggar, whereas topo VI DNA cleavage sites are staggered by 2 nucleotides [80]. Topo VI is a potent decatenase and recognises DNA crossings close 90°, which are commonly found in catenated substrates, but can also relax negative and positive supercoils with reduced efficiency [84].

Topo VIII diverge from topo VI, because the ATPase and TOPRIM domain are located on the same polypeptide chain, like with the type IIA topoisomerases. Topo VIII contains the topo IIB characteristic H2TH domain [82]. Topo VIII can relax positive and negative supercoils. The role of ATP is less characterised for this subgroup, since *Microscilla marina* topo VIII was found to not only relax DNA independently of ATP, but also the DNA relaxation and cleavage activities were inhibited by the presence of ATP [82].

1.4 The DNA cleavage and resealing reaction by type II topoisomerases

The cleavage and resealing of the G-segment has to be tightly regulated and fast, since the reaction must be coordinated with T-segment passage, and unrepaired double-stranded DNA breaks are lethal. The DNA cleavage site of type II topoisomerases is formed from the WHD, which contains the catalytic tyrosine and an adjacent conserved arginine residue, and the TOPRIM domain, which contains the conserved E DXD motif which binds to catalytic metal ions. There are two DNA cleavage sites per topoisomerase complex, and type IIA enzymes cleave DNA with a 4 bp stagger. DNA cleavage is achieved by forming a phosphotyrosyl linkage with the $5'$ phosphate of the DNA backbone [fig. 1.5].

The cleavage of the DNA strands in the DNA duplex by type II topoisomerases are cleaved consecutively, therby proceeding via a nicked intermediate [85], [86]. There is asymmetry in the mechanism of strand scission between the two DNA cleavage active sites on the type II topoisomerase-DNA complex, where the cleavage of the first strand of DNA increases the rate of the cleavage of the opposite DNA strand, which results in coordinated DNA cleavage. This increases effectivity by raising the chances of the enzyme making a double-stranded break. Mechanistically, type II topoisomerases bend the G-segment at the cleavage site by up to 150° [27], [28], converting the DNA from the B-form like DNA to resemble the A-from. Once this strain is released after the first strand scission event, the increased flexibility aids the cleavage at the opposite strand on the duplex. If an artificial nick is introduced into the DNA, the DNA is a more efficient substrate for type II topoisomerases which increases the rate of DNA cleavage [87].

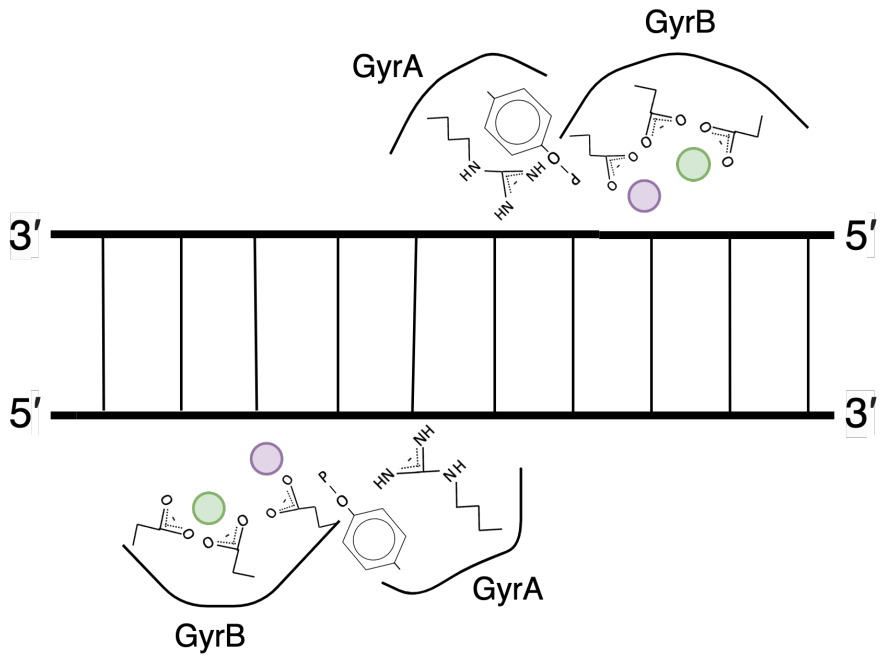

(a)

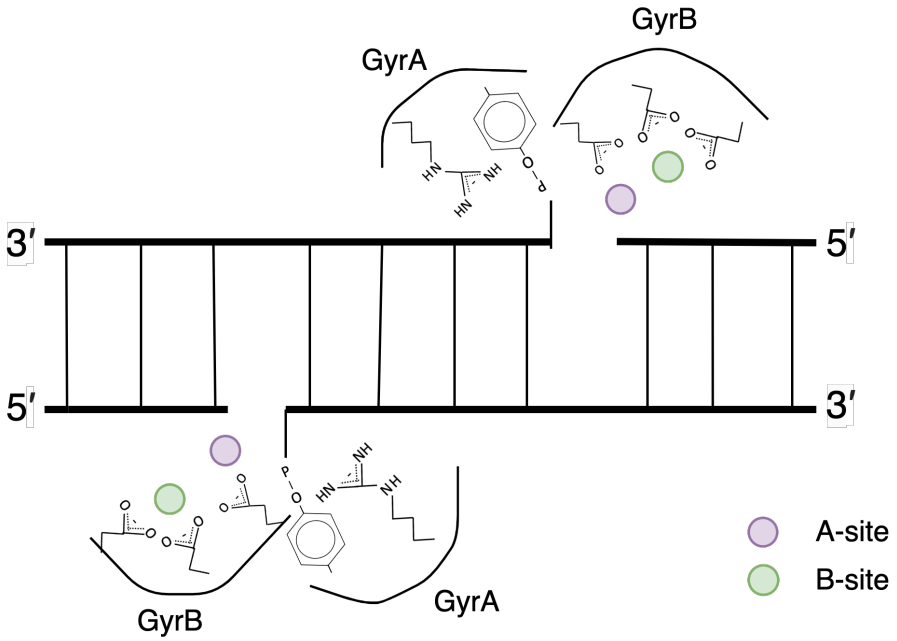

(b)

Figure 1.5: Bacterial type II topoisomerases in the uncleaved and cleaved state. The GyrA catalytic tyrosine, and the acidic metal ion coordinating GyrB amino acids are shown. There are two metal ion binding sites per DNA cleavage site: the catalytic A-site, and the non-catalytic B-site, which are shown in purple and green respectively. The metal ions are coordinated by the GyrB acidic residues and the DNA. **(a)** The gyrase-DNA complex with uncleaved DNA. **(b)** The catalytic tyrosine forming a phosphotyrosine linkage with the scissile phosphate; there is a 4 bp stagger between the two DNA cleavage sites.

There are two sites for divalent metal to bind, the A-site and the B-site, which are coordinated by the acidic triad of a glutamate and two aspartates that form the conserved E DxD motif [fig. 1.6]. The B-site metal ion is coordinated by D508 and D510 (*S. aureus* gyrase numbering) and is the binding site for the non-catalytic metal ion. The B-site metal ion is thought to dock the non-scissile phosphate via the non-bridging oxygen on the DNA phosphate located 5′ to the scissile phosphate. The A-site metal ion is known as the catalytic metal ion, which stabilises the transition state and the bridging oxygen leaving group. This aids the tyrosine to attack the phosphate to cleave the DNA and form a covalent linkage. The A-site metal ion is coordinated by D508 and E435, two water-metal ion bridges with D510, and the bridging and non-bridging oxygens from the scissile phosphate (*S. aureus* gyrase numbering) [39]. Since D508 coordinates both the A- and B-site metal ions, the residue has been observed to rotate in crystal structures. In crystal structures, the two metal ion binding sites have been observed 2.8 Å apart. There are two models in the literature which describe the mechanism by which the metal ions catalyse the DNA cleavage and resealing reaction for type II topoisomerases.

The two-metal model hypothesises that both the A- and B-sites are occupied simultaneously to catalyse DNA cleavage and resealing on both sides of the enzyme [88], [89], [90], [91]. The moving-metal model proposes that a metal ion is present at either the A-site or the B-site at each DNA cleavage site. The metal ion moves between the two sites, starting by binding to the B-site to dock the DNA. The metal ion then moves to the A-site to catalyse strand scission. Post cleavage, the metal ion moves back to the B-site, and then to the A-site to catalyse religation [39], [92]. A wealth of evidence is avaliable in the literature to support both metal ion mechanisms, primarily from X-ray crystallography structures, where the catalytic metal ion can be visualised, and from biochemical studies [fig. 1.7].

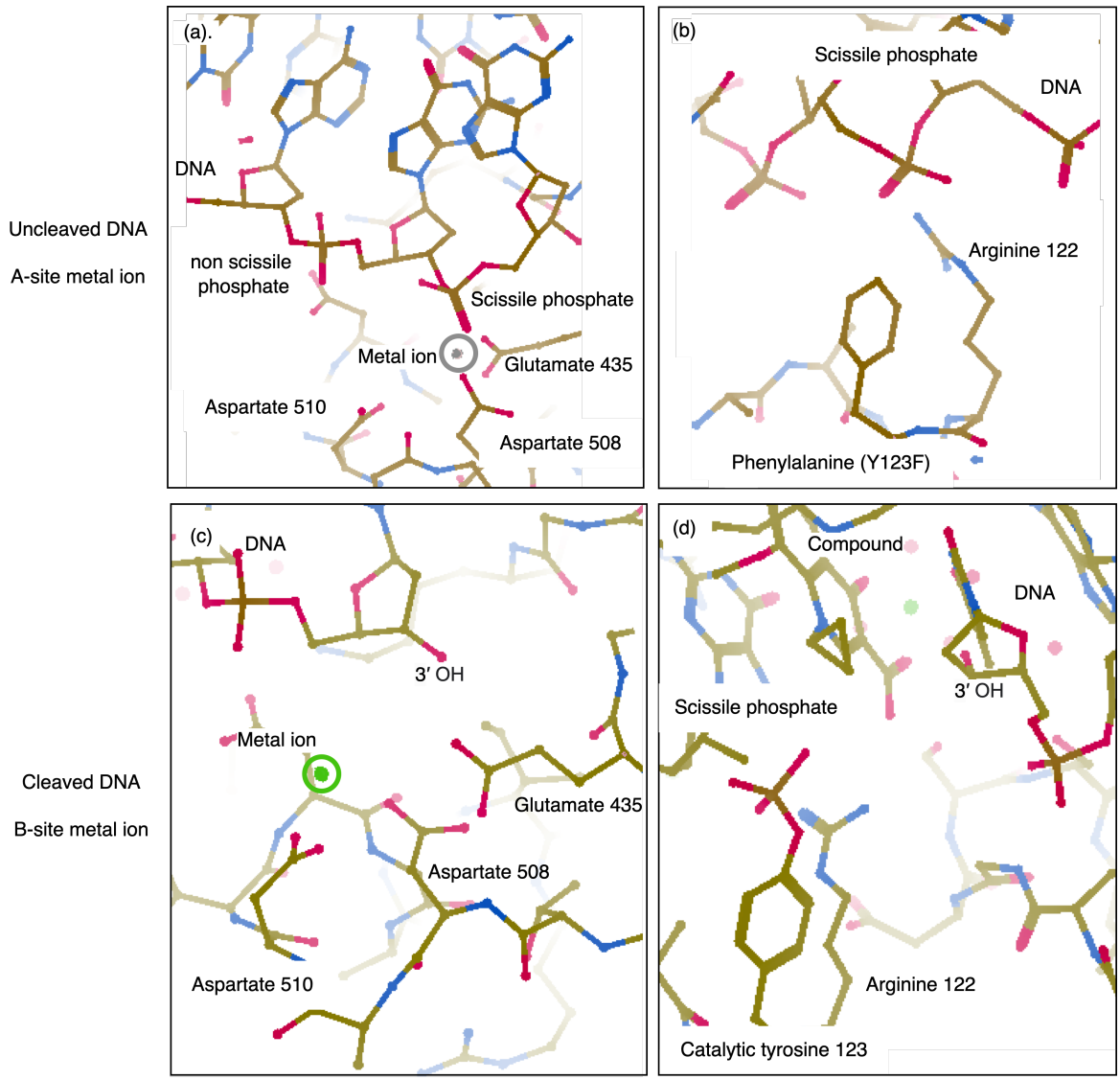

Figure 1.6: *S. aureus* gyrase pre-cleavage, and post cleavage state. An *S. aureus* gyrase crystal structure representing a metal ion occupying the A-site and the scissile phosphate poised to cleave DNA, and an *S. aureus* gyrase crystal structure showing gyrase in the cleaved conformation with the metal ion at the B-site, and the phosphotyrosyl linkage. The *S. aureus* gyrase core fusion crystal structure with uncleaved DNA in two different views **(a-b)** (PDB 6FM4 [93]). **(a)** The GyrB metal-coordinating acidic residues, aspartate 508 and glutamate 435 coordinates the catalytic metal ion at the A-site (circled in grey). The metal ion is also coordinated by the scissile phosphate. **(b)** The GyrA catalytic tyrosine (mutated to phenylalanine in this structure), pointing towards the scissile phosphate. The *S. aureus* gyrase core fusion structure, with the gyrase-DNA complex in the cleaved state with the cleavage-stabilising compound moxifloxacinin two different views **(c-d)** (PDB 5CDQ [46]). **(c)** The GyrB metal ion coordinating acidic residues, depicting aspartate 510 and aspartate 508 coordinating a metal ion at the non-catalytic B-site. The metal ion is circled in green. **(d)** The catalytic tyrosine forming a phosphotyrosine bond with the scissile phosphate.

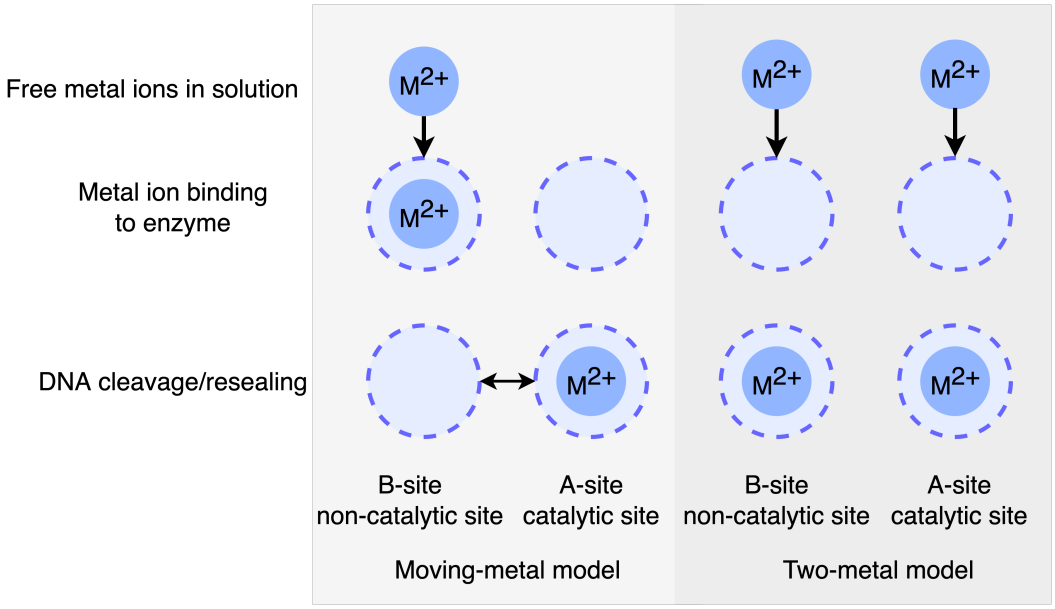

Figure 1.7: The existing metal ion models in the literature for the catalysis of the DNA cleavage and resealing reaction by type II topoisomerases. There are two models for how divalent metal ions catalyse DNA cleavage and resealing. One model proposes only one metal ion is sufficient to catalyse DNA cleavage and resealing, and can move between the two metal ion binding sites [39]. The other metal ion model proposes that two metal ions are required to be simultaneously present to catalyse DNA cleavage and resealing [88]. When the metal ion is at the B-site, the metal ion aids DNA binding and positions the DNA in the correct orientation. The A-site metal ion catalyses the DNA cleavage and resealing reaction.

Despite the two contrasting models describing the occupancy of the metal ion binding sites in type II topoisomerases, the catalytic mechanism for the DNA cleavage and reunion reaction are in general agreement. Type II topoisomerases use general acid-base chemistry to cleave and reseal DNA [fig. 1.8]. A base, which has been proposed to be a conserved histidine residue or a metal-associated water molecule, deprotonates the active-site nucleophilic tyrosine [88], [94]. The catalytic tyrosine forms a covalent phosphotyrosine linkage with the 5′ phosphate on the DNA backbone [95]. The pentavalent negatively-charged transition state is stabilised by the metal ion present at the A-site, as well as a conserved arginine, located adjacent to the catalytic tyrosine [95]. The metal ion coordinates the 3′ hydroxyl leaving group, which is protonated by an acid. The DNA gate is then opened, pulling the DNA apart. During this stage, the scissile phosphate is separated from the E DxD motif and therefore the metal ion binding site is disrupted. Following T-segment passage, the DNA gate is closed and the A-site is reformed. Ligation proceeds by deprotonating the 3′ hydroxyl group to attack the phosphotyrosyl bond. The A-site metal ion and arginine stabilises the negative charge during this stage.

In the two metal-ion model, metal ions have to be simultaneously present during DNA cleavage; the A-site metal ion would have to either rebind from solution, or be retained by the acidic residues during DNA gate opening. The metal ion mechanism for this model is a non-canonical two metal ion mechanism. The classical two-metal ion model was proposed for some enzymes, including polymerases, where one metal ion activates the nucleophile, and another metal ion stabilises the developing negative charge on the transition state [96], [97]. The type II topoisomerase metal-ion mechanism is non-canonical, because the B-site metal ion coordinates the non-scissile phosphate. The moving metal model suggests the B-site metal ion is captured first to anchor and orientate the DNA. The metal ion moves to the A-site to catalyse DNA cleavage, which then moves back to the B-site following gate opening. The metal ion can then move to the A-site to catalyse rejoining [39], [92].

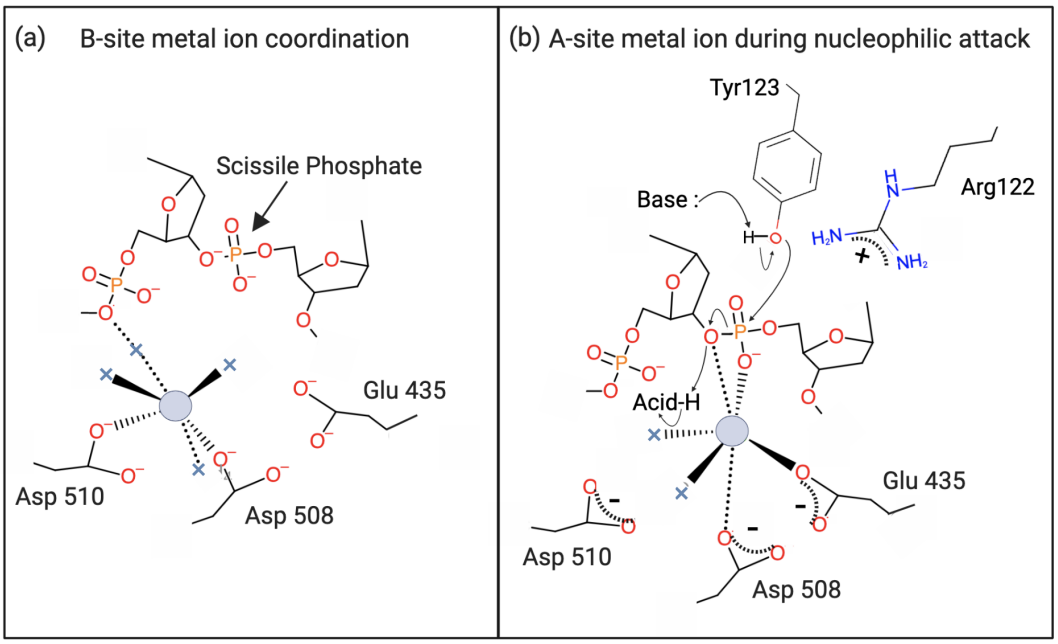

Figure 1.8: The metal ion coordination of the B-site metal ion, and the A-site metal ion during nucleophilic attack. (a) The B-site metal ion is coordinated by the non-scissile phosphate, and two aspartates, GyrB D510 and D508 (*S. aureus* gyrase numbering). **(b)** The A-site metal ion stabilising the scissile phosphate during nucleophilic attack from the tyrosine. The A-site metal ion is coordinated by GyrB D508 and E435 (*S. aureus* gyrase numbering).

1.4.1 Evidence for the metal ion mechanisms to catalyse DNA cleavage and resealing

The two-metal ion mechanism was first proposed in 2002 in a series of mutagenesis studies on the acidic residues at the DNA cleavage active site of *E. coli* DNA gyrase. The DNA relaxation levels from the GyrB metal ion coordinating residue D500H mutant were measured in the

presence of both magnesium and calcium ions. The relaxation activity was enhanced in the presence of both metal ions, compared to the sum of the relaxation activities catalysed by the individual metal ions. This co-stimulation effect was not observed for wild-type gyrase [88]. DNA cleavage enhancement in the presence of two different metal ions has been observed with human topoisomerase II. Manganese ions with magnesium ions or calcium ions showed increased total cleavage using DNA with the 3′-bridging oxygen modified to a sulphur (phosphorothiolate bonds). The S-P bond is unable to be reformed following cleavage, inhibiting DNA religation, as opposed to the native O-P, creating a suicide substrate. The study also showed biphasic concentration dependence for DNA cleavage activity with manganese and calcium ions with both a wild-type DNA substrate, and a mutated DNA substrate with a phosphorothiolate bond at the DNA cleavage site. The sigmoidal shaped curve was suggested to represent the sequential binding of each metal ion [89]. Similar experiments have also been replicated in other type II topoisomerases, such as *E. coli* topo IV [98].

Crystallographic studies primarily visualise one metal ion at the DNA cleavage site, however there are a handful of crystal structures which depict two metal ions simultaneously occupying both the A-site and the B-site. These structures generally have asymmetry within the structure, or the metal ions are modelled at half occupancy. The 3-Å resolution crystal structure of *Saccharomyces cerevisiae* topoisomerase II DNA-binding region visualises the catalytic tyrosines covalently attached to an asymmetric DNA substrate. At the cleavage site, one phosphodiester bond was modified to a phosphorothiolate bond (O-P to S-P), and at the other cleavage site, there is an artificial nick in the DNA. The crystal structure visualises zinc ions at the A- and B-site, 3.5 Å apart [94]. Zinc metal ions are unable to catalyse DNA cleavage and therefore the positions of the native metal ion, magnesium, may differ.

Additional crystal structures visualise two metals at the DNA cleavage site. The 2.45-Å resolution structure of *Staphylococcus aureus* gyrase which has a mutation of the active site tyrosine to a phenylalanine, an artificial doubly-nicked DNA substrate and the DNA cleavage-stabilising agent etoposide shows two manganese ions occupying the A-site and the B-site at one out of the two DNA cleavage sites [fig. 1.9] [46]. Etoposide intercalates into the cleaved DNA site on one side of the dimeric enzyme, introducing asymmetry into the structure. A single manganese ion at the B-site was observed on the side with etoposide intercalation, and two manganese ions at both the A- and B-site were observed on the opposite side. These metal ions were modelled with 60 and 40% occupancy for the A-site and B-site respectively. This may suggest the metal ions are weakly bound, or, static disorder within the crystal structure

depicts the metal ions in the two positions.

Another structure showing one metal ion at one of the enzyme's cleavage site, and two metal ions at the other DNA cleavage site is the wild-type *S. aureus* gyrase 2.37-Å resolution crystal structure [99]. The DNA substrate used was uncleaved DNA with gepotidacin, which stabilises single-stranded DNA cleavage. The metal is visualised at the A-site on one side, and the A- and B-site on the other. The occupancy of the metal ions is low for the metal ions, which were modeled at between 25-40% occupancy. An asymmetric complex is formed because the compound binds in two orientations, and because there is one phosphotyrosine linkage per enzyme complex.

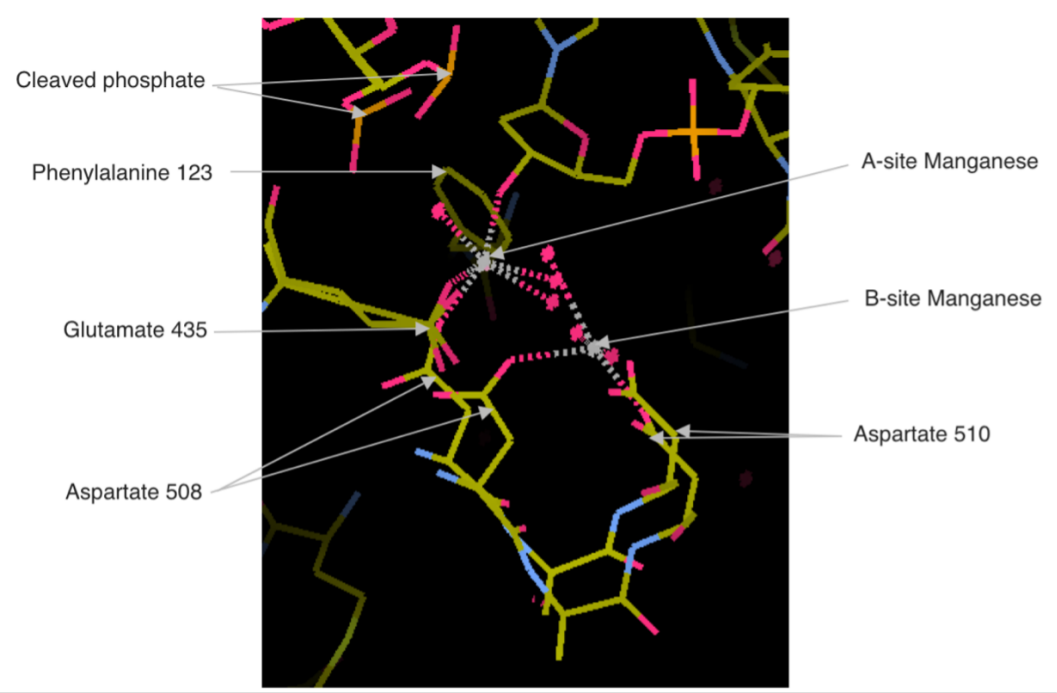

Figure 1.9: The DNA cleavage site of *S. aureus* gyrase, with a manganese ion present at the two metal ion binding sites. Two metals can be seen at the active site. The catalytic tyrosine (mutated to phenylalanine in this structure) can be seen pointing to the cleaved phosphate. The A-site metal ion is coordinated by GyrB E435, D508 and the 3′ hydroxyl group. The B-site metal ion is coordinated by GyrB D508 and D510. The residues have been modelled in two orientations. Phenylalanine can be seen pointing to the cleaved phosphate. This structure was obtained using artificially nicked DNA, and one molecule of the cleavage-stabilising compound etoposide is bound per gyrase complex. The A- and B-site metal ions at the DNA cleavage site without a compound bound were modeled with 60 and 40% occupancy, respectively. This figure was created in coot using PDB 5CDP [46].

The moving metal mechanism was hypothesised because metal was visualised at either the A- or B-site in numerous structures of type II topoisomerase from different species. The structures generally represent the pre-cleavage and post-cleavage enzyme conformations respectively. A

2.1-Å resolution crystal structure of *S. aureus* DNA gyrase captures the enzyme in a pre-cleavage conformation with a single manganese ion at the A-site [fig. 1.10]. The enzyme has the active-site tyrosine mutated to phenylalanine to prevent cleavage of the DNA 20-mer, and so the DNA is intact in the crystal structure [39].

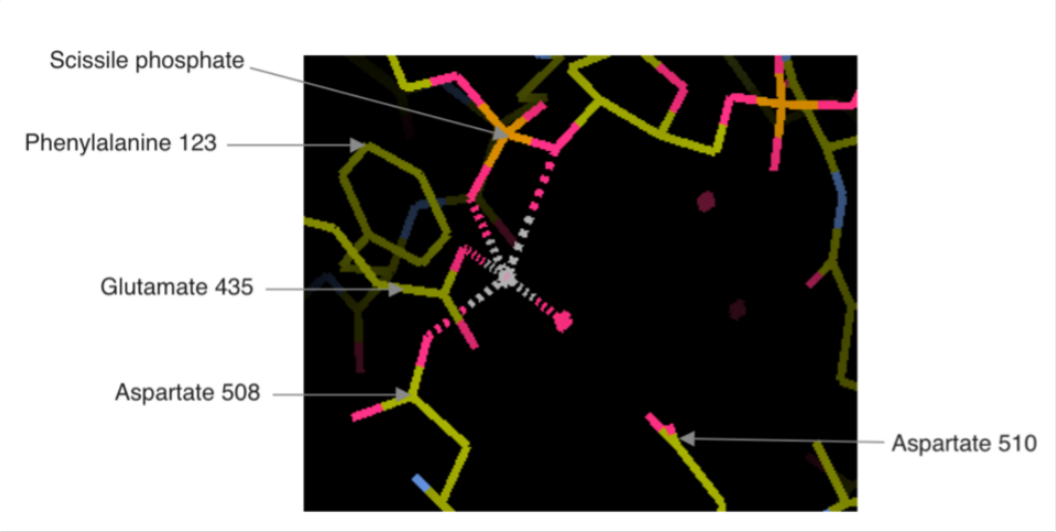

Figure 1.10: The DNA cleavage site of *S. aureus* gyrase, with a manganese ion present at the catalytic A-site. The structure of *S. aureus* gyrase Y123F mutant crystallised with the cleavage-stabilising compound GSK299423, and uncleaved DNA. In this state, gyrase is poised to cleave DNA (pre-cleavage). A manganese ion is visualised at the A-site on both sides of gyrase. This metal ion is coordinated by GyrB D508, E435 and the scissile phosphate. The phenylalanine can be seen pointing towards the scissile phosphate. This figure was made by using the model PDB 2XCS in coot [39].

The DNA cleavage site where metal ions are complexed to the B-site metal is often visualised when the enzyme is in the post-cleavage conformation. The metal ion at the B-site and enzyme in the cleaved conformation is the most common configuration of type II topoisomerases which has been captured by X-ray crystallography. This may be achieved either through enzyme-cleaved DNA via covalent attachment of the tyrosine to the 5′ phosphate, or artificially cleaved DNA and with either wild-type enzyme, or the tyrosine mutated to a phenylalanine. These structures are also often achieved with cleavage-stabilising compounds to stabilise the cleaved conformation. For example, the wild-type *S. aureus* DNA gyrase crystal structure at 2.95 Å resolution in the presence of the DNA cleavage stabilising compound moxifloxacin depicts the magnesium ions at the B-site at both DNA cleavage sites [fig. 1.11]. The enzyme-cleaved DNA captures the tyrosine covalently bound to the DNA and the B-site metal coordinated by two aspartates and an important water bridge with the non-bridging oxygen 5′ to the cleavage site [46].

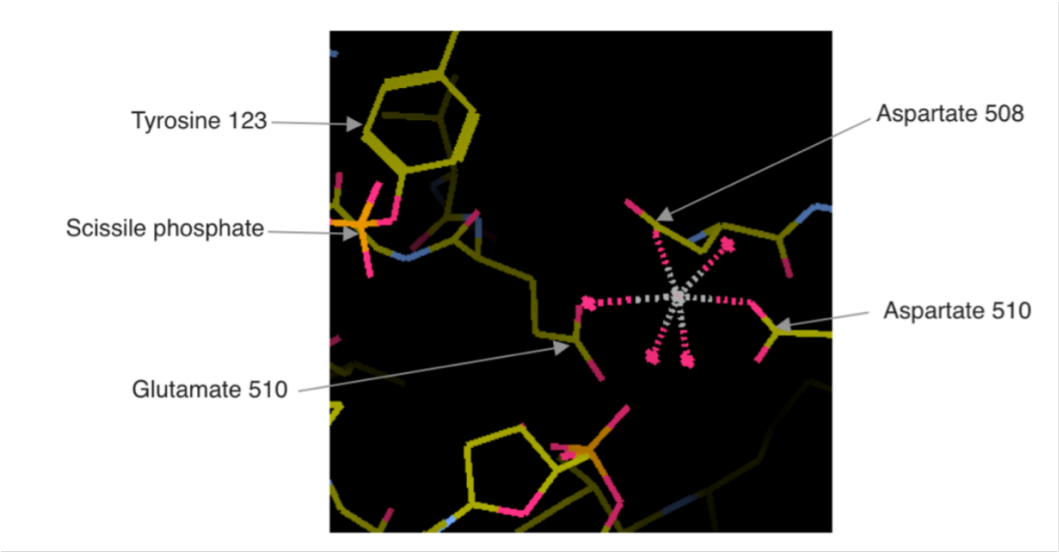

Figure 1.11: The DNA cleavage site of *S. aureus* gyrase, with a manganese ion present at the B-site. The active site of *S. aureus* gyrase wild type in the post-cleavage conformation, crystallised with magnesium and the DNA cleavage-stabilising compound moxifloxacin. The catalytic tyrosine is visualised forming the covalent phosphotyrosyl bond with the DNA backbone. The metal is visualised at the B-site on both sides of the gyrase complex, coordinated by D508, D510 and the non-scissile DNA phosphate. This figure was made using coot and the model PDB 5CDQ [46].

DNA cleavage-stabilising compounds generally act by distorting the DNA to inhibit the religation of DNA cleavage complexes. Wendorff and colleagues [100] provide suggestions to why only one metal ion may be present in many type II topoisomerase crystal structures. In the presence of DNA cleavage-stabilising drugs, which intercalate into the DNA, the compound distorts the DNA such that the scissile phosphate is shifted out of position, resulting in A-site metal ion binding incompatibility. This would provide an explanation to why only the B-site metal is visualised in these types of type II topoisomerase crystal structures. In crystal structures of type II topoisomerases which visualise the A-site metal ion only, the acidic metal ion residues were suggested to be misaligned, physically preventing the B-site metal from binding. Therefore, there is crystallographic evidence to support both a one metal, and two metal ion model to catalyse the DNA cleavage and reunion reaction.

1.4.2 The metal ion mechanism of type I topoisomerases and nucleotide transferring enzymes

Magnesium ions are required to catalyse the reactions of a diverse range of enzymes, which include the nucleotide transfer reaction, which involves forming and/or breaking the phosphodiester bond. There are variations in the number of metal ions which catalyse these nucleic acid chemistries. For example, one metal ion catalyses the DNA cleavage and resealing in the type

IA topoisomerases, and metal ions are not required for catalysis in type IB topoisomerases. The number of metal ions and the metal ion mechanisms of structurally and functionally similar enzymes may elucidate the metal ion mechanism of the type II topoisomerases.

The type IA topoisomerases possess the TOPRIM domain, where the metal ion coordinating residues are situated. The scission activity of this enzyme subclass generally requires a divalent metal ion, some enzymes can cleave in the absence of metal ions, although the activity is enhanced by the presence of divalent metal ions. The reverse reaction, DNA rejoining, is dependent on metal ions. In *Mycobacterium tuberculosis* topoisomerase I (topo I), a type IA enzyme, a water molecule acts as a base to activate the catalytic tyrosine, the positive charge in the transition state is stabilised by a nearby arginine. Additionally, a glutamate residue acts as an acid to donate a proton to the hydroxyl leaving group via a proton relay system. Metal ions are essential for religation in *Mycobacterium tuberculosis* topo I, and glutamate is thought to position the catalytic metal ion to increase the nucleophilic properties of the $3'$ hydroxyl broken end [101]. Further, since topo I can cleave single-stranded DNA, the bases are not constrained to Watson Crick base pairing. Therefore, the metal ion is important during DNA resealing to position the $3'$ -OH group for attack on the phosphotyrosyl bond. In *E. coli* topo I, a spatially adjacent conserved arginine is important in stabilising the negative charge on the catalytic tyrosine during DNA religation, since mutating this residue led to the accumulation of topo I-DNA cleavage complexes [102]. Human topoisomerase IIIβ (top3B) also does not require metal ions for DNA cleavage, but are essential for DNA resealing. The role of the metal ion in DNA cleavage is replaced by a conserved lysine residue in the topo III enzymes, since mutation of the lysine residue abolished metal ion-dependent DNA cleavage activity. The lysine coordinates the scissile phosphate for correct positioning with respect to the catalytic tyrosine, and stabilising the negative charge in transition states [17]. The topo IA enzymes do not require two metal ions for catalysis like the type II enzymes, due to the presence of positively charged residues at the DNA cleavage sites, such as arginine and lysine residues.

The type IB topoisomerases lack the TOPRIM domain, and therefore the conserved DXD motif which coordinates the catalytic metal ions is not present. These enzymes act in a metal ion independent mechanism. The enzyme can achieve this by additional positively charged residues present at the DNA cleavage active site. *Leishmania donovani* topo I has 4 positively charged residues, 2 arginines, 1 lysine and a histidine, residing on the catalytic core domain, which all coordinate the pentavalent transition state and stabilise the negative charge [103].

The type II topoisomerase have the adjacent arginine to the catalytic tyrosine, however, there are no obvious positively charged residues near the DNA cleavage site.

The OLD family nucleases contain the TOPRIM domain, where the acidic metal ion binding residues are located. *Burkholderia pseudomallei* class 2 OLD nuclease uses divalent cations, namely Mg^{2+}, Ca^{2+} and Mn^{2+}. The crystal structure of the enzyme revealed two magnesium ions present at on the TOPRIM domain, which were coordinated by 6 acidic amino acids. The magnesium ions had octahedral geometry with a water bridge between the two magnesium ions, which were spaced 4.9 Å apart, significantly further than the distance between the two metal ion binding sites for type II topoisomerases. The magnesium ions from the OLD nuclease are situated around the scissile phosphate, whilst the type II topoisomerase metal ions coordinate the scissile phosphate, and the non-scissile phosphate [44].

A crystal structure of *S. aureus* DnaG primase, which contains a TOPRIM domain, revealed three manganese ions coordinated by the TOPRIM acidic residues [43]. In both of these DnaG primase and OLD nuclease structures, there are additional acidic residues, and the catalytic metal ions are spatially separated compared with the type II topoisomerases. Another non-topoisomerase protein which contains a TOPRIM domain is RecR proteins, which is involved in DNA repair. There was no biochemical or structural data on the metal ion mechanism for these proteins.

The two metal ion mechanism in the OLD family nucleases, DNA polymerase I, and MutH/RNase H nucleases use a canonical two-metal ion mechanism [104], [97]. The utilisation of two, divalent metal ions to catalyse nucleic acid chemistry often follows a canonical, two metal ion mechanism. One metal ion activates and positions the nucleophile, which is often a water molecule, and coordinates with one of the oxygens from the scissile phosphate. The other metal ion coordinates two oxygens from the scissile phosphate, and coordinates the leaving group. Both metal ions are required to stabilise the negative charge of the pentavalent phosphate transition state (the phosphorous is bound to 2 oxygens, the nucleophile, and DNA strands). There are variations to this metal ion mechanism; the LAGLIDADG homing endonucleases, which hydrolyse DNA, utilise three metal ions per two DNA cleavage sites. The two catalytic sites each have a divalent metal ion to activate the water nucleophile, whilst share a metal ion which stabilises the transition state [105].

There are also examples of enzymes which catalyse the phosphotransfer reaction using a one metal ion mechanism. HUH endonuclease and relaxase TrwC nicks DNA using a nucleophilic

tyrosine. The divalent metal ions are coordinated by a pair of histidines, which polarise the phosphotyrosine bond to facilitate nucleophilic attack, however this metal ion is too far away to activate the OH group of the nucleophile [106], [107]. DNA polymerase η, β and μ have been proposed to require three divalent metal ions to catalyse phosphoryl transfer, which diverges from the conserved canonical two metal ion mechanism for other polymerases [108], [109], [110]. The three metal ion mechanism of polymerases was identified by transition state structures. The mechanism still uses the principles of the canonical two metal ion mechanism, but with a third metal ion that coordinates a nucleotide phosphate to help overcome the energy barrier for DNA synthesis [111].

The activity of type II topoisomerases is inhibited at high concentrations of metal ions [91]. This result could represent changes in the ionic strength, or, non-specific metal ion binding on the topoisomerase which is detrimental to the enzyme's activity. Alternatively, at higher concentrations of metal ions, the two metal ion binding sites are more likely to be simultaneously occupied, which could be inhibitory to the DNA cleavage and resealing activities of the topoisomerase. Inhibition of the endonuclease APE-1 enzyme at high concentrations of metal ions was proposed to arise by the simultaneous occupation of the two metal ion binding sites, and therefore a moving metal ion model was proposed for this enzyme [112]. The APE-1 enzyme cleaves DNA using water as the nucleophile, and the metal ion is coordinated by two aspartates and one glutamate.

1.5 DNA topoisomerases as drug targets

The topoisomerase enzymes are of great interest as drug targets for the development of broad spectrum antibiotics and chemotherapeutic anti-cancer agents.

One class of topoisomerase inhibitors, termed poisons, manipulate the DNA cleavage and religation reaction by stabilising the topoisomerase in the cleaved state. Poisons associate with the topoisomerase-DNA complex and stabilise the covalent single- and double-stranded DNA-topoisomerase cleavage complexes by distorting the DNA such that the scissile phosphate is misaligned for DNA resealing. Therefore, poisons increase the lifespan of the transiently cleaved DNA state. Trapped topoisomerase cleavage complexes block DNA replication and transcription, which inhibits cell growth and division. The topoisomerase-associated DNA breaks can be processed into lethal DNA breaks which results in the loss in genomic integrity and activation of apoptosis [113].

The second class of topoisomerase inhibitors are the catalytic inhibitors. Catalytic inhibitors inhibit the overall activity of topoisomerases by reducing the rate of DNA relaxation, supercoiling or decatenation. These inhibitors target different functionalities of the topoisomerases, such as ATPase binding and hydrolysis, DNA binding or the DNA cleavage-resealing reaction. These inhibitors prevent the topoisomerase from their essential functions, such as relieving topological strains and separating intertwined daughter chromosomes, from forming interactions with other proteins on DNA, or trapping the T-segment between the N- and DNA-gate [114].

1.5.1 Inhibitors to the type I topoisomerases

Camptothecin is a natural product isolated from the tree bark of *Camptotheca acuminata*, which was identified to have anti-cancer properties [115], and later discovered to be an inhibitor of type I topoisomerases [115]. Clinical usage of camptothecin were withdrawn due to side effects [116]. This led to the development of water-soluble analouges, topotecan and irinotecan, which are used clinically to treat ovarian and colon cancers respectively [117], [118], and are the only type I topoisomerase inhibitors currently clinically approved by the US Food and Drug Administration. Camptothecin and derivatives stabilise single-stranded DNA cleavage complexes by blocking the scissile phosphate from religating following DNA cleavage. The compounds are interfacial poisons which bind at the interface between the type I topoisomerases, and the DNA at the site of DNA cleavage [118].

Bacterial type I topoisomerase inhibitors are being developed for antibiotics, however none have been approved clinically. Type I topoisomerase inhibitors have potential against numerous infectious bacteria, including *Mycobacterium tuberculosis*, the causative agent of tuberculosis, since it contains only one type IA topoisomerase which is essential for cell viability [119].

1.5.2 DNA cleavage-stabilising type IIA topoisomerase inhibitors

Interfacial poisons targeting the type II topoisomerases bind at the interface between DNA and the protein. A number of poisons intercalate into the DNA at the site of DNA cleavage and stabilise double-stranded DNA breaks. These compounds are also coordinated by the TOPRIM and WHD domains and two compounds bind per topoisomerase complex [fig. 1.12a]. Compounds which intercalate at the site of DNA cleavage include the bacterial-targeting quinolones, antibiotics in development, such as the imidazopyrazinones and the quinazoline diones, and the anti-cancer drug etoposide [120], [121], [46], [39]. Another class of type II topoisomerase inhibitors, which target the bacterial DNA gyrase and topo IV, are the

Novel Bacterial Topoisomerase Inhibitors (NBTIs), which includes the antibiotic gepotidacin. Gepotidacin has reached phase III clinical trials [122]. These compounds intercalate at the centre of the G-segment and stabilises single-stranded DNA breaks [fig. 1.12b] [123].

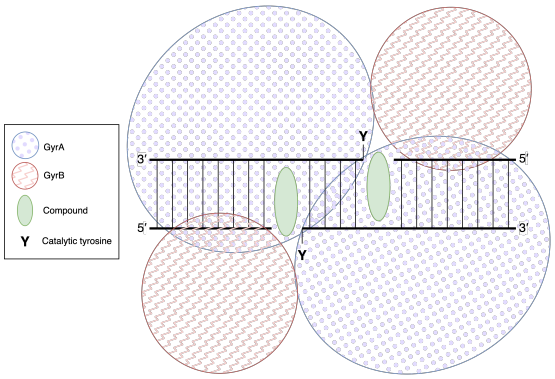

(a)

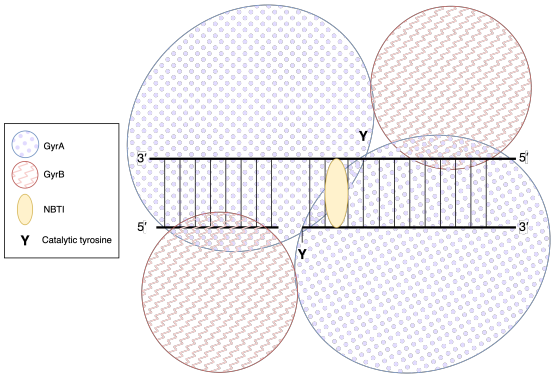

(b)

Figure 1.12: The effect of DNA cleavage stabilising compounds on gyrase-DNA complexes. **(a)** Poisons stabilising double-stranded DNA breaks, depicting two inhibitors per enzyme, intercalating into the DNA at the DNA cleavage site. These poisons include fluoroquinolones, imidazopyrazinones, quinazoline diones and etoposide. **(b)** An NBTI intercalating in between the two DNA cleavage sites; one compound binds per enzyme complex, which results in a single-strand DNA break.

The bacterial topoisomerases are the target of the fluoroquinolones, which are one of the most successful and widely used antibiotic series in clinical use [124]. The quinolone interfacial poison antibiotics dual-target the bacterial topoisomerases: DNA gyrase and topoisomerase IV and are broad spectrum antibiotics. The first quinolone developed, nalidixic acid and other first generation quinolones were used to treat urinary tract infections from Gram-negative bacteria [125]. The addition of a fluorine atom to the quinolone scaffold led to 2^{nd}, 3^{rd} and 4^{th} generation

quinolones, which are called fluoroquinolones [fig. 1.13]. The nine antibiotics approved for clinical use which target the bacterial type II topoisomerases are all fluoroquinolones [126]. The fluoroquinolones can target Gram-negative and Gram-positive bacteria, and can be used to treat a variety of bacterial infections, including pneumonia, bronchitis and urinary tract infections. In the US, the fluoroquinolones were all approved between 1986-1999. Since then, the fluoroquinolones have been extensively diversified, however no more have been approved for clinical use. The success of the fluoroquinolones led to widespread usage and escalating rates of fluoroquinolone-resistant bacteria [127], [128].

Hotspots for quinolone-resistance mutations in bacterial topoisomerases occur at the quinolone binding site, named the quinolone-resistance-determining region (QRDR) [129]. Resistance of fluoroquinolones in *Neisseria gonorrhoeae* arises through mutations in the QRDR; in South Asia, 50% of clinical isolates of *Neisseria gonorrhoeae* were quinolone resistant [130]. Fluoroquinolones require a water-metal ion bridge between the compound and the enzyme to bind to the bacterial topoisomerases. This metal ion is structural and is not involved in the catalytic metal ion mechanism to cleave and reseal DNA. The water-metal ion bridge is commonly coordinated by a GyrA/ParC serine and glutamate, located in the QRDR. Therefore, mutations of these residues give rise to antibiotic resistant bacteria [129]. The fluoroquinolones have been a triumph over the last 30 years, however, their success was undermined by substantial use and misuse, which has increased the prevalence of antibiotic-resistant bacteria. Therefore, alternatives are critical.

Antimicrobial resistance (AMR) is a global challenge. Nearly 5 million deaths each year have been estimated to attribute to AMR, which has been predicted to rise to 10 million annually by 2050 [131]. Not only will pathogens become more deadly, AMR is economically impactful and will disproportionately affect the livelihoods of societies most vulnerable. A number of pathogenic bacteria, including *Salmonella* species, *Shigella* species, *Campylobacter* species, and *Naisseria gonorrhaeae* are on the World Health Organisation's list of priority pathogens, on account of their resistance to the fluoroquinolones [132].

The success of fluoroquinolones highlight the power of targeting the bacterial topoisomerases, and the search for alternatives led to the development of new classes of antibiotics targeting the bacterial topoisomerases. To date, none of the new antibiotic classes have been approved clinically. The imidazopyrazinones (IPY) and the quinazoline diones bind in the quinolone binding pocket at the site of DNA cleavage and are under current investigation for development

into antibiotics [120], [121] [fig. 1.13]. These synthetic compounds do not require a water-metal ion bridge for binding, and therefore are promising against bacteria with mutations in the residues which coordinate the fluoroquinolone water-metal ion bridge. The IPYs were shown to be more active at inhibiting the *in vitro* DNA supercoiling activity of the *E. coli* gyrase GyrA S83L and GyrA D87N mutants than one of the most successful fluoroquinolone antibiotics, ciprofloxacin [120]. Since IPYs bind in the quinolone binding pocket, there are mutants resistant to both IPYs and fluoroquinolones.

Antibiotics which bind in the quinolone-binding pocket are likely to exhibit cross resistance with fluoroquinolone resistant bacterial strains. The development of the NBTIs, which are also interfacial bacterial topoisomerase poisons, do not bind at the DNA breakage point [fig. 1.13]. The NBTI's primary target in Gram-negative bacteria is DNA gyrase, and in Gram-positive bacteria, the primary target is topo IV [133]. The NBTI gepotidacin has promising minimum inhibitory concentrations (MIC) against fluoroquinolone resistant bacteria. The compound recently entered phase III clinical trials to treat uncomplicated urinary tract infections [134], and trials were halted early due to promising efficacy [122].

Etoposide [fig. 1.13] is a topo II poison which is approved for use against small cell lung cancer and testicular cancer [135]. Etoposide intercalates into the G-segment DNA at the DNA cleavage site of human topooisomerase II, in the same location as quinolones. Cancer cells can gain resistance to etoposide by numerous mechanisms, including increasing drug efflux and alterations in topoisomerase expression levels. Another clinically available anti-cancer chemotherapeutic agent is the anthracyclin doxorubicin, which is approved to treat a broad range of cancers [136]. Doxorubicin can act by the generation of free radicals and oxidative damage, and also intercalates into the DNA which inhibits human topo II [137]. Doxorubicin acts differently to the topoisomerase poisons, because it does not intercalate into the G-segment DNA at the DNA cleavage site.

Stabilising the cleaved state of the bacterial topoisomerases is an effective mechanism at killing bacteria, as exemplified by the fluoroquinolones. A new series of antibiotics - the thiophenes, allosterically inhibit the bacterial topoisomerases by stabilising topoisomerase-DNA cleavage complexes [138]. The compounds were shown to stabilise both single- and double-stranded DNA breaks. Discovering novel binding pockets to allosterically inhibit the topoisomerases is promising in terms of new pockets to explore for medicinal chemistry to target the topoisomerases. The thiophenes are not shown to be cross-resistant to bacteria

resistant to the fluoroquinolones, due to the allosteric binding pocket being distal from the QRDR.

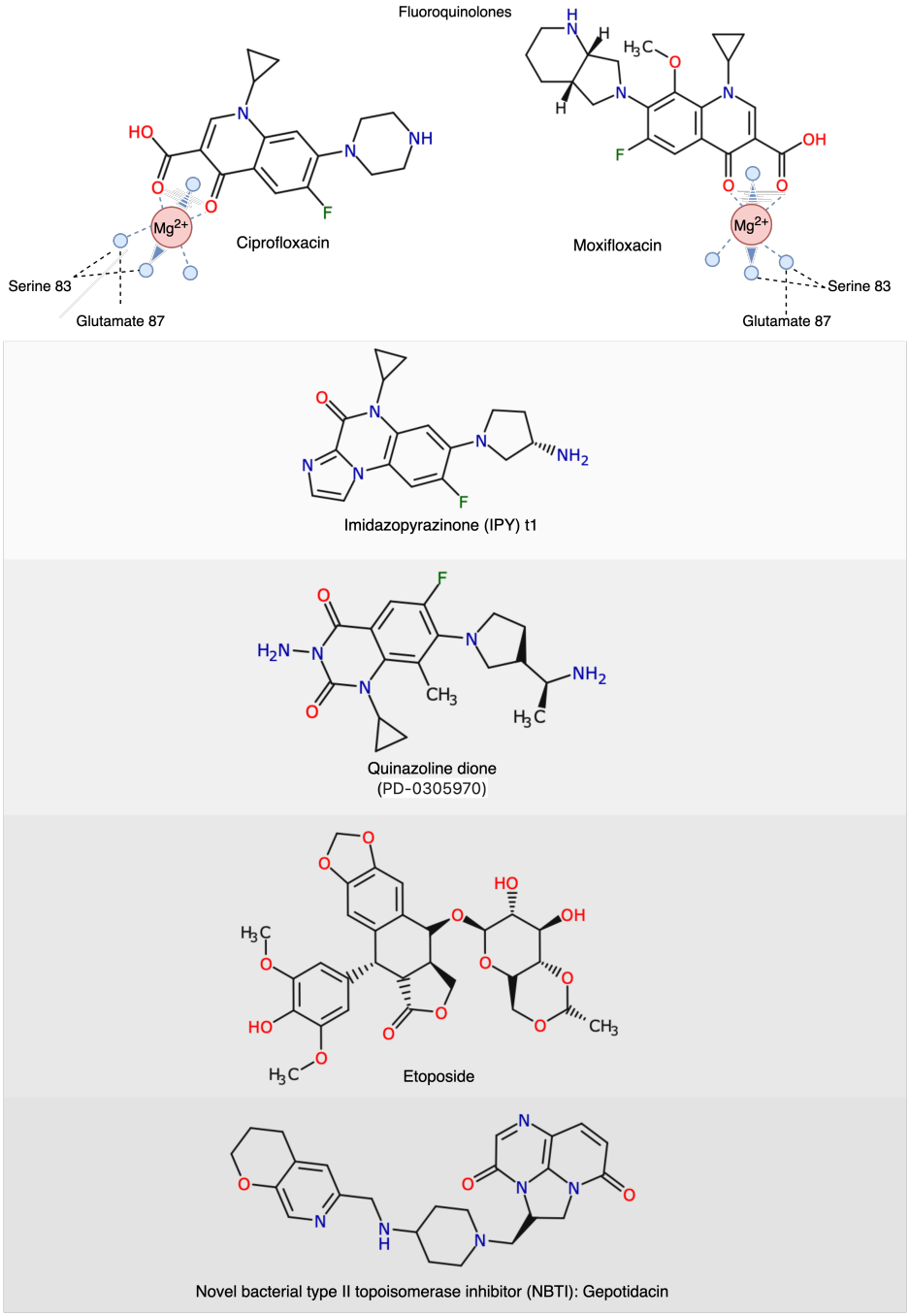

Figure 1.13: The compound structures of cleavage-stabilising type II topoisomerase inhibitors. The structure of the fluoroquinolones ciprofloxacin and moxifloxacin, showing the water-metal ion bridge required for compound binding to *E. coli* gyrase. The compound structures of the imidazopyrazinone t1, the quinazoline dione PD-0305970, etoposide and the NBTI gepotidacin.

1.5.3 Catalytic inhibitios of type II topoisomerases

Different aspects of the type II topoisomerases catalytic cycle can be targeted with inhibitors. The aminocoumarins are antibiotics which target the ATPase domain. Novobiocin is a natural product produced by *Streptomyces nivens* and targets the bacterial type II topoisomerases. Novobiocin is more potent against DNA gyrase over topo IV [139], and has poor activity against the human topoisomerase II [129]. The compound has greater activity against Gram-positive bacteria, because the novobiocin struggles to cross the lipopolysaccharide membrane of Gram-negative bacteria. Novobiocin competitively competes with ATP on the ATPase domain by partially covering the ATP-binding site. This inhibits topoisomerase relaxation activity, and the DNA gyrase supercoiling activity [113]. Novobiocin is not currently approved for clinical use as an antibiotic on the grounds of toxicity and undesirable pharmacokinetic properties.

Simocyclinone D-8 is a natural product isolated from *Streptomyces antibioticus* Tü 6040 [140] and contains an aminocoumarin moiety. The compound targets DNA gyrase using a different mechanism to the aminocoumarins. The compound has not been shown to target topo IV. The compound also has anti-cancer properties. Simocyclinone D-8 inhibits gyrase prior to DNA cleavage by inhibiting DNA binding to the enzyme, by binding to GyrA at a site adjacent to the quinolone binding site [141]. The two binding sites do not overlap, however simocyclinone D-8 exhibited cross resistance to fluoroquinolone-resistant mutants in the QRDR [142], [143].

1.6 Project aims

The DNA cleavage and resealing activities of type II topoisomerases are manipulated by successful antibiotic and anti-cancer agents. Whilst the reactions are well-studied, there remains contrasting evidence in the literature, as to the metal ion mechanism required for catalysis, particularly with respect to the occupancy of the two metal ion binding sites during each step in the reactions, and the fate of the metal ions prior to DNA resealing is not fully understood. Following DNA cleavage, the catalytic metal ion site is destroyed on opening of the DNA-gate. This project aims to gain a deeper understanding of the equilibrium between the cleaved and resealed state of DNA formed by the bacterial type II topoisomerases, focussing on the DNA resealing reaction. The role of divalent metal ions is explored, as well as the contributions of individual amino acids and domains to the reactions.

New antibiotics are required to combat the emergence of antibiotic resistance. Manipulation of the DNA cleavage and resealing reaction has proved to be successful in drug development, and therefore novel compounds targeting this equilibrium were explored in this thesis. These synthetic antibiotics developed by Uppsala University are called the quinazoliniums and kill clinically important Gram-negative bacteria. These compounds were thought to target DNA gyrase. In this project, the quinazolinium mechanism of inhibition against gyrase is investigated. The potency of these compounds against gyrase from Gram-positive and Gram-negative species is calculated, as well as the compound activity against other type II topoisomerase enzymes. This project aims to define the binding site for the quinazoliniums, and to assess biochemically any cross resistance against fluoroquinolone-resistant gyrase mutants.

Chapter 2

Materials and Methods

2.1 Bacteriology

Escherichia coli Strain	Genotype
5-alpha (NEB)	ϕ80Δ(lacZ)M15 fhuA2 Δ(argF-lacZ)U169 phoA glnV44 gyrA96 reacA1 relA1 endA1 thi-1hsdR17
α-Select Gold (Bioline)	F - deoR endA1 recA1 relA1 gyrA96 hsdR17(rk - , mk +) supE44 thi-1 phoA Δ(lacZYA argF)U169 Φ80lacZΔM15λ -
DH5-alpha (Thermofisher Scientific)	Δ(argF-lac)169, ϕ80dlacZ58(M15), ΔphoA8, glnX44(AS), deoR481, rfbC1, gyrA96(NalR), recA1, endA1, thiE1 and hsdR17
Stellar (TakaraBio)	F–, endA1, supE44, thi-1, recA1, relA1, gyrA96, phoA, Φ80d lacZΔ M15, Δ (lacZYA - argF) U169, Δ (mrr - hsdRMS - mcrBC), ΔmcrA, λ–
JM109 (Promega)	endA1, recA1, gyrA96, thi, hsdR17 (r_k^-, m_k^+), relA1, supE44, Δ(lac-proAB), [F´ traD36, proAB, $laqI^qZ\Delta M15$]
BLR (Novagen)	F- ompT hsdSB(rB-mB-) gal lac ile dcm Δ(srl-recA)::Tn10 (tetR)(DE3)
OneShot BL21 (DE3) Star	F-ompT hsdSB (rB-, mB-) galdcmrne131
Rosetta2 pLysS (Novagen)	F- ompT hsdSB(rB- mB-) gal dcm (DE3) pLysSRARE2 (CamR)

Table 2.1: The *E. coli* bacterial competent cells used for plasmid and protein expression.

2.2 Molecular biology

2.2.1 Protein constructs

The plasmids for expressing and purifying *E. coli* gyrase and *S. aureus* gyrase wild-type enzymes or mutant enzymes were either gifted, or made using PCR mutagenesis [tbl. 2.2].

Species	Protein	Plasmid	Source
E. coli	GyrA	pPH3	Gifted from Dr. Thomas Germe
E. coli	GyrB	pAG111	Gifted from Dr. Thomas Germe
E. coli	GyrB	pET28b	Girfted from Ghilarov lab
E. coli	GyrB E424A	pAG111	Mutagenesis of wild-type
E. coli	GyrB D500H	pET28b	Mutagenesis of wild-type
E. coli	GyrB ∆Greek Key domain	pAG111	Mutagenesis of wild-type
E. coli	GyrA	pET28b	Girfted from Ghilarov lab
E. coli	GyrBA fusion	pTTQ18	Gifted from Dr. Thomas Germe
E. coli	$GyrB_{D500H}A$	pTTQ18	Mutagenesis of wild-type
E. coli	$GyrBA_{R121L,Y122L,T123L}$	pTTQ18	Gifted from Dr. Thomas Germe
E. coli	$GyrB_{E424A}A$	pTTQ18	Mutagenesis of wild-type
E. coli	GyrB K740A	pET28b	Girfted from Ghilarov lab
E. coli	GyrA	pACYC-duet	Gifted from Dr. Thomas Germe
S. aureus	GyrA	pET11	Gifted from Dr. Thomas Germe
S. aureus	GyrB	pET11	Gifted from Dr. Thomas Germe
S. aureus	GyrB K740A	pET11	Mutagenesis of wild-type
S. aureus	GyrB ∆Greek Key domain	pET11	Mutagenesis of wild-type
S. aureus	GyrBA core fusion	pET11	Gifted from Dr. Thomas Germe
S. aureus	GyrBA core fusion GyrA Y123F	pET11	Gifted from Dr. Thomas Germe

Table 2.2: The source of *E. coli* and *S. aureus* gyrase wild-type and mutant plasmids. pPH3 and pAG111 are vector constructs originally in pTTQ18 [144]. Plasmids: pACYC-duet (Novagen), pTTQ18 was a gift from Michael Stark (Addgene plasmid 69122), pET28b (Novagen), pET11 (Novagen).

2.2.2 Cloning for site-directed mutagenesis and deletion

2.2.2.1 Primer design

Constructs were designed for site-directed mutagenesis or domain deletion using InFusion cloning (TakaraBio). Forward and reverse primers were designed to contain a 15 bp overlap region containing the codon for the point mutation change. For domain deletions, primers were designed such that the 15 bp primer pair overlap could delete a region [tbl. 2.3].

2.2.2.2 Polymerase chain reaction mix

PCR mixes were made with the CloneAmp HiFi PCR premix, 0.2 μM of forward and reverse primer and 50 ng of plasmid template per 25 μL reaction in 0.2 mL PCR tubes.

2.2.2.3 Polymerase chain reaction cycle

The PCR reaction was performed by heating to 98°C for 2 minutes to denature the template, followed by 30 cycles of (98°C for 15 seconds, primer Tm - 5°C for 15 seconds to anneal the primers, and 72°C for 0.5 minutes/kbp of the protein construct for extension), followed by 72°C for 7 minutes to complete extension.

Species	Mutant	Plasmid	Forward Primer	Reverse Primer
S. aureus	GyrB ΔGreek Key domain	pET11	CGCCGACCGGAAAAGGTCTGGGTGAAATGAATGCAG	CTTTTCCGGTCGGCGGCTGTGCAATATAAAC
S. aureus	GyrB K581A	pET11	ACGTTATGGAGGTCTGGGTGAAATGAATGC	AGACCTCCATAACGTGCAATAGACCATTTCGG
E. coli	GyrB ΔGreek Key domain delete amino acids 534-561	pAG111	GCCGCCGGGGCGACGGCGCAACGCTGCAC	CCGTCGCCCGGCGGCTGAGCGATATAGAC
E. coli	GyrB ΔGreek Key domain delete amino acids 735-739	pAG111	CGGCCTCGGCAAAGGTCTGGGCGAGATGAACC	CCTTTGCCGAGGCCGCGACGGGACTCTTTCACC
E. coli	GyrB D500H	pET28b	CCGATGCGCACCGTCGACGGCTCGCACATTC	CGACGTGCGCATCGGTCATGATGATGATG
E. coli	GyrBA fusion GyrB D500H	pTTQ18	CCGATGCGCACCGTCGACGGCTCGCACATTC	CGACGTGCGCATCGGTCATGATGATGATG
E. coli	GyrB E424A	pAG111	CTGGTGGCAGGGGACTCCGCGGGCGGCTCTG	GTCCCCTGCCACCAGGTACAGTTCGGAAAGCGCCGGATCGCGTTC
E. coli	GyrBA fusion GyrB E424A	pTTQ18	CCTGGTGGCAGGGGACTCCGCGGGCGG	TCCCCTGCCACCAGGTACAGTTCGGAAAGC

Table 2.3: The primers used for the mutagenesis of DNA sequences for the production of new DNA plasmid constructs to express gyrase mutants.

2.2.2.4 PCR product purification

The PCR mix was digested with 1 μL Dpn1 (NEB) per 50 μL of PCR reaction for 15 minutes at 37°C to degrade the template wild-type methylated DNA. The digested PCR mix was cleaned up using the QIAquick PCR Purification Kit (Qiagen), following the manufacturer's instructions. The entire DNA sample with 1x Gel Loading Dye, Purple (NEB) was loaded onto a 1% agarose gel with 0.5 μg/mL ethidium bromide [subsection. 2.4.3]. The gel was visualised using UV, and the DNA band at the correct size was excised with a razor blade. The excised gel piece and 200 μL of 1x TAE [tbl. 2.9] was placed into SnakeSkin Dialysis Tubing with a 10k MWCO, 22 μm (Thermo Fisher Scientific), which was sealed with clips. The dialysis tubing was placed in a gel tank in 1x TAE [tbl. 2.9] and run at 80 V for 45 minutes. The buffer around the gel piece was aspirated and concentrated using the QIAquick PCR Purification Kit (Qiagen). The DNA concentration was estimated using the NanoDrop One by measuring the absorbance at 280 nm.

2.2.2.5 The InFusion reaction

The InFusion reaction was set up to ligate the linearised PCR product, using up to 100 ng of the PCR plasmid product and 2 μL of the In-Fusion Snap Assembly Master Mix, which was made to 10 μL in water. The InFusion reaction was incubated at 50°C for 15 minutes. 2-5 μL of InFusion reaction were transformed into *E. coli* Stellar competent cells.

2.2.3 Media, agar and antibiotics

The media for bacteria growth for plasmid and protein expression.

LB (Millar): 1% (w/v) Tryptone, 0.5% (w/v) Yeast Extract, 1% NaCl (w/v).

LB-agar: LB (Millar) media with 1.1% agar. 2x YT (Yeast Extract Tryptone): 1.6% Tryptone, 1% Yeast Extract, 0.5% NaCl.

SOC media (Super Optimal broth with Catabolite repression): 2% (w/v) Tryptone, 0.5% Yeast Extract, 0.58% NaCl, 0.186% KCl, 21.3 mM $MgCl_2$, 16.3 mM $MgSO_4$, 20 mM glucose.

The appropriate antibiotics were added to the media, or melted agar cooled to 50°C. The concentration of antibiotics were: 50-100 μg/mL ampicillin, 30 μg/mL chloramphenicol (dissolved in 100% ethanol), and 35 μg/mL kanamycin.

2.2.4 Plasmid transformations

Defrosted chemically competent cells were combined with 50-300 ng of plasmid or up to 5 μL of InFusion cloning reaction, and incubated on ice for 30 minutes. The cells were transformed by incubating the cells at 42°C for 45 seconds, followed by incubation on ice for 2 minutes. 450 μL of SOC media pre-warmed to 37°C was added to the transformed cells, which were then incubated for 30-60 minutes at 37°C in a shaking hot block (800 rmp). 50 μL of transformation, or the whole transformation (centrifuged at 2k xg and cells resuspended in 50 μL of LB) were spread on agar plates with appropriate antibiotics. Agar plates were incubated overnight at 37°C.

2.2.5 DNA plasmid amplification and purification

The plasmid of interest, or the InFusion cloning reaction for plasmid mutagenesis, was transformed into either *E. coli* Stellar competent cells (TakaraBio), *E. coli* α-competent cells (Bioline), *E. coli* 5-alpha competent cells or *E. coli* DH5α cells (Thermo Fisher). Colonies were picked and inoculated into 5-10 mL of LB with appropriate antibiotics, and incubated at 37°C overnight at 200 rpm. The plasmids were extracted and purified from 1-5 mL of cell culture using the QIAprep Spin Miniprep Kit (Qiagen), following the manufacturer's instructions. The DNA concentration from the purified plasmid product was estimated using the NanoDrop 1.

2.2.6 DNA sequencing

To sequence plasmids to ensure the correct mutations were incorporated, Sanger sequencing using the Mix2Seq kit (Eurofins) was used, following the manufacturer's instructions to prepare the sequencing samples. Sequencing primers were designed to sequence the whole plasmid. Primers were selected at 700-800 bp intervals and designed to be of length 18-22 bases with a melting temperature between 50-55°C.

2.3 Protein expression and purification

2.3.1 Expression of *E. coli* and *S. aureus* proteins

A fresh colony (1-2 days post transformation) expressing the plasmid containing the gene for the protein of interest was picked and inoculated into 10-100 mL of media with appropriate antibiotics. The culture was incubated overnight at 37°C whilst shaking at 200 rpm. 10 mL of

overnight culture was inoculated into 1 L of media with appropriate antibiotics in 2 L shake flasks. The cell culture was incubated at 37°C at 200 rpm. The OD_{600} was measured every hour using a spectrometer until the desired optical density was reached. The culture was induced with IPTG and the protein was expressed at the desired temperature and expression time [tbl. 2.4]. The cells were harvested at 3.5k xg for 20 minutes, the cell pellet was flash frozen in liquid nitrogen and stored at -80°C.

Species	Protein	Vector	Antibiotic	Protein expression conditions
E. coli	GyrA, GyrB, GyrB E424A, GyrB Δ Greek Key domain	pAG111 for GyrB, pPH3 for GyrA	Ampicillin	Plasmid transformed into *E. coli* JM109 competent cells. LB overnight culture. Cells expressed in LB at 37°C until the OD_{600} was between 0.4-0.6 for GyrA, and 0.3 for GyrB. Cells induced with 0.5 mM IPTG and grown for 2.5 hours at 37°C
E. coli	GyrA, GyrB, GyrB K740A, GyrB D500H	pET28b	Kanamycin	Plasmid transformed into OneShot BL21 (DE3) Star *E. coli*. Overnight culture in 2xYT media. Cells expressed in 2xYT media at 37°C until the OD_{600} was between 0.4-0.6. Cells induced with 0.5 mM IPTG and grown overnight at 20°C
E. coli	Homodimer, homodimer mutants	pTTQ18	Ampicillin	Plasmid transformed into *E. coli* BLR competent cells. Colony inoculated into LB overnight culture grown at 37°C. Overnight culture inoculated into LB until the OD_{600} was between 0.4-0.6. Cells induced with 0.5 mM IPTG and grown for 3 hours at 37°C
E. coli	Heterodimer, heterodimer mutants,	pTTQ18 and pACYC-duet	Ampicillin and Chloramphenicol	Plasmids transformed into *E. coli* BLR competent cells. Colony inoculated into LB overnight culture grown at 37°C. Overnight culture inoculated into LB until the OD_{600} was between 0.4-0.6. Cells induced with 1 mM IPTG and grown for 3 hours at 37°C
S. aureus	GyrA	pET11	Ampicillin and Chloramphenicol	Plasmids transformed into *E. coli* Rosetta2 pLysS competent cells. Colony inoculated into LB + 10% glucose overnight culture grown at 37°C. Overnight culture inoculated into LB + 10% glycerol until the OD_{600} was between 0.4-0.6. Cells induced with 0.5 mM IPTG and grown for 3 hours at 28°C
S. aureus	GyrB, GyrB K581A, GyrB ΔGreek Key domain	pET11	Ampicillin	Plasmid transformed into *E. coli* BLR competent cells. Colony inoculated into LB overnight culture grown at 37°C. Overnight culture inoculated into LB until the OD_{600} was between 0.4-0.6. Cells induced with 0.5 mM IPTG and grown for 3 hours at 28°C
S. aureus	GyrBA core fusion wild-type and Y123F mutant	pET11	Ampicillin	Plasmid transformed into *E. coli* BLR competent cells. Colony inoculated into LB overnight culture grown at 37°C. Overnight culture inoculated into LB until the OD_{600} was between 0.4-0.6. Cells induced with 0.5 mM IPTG and grown overnight at 18°C

Table 2.4: The protein expression of *E. coli* and *S. aureus* gyrase proteins.

2.3.2 Protein purification overview

2.3.2.1 Cell lysis

The cell pellet was defrosted and resuspended in pellet resuspension buffer [tbl. 2.6] and 1 EDTA-free proteinase inhibitor tablet per 2 L of cell culture. The cells were lysed at 40 psi using either the Avestin EmulsiFlex C3, or the Avestin EmulsiFlex-B15. Lysed cells were clarified by centrifugation at 37k xg at 4°C for between 45-60 minutes. The supernatant was aspirated and filtered in a 0.45 μm filter.

2.3.2.2 Protein purification

Proteins were purified using the ÄKTA pure chromatography systems (Cytivia) and purified using relevant columns [tbl. 2.5] and purification buffers [tbl. 2.6]. When gradients were run over columns, gradients were run over 30 mL. After each purification column, samples were analysed on 8 or 10% polyacrylamide Tris-glycine gels.

2.3.2.3 Dialysis

If protein samples required dialysis, samples were placed into SnakeSkin Dialysis Tubing with a 10k MWCO, 22 μm (Thermo Fisher Scientific) and sealed with food clips with a polystyrene float. The dialysis tubing was placed into 2 L of pre-cooled buffer, and incubated overnight at 4°C whilst stirring with a magnetic stirrer bar.

2.3.2.4 Affinity tag cleavage

If proteins required affinity tag removal (His tag and strep tag), TEV and 3C protease were added to the protein sample at a ratio of 1:100 w/w protease:protein sample, and cleaved overnight at 4°C.

Species	Protein	Plasmid	Cell lysis buffer	Column 1	Column 2	Column 3
E. coli	GyrA	pPH3	TED	5 mL heparin column in TED eluted in 0-100% TED + 1M NaCl. Eluted protein dialysed vs TED	1 mL MonoQ in TED, eluted from 0-100% TED + 1 M NaCl. Protein dialysed vs storage buffer 2	
E. coli	GyrB, GyrB E424A, GyrB ΔGreek Key domain	pAG111	TGED	5 mL heparin column in TGED eluted in 0-100% TED + 1M NaCl. Eluted protein dialysed vs TED	1 mL MonoQ in TED, eluted from 0-100% TED + 1 M NaCl. Protein dialysed vs storage buffer 2	
E. coli	GyrA, GyrB, GyrB D500H	pET28b	HisTrap binding buffer	5 mL HisTrap equilibrated inHisTrap binding buffer. Protein eluted over 0-100% HisTrap binding buffer + 250 mM imidazole	5 mL StrepTrap HP in StrepTrap binding buffer, eluted in 0-100% StrepTrap binding buffer + 3 mM desthiobiotin. Overnight TEV and 3C protease digestion.	5 mL HiTrap Q HP in HGED. Protein eluted over HGED + 1M NaCl
E. coli	GyrBA·A, $GyrB_{D500H}$·A, $GyrB_{E424A}$·A, $GyrBA_{LLL}$·A, $(GyrBA)_2$, $(GyrB_{D500H}A)_2$	pTTQ18, pACYC-duet	TED + 50 mM KCl	5 mL Q Sepharose column pre-equilibrated in TGED, eluted from 0-100% in TGED + 1M NaCl	5 mL HisTrap pre-equilibrated in TED + 20 mM imidazole, protein eluted in TED + 500 mM imidazole	Protein was concentrated to <2 mL and injected onto an S200 HiLoad gel filtration column pre-equilibrated in TED + 100 mM KCl
S. aureus	GyrA	pET11	TGED	5 mL HiTrap Q in TGED, eluted from 0-100% TGED + 1M NaCl	Pooled protein made up to 1 M ammonium sulphate, loaded onto a 5 mL phenyl sepharose column in TGED + 1 M ammonium sulphate. Eluted from 1-100% TGED. Protein dialysed vs TGED + 200 mM NaCl	5 mL heparin column in TGED eluted in 0-100% TGED + 1M NaCl. Eluted protein dialysed vs storage buffer 1
S. aureus	GyrB, GyrB K581A, GyrB Δ Greek Key domain	pET11	TGED + 50 mM NaCl	5 mL heparin column in TGED, eluted from 0-100% TGED + 1 M NaCl, protein dialysed vs TGED + 50 mM NaCl	5 mL Q Sepharose column in TGED + 50 mM NaCl, eluted in TGED + 1 M NaCl. Protein dialysed vs storage buffer 1	
S. aureus	GyrBA core fusion, GyrBA core fusion Y123F	pET11	TGED	5 mL heparin column in TGED, eluted in 0-100% TGED + 1M NaCl. Protein dialysed vs TGED	Protein concentrated to <2 mL and loaded onto an S200 HiLoad gel filtration column pre-equilibrated in gel filtration buffer	

Table 2.5: The protein purification columns to purify *E. coli* and *S. aureus* gyrase proteins and mutants.

Buffer	Buffer Components
TED	50 mM Tris-HCl pH 7.5, 1 mM EDTA, 1 mM DTT
TGED	50 mM Tris-HCl pH 7.5, 10% glycerol, 1 mM EDTA, 1 mM DTT
HGED	50 mM HEPES pH 8.0, 10% glycerol 1 mM EDTA, 2 mM DTT
Storage buffer 1	50 mM Tris-HCl pH 7.5, 40% glycerol, 1 mM DTT, 100 mM NaCl
HisTrap binding buffer	50 mM Tris-HCl pH 7.5, 300 mM NaCl, 10% glycerol, 20 mM imidazole
StrepTrap binding buffer	20 mM HEPES pH 8.0, 60 mM NaCl, 10% glycerol, 1 mM EDTA, 1 mM DTT
Gel filtration buffer	100 mM Na_2SO_4, 20 mM HEPES pH 8.0
Storage buffer 2	100 mM KCL, 10% glycerol, 1 mM EDTA, 2 mM DTT, 50 mM Tris-HCl pH 7.5

Table 2.6: The buffers used to purify *E. coli* and *S. aureus* gyrase proteins and mutants.

2.3.2.5 Protein concentration determination

Protein concentration was measured using the NanoDrop One (Thermofisher Scientific) by taking the absorbance at 280 nm. Typically, 1-2 μL of sample was loaded onto the NanoDrop, and the NanoDrop was blanked with buffer prior to taking protein readings. The protein concentration was determined from the Beer Lambert Law, using the protein molecular weight and theoretical extinction coefficient. The theoretical extinction coefficient was determined by entering the protein sequence into ExPASy ProtParam [145].

2.3.2.6 Protein concentration and storage

Protein samples were concentrated to the desired concentration in Amicon® Ultra Centrifugal filters (Merck). The desired MWCO was selected (10 - 100 kDa), based on the molecular weight of the protein. The concentrators were centrifuged at 3.5k xg at 4°C in a benchtop centrifuge (Thermo Sorvall Legend XTR). Purified concentrated protein were flash frozen in liquid nitrogen in aliquots between 5-100 μL, and stored at -80°C.

2.3.3 SDS-polyacrylamide gel electrophoresis (SDS-PAGE)

Proteins were analysed on Tris-glycine gels on either 8 or 10% SDS polyacrylamide gels depending on the protein size, made using glass casting plates (Bio-Rad). Protein samples were diluted 2-fold in 2x protein loading buffer, boiled for 5 minutes and centrifuged for 2 minutes at 16.1k xg. Typically, 10 μL of protein sample were loaded onto the acrylamide gel, and run at 180 V for 60 minutes. Gels were stained with 10 mL of InstantBlue™ protein stain (Expedeon) for 2-5 hours, and destained in water. Gels were imaged using visible light in a Syngene gel doc system. The gel solutions, gel running buffer and protein loading dye are indicated in table 2.7.

Buffer	Buffer Components
Stacking gel	4% acrylamide (v/v), 130 mM Tris-HCl pH 6.8, 0.1% SDS (w/v), 0.1% ammonium persulfate (v/v), 0.1% (v/v) N,N,N',N'-Tetramethylethylenediamine
Resolving gel	8 or 10% acrylamide (v/v), 390 mM Tris-HCl pH 8.8, 0.1% SDS (w/v), 0.1% ammonium persulfate (v/v), 0.1% (v/v) N,N,N',N'-Tetramethylethylenediamine
Running buffer	25 mM Tris, 192 mM glycine, 0.1% SDS (w/v), pH 8.3
2x protein loading dye	100 mM Tris-HCl pH 6,8, 4% SDS (v/v), 20% glycerol (v/v), 0.1% bromophenol blue (w/v), 200 mM DTT

Table 2.7: The recipe for preparing 8 or 10% acrylamide Tris-glycine resolving and stacking gels and running buffer.

2.4 DNA topology assays

2.4.1 DNA cleavage, supercoiling, relaxation and intercalation assays

DNA cleavage, supercoiling, relaxation and intercalation assays were performed in 1.5 mL Eppendorf tubes and had a reaction volume of 30 μL. Assay buffer (1x) [tbl. 2.8], 500 ng of pBR322* DNA (Inspiralis), relevant compounds and 4 mM $MgCl_2$ (unless otherwise stated) were combined and made up to 28 μL with water. The DMSO concentration was kept constant across assays and ranged from 0-10%. Negatively supercoiled pBR322* DNA for DNA cleavage and relaxation assays, relaxed pBR322* DNA for supercoiling assays, and relaxed and negatively supercoiled pBR322* for intercalation assays were used (Inspiralis). The assays were started on addition of 2 μL of enzyme stock at 15 times the required concentration, in dilution buffer [tbl. 2.9]. The samples were vortexed for 1-3 seconds and incubated for 30 minutes at 37°C. DNA supercoiling and relaxation assay samples were stopped by the addition of 30 μL chloroform:isoamylalcohol 24:1, and 30 μL of STEB [tbl. 2.9]. DNA cleavage samples were trapped by the addition of 7.5 μL SDS of 1%, and digested by proteinase K (Roche) at 0.5 mg/mL for 30 minutes at 37°C. The reaction was stopped by the addition of 20 μL STEB.

Assay Buffer	Enzyme	Components
Cleavage & Relaxation	*E. coli* gyrase	35 mM Tris.HCl (pH 7.5), 24 mM KCl, 2 mM DTT, 1.8 mM spermidine, 6.5% glycerol, 0.1 mg/ml, acetylated serum albumin (and 4 mM $MgCl_2$ unless otherwise stated)
Supercoiling	*E. coli* gyrase	35 mM Tris.HCl (pH 7.5), 24 mM KCl, 2 mM DTT, 1.8 mM spermidine, 6.5% glycerol, 1 mM ATP, 0.1 mg/ml acetylated serum albumin and 4 mM $MgCl_2$
Cleavage & Relaxation	*E. coli* topo IV	Supplied by Inspiralis: 40 mM HEPES.KOH (pH 7.6), 100 mM potassium glutamate, 10 mM magnesium acetate, 10 mM DTT, 1 mM ATP, and 50 µg/ml acetylated serum albumin
Cleavage	*S. aureus* gyrase	35 mM Tris-HCl (pH 7.5), 24 mM KCl, 2 mM DTT, 1.8 mM spermidine, 6.5% glycerol, 0.1 mg/ml, acetylated serum albumin, 100 mM potassium glutamate (and 4 mM $MgCl_2$ unless otherwise stated)
Supercoiling	*S. aureus* gyrase	40 mM HEPES-KOH (pH 7.6), 10 mM DTT, 2 mM ATP, 500 mM potassium glutamate, 0.05 mg/ml, acetylated serum albumin (and 4 mM $MgCl_2$ unless otherwise stated)
Cleavage & Relaxation	*M. mazei* topo VI	20 mM bis-tris propane pH 7.0, 100 mM potassium glutamate, 1 mM ADPNP, 12 mM $MgCl_2$ and 1 mM DTT
Cleavage & Relaxation	Human topoisomerase IIα	50 mM Tris.HCl (pH7.5) 125 mM NaCl 10 mM $MgCl_2$ 5 mM DTT 100 µg/ml acetylated albumin 1 mM ATP
Intercalation	Wheat germ topoisomerase I	50 mM Tris.HCl (pH 7.9) 1 mM EDTA 1 mM DTT 20% glycerol 50 mM NaCl

Table 2.8: The assay buffer used in DNA topology assays.

Buffer	Enzyme	Components	Supplier
STEB		100 mM Tris-HCl pH 8.0, 40% (w/v) sucrose, 1 - 10 mM EDTA, Bromophenol Blue (to colour)	
Dilution	*E. coli* gyrase	50 mM Tris·HCl pH 7.5, 100 mM KCl, 2 mM DTT, 1 mM EDTA, 50% (v/v) glycerol	
Dilution	*S. aureus* gyrase	50 mM Tris.HCl pH 7.5, 1 mM DTT, 1 mM EDTA, 40% (v/v) glycerol	
Dilution	*E. coli* topo IV	40 mM HEPES.KOH pH 7.6, 100 mM potassium glutamate, 1 mM DTT, 1 mM EDTA, and 40% (v/v) glycerol	Insperalis
Dilution	human topoisomerase Iiα	50 mM Tris.HCl pH 7.5, 100 mM NaCl, 1 mM DTT, 0.5 mM EDTA, 50 μg/ml albumin, 50% (v/v) glycerol	Inspiralis
Dilution	*M. mazei* topo VI	20 mM HEPES pH 7.5, 100 mM potassium glutamate, 2 mM β-mercaptoethanol, 10% (v/v) glycerol	
Dilution	Wheat germ topo I	50 mM Tris.HCl pH 7.9, 1 mM EDTA, 500 mM NaCl, 1 mM DTT, 50% (v/v) glycerol	Insperalis
TAE		40 mM Tris base, 20 mM glacial acetic acid and 1mM Na_2EDTA	Formedia

Table 2.9: The dilution buffers in enzyme assays and buffers associated with running agarose gel electrophoresis.

2.4.2 DNA resealing assays with EDTA, dilution, dialysis and desalt spin columns

The DNA cleavage-resealing equilibrium was formed as described for DNA cleavage assays in section 2.4.1 prior to stimulation of DNA resealing. Trapping with SDS and digestion with proteinase K was performed after the DNA resealing steps.

2.4.2.1 DNA resealing stimulated with EDTA

For resealing assays stimulated with EDTA, 7.5 μL of EDTA at pH 8.0 at concentrations stated in the experiment, were added to the 30 μL DNA cleavage assay and vortexed for 1-3 seconds. The reaction was incubated for between 0.5-90 minutes at 37°C, and stopped with SDS and digested with proteinase K as described for DNA cleavage assays in section 2.4.1.

2.4.2.2 Removing metal ions with desalt spin columns

To reseal DNA with desalt columns, 30 μL of DNA cleavage reaction formed with 50 nM of *E. coli* gyrase, 20 μM of the IPY t1 and 0.25 mM $MgCl_2$ was added to a micro Bio-spin p30 column with an MWCO of 40k Da (Bio-Rad). The column was pre-equilibrated in assay buffer [tbl. 2.8]. The columns were immediately centrifuged at 1k xg for 4 minutes. Reactions were incubated for 0-10 minutes at room temperature before processing by trapping with SDS and proteinase K digestion as described in 2.4.1. To samples with the 0 minutes time point, SDS was pre-added to the Eppendorf tube at the bottom of the spin column for immediate trapping.

2.4.2.3 DNA resealing using dialysis

For DNA resealing stimulated by removing the metal ions using dialysis, 100 μL of cleavage reaction formed with 50 nM of *E. coli* gyrase with 20 μM of the IPY t1 and 0.25 mM $MgCl_2$ was added to Slide-A-Lyzer MINI Dialysis Devices with a 10k MWCO (Thermo Scientific). The dialyser was placed in 50 mL of assay buffer [tbl. 2.8], and incubated between 0-120 minutes at room temperature. To stop the reaction, 30 μL was aspirated from the dialyser and processed as with a DNA cleavage assay by trapping with SDS and proteinase K digestion 2.4.1.

2.4.2.4 DNA resealing with dilution

To reseal DNA via dilution, 30 μL of DNA cleavage reaction was diluted with assay buffer 5-10 - fold and incubated at 37°C. Reactions were stopped with the addition of SDS to 0.2% and digested with 5 μL of 20 mg/mL proteinase K for 30 minutes at 37°C. Samples were ethanol precipitated with 1 mL of ice-cold 100% ethanol and 1 μL of 20 mg/mL glycogen (Thermo Scientific), and incubated at -20°C for 20 minutes. The samples were centrifuged at 4°C for 45 minutes at 16.1k xg. The ethanol was discarded, and the pellet was washed with 500 μL of ice-cold 70% ethanol. Samples were centrifuged for 15 minutes at 4°C at 16.1k xg. The ethanol was removed, the pellet air dried, and resuspended in 20 μL of 1x STEB [tbl. 2.8].

2.4.3 Agarose gel electrophoresis

Samples were centrifuged for 60 seconds at 16.1k xg prior to gel-loading. Agarose gels were prepared by melting 1% agarose in 1x TAE [fig. 2.9]. Typically, 20 μL of sample was loaded onto a 1% agarose gel and run in 1x TAE. For ethidium bromide gels, ethidium bromide was added into the semi-cooled melted agarose for gel casting, and into the running buffer, for a final ethidium bromide concentration of 0.5 μg/mL. For chloroquine gels, chloroquine was added to 1 μg/mL into melted agarose cooled to 50°C, and into the running buffer.

Gels were typically run for 2 hours at 80 V, or for 18 hours at 17 V. If samples had potassium glutamate present in the assay buffer, samples were loaded into the wells of the agarose gel and incubated for 30 minutes prior to gel running, and run at a maximum of 60 V. Gels run in the absence of ethidium bromide were stained for 15 minutes in 0.5 μg/mL ethidium bromide, and destained in Milli Q water for 10 minutes. Chloroquine gels were first destained in Milli Q water, before staining with ethidium bromide and destaining in Milli Q water. Gels were imaged by UV in a Syngene gel doc system.

2.4.4 Phenol Extractions

DNA cleavage complexes were formed as described for a DNA cleavage assay [subsection 2.4.1], but were trapped by the addition of 2% SDS at 1:1 v/v. 3.6 μL of 5 M NaCl and 2.4 μL of 250 mM EDTA were added to the 60 μL sample and vortexed. The gyrase-DNA adducts were separated from the naked DNA by phenol extractions. Phenol saturated with 10 mM Tris-HCl pH 8.0 and 1 mM EDTA (Sigma-Aldrich) was added to the samples at 1:1 v/v, vortexed and centrifuged. The aqueous layer on the top (containing free DNA) was aspirated into a separate tube. The process was repeated twice more to remove any protein-DNA adducts which remained in the aqueous phase. The phenol phases were combined, and, to extract free DNA in the buffer remaining above the phenol phase, the samples were washed with extraction buffer (50 mM Tris-HCl pH 8.0, 10 mM EDTA, 300 mM NaCl, 1% SDS) at a 1:1 ratio. The aqueous layer was aspirated and combined into the aqueous phase. The extraction process was repeated twice more.

The naked DNA in the aqueous phase were precipitated with the addition of 1 mL of 100% ice-cold ethanol and 1 μL of 10 mg/mL glycogen (Thermo Scientific). The protein-DNA adducts present in the phenolic phase were precipitated with 1 mL of ice-cold 100% acetone and 1 μL of 10 mg/mL of bovine serum albumin (Sigma-Aldrich). The samples were incubated for at least 20 minutes at -20°C and centrifuged for 40 minutes at 4°C at 11k xg. The ethanol or acetone were discarded, and the pellets were washed with 500 μL of ice-cold 70% ethanol and centrifuged for 15 minutes at 4°C. The ethanol was discarded, the pellets were air-dried and resuspended in 20 μL of resuspension buffer (50 mM Tris-HCl pH 8.0, 10 mM EDTA, 0.1% SDS). The samples were digested with 1 μL of 20 mg/mL proteinase K and incubated for 30 minutes at 37°C. 6 μL of STEB loading dye was added to the samples, which were analysed by agarose gel electrophoresis.

2.4.5 Quantification of gel bands

Gels were quantified using densitometric analysis using Fiji and ImageJ [146], [147]. For DNA supercoiling and relaxation assays, the individual relaxed topoisomer bands were grouped to quantify the relaxed topoisomers. The percentages of relaxed and supercoiled DNA were calculated against the sum of relaxed and supercoiled DNA. For DNA cleavage assays, the percentage of nicked, linear and supercoiled DNA were calculated.

2.4.6 Plotting DNA cleavage, relaxation and supercoiling assay data

Data from quantified bands were plotted using python using the libraries sciPy.optimize curve_fit (fig. 2.2) [148], pandas [149], Matplotlib [150], NumPy [151] and seaborne [152].

2.4.7 Quinazolinium potency determination

The quinazoliniums were obtained in powder form from Marcus Söderström from Uppsala University. The compounds were stored at -20°C. Stock concentrations were made by dissolving the compound into 100% DMSO and vortexing for 10 minutes [tbl. 2.10].

Compound	Molecular weight (g/mol)	Approx. solubility (mg/mL) (DMSO)	Stock (mM) (DMSO)
BT9701	294.31	25.0	30.0
1488	310.31	1.9	5.0
1529	324.34	10.0	30.0
1532	328.30	1.7	5.0
2086	310.31	2.0	5.6

Table 2.10: The molecular weight, solubility in 100% DMSO and stock concentration made in 100% DMSO of the quinazoliniums.

The quinazoliniums were tested for activity against wild-type *E. coli* gyrase and *S. aureus* gyrase, which were purified in-house. The compounds were also biochemically assayed against other topoisomerase enzymes and mutants, the source of which is detailed in table 2.11.

Protein	Source
E. coli GyrA G81A	Inspiralis
E. coli GyrA D82N	Gifted by Ghilarov lab
E. coli GyrA S83L	Gifted by Ghilarov lab
E. coli GyrA A84S	Inspiralis
E. coli GyrA D87N	Inspiralis
E. coli GyrB K447E	Gifted by Ghilarov lab
E. coli GyrB S464Y	Inspiralis
S. aureus GyrB R458K	Inspiralis
Wheat germ topoisomerase I	Inspiralis
Human topoisomerase IIα	Inspiralis
E. coli topoisomerase IV	Inspiralis
M. mazei topoisomerase VI	Gifted by Adam Allen

Table 2.11: The source of the purified wild-type and mutant topoisomerase enzymes used in the DNA supercoiling inhibition assays, DNA relaxation inhibition assays, DNA cleavage stabilisation assays or intercalation assays with the quinazoliniums.

The quinazoliniums were tested for inhibition of DNA supercoiling, relaxation or cleavage

activity against *E. coli* gyrase, *S. aureus* gyrase, *E. coli* topo IV, *M. mazei* topo VI and human topoisomerase IIα. If good activity was observed, the compounds were titrated against a constant enzyme concentration to determine IC_{50} and CC_{50} values in DNA supercoiling, relaxation and cleavage assays. The enzyme concentration was defined by the concentration required to relax or supercoil DNA to almost completion for relaxation and supercoilng assays respectively. For DNA cleavage assays, the enzyme concentration was determined by the concentration required for 50% double-stranded DNA cleavage stabilised by a relevant drug or cleavage stabilising agent, such as ciprofloxacin, moxifloxacin, etoposide or ADPNP. The DMSO concentration was kept constant for each QZM concentration and relevant controls were run, including samples without enzyme or drug, or with novobiocin for negative controls, and positive controls were run with a drug known to target the enzyme. Three replicates were generated for each dataset.

The data from the DNA supercoiling, cleavage and relaxation assays were fitted to 4-parameter IC_{50} and CC_{50} curves in python (fig. 2.1) by using the sciPy.optimize curve_fit (fig. 2.2) [148]. Other libraries used were pandas [149], Matplotlib [150], NumPy [151] and seaborne [152]. Standard deviation was calculated and plotted. These equations were also used to calculate the C_{50} values (the enzyme concentration at which the DNA cleavage or supercoiling activity is half).

```
def logistic4(x, Min, Max, IC50, HillSlope):
y = Min + ((Max - Min)/(1 + (x/IC50)**HillSlope))
return y
```

(a)

```
def logistic4(x, Min, Max, CC50, HillSlope):
y = Min + ((Max - Min)/(1 +(x/CC50)**HillSlope))
return y
```

(b)

Figure 2.1: Python code for IC_{50} (a) and CC_{50} (b) curve fitting

```
def tora_curve_fit(df, colname):
parameter, _ = curve_fit(logistic4, X, Y, maxfev=20000)
return parameter
```

Figure 2.2: Python code for returning IC_{50} and CC_{50} values.

2.5 Crystallography

2.5.1 Protein constructs for crystallisation

Crystallisation trials were set up between QZMs 1488, 1529 and 1532, *S. aureus* gyrase and DNA. The *S. aureus* gyrase core fusion construct, developed by Bax *et al.* [39],[52], consists of a fusion between GyrB residues 410-640 and GyrA residues 1-491 with a TG amino acid linker. The N-terminal ATPase domain from GyrB, the C-terminal domain of GyrA, and the flexible Greek Key motif in the TOPRIM domain of GyrB (amino acids 544-579) were deleted in this construct. Both the wild-type, and the catalytic tyrosine mutant (GyrA Y123F) were used in crystallisation screens.

2.5.2 DNA in the crystallisation trials

20-bp palindromic DNA duplexes for crystallography were formed from annealing single-stranded oligos by heating to 85°C and cooling at 1°C/min in a PCR machine [39],[52]. The DNA used for the crystallisation trials with *S. aureus* gyrase core fusion Y123F mutant was formed from 4 oligos: two 12-mers with 5′ phosphates, and two 8-mers which anneal to form a 20-bp duplex with two artificial nicks staggered by 4 bp. The duplex, called 20-12p-8 was formed from the sequences 5′-AGCCGTAG-3′ and 5′-GTACCTACGGCT-3′. For crystallisation trials with wild-type *S. aureus* gyrase core fusion, DNA called 20-448T was used with the sequence 5′-GAGCGTATGGCCATACGCTT-3′. The 20-448T DNA is palindromic except for the end base pairs.

2.5.3 Crystallisation screening conditions and optimisations

Between 3-5 mg/mL of protein, 0.25 mM of pre-annealled DNA, QZM (∼0.4 mM for QZM 1488 and 1532, and 1.5 mM for QZM 1529), 10 mM Tris-HCl pH 7.5, 25 mM NaCl at 5% DMSO and 3.5% glycerol were incubated on ice prior to crystallisation trials. Sitting drop vapour diffusion was performed using the commercial screen from Molecular Dimensions, MIDASplus™ in a swissci 96-well 2-drop plate. Optimisation of the crystallisation conditions were designed around C11 and H1 from MIDASplus™ [tbl. 2.12]. The optimisation screens were dispensed from reagents directly into the reservoir of the swissci 96-well 2-drop plates using the Oryx8 robot (Douglas Instruments). The total volume in the reservoir was 500 μL.

Optimisation plate based of the MIDASplus™ C11 crystallisation condition (Molecular Dimensions)

Reagent	Optimisation	Incriment
Pentaerythritol ethoxylate 15/4 EO/OH (%)	25.0 - 32.5	2.5
Tris-HCl 0.1 M (pH)	8.00 - 8.75	0.025
Metal ions	a) 50 mM magnesium formate b) 50 mM $MgCl_2$ and 50 mM $MnCl_2$ c) 50 mM $MgCl_2$ d) 50 mM $MnCl_2$ e) 50 mM $CoCl_2$ f) 3.75 mM $MnCl_2$	Constant

(a)

Optimisation plate based of the MIDASplus™ H1 crystallisation condition (Molecular Dimensions)

Reagent	Optimisation	Incriment
SOKERLAN CP-42 (%)	20.0 - 27.5	2.5
Bis-Tris 0.1 M (pH)	5.8 - 6.4	0.2
Metal ions	a) 50 mM magnesium formate b) 50 mM $MgCl_2$ and 50 mM $MnCl_2$ c) 50 mM $MgCl_2$ d) 50 mM $MnCl_2$ e) 50 mM $CoCl_2$ f) 3.75 mM $MnCl_2$	Constant

(b)

Table 2.12: The crystallisation optimisation screening conditions based on MIDASplus™ C11 (a) and H1 (b). The optimisation screen for the crystallisation of *S. aureus* gyrase core fusion wild-type and Y123F mutant with DNA and the QZMs.

2.5.4 Conducting crystallisation screens

The protein-DNA-compound premix, and the crystallisation screening conditions were dispensed using the Oryx8 (Douglas Instruments) at a 1:1 ratio with a drop size of either 0.6 or 0.7 μL. The plates were sealed with optically clear adhesive seal sheets (Thermo Scientific), stored at 15°C and checked every 1-14 days over 2 months for crystals with a light microscope.

2.5.5 Crystal Harvesting

Crystals were protected with cryoprotectant by either adding the cryoprotectant to the drop, or soaking. Cryoprotectant was made to match the mother liquor from the crystallisaition condition and included relevant drugs and metal ions, with the addition of 25-30% glycerol or ethylene glycol. Crystals were fished with mounted rounded LithoLoops (Molecular Dimensions) by Dr Clare Stevenson, and directly flash cooled in liquid nitrogen for storage and transport.

2.5.6 X-ray data collection

Data collection was carried out in collaboration with Prof. Dave Lawson and Dr Clare Stevenson. Crystals were sent to the Diamond Light Source synchrotron, Oxford, UK. Data collection was performed on the iO4 beamline under cryogenic conditions maintained at -173°C with a cryojet. The wavelength was set to 0.9795 Å and the beamsize was 43x30 μm at 100% transmition, images were taken with a 0.1° oscillation. Datasets were autoproceessed on the Diamond computers and solutions were taken from ISpYB.

2.5.7 Data Processing

Data processing was performed with the guidance of Prof. Dave Lawson. The autoPROC dataset [153], which was autoprocessed with scaling and integration, were merged with no further scaling in AIMLESS [154]. Images 1-3600, and 7401-11,000 were excluded, and the resolution was cut to 3 Å. Molecular replacement was performed with PHASER [155], using a previous in-house *S. aureus* gyrase structure as the model for molecular replacement. Iterative rounds of REFMAC [156] and editing in the manual model builder coot [157] were performed to fix Ramachandran outliers, and to satisfy statistics. The quinazolinium was drawn in ligand builder in coot, and fitted into the model using ligand fitter prior to final refinement in REFMAC.

2.6 Quinazolinium toxicity in *Galleria mellonella*

The following was performed by Harriet Gooch at the John Innes Centre: *G. mellonella* larvae were taken from a colony maintained at the John Innes Centre. The larvae selected were between 180 and 220 mg. Larvae were injected with 16 μL of 1 mg/mL of quinazoliniums 1488, 1529, 1532 and 2086 at 20% DMSO. This corresponds to 16 μg of compound per larvae, or 80 mg/kg of larvae body weight, and therefore approximately 20 times the MIC of *E. coli* wild-type with QZM 1488. PBS at 20% DMSO was used as a control. This was repeated 3 times. Each set of 5 larvae were kept in a Petri dish and incubated without food for 24 hrs at 30°C.

The larvae mortality was assessed visually and by poking with tweezers to elicit larvae movement. 60% mortality rate was used to evaluate compound toxicity, as stated by Ignasiak and Maxwell [158].

Chapter 3

DNA gyrase DNA Resealing Dynamics

3.1 Introduction

Type II DNA topoisomerases form transient double-stranded DNA breaks to alter DNA topology, which can be stabilised by drugs by blocking the reverse reaction - DNA religation. The DNA breaks result in a covalent phosphotyrosine linkage formed between the catalytic tyrosine on the enzyme and the $5'$ scissile phosphate, and are reversible. The formation of stable topoisomerase-DNA cleavage complexes leads to genomic instability; DNA replication and transcription machinery can stall, and processing to remove the trapped topoisomerase releases double-stranded DNA breaks, leading to genomic rearrangements and cytotoxicity [159], [160]. The DNA-topoisomerase cleavage complexes are resealed by the enzyme as part of its catalytic cycle, or when a topoisomerase poison stabilising the DNA cleavage complex dissociates. The reaction proceeds asymmetrically; one of the two DNA cleavage sites on the topoisomerase complex will reseal first, followed by the resealing of the second DNA break at the DNA cleavage site on the opposite side. Thus, DNA resealing proceeding via a nicked intermediate [85], [86].

3.1.1 Type II topoisomerase poisons lead to the accumulation of double-stranded DNA breaks by blocking the DNA religation reaction

Type II topoisomerase poisons are clinically available as either antibiotics or anti-cancer agents. There are currently 9 antibiotics which target type II topoisomerases approved by the FDA; the antibiotics are all fluoroquinolones and are topoisomerase poisons [161]. The fluoroquinolone antibiotics, as well as other antibiotic classes which are not clinically in use, such as the imizadopyrazinones or the quinazoline diones, stabilise double-stranded DNA breaks by blocking the topoisomerases from resealing the DNA. Fluoroquinolones distort DNA, such that the $3'$ -OH group on the broken DNA strand is prevented from performing a nucleophilic attack on the covalent phosphotyrosine linkage, greatly reducing the probability of DNA resealing [39]. The persistence of drug-associated topoisomerase-DNA cleavage complexes has been associated

with the stability of the cleavage complexes. Crosslinking the fluoroquinolone ciprofloxacin to gyrase resulted in greater resistance to DNA resealing, compared to non-crosslinked ciprofloxacin [162].

The NBTIs also stabilise DNA breaks formed by topoisomerases, however stabilise only single-stranded breaks. NBTIs intercalate into the DNA between the two DNA cleavage sites, resulting in the rotation of an adjacent base which positions the scissile phosphate to be inaccessible to the catalytic metal ion at the A-site, thereby blocking DNA resealing [163]. The position of both the $3'$ end and $5'$ phosphate is determined by interactions between other bases, non-covalent topoisomerase interactions, and the covalent phosphotyrosine linkage. The correct position of the $3'$ hydroxyl group and $5'$ phosphate is essential to reseal the DNA [164]. By blocking the resealing of the DNA, the antibiotics inhibit the enzyme's catalytic function.

Poisons approved for chemotherapy include etoposide which targets human topoisomerase II. Etoposide binds at the DNA cleavage site, and acts by blocking DNA resealing. There is a link between the cytotoxicity of etoposide, and the persistence of topoisomerase-DNA cleavage complexes which the drug stabilises [165]. Topoisomerase poisons often distort the DNA around the DNA cleavage site, such that DNA geometry is not favoured for the enzyme to religate the DNA. The inhibition of DNA religation is the most common mechanism of action for poisons. For some topoisomerase poisons, the rate of DNA resealing is unaffected. These poisons act by increasing the rate of formation, or the stability of the DNA-topoisomerase cleavage complexes. The drugs thought to act through this mechanisms include ellipticines [166] and thiosemicarbazones [167].

Since topoisomerase poisons have different mechanisms of action, studying the religation reaction with compounds gives insights into how they inhibit the enzyme. Additionally, the stability of the DNA cleavage complex can be studied biochemically to give insight into the persistence and cytotoxicity of the drug in cells.

The persistence of the gyrase-DNA cleavage complexes during DNA resealing reactions does not always translate directly to the potency of the drug *in vitro* or against bacterial cells. Comparing the quinolones and the quinazoline diones, the quinolones are 10-100 - fold more active at stabilising double-stranded DNA breaks in DNA cleavage assays [121]. The quinazoline dione associated cleavage complexes, however, are more resistant to DNA religation stimulated by EDTA or salt, which could be explained by the stability of the water-metal ion bridge present in only the quinolones [168].

3.1.2 Biochemical studies of the DNA religation reaction by type II topoisomerases

The type II topoisomerase DNA cleavage and resealing equilibrium can be pushed to favour resealing *in vitro*. Typically, the DNA cleavage complexes are short-lived; in absence of drug and in the presence of magnesium ions, topoisomerase-DNA cleavage complexes will represent under 1% of the total enzyme conformations at equilibrium [169]. *In vitro*, DNA cleavage complexes can be stimulated to reseal using the metal chelator EDTA, high salt, changes in temperature or diluting out the metal ions.

There remains questions to the mechanism of why DNA reseals in the presence of EDTA. Fluoroquinolones inhibit gyrase by stabilising DNA cleavage. Fluoroquinolones require a water-metal ion bridge to bind to the enzyme. Resealing stimulated by EDTA of DNA cleavage complexes formed with drug have been suggested to be driven by chelating the structural non-catalytic metal ion required for fluoroquinolones to bind to topoisomerases [121]. Since fluoroquinolones inhibit DNA resealing, compound dissociation would lift the block on DNA resealing. Compound persistence assays measure the stability of drug-enzyme complexes. EDTA is often used to stimulate DNA resealing in compound persistance assays. Dissociation of the drug is thought to drive DNA resealing. Using EDTA to initiate DNA resealing for compound persistence assays has limitations, since metal ions are also required catalytically for DNA cleavage and DNA resealing. Therefore, the assays would inadvertently be measuring DNA resealing as a result of compound dissociation and by altering the DNA cleavage-resealing equilibrium with metal ions.

Since both DNA cleavage and resealing requires catalytic metal ions, there is confusion to why DNA is stimulated to reseal on removal of these metal ions with the metal chelator EDTA. The effects of the free metal ions in solution have not been thoroughly investigated with respect to the DNA cleavage and resealing equilibrium. Additionally, there are hypotheses where the first stage of DNA resealing, resealing one strand of the DNA break, can occur using a metal-independent mechanism, since nicked DNA (single-stranded DNA cleavage) accumulates on removal of metal ions with EDTA [121], [46]. Further evidence to this was provided by some type I topoisomerase enzymes, which have homologous domains at the catalytic core, can replace the role of the catalytic metal ion with a lysine residue to support DNA resealing [170], [94].

The number of catalytic divalent metal ions at the DNA cleavage site is debated, ie. whether two metal ions are simultaneously present to catalyse DNA cleavage, or one moving metal

ion can move between the two metal-ion binding sites [fig. 1.7]. There is biochemical and structural evidence to support both metal models [88], [39], [120], however the data focuses on the role and number of metal ions during the DNA cleavage reaction, as opposed to religation. For example, following DNA cleavage and gate-opening, the catalytic metal site, or "A-site" which is formed from the acidic amino acids and the scissile phosphate, would not exist. The scissile phosphate is spatially separated from the metal-binding sites to open the DNA gate. Therefore, there must be stages during the enzyme's reaction cycle where there is either one, or no catalytic metal ions bound to the enzyme. Catalysis achieved with one metal ion has been modelled to be one metal ion which is stored at the non-catalytic site, or "B-site" until catalysis [92], however whether the metal ion is dynamic with respect to the free metal ions in solution has not been thoroughly explored.

3.1.3 Chapter aims

This chapter aims to explore in greater detail to why the DNA cleavage and resealing equilibrium is affected by metal ions. The impact of the concentration of metal ions and EDTA will be investigated, and how the parameters effect DNA-cleavage complexes stabilised with drugs such as fluoroquinolones and imidazopyrazinones. Fluoroquinolones require a structural metal ion to bind, whereas imidazopyrazinones do not. The effects of DNA resealing with altered EDTA concentration have not been investigated or discussed in depth with respect to the concentration of free metal ions in solution. The different catalytic metal ion models for DNA cleavage and resealing will be discussed with respect to the findings in this chapter. Understanding the conditions for the reversal of drug-stabilised DNA cleavage complexes will guide the chemical development of compound series to take into consideration compound persistence when assaying next generation drugs. By designing the optimal conditions to investigate the inhibition of DNA resealing with different drugs, more comparable assays can be performed to compare the stability of DNA cleavage complexes. Robust assays should be performed for DNA resealing assays, and therefore resealing DNA cleavage complexes stimulated by EDTA, dilution, dialysis or buffer exchange columns is investigated here. These techniques all lower the concentration of free metal ions in solution.

Additionally, this work will study how the enzyme natively cleaves and reseals DNA to gain insights into the enzyme mechanism and the role of catalytic divalent metal ions. How DNA gyrase from clinically relevant species, such as *E. coli* and *S. aureus*, reseal DNA will be compared. The concentration of free metal ions in solution required to modulate the DNA

cleavage-resealing equilibrium and push towards resealing has not been calculated. This chapter will explore the metal ion concentration ranges to support DNA cleavage or DNA resealing. Many of the DNA cleavage and resealing data from the literature are from experiments using type II topoisomerases. DNA gyrase may have different DNA cleavage and resealing mechanisms, particularly as DNA gyrase uniquely negatively supercoils DNA.

3.2 Results and discussions

A number of experiments described in this chapter were performed as single experiments (n=1). Experiments have been repeated under similar conditions, and example data has been selected for this chapter for story-telling purposes. Additionally, the results from this chapter are self-consistent. This has allowed conclusions to be drawn.

3.2.1 The concentration of free magnesium ions on the rate of resealing DNA cleavage complexes stimulated by EDTA

DNA resealing assays are often performed to determine the persistence of a type II topoisomerase-DNA cleavage complex stabilised by a drug. The concentration of EDTA required to stimulate DNA resealing is not standardised. Therefore, the concentration of EDTA used to stimulate the DNA resealing of a pre-formed DNA cleavage equilibrium with *E. coli* gyrase stabilised by the fluoroquinolone ciprofloxacin was varied. The concentrations of EDTA were chosen from preliminary experiments; 40 and 80 mM EDTA were chosen, which nicely demonstrated the DNA resealing reaction. The percentages of nicked, supercoiled and linear DNA was measured during the time-course of DNA resealing [fig. 3.1, 3.2].

In these experiments, linear DNA represents double-stranded DNA cleavage of a plasmid - the plasmid is linearised following protein digestion with proteinase K. Stimulating DNA to reseal with 40 mM EDTA resulted in the linear DNA resealing almost to completion in 60 minutes, whereas in the same time period, 50% of the linear DNA resealed with 80 mM EDTA [fig. 3.1a]. Scaling the data to 100%, the linear DNA resealed at a faster rate at the lower EDTA concentration [fig. 3.1b].

The nicked DNA increased as on addition of EDTA. DNA is resealed asymmetrically via a nicked intermediate, and therefore the accumulation and disappearance of the nicked DNA was visualised. The nicked DNA appeared faster at the lower EDTA concentration, plateauing after 20 minutes [fig. 3.1c]. The resealing of the second strand of DNA is slower than the resealing of

the first strand, this allows the nicked intermediate to be observed [85]. The supercoiled DNA only accumulated using 40 mM EDTA, since the reaction was faster than at 80 mM EDTA [fig. 3.1d].

EDTA chelates metal ions. At high concentrations of EDTA, the concentration of free metal ions in solution would be lower. With less free metal ions available in solution, the resealing of gyrase-DNA cleavage complexes was slower. This demonstrated that DNA resealing requires metal ions, and the rate can be controlled by the concentration of free metal ions in solution. Additionally, since the rate of DNA resealing was affected by the concentration of free metal ions, metal ions must leave the enzyme post DNA cleavage, and rebind to reseal DNA.

EDTA experiments have limitations; high EDTA concentrations may alter the ionic strength of the solution, metal ions may have structural or regulatory roles to the gyrase, and the discussed experiment was in the presence of ciprofloxacin, which requires a metal ion for binding. Therefore, there are a number of assumptions made when concluding the affects of metal ions to reseal DNA, which will be addressed in this chapter.

EDTA has acid-base properties, and EDTA has 4 carboxyl groups with pKa values below the pH the assays are run (pH 7.5-8.0) [171]. Changes in charge in solution could lead to protein denaturation, or effect the charge of amino acid side chains on gyrase critical for activity. Higher EDTA concentrations may also lead to chelation of the structural metal ions bound to gyrase which are required for activity, which could lead to protein denaturation or aggregation [172]. Metal ions can also be regulatory, removal of which could lead to a reduction in activity [173]. To this end, the EDTA concentration was kept constant during a DNA resealing assay with *E. coli* DNA gyrase in the presence of the fluoroquinolone moxifloxacin, and the concentration of metal ions used to form the gyrase-DNA cleavage complexes were varied [fig. 3.3]. Experiments in this chapter involving fluoroquinolones have either been performed with ciprofloxacin or moxifloxacin, results are similar when using either compound.

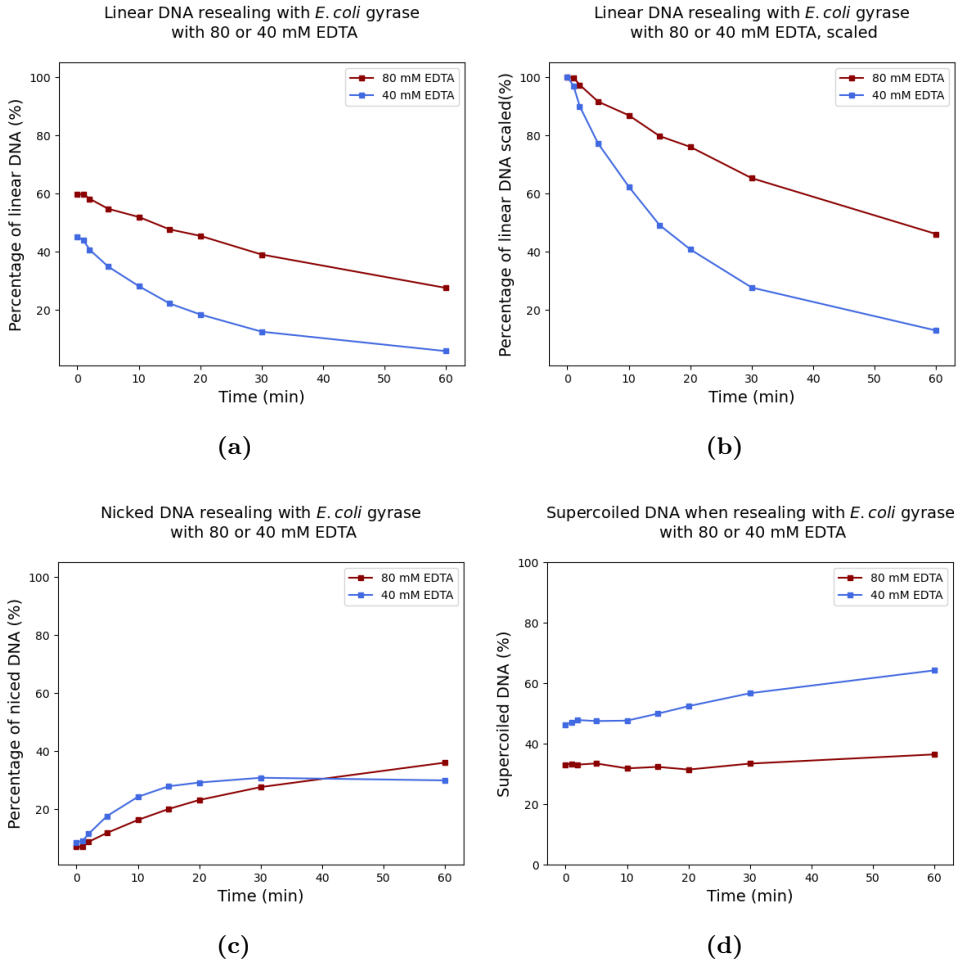

Figure 3.1: The effect of EDTA concentration on the linear, nicked and supercoiled DNA during a DNA resealing assay with *E. coli* gyrase. A DNA cleavage equilibrium was formed with 50 nM *E. coli* gyrase in the presence of 20 μM ciprofloxacin and 0.5 mM $MgCl_2$. The DNA cleavage complexes were stimulated to reseal with 40 or 80 mM EDTA. **(a)** Linear DNA. **(b)** Linear DNA scaled to the starting percentage of double-stranded DNA cleavage. **(c)** Nicked DNA. **(d)** Supercoiled DNA. Time points during the course of DNA resealing were taken by trapping with SDS and digestion with proteinase K. Samples were analysed on an agarose gel and band intensity was quantified using densitometry.

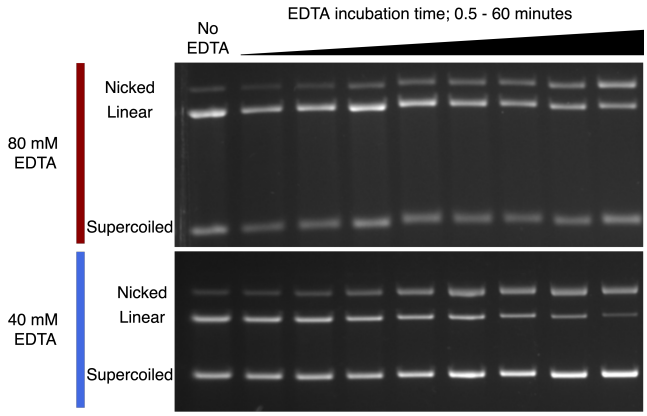

Figure 3.2: The effect of EDTA concentration on the linear, nicked and supercoiled DNA during a DNA resealing assay with *E. coli* gyrase and accompanying gels. A DNA cleavage equilibrium was formed with 50 nM *E. coli* gyrase in the presence of 20 μM ciprofloxacin and 0.5 mM $MgCl_2$. The DNA cleavage complexes were stimulated to reseal with 40 or 80 mM EDTA, and timepoints were taken by trapping with SDS, and digestion with proteinase K.

The linear DNA resealed at a faster rate when stimulated with EDTA from DNA cleavage complexes initially formed with 2 mM of $MgCl_2$ than 0.5 mM $MgCl_2$. The resealing of the first strand of DNA was completed after 10 and 20 minutes respectively, as indicated by the disapearance of linear DNA [fig. 3.3a, 3.3b]. On addition of EDTA, an equilibrium forms between EDTA and free metal ions. At the higher total concentration of magnesium ions, there will be a higher concentration of free metal ions in solution. Therefore, when there are more free magnesium ions available in solution, DNA is able to reseal faster. This data agrees with [fig. 3.1], where DNA was resealed faster at a lower concentration of EDTA, where there would be a higher concentration of free metal ions in solution. There would be a higher free metal ion concentration in solution at 2 mM $MgCl_2$ than 0.5 mM $MgCl_2$ in the presence of EDTA. Since the data suggests that the rate of DNA resealing depends on the concentration of free metal ions in solution, this does not support the hypothesis that the catalytic metal ions are stably-bound to the enzyme. To be instantly affected by changes to the metal ion concentration, there may be a dynamic equilibrium between the metal ions bound at the DNA cleavage site and solution. This would not support a moving metal model, where the same metal ion moves between the two metal ion binding sites during the DNA cleavage and resealing reaction cycle.

The nicked DNA initially accumulated to higher quantities at 0.5 mM $MgCl_2$, representing the slower resealing of the first strand of DNA [fig. 3.3c]. Additionally, the accumulated nicked intermediate took longer to reseal at the lower concentration of $MgCl_2$. Together, this data suggests that the resealing of both strands of DNA requires metal ions and does not occur

independently of metal ions, since religation rates were affected for both resealing events. Since the resealing each strand of the DNA break was faster at higher magnesium ion concentrations, the appearance of supercoiled DNA also accumulated at a faster rate at 2 mM $MgCl_2$ [fig. 3.3d]. The accumulation of nicked DNA at higher EDTA concentrations is observed in the literature [121], however, these nicked intermediates were thought to not reseal because the experiments performed were not timecourses. Since the concentration of EDTA was kept constant in this experiment, it controls for ionic strength effects on the DNA cleavage and resealing equilibrium, and for removal of structural and regulatory metal ions controlling the DNA cleavage and resealing equilibrium.

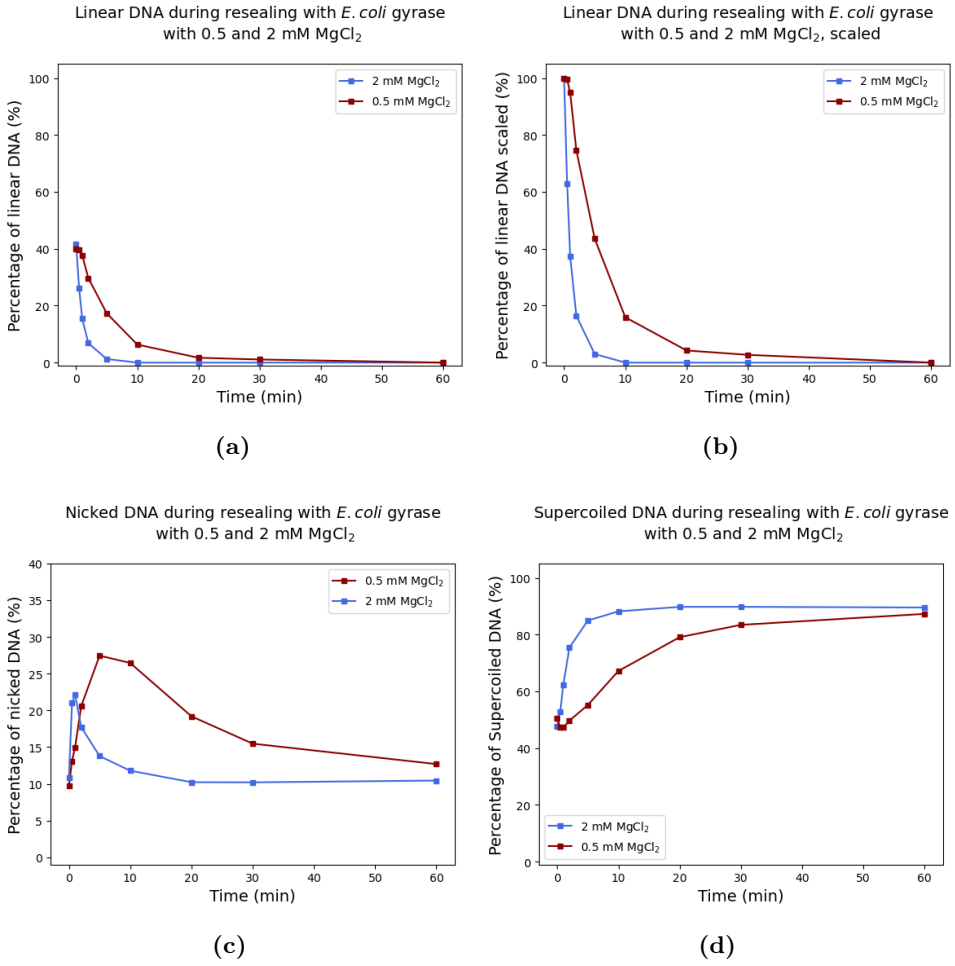

Figure 3.3: The effect of the initial concentration of $MgCl_2$ on the linear, nicked and supercoiled DNA during a DNA resealing assay with *E. coli* gyrase. A DNA cleavage equilibrium was formed with 50 nM *E. coli* gyrase in the presence of 20 μM moxifloxacin at either 0.5 mM, or 2 mM $MgCl_2$. The DNA cleavage complexes were stimulated to reseal with 20 mM EDTA. **(a)** Linear DNA. **(b)** Linear DNA scaled to the starting percentage of double-stranded DNA cleavage. **(c)** Nicked DNA. **(d)** Supercoiled DNA. Time points during the course of DNA resealing were taken by trapping with SDS and digested with proteinase K. Samples were analysed on an agarose gel and band intensity was quantified using densitometry.

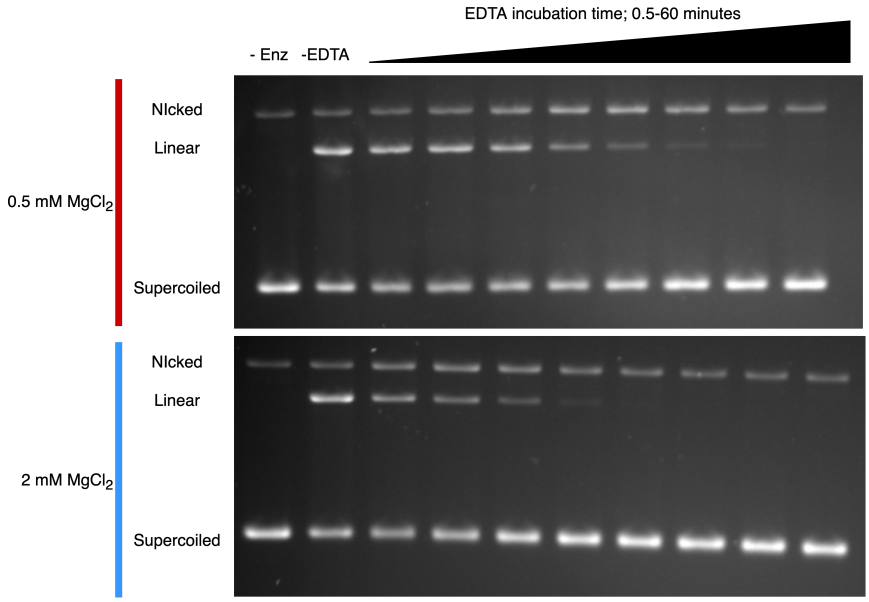

Figure 3.4: The effect of the initial concentration of $MgCl_2$ on the linear, nicked and supercoiled DNA during a DNA resealing assay with *E. coli* gyrase, accompanying gels. A DNA cleavage equilibrium was formed with 50 nM *E. coli* gyrase in the presence of 20 μM moxifloxacin at either 0.5 mM, or 2 mM $MgCl_2$. The DNA cleavage complexes were stimulated to reseal with 20 mM EDTA, and trapped after incubation with EDTA with SDS, followed by proteinase K digestion.

3.2.2 A comparison of resealing DNA cleavage complexes stimulated by EDTA in the presence of a fluoroquinolone, or an imidazopyrazinone

The fluoroquinolones ciprofloxacin and moxifloxacin require a water-metal ion bridge to bind and inhibit DNA gyrase. Resealing assays stimulated by EDTA have been suggested to be driven by removal of this compound-associated metal ion, resulting in compound dissociation and therefore removal of the inhibition of DNA resealing [121]. Therefore, the effects of the IPYs on DNA resealing, which stabilise double-stranded DNA cleavage but do not require a water-metal ion bridge to bind, and bind at the same site as fluoroquinolones [120], were investigated using *E. coli* DNA gyrase [fig. 3.5, 3.6].

The concentration of the metal ions used to set up the DNA cleavage equilibrium (0.5 mM and 2 mM) was altered, and the DNA was stimulated to reseal with 20 mM EDTA. Linear DNA resealed faster at 2 mM of $MgCl_2$ [fig. 3.5a, 3.5b]. Directly comparing the linear resealing of the IPY and moxifloxacin, at 0.5 mM $MgCl_2$, the DNA resealed at the same rate, the linear DNA was resealed in 60 minutes [fig. 3.5c, 3.5d]. This data suggests that the disruption of the water-metal ion bridge during resealing with fluoroquinolones is not the main causality of DNA resealing with EDTA.

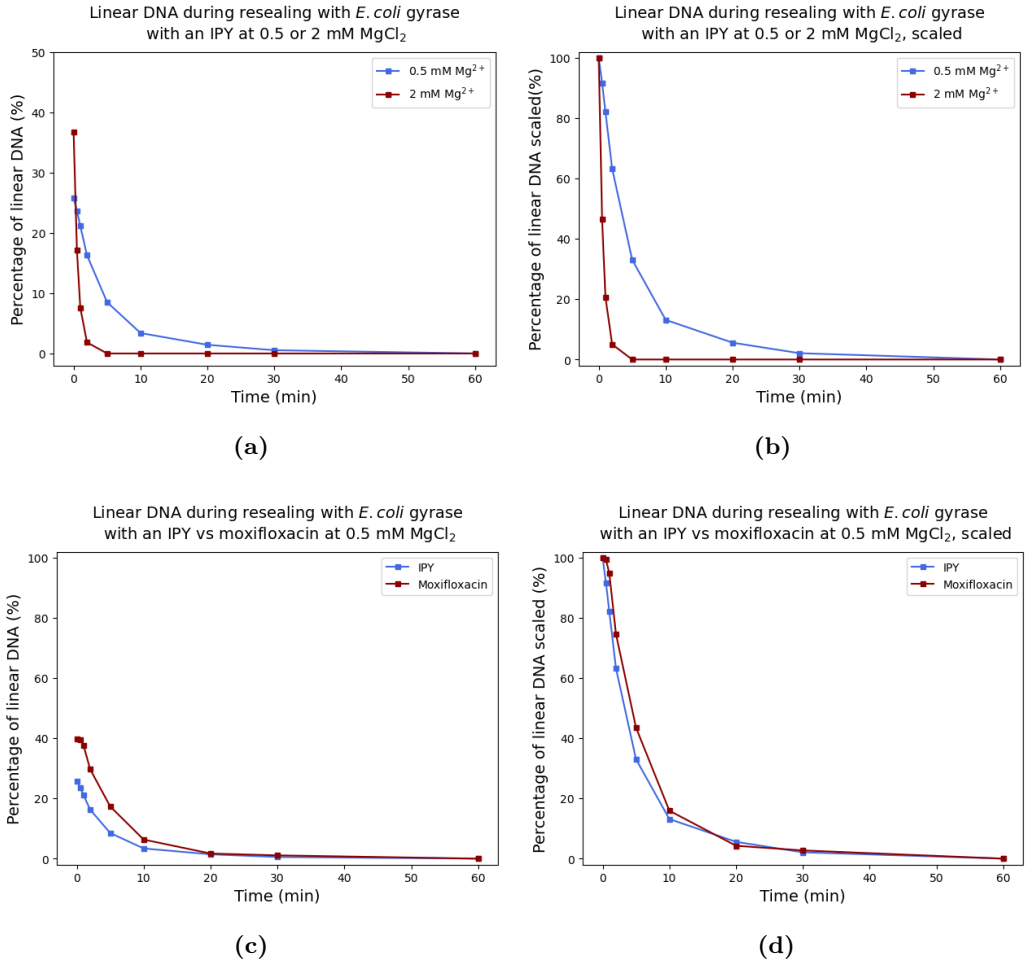

Figure 3.5: A comparison of DNA resealing with the imidazopyrazinone t1 and the fluoroquinolone moxifloxacin in a DNA resealing assay with *E. coli* gyrase. A DNA cleavage equilibrium was formed with 50 nM *E. coli* gyrase in the presence of either 20 μM of the imidazopyrazinone t1 or moxifloxacin. The DNA cleavage complexes were stimulated to reseal with 20 mM EDTA. DNA cleavage complexes stabilised by the IPY t1 formed in the presence of 0.5 mM, or 2 mM $MgCl_2$, stimulated to reseal with 20 mM EDTA. The percentage of linear DNA **(a)**, or linear DNA scaled **(b)** was calculated. A comparison of the linear DNA resealing rates with the IPY t1 and moxifloxacin, using an initial starting metal ion concentration of 0.5 mM $MgCl_2$ **(c)**, and **(d)** (scaled). Time points during the course of DNA resealing were taken by trapping with SDS and digestion with proteinase K. Samples were analysed on an agarose gel and band intensity was quantified using densitometry.

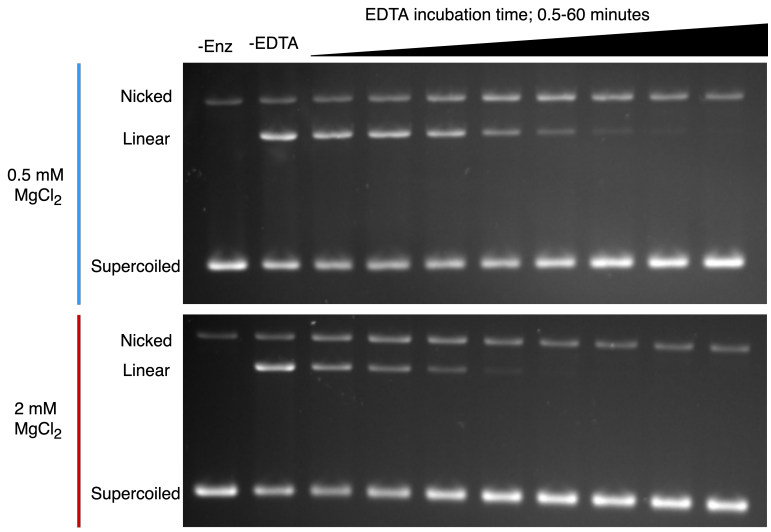

Figure 3.6: A comparison of DNA resealing with the imidazopyrazinone t1 and the fluoroquinolone moxifloxacin in a DNA resealing assay with *E. coli* gyrase, accompanying gels. A DNA cleavage equilibrium was formed with 50 nM *E. coli* gyrase in the presence of either 20 μM of the imidazopyrazinone t1 or moxifloxacin. The DNA cleavage complexes were stimulated to reseal with 20 mM EDTA. DNA cleavage complexes stabilised by the IPY t1 formed in the presence of 0.5 mM, or 2 mM $MgCl_2$, stimulated to reseal with 20 mM EDTA. The DNA was incubated with EDTA, and trapped with SDS and digested with proteinase K.

From the DNA resealing results in this chapter, the concentration of free metal ions, which can be altered by either changing the starting concentration of metal ions, or the concentration of EDTA used to stimulate DNA resealing, affect the rate of DNA resealing by *E. coli* gyrase. In the literature, DNA resealing end point experiments have been performed, where the concentration of EDTA was varied, and the proportion of DNA resealed after 20 minutes was measured [121]. To see how the resealing results in this chapter fit with the literature results, an end point DNA resealing experiment was performed [fig. 3.7, 3.8].

The starting concentration of $MgCl_2$, and the concentration of EDTA to stimulate DNA resealing was varied, to see the relationship between the amount resealed and the metal ion concentration. When varying the EDTA concentration, and keeping the metal ion concentration constant, the data had a sigmoidal shape. This shape mimics an EDTA titration curve for the binding of metal ions, the mid-point in a titration curve represents the equivalence point, where there are some free metal ions in the equilibrium between metal ions and EDTA [174]. At high EDTA concentrations, there will be a low concentration of free metal ions in solution. The shape of the curve is similar to the literature, however the curve in the literature does not plateau at high concentrations of EDTA [121]. The experiments presented here explored a greater range of EDTA and metal ion concentrations and therefore the plateau was observed.

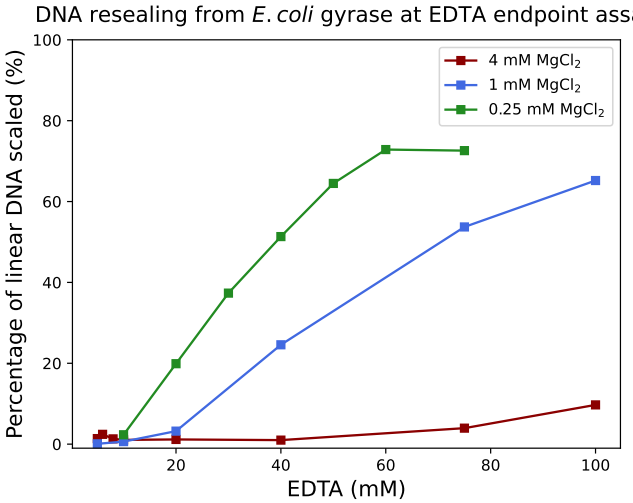

Figure 3.7: The effect of EDTA concentration and initial $MgCl_2$ concentration on DNA resealing after 20 minutes with *E. coli* gyrase in the presence of the IPY t1. A DNA cleavage reaction was set up with *E. coli* gyrase, stabilised with the imidazopyrazinone t1. The DNA cleavage complexes were stimulated to reseal with different concentrations of EDTA, and incubated for 20 minutes before trapping with SDS and digestion by proteinase K. Samples were run on an agarose gel and the band intensity quantified. The percentage of double-stranded DNA cleavage was plotted using python.

3.2.3 Different techniques to resealing DNA cleavage complexes

The resealing of DNA cleavage complexes by *E. coli* gyrase stabilised by a fluoroquinolone may be driven by the dissociation of the compound, or removal of catalytic metal ions. The DNA resealed as a result of fluoroquinolone dissociation, and removal of metal ions were compared [fig. 3.9, 3.10]. DNA complexes were formed by *E. coli* gyrase stabilised by ciprofloxacin. The reaction was diluted 10-fold in different dilution buffers, and the resealing reaction was stopped at time points by trapping with SDS.

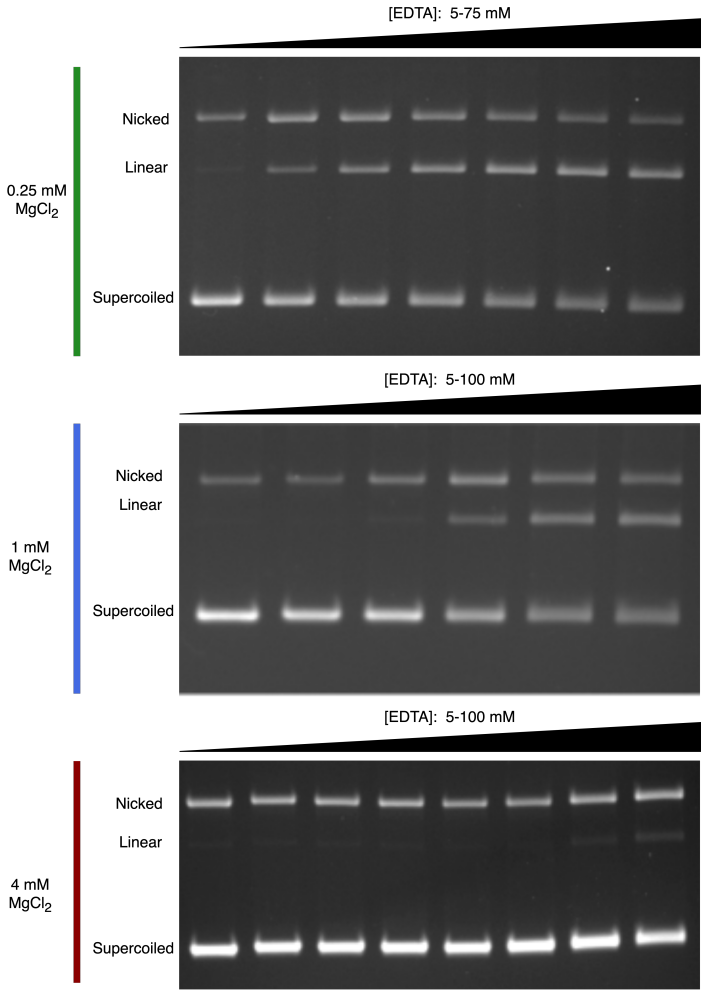

Figure 3.8: The effect of EDTA concentration and initial $MgCl_2$ concentration on DNA resealing after 20 minutes with *E. coli* gyrase in the presence of the IPY t1, accompanying gel. A DNA cleavage reaction was set up with *E. coli* gyrase, stabilised with the imidazopyrazinone t1. The DNA cleavage complexes were stimulated to reseal with different concentrations of EDTA, and incubated for 20 minutes before trapping with SDS and digestion by proteinase K. Samples were run on an agarose gel.

When the DNA cleavage reaction was diluted in dilution buffer, which contained $MgCl_2$ and ciprofloxacin concentrations equivalent to the DNA cleavage reaction, there was no change to DNA cleavage-resealing equilibrium. The dilution buffer was altered to omit ciprofloxacin, but retain the magnesium ions, so that resealing due to compound dissociation, and not resealing due to disruption of the water-metal ion bridge could be measured. The DNA resealed at a slow rate, after 60 minutes, 43% of the linear DNA resealed. The metal ions were the omitted from the dilution buffer, which resealed at the same rate in the presence and absence of ciprofloxacin in the dilution buffer. The linear DNA resealed after a 30-minute incubation. The data suggests that removal of metal ions is the most impactful parameter for resealing DNA by dilution. However, although ciprofloxacin was present in the dilution buffer in the absence of metal ions,

the water-metal ion bridge may have been disrupted. With the knowledge of hindsight, the experiment could be repeated with an IPY, which do not require metal ions to bind to the gyrase, to measure the effects of compound dissociation vs resealing stimulated by low metal ion concentrations. The conclusions drawn from the resealing by dilution assay can be applied to resealing assays with EDTA, suggesting that removal of metal ions and not compound dissociation drives DNA resealing.

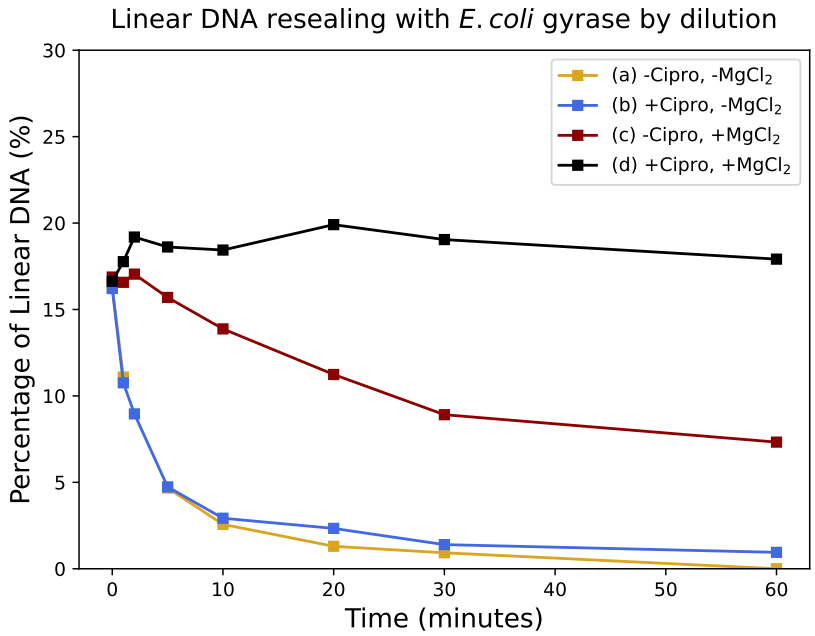

Figure 3.9: The effect of fluoroquinolones and magnesium ions on *E. coli* gyrase linear DNA resealing by dilution. *E. coli* gyrase DNA cleavage complexes stabilised with 20 μM of ciprofloxacin at 0.25 mM $MgCl_2$ for 30 minutes at 37°C were diluted 10-fold to stimulate DNA resealing. Four dilution buffers were tested: (a) assay buffer, (b) assay buffer and 20 μM ciprofloxacin, (c) assay buffer and 0.25 mM $MgCl_2$, and (d) assay buffer, 20 μM ciprofloxacin and 0.25 mM $MgCl_2$. Dilution buffer was made up of assay buffer and time points during DNA resealing were taken by trapping the samples at 0.2% SDS. Samples were digested with proteinase K, ethanol precipitated and analysed by agarose gel electrophoresis. The DNA cleavage complexes were formed using 10 nM of *E. coli* gyrase and negatively supercoiled pBR322.

DNA resealing stimulated by dilution is a method to reseal DNA cleavage complexes without the requirement to use reagents which may affect protein structure and stability such as EDTA, high salt, or high temperatures which may denature the enzyme. Dilution does affect the concentration of the protein and requires an ethanol precipitation step. New methods to reseal DNA, which involved removal of metal ions, were investigated which did not affect protein concentration and kept the overall assay volume constant [fig. 3.11, 3.12].

Dialysis is a technique to slowly exchange buffer. Using dialysis to remove metal ions would

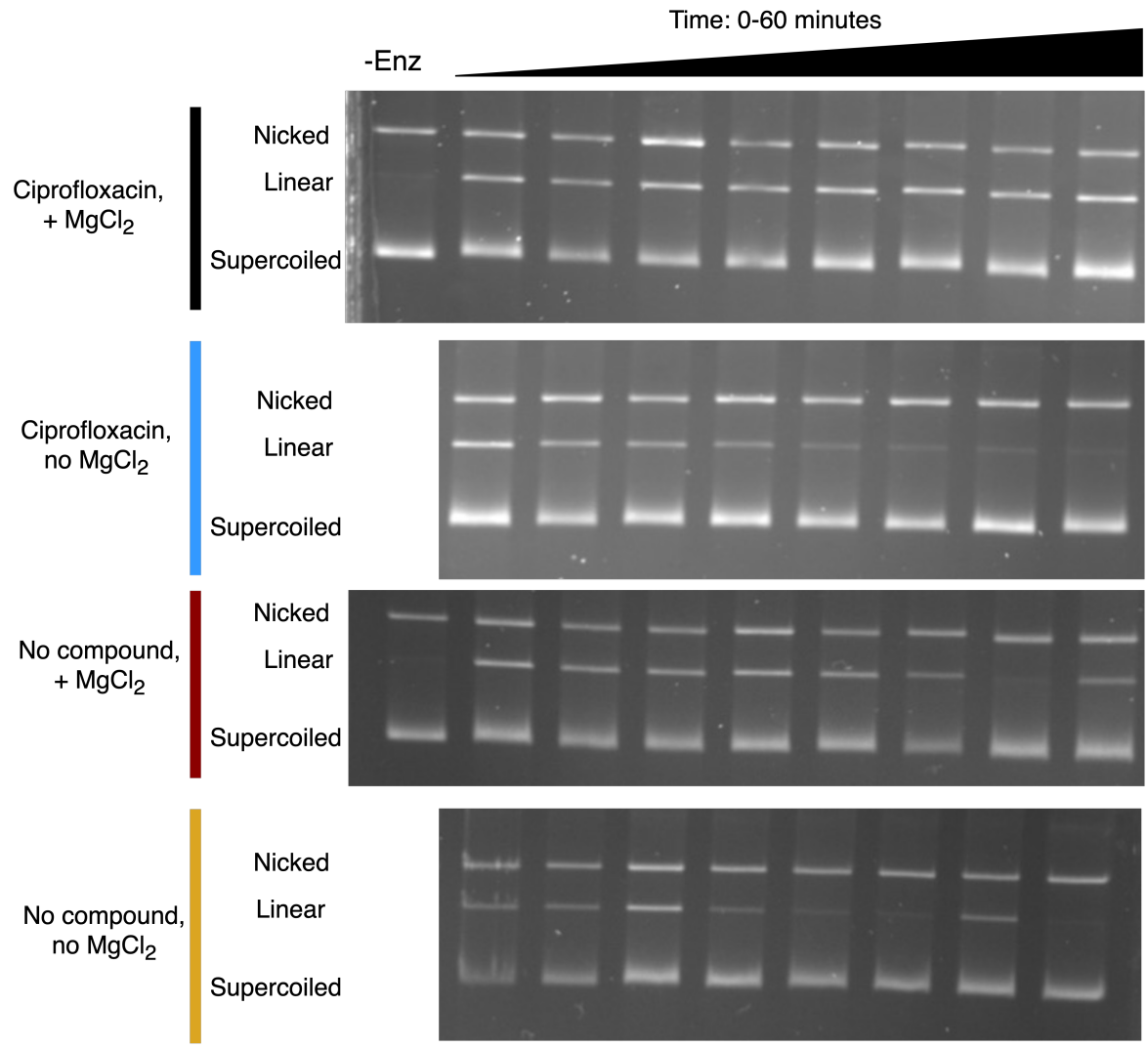

Figure 3.10: The effect of fluoroquinolones and magnesium ions on *E. coli* gyrase linear DNA resealing by dilution, accompanying gels. *E. coli* gyrase DNA cleavage complexes stabilised with 20 μM of ciprofloxacin at 0.25 mM $MgCl_2$ for 30 minutes at 37°C were diluted 10-fold to stimulate DNA resealing. Four dilution buffers were tested. Samples were digested with proteinase K, ethanol precipitated and analysed by agarose gel electrophoresis. The DNA cleavage complexes were formed using 10 nM of *E. coli* gyrase and negatively supercoiled pBR322. Lane 8 from the no compound, + $MgCl_2$, and Lane 7 from the no compound, no $MgCl_2$ gel were swapped when running the agarose gel.

change the concentration slowly, in contrast to alternative methods such as EDTA and dilution, where the metal ion concentration drops almost instantaneously. After a DNA cleavage reaction with *E. coli* gyrase and an IPY was added to a dialyser to exchange the assay reaction buffer with assay buffer without metal ions, DNA resealed slowly over 2 hours [fig. 3.11a]. Previously, DNA resealing experiments with EDTA revealed that slow DNA resealing occurred when the metal ion concentration dropped quickly and significantly [fig. 3.1, 3.3]. However, resealing stimulated by dialysis lowered the metal ion concentration slowly over a long time period. This can be explained by the metal ion concentration achieved during the dialysis process can still support DNA cleavage. Lowering the metal ion concentration by a small amount still impacts the DNA cleavage-resealing equilibrium. This is observed in [fig. 3.5a], where the maximal DNA cleavage achieved was 36.8% of linear DNA at 2 mM $MgCl_2$, and 25.8% of linear DNA at 0.5 mM $MgCl_2$. The position of equilibrium between DNA cleavage and resealing can therefore be modulated by the concentration of free metal ions in solution [fig. 3.13].

A faster method to exchange buffer, and therefore remove metal ions without changing the protein concentration is to use desalt spin columns. The DNA cleavage reaction with *E. coli* gyrase in the presence of an IPY was placed in a desalt spin column, pre-equilibrated in assay buffer with metal ions omitted, centrifuged to exchange the buffer, and trapped with SDS [fig, 3.11b]. The linear DNA resealed quickly over 15 minutes. Following buffer exchange, the metal ion concentration remaining must be sufficient to support fast DNA resealing. Since DNA resealing could be stimulated by dialysis and spin columns, the data shows that lowering the protein concentration, and the acid properties from EDTA would be unlikely to significantly affect DNA resealing.

Therefore, both the DNA cleavage and resealing reaction require metal ions, but the metal ion dependency differs between the two processes. Often, DNA resealing is thought as the exact reverse process of DNA cleavage. It is important to consider the reaction as having different requirements and mechanism of action than the DNA cleavage reaction [fig. 3.13].

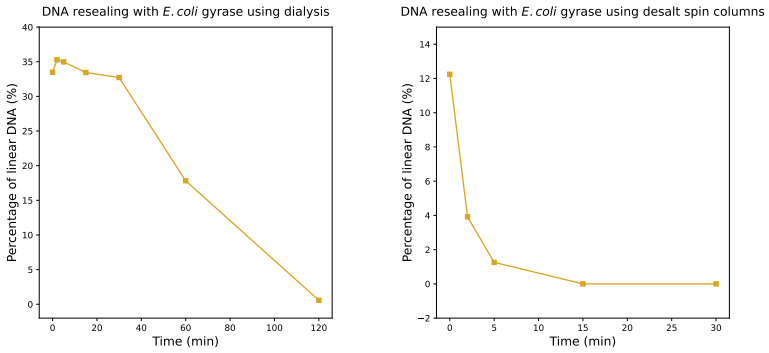

(a) **(b)**

Figure 3.11: Alternative methods to lowering the concentration of free metal ions to stimulate the resealing of *E. coli* gyrase DNA cleavage complexes. DNA cleavage complexes were formed by 50 nM of *E. coli* gyrase stabilised with 20 μM of the IPY t1 at 0.25 mM $MgCl_2$. **(a)** Removal of metal ions to stimulate DNA resealing by dialysing the DNA cleavage reaction in a 10k MWCO dialyser against assay buffer. **(b)** DNA resealing stimulated by passing the DNA cleavage reaction through a desalt spin column pre-equilibrated in assay buffer without metal ions or compound. Time points were taken by trapping with SDS and digestion with proteinase K. Samples were analysed by agarose gel electrophoresis, the bands were quantified and the percentage of linear pBR322 (double-stranded DNA cleavage products) were plotted using python.

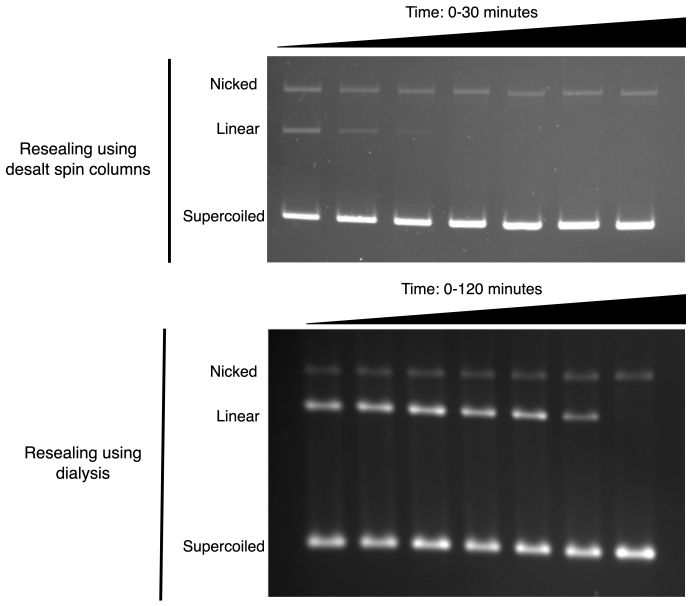

Figure 3.12: Alternative methods to lowering the concentration of free metal ions to stimulate the resealing of *E. coli* gyrase DNA cleavage complexes, accompanying gels. DNA cleavage complexes were formed by 50 nM of *E. coli* gyrase stabilised with 20 μM of the IPY t1 at 0.25 mM $MgCl_2$. DNA cleavage was either stimulated by lowering the free metal ion concentration with buffer exchange desalt spin columns, or by dialysing out the metal ions.

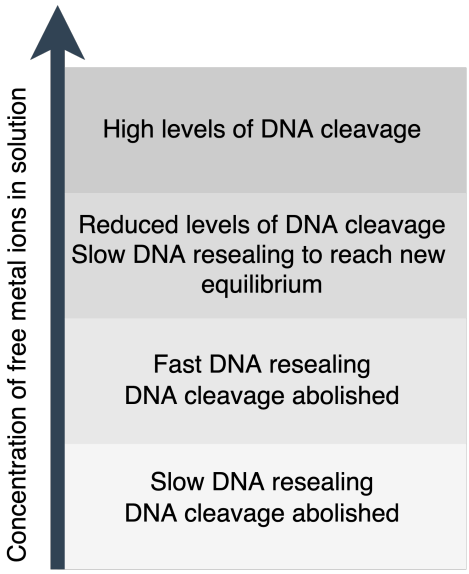

Figure 3.13: A summary of the relationship between the free metal ion concentration in solution, and the effect on the DNA cleavage and resealing equilibrium. The concetration of free metal ions in solution affects the observed levels of DNA cleavage in assays.

3.2.4 The impact of a DNA cleavage stabilising drug on the resealing of DNA cleavage complexes with EDTA

Resealing DNA assays can be used to elucidate the mechanism of action of the compound, and give indications regarding persistence of the type II topoisomerase DNA cleavage complex with compound. DNA resealing is easier to study in the presence of cleavage-stabilising compounds, since higher levels of cleavage can be reached at lower enzyme concentrations, making the linear DNA cleavage band clearer during agarose gel electrophoresis. Since topoisomerase poisons can inhibit DNA resealing, drugs cannot be used to draw conclusions about how the enzyme natively reseals DNA. Therefore, the DNA resealing reaction was compared in the presence and absence of the fluoroquinolone ciprofloxacin [fig. 3.14, 3.2, 3.17].

In the presence of a fluoroquinolone, at 50 nM of *E. coli* DNA gyrase, 45.6% of the DNA was linear. The nicked intermediate appeared, which was then resealed, and the supercoiled DNA increased with the rate of linear to nicked, and nicked to sealed [fug. 3.14a]. Using 1 μM of *E. coli* gyrase in the absence of a drug, 7.5% of the DNA was linear before initiating DNA resealing with EDTA [fig. 3.14b]. The linear DNA resealed over 10 minutes before reaching an equilibrium at 1% linear DNA. The low level of DNA cleavage could be background levels of the intrinsic DNA resealing failure rate of DNA cleavage complexes which cannot be resealed from faulty enzymes. Gyrase was purified *in vitro* and therefore the protein product is unlikely

to be perfectly folded. Natively, any DNA cleavage complexes which cannot be resealed would be repaired by the bacterial cell.

In the absence of a cleavage-stabilising drug, the nicked DNA initially increased by 22% on addition of EDTA. This increase was larger than expected, since the percentage of double-stranded DNA cleavage at the start of the assay was only 7%. Further, the percentage of intact DNA (sealed) decreased, corresponding to the increase in single-strand DNA cleavage. This was not observed during resealing assays with a fluoroquinolone.

The nicked DNA did not reseal to completion, which plateaued after 10 minutes. The slight resealing of the accumulated intermediate corresponded with the same decrease in linear DNA. Since the supercoiled DNA (intact/sealed) decreased as the nicked (single-stranded DNA cleavage) increased, a new equilibrium formed at the lower metal ion concentration between sealed and nicked DNA [fig. 3.15]. The breakage of the first strand of DNA may be acheived at a lower metal ion concentration than the second stage, introducing asymmetry into the consecutive reaction. The binding of metal ions may have a lower K_d for the first DNA cleavage event, or additional structural, regulatory or catalytic metal ions may be required to support DNA cleavage of the second strand. Usually, the cleavage of one strand of DNA increases the rate of second-strand DNA cleavage by type II topoisomerases [175]. The data presented here suggests this is only the case when metal ions are not limiting.

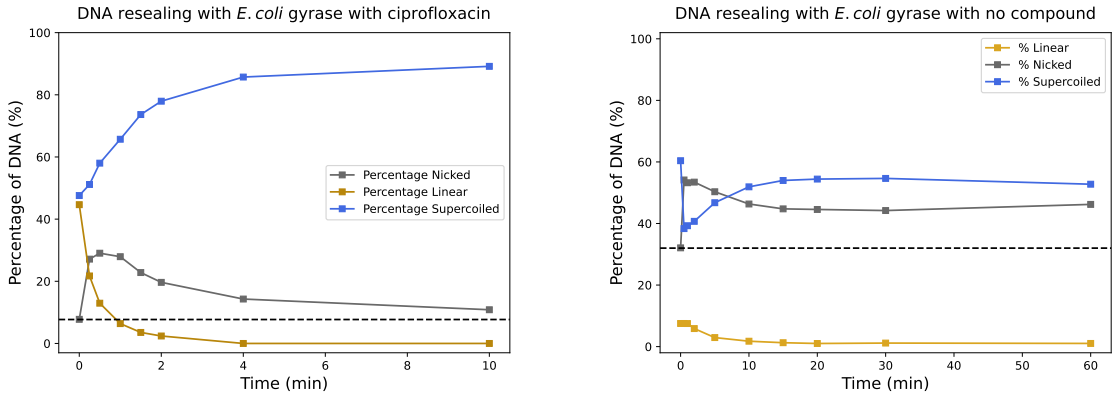

(a) **(b)**

Figure 3.14: A comparison of the *E. coli* gyrase DNA resealing assay timecourse in the presence and absence of a cleavage-stabilising drug. DNA cleavage complexes were formed by incubating negatively supercoiled pBR322 DNA with *E. coli* gyrase. Cleavage complexes were resealed by the addition of EDTA. **(a)** DNA cleavage complexes stabilised by 20 μM of ciprofloxacin. 50 nM of enzyme, 0.5 mM $MgCl_2$ and 40 mM EDTA was used. **(b)** 1 μM of *E. coli* gyrase cleavage complexes formed at 0.5 mM $MgCl_2$ with no drug present. DNA was stimulated to reseal with 10 mM EDTA.

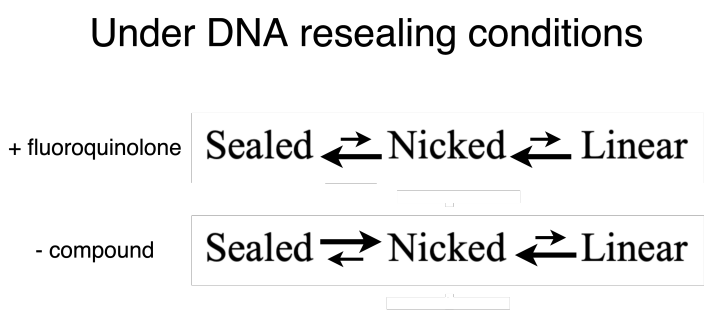

Figure 3.15: The effect of EDTA addition to the position of the DNA cleavage and resealing equilibrium, in the presence or absence of a fluoroquinolone. Under DNA resealing conditions, the position of equilibrium between the cleaved and sealed states are shifted. This effect is dependent on whether there is a DNA cleavage stabilising compound present or not.

The concentration of free metal ions in solution were varied by altering the concentration of EDTA during a DNA resealing assay with *E. coli* gyrase in the absence of drugs [fig. 3.16, 3.17]. The double-stranded DNA cleavage resealed at a slower rate when the DNA cleavage complexes were stimulated to reseal with a higher concentration of EDTA [fig. 3.16a], which was in agreement with the findings of linear DNA resealing in the presence of a topoisomerase poison [fig. 3.1, fig. 3.5].

When comparing the resealing of the nicked intermediate (single-strand DNA cleavage) with EDTA in the presence of drug, the nicked DNA resealed slower when there was less availability of free metal ions, as well as accumulating higher quantities of nicked DNA [fig. 3.3c]. To compare whether the drop in supercoiled DNA, and resealing of nicked DNA in the absence of cleavage-stabilising compound was affected by the concentration of free metal ions, the percentage of supercoiled DNA was compared at different EDTA concentrations [fig. 3.16b]. The supercoiled DNA decreased instantaneously on addition of EDTA, and the drop in proportion of supercoiled DNA was independent of the EDTA concentration. This may be because between 10-80 mM EDTA, the free metal ion concentrations were all too low to continue the DNA cleavage of the second strand of DNA, and equally sufficient to continue the cleavage of the first strand of DNA. The increase in supercoiled DNA can be directly correlated to the resealing of the nicked intermediate during DNA resealing. At a lower EDTA concentration, the recovery of the supercoiled DNA was slower and therefore resealing of the nicked intermediate is dependent on the concentration of free metal ions.

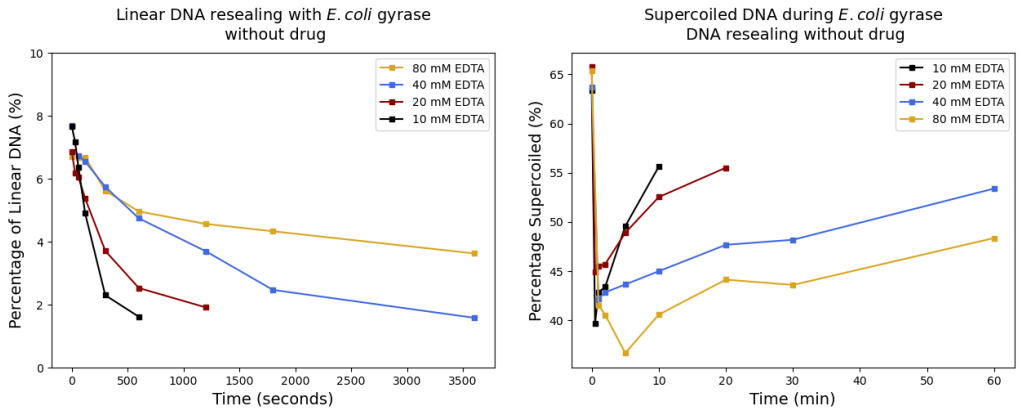

(a) **(b)**

Figure 3.16: The effect of EDTA concentration during a DNA resealing assay with *E. coli* gyrase on the linear and supercoiled DNA in the absence of drug. DNA cleavage complexes formed by 500 nM of *E. coli* gyrase in the absence of drug with 0.5 mM $MgCl_2$. The DNA cleavage complexes were resealed with 10, 20, 40 and 80 mM EDTA and time points were trapped with SDS and digested with proteinase K. **(a)** The resealing of double-stranded DNA. **(b)** The change in supercoiled DNA during DNA resealing at different EDTA concentrations.

3.2.5 Resealing DNA cleavage complexes formed by *S. aureus* gyrase

E. coli DNA gyrase is often used as a model enzyme for studying DNA gyrase, however between bacterial species, the enzyme varies in terms of sequence, domain architecture, and activity. For example, the *E. coli* gyrase gene contains a 174 bp insert in the middle of the Greek Key domain and TOPRIM domain, which the majority of gyrases lack, and there are key amino acid residue differences at the DNA cleavage sites between the enzymes from the two species. Additionally, *E. coli* gyrase is from a Gram-negative bacterial species. Therefore, DNA resealing by a gyrase from the Gram-positive species, *S. aureus* was investigated in the presence and absence of moxifloxacin [fig. 3.18, 3.19].

Like with *E. coli* gyrase, the linear DNA completely resealed in the presence of a fluoroquinolone, and resealed almost to completion without a drug present, forming an equilibrium at 3% linear [fig. 3.18a, 3.18b]. This background linear DNA is may be un-resealable gyrase-DNA cleavage complexes which are faulty in DNA resealing due to mis-folding, or because the enzyme wore out after multiple DNA cleavage-resealing cycles. In the presence of moxifloxacin, following the appearance of the nicked intermediate, only 28% of the single-stranded intermediate resealed, plateauing at 33% nicked DNA. Comparing this with *E. coli* gyrase, the nicked intermediate was completely resealed [fig. 3.14a]. This increase in nicked DNA corresponds with the decrease in linear DNA. The resealing of the second strand of DNA may therefore require a higher

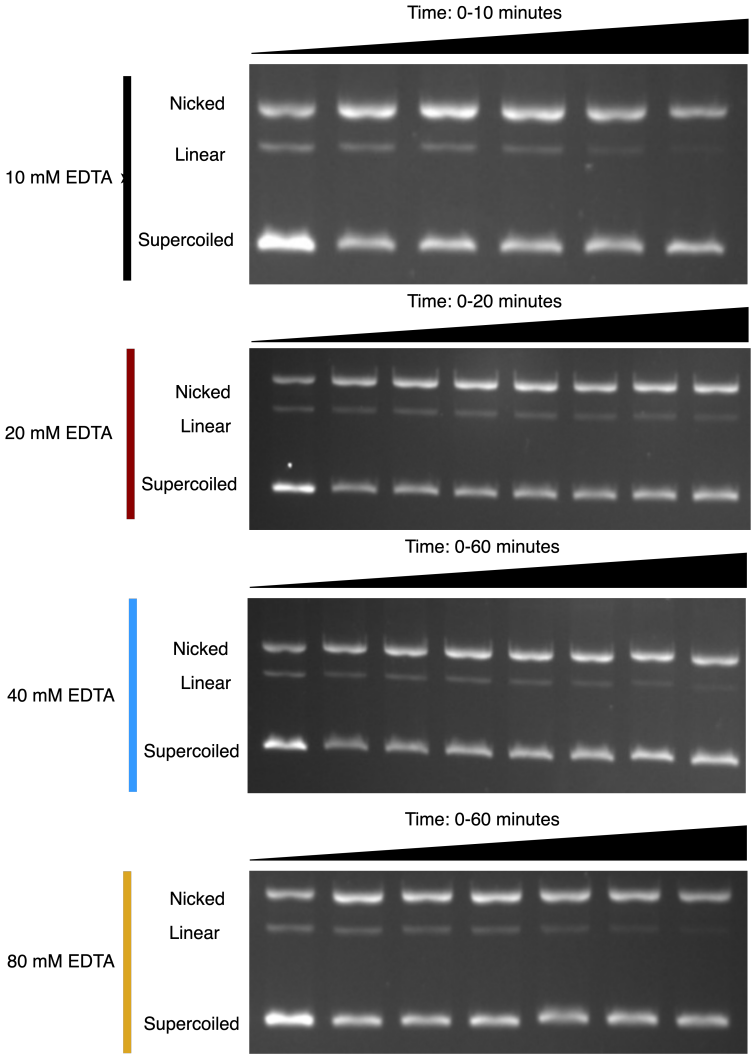

Figure 3.17: The effect of EDTA concentration during a DNA resealing assay with *E. coli* gyrase on the linear and supercoiled DNA in the absence of drug, accompanying gels. DNA cleavage complexes formed by 500 nM of *E. coli* gyrase in the absence of drug with 0.5 mM $MgCl_2$. The DNA cleavage complexes were resealed with 10, 20, 40 and 80 mM EDTA and time points were trapped with SDS and digested with proteinase K.

concentration of metal ions to proceed, since only partial resealing was observed.

When resealing DNA cleavage complexes formed with *S. aureus* gyrase in absence of drugs, the nicked intermediate increases by 47%, and showed minimal resealing over 1 hour. The nicked intermediate increased significantly more than the disappearance of linear DNA, which was also observed with *E. coli* gyrase [fig. 3.14b]. The increase in nicked DNA was much greater than the increase from the *E. coli* gyrase experiments.

Since there were differences in the nicked DNA between *E. coli* gyrase and *S. aureus* gyrase, the concentration of EDTA was varied for DNA resealing assays with *S. aureus* gyrase [fig. 3.18c, 3.18d]. In the presence of moxifloxacin, resealing DNA cleavage complexes with a higher concentration of EDTA resulted in the accumulation of more nicked intermediate, and slower resealing of the nicked intermediate [fig. 3.18c]. This result agrees with the results from *E. coli* gyrase resealing with fluoroquinolones. In the absence of drug, the accumulation of the nicked intermediate, and the resealing of the nicked intermediate was not different when the cleavage complexes were stimulated with either 5 or 20 mM EDTA [fig. 3.18d].

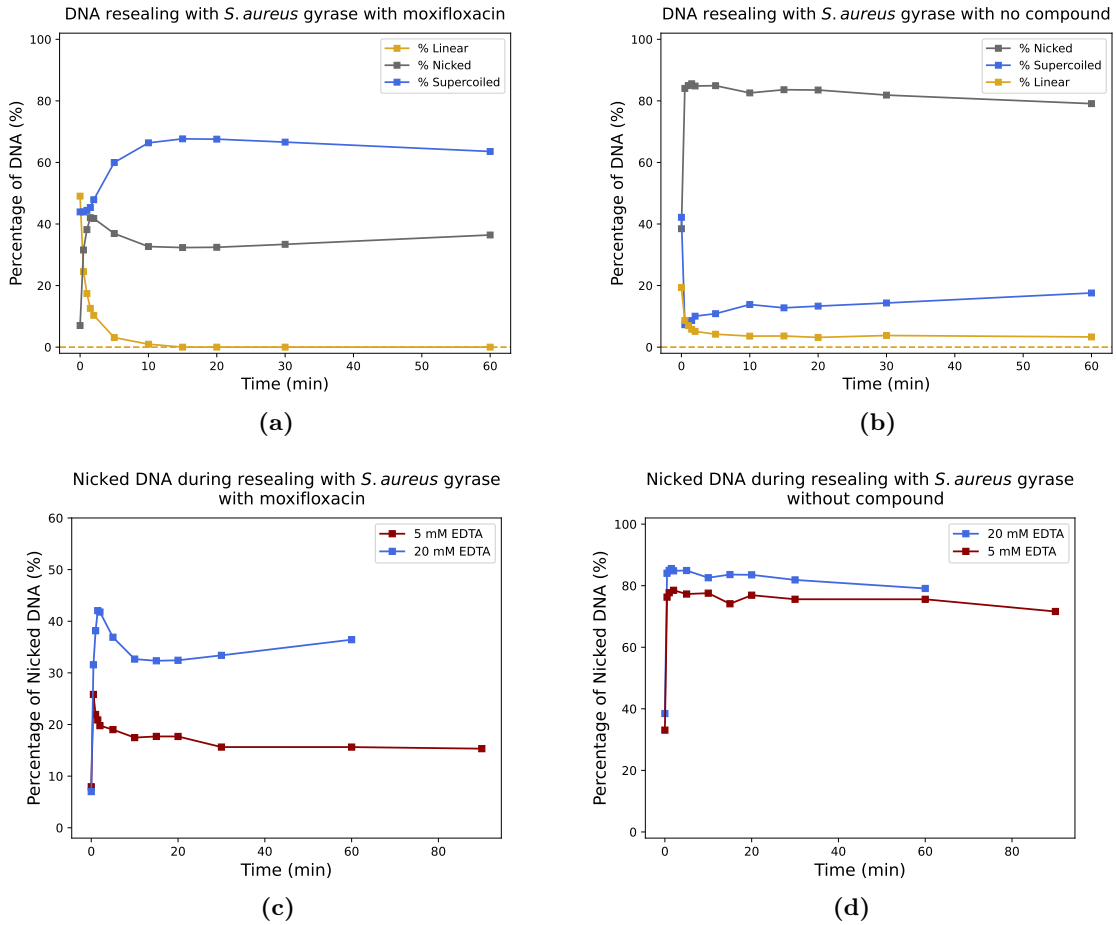

Figure 3.18: *S. aureus* gyrase DNA resealing with moxifloxacin and without a cleavage-stabilising drug. DNA cleavage complexes formed by 50 nM or 500 nM *S. aureus* gyrase when using 20 μM moxifloxacin or no drug respectively at 0.5 mM $MgCl_2$. Cleaved DNA was stimulated to reseal with 20 mM EDTA in the presence of moxifloxacin **(a)** or no drug **(b)**. The effect of 5 mM and 20 mM EDTA was compared in the presence of moxifloxacin **(c)** or without a cleavage-stabilising drug present **(d)**. Following the addition of EDTA, samples were incubated and trapped with SDS and digested with proteinase K. Agarose gel electrophoresis was performed on the DNA and the bands were quantified to be plotted using python.

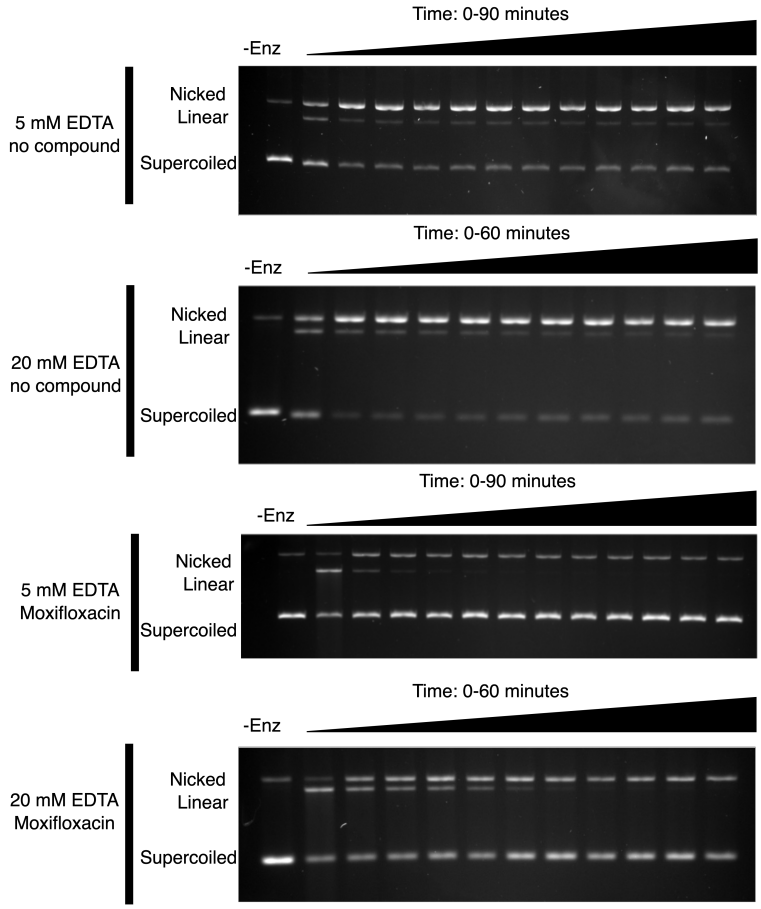

Figure 3.19: *S. aureus* gyrase DNA resealing with moxifloxacin and without a cleavage-stabilising drug, accompanying gels. DNA cleavage complexes formed by 50 nM or 500 nM *S. aureus* gyrase when using 20 μM moxifloxacin or no drug respectively at 0.5 mM $MgCl_2$. DNA cleavage complexes were stimulated to reseal with either 5 or 20 mM EDTA.

3.2.6 Altering the catalytic divalent metal ion in DNA resealing assays with *E. coli* gyrase

Natively, DNA gyrase uses magnesium ions for catalysis of DNA cleavage and resealing, however other divalent metal ions, including manganese and calcium can support this reaction [94]. The DNA resealing profiles were compared for *E. coli* gyrase DNA cleavage complexes generated with manganese ions, stimulated by EDTA in the presence or absence of the fluoroquinolone moxifloxacin [fig. 3.20, 3.21]. In the presence of moxifloxacin, the linear DNA resealed completely, and there was no notable increase in the nicked DNA, which represents the nicked intermediate generated during resealing from the linear DNA. This suggests that the resealing of the second-strand is very efficient with respect to the resealing of the first-strand in the presence of manganese ions [fig. 3.20a]. In absence of drug, the linear DNA partially resealed, forming an equilibrium at 5% linear [fig. 3.20b]. The nicked intermediate also did not reseal.

This was similar to what was observed with magnesium ions, where there was a large increase in the nicked intermediate. However, partial resealing of the nicked intermediate with magnesium ions was observed, which was not observed with manganese ions.

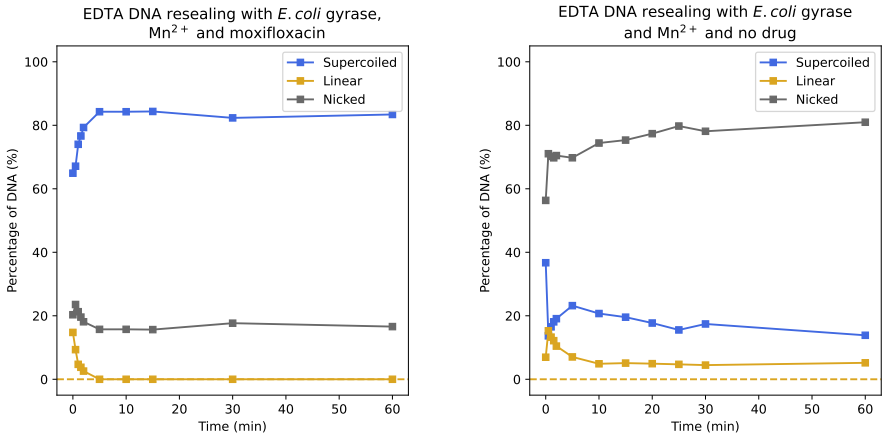

(a) **(b)**

Figure 3.20: DNA resealing by *E.coli* gyrase using manganese ions and EDTA. DNA cleavage complexes formed at 4 mM $MnCl_2$ with *E. coli* gyrase, time points were trapped with SDS and digested with proteinase K. The ratio between the EDTA and $MgCl_2$ concentration was 1.25:1. **(a)** DNA cleavage complexes were stabilised with 20 μM moxifloxacin by 40 nM gyrase. **(b)** Cleavage complexes were formed without drug present, using 500 nM of gyrase.

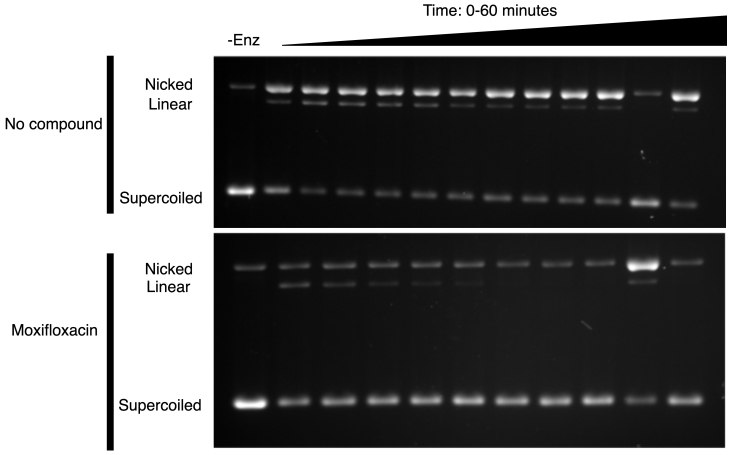

Figure 3.21: DNA resealing by *E.coli* gyrase using manganese ions and EDTA accompanying gels. DNA cleavage complexes formed at 4 mM $MnCl_2$ with *E. coli* gyrase, time points were trapped with SDS and digested with proteinase K. The ratio between the EDTA and $MgCl_2$ concentration was 1.25:1.

Calcium ions stabilise higher levels of native DNA cleavage than other metal ions [176], and therefore, DNA resealing by *E. coli* gyrase stimulated with EDTA was investigated in absence of drugs [fig. 3.22, 3.23]. The linear DNA resealed completely, which was not the case

for magnesium or manganese ions [fig. 3.14, 3.20]. Additionally, the accumulation of the nicked intermediate corresponds with the resealing of the linear DNA, and not due to a decrease in the supercoiled DNA like for magnesium and manganese ions. The nicked intermediate resealed back to the original background level. This data does not agree with an experiment in the literature, where DNA cleavage complexes generated by *E. coli* gyrase and calcium ions were stimulated by EDTA and the nicked intermediate did not reseal. The ratio between calcium and EDTA ions used by Germe *et al.* was 1:2, whereas the experiment in this chapter used a ratio of 1:1.25. The ratio between metal ions and EDTA was very important when optimising this experiment, because at higher ratios, EDTA chelated more calcium ions, resulting in a lower concentration of free calcium ions. Therefore, DNA resealing was too slow to observe. Calcium ions have previously acted differently to other divalent metal ions due to stabilising higher levels of cleaved DNA by altering the DNA cleavage and resealing equilibrium [176]. The DNA cleavage and resealing reaction may therefore act in a more coordinated manner with less asymmetry than observed with magnesium or manganese ions.

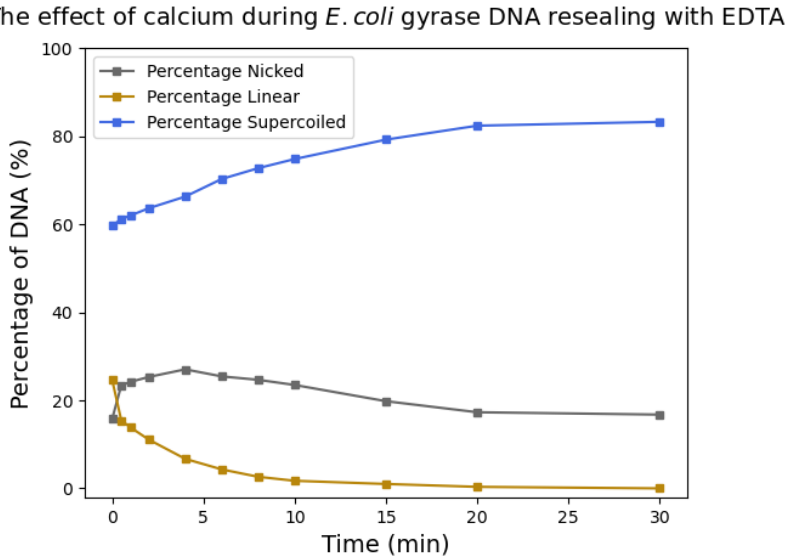

Figure 3.22: The effect of calcium on the DNA resealing reaction by *E. coli* gyrase stimulated by EDTA. A DNA resealing timecourse assay with 40 nM *E. coli* gyrase and 4 mM $CaCl_2$. The DNA was resealed at 5 mM EDTA and time points were taken by trapping samples with SDS and digesting with proteinase K. Data were averaged from 2 datasets and the percentage of each DNA type form the agarose gel was quantified and plotted.

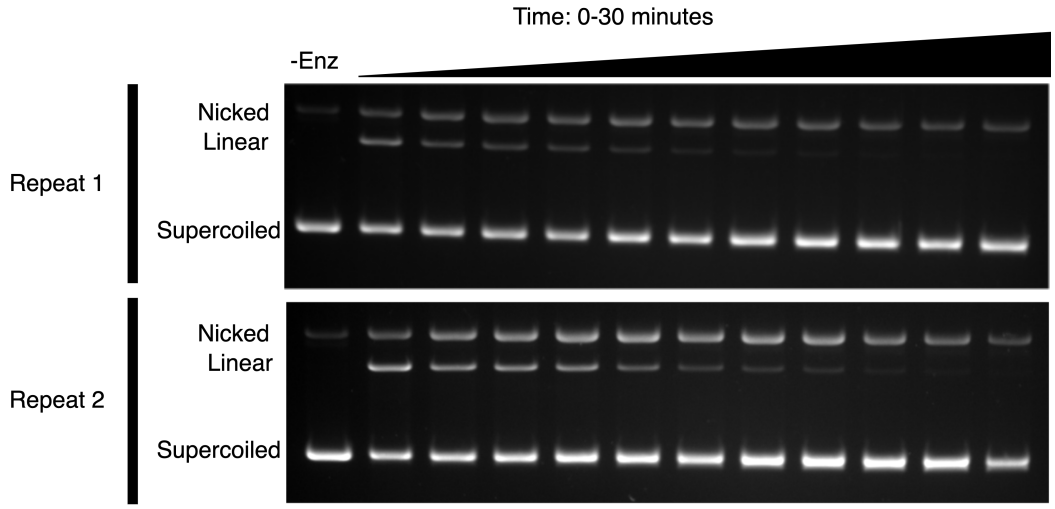

Figure 3.23: The effect of calcium on the DNA resealing reaction by *E. coli* gyrase stimulated by EDTA, accompanying gels. A DNA resealing timecourse assay with 40 nM *E. coli* gyrase and 4 mM $CaCl_2$. The DNA was resealed at 5 mM EDTA and time points were taken by trapping samples with SDS and digesting with proteinase K. Data were averaged from 2 datasets and the percentage of each DNA type form the agarose gel was quantified and plotted.

The resealing of *E. coli* gyrase DNA cleavage complexes stimulated by EDTA in the presence of ciprofloxacin and either magnesium, manganese or calcium ions were compared [fig. 3.24, 3.25]. The linear DNA resealed the fastest in the presence of magnesium ions, followed by calcium ions and manganese ions. DNA resealing by EDTA is not an appropriate method to compare the resealing rates with different metal ions, because EDTA has different affinities for each metal ion. The equilibrium constant for metal chelation is known as the stability constant. A large stability constant represents a strong interaction for the metal-EDTA complex. Magnesium ions have the lowest logarithmic stability constant, 8.79, followed by calcium ions at 10.65, then manganese ions at 13.45 (measured at 25°C and 0.1 M ionic strength) [177]. Therefore, magnesium ions have a weaker interaction with EDTA, resulting in a higher concentration of free metal ions, leading to faster DNA resealing. Additionally, different metal ions will have different roles in the gyrase reaction cycle, for example, calcium ions have been shown to assist DNA binding [176]. Different metal ions may function better at regulating and structurally stabilising the gyrase-DNA complex.

Since comparisons cannot be made between the DNA resealing rates of *E. coli* gyrase DNA cleavage complexes from different metal ions with EDTA, resealing by dilution was explored [fig. 3.24b]. DNA cleavage complexes formed in the presence of an IPY were resealed by diluting the DNA cleavage reaction 5-fold with assay buffer with metal ions omitted. The linear DNA resealed to completion in 30 minutes for DNA cleavage complexes with calcium. Gyrase

resealed 37% of the linear DNA in 120 minutes when the cleavage complexes were formed with magnesium ions. The DNA cleavage could be sustained, albeit at a lower proportion, when the magnesium ions were lowered. This data fits with literature findings, where the optimum concentration for DNA cleavage with magnesium ions is lower than the optimum concentration for calcium ions [176], [88].

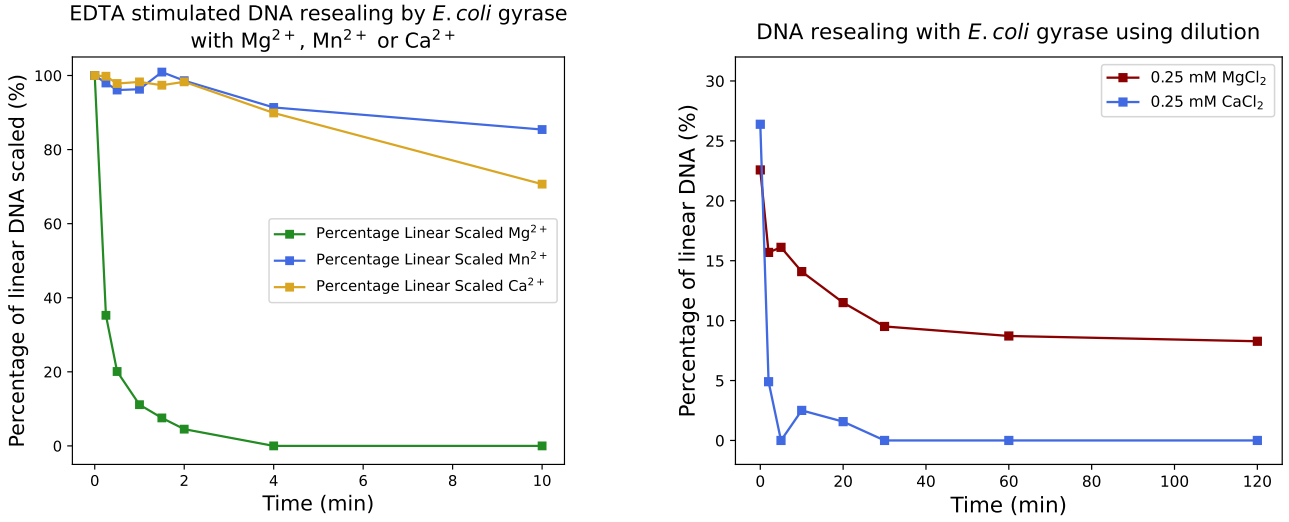

Figure 3.24: A comparison of magnesium, manganese and calcium on resealing DNA cleavage complexes formed by *E. coli* gyrase. (a) A DNA cleavage assay with 50 nM *E. coli* gyrase and 20 μM ciprofloxacin where the divalent metal ion used was either 1 mM of magnesium, manganese or calcium ions. The cleaved DNA was resealed with 10 mM EDTA over 10 minutes. **(b)** A DNA resealing timecourse assay using *E. coli* gyrase and 20 μM of the IPY t1. The cleavage equilibrium was formed with 40 nM of *E. coli* gyrase and 0.25 mM of either $MgCl_2$ or $CaCl_2$. DNA resealing was achieved by diluting the sample 5-fold in assay buffer.

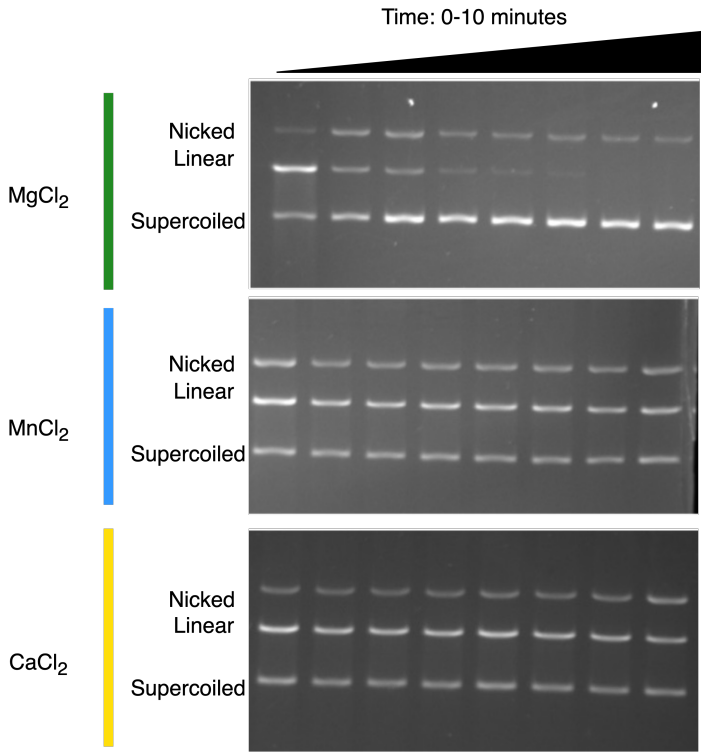

Figure 3.25: A comparison of magnesium, manganese and calcium on resealing DNA cleavage complexes formed by *E. coli* gyrase, accompanying gels.

3.2.6.1 Estimating the concentration of free magnesium ions in solution following chelation by EDTA

The results in this chapter suggested that the concentration of free metal ions strongly influenced the rate at which DNA resealed. The theoretical concentration of free metal ions in solution was calculated, to investigate which concentrations of metal ions are optimal for pushing the position of equilibrium towards DNA resealing. For dilution, the change in metal ions can be calculated by dividing the initial metal ion concentration by the dilution factor. For the dilution experiment in fig. 3.9, the metal ion concentration was diluted from 250 μM to 25 μM. This concentration resulted in DNA resealing, and the total metal ion concentration equates to 2500 times the enzyme concentration.

In experiments where the DNA was stimulated to reseal by the addition of EDTA, metal ions exist in three states: bound to the enzyme, bound to EDTA and free in the solution. The fraction of magnesium ions complexed with EDTA can be calculated from the K_d value for EDTA and magnesium ions, and the total concentration of EDTA and magnesium ions [eqn. 3.1-3.6]. Since the enzyme concentration used was very low compared with the EDTA concentration (nM vs mM), and for simpler calculations, the free metal ions, and the metal

ions bound to the enzyme or DNA were considered as one pool [fig. 3.26]. The K_d value used for the calculations was 0.6 μM [178], which was calculated using ITC at 25°C. The concentration of free metal ions at equilibrium with EDTA was calculated at different total EDTA and magnesium ion concentrations [fig. 3.27].

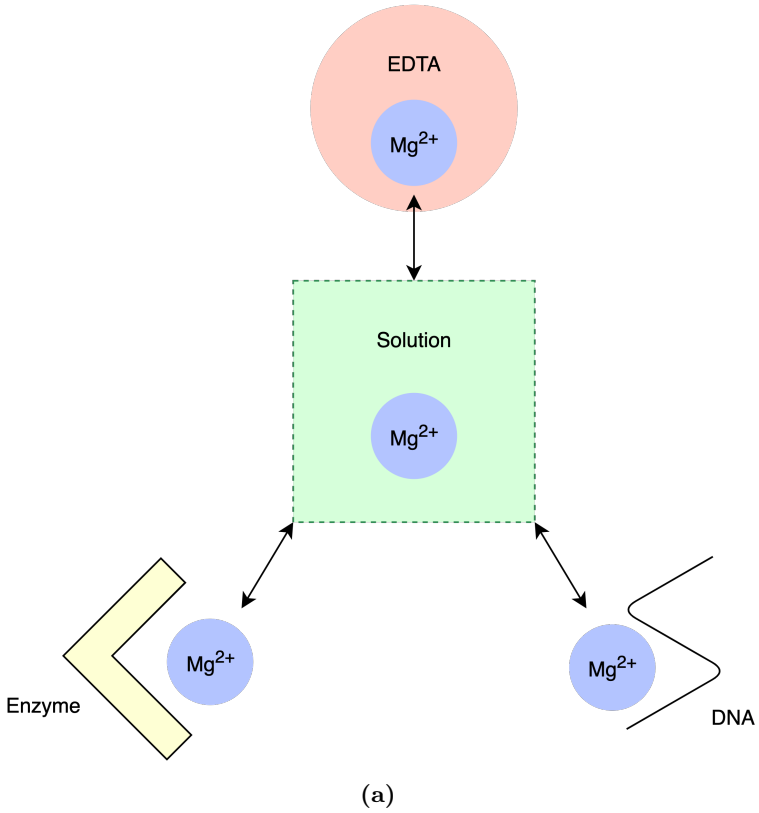

(a)

Figure 3.26: The distribution of the magnesium ions during a DNA resealing assay. On addition of EDTA to gyrase-DNA cleavage complexes, metal ions will either be chelated by EDTA, bound to gyrase (either catalytic, structurally or regulatory), bound to DNA, or free in solution.

As the [EDTA] increased, the [magnesium$_{free}$] decreased, which plateaued at high [EDTA]. At 4 mM total $MgCl_2$ and high [EDTA], the [magnesium$_{free}$] plateaued at a higher concentration than at 0.1 mM $MgCl_2$. This indicated that in large excess of EDTA, there would still subtle differences in the fraction of unbound magnesium ions at different total magnesium ion concentrations [fig. 3.27a]. To calculate the theoretical free magnesium ion concentration used in experimentally in DNA resealing assays, the EDTA concentration where DNA cleavage complexes resealed experimentally was plotted for each total magnesium ion concentration [fig. 3.27b]. The concentration of free metal ions ranged from 1-15 μM, which was still in excess compared to the enzyme concentration, and on a similar scale to the calculated concentration of free metal ions for the dilution method (25-250 μM). Theoretically calculating the [magnesium$_{free}$] on addition of EDTA has limitations. EDTA will not reach equilibrium

immediately, therefore the free magnesium ions initially would be higher. The literature value for the K_d, 0.6 μM [178], was calculated at 25°C in a different buffer than the assay buffer used for these experiments. Additionally, these calculations did not take into consideration magnesium ions bound to the enzyme or DNA, however these metal ions may be neglible. These calculations aimed to give an indication to the magnesium ion concentration where the DNA cleavage and resealing reactions could proceed.

$$[Mg_f] + [EDTA_f] \rightleftharpoons [EDTA \cdot Mg] \tag{3.1}$$

$$[K_d] = \frac{[EDTA_f][Mg_f]}{[EDTA \cdot Mg]} \tag{3.2}$$

$$[EDTA_t] = [EDTA_f] + [EDTA \cdot Mg] \tag{3.3}$$

$$[Mg_t] = [Mg_f] + [EDTA \cdot Mg] \tag{3.4}$$

$$K_d = \frac{([EDTA_t] - [EDTA \cdot Mg])([Mg_t] - [EDTA \cdot Mg])}{[EDTA \cdot Mg]} \tag{3.5}$$

$$[EDTA \cdot Mg] = \frac{([EDTA_t] + [Mg_t] + K_d) \pm \sqrt{([EDTA_t] + [Mg_t] + K_t)^2 - 4([EDTA_t][Mg_t])}}{2} \tag{3.6}$$

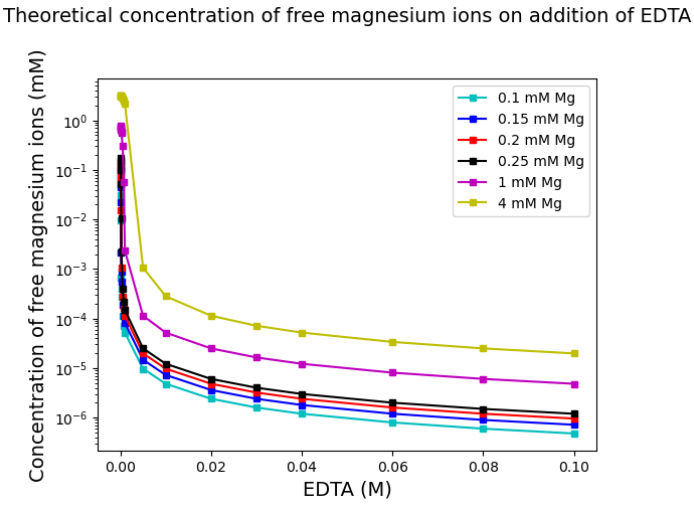

(a)

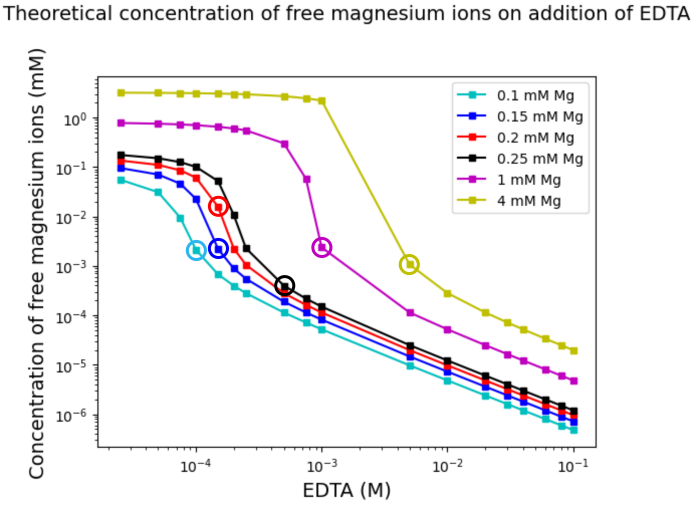

(b)

Figure 3.27: The effect of the EDTA concentration on the theoretical concentration of free metal ions in solution. The theoretical concentrations of the free metal ions were calculated from the total magnesium ion and EDTA concentrations in solution, and the literature value for the K_d of EDTA and magnesium ions at 25°C, 0.6 μM [178]. The concentration of free magnesium ions were plotted on a logarithmic scale. The total magnesium ion values quoted correspond to the initial metal ion concentration that would be used to set up the DNA cleavage equilibrium. On addition of EDTA, the volume of the cleavage reaction changes from 30 μL to 37.5 μM, therefore the total magnesium concentration would be reduced by $1/5^{th}$. This dilution effect was incorporated into the free metal ion calculations. **(a)** The data plotted on a logarithmic scale on the y-axis. **(b)** A log scale was used on the y and x-axis. The concentration of EDTA which the DNA resealed experimentally with *E. coli* gyrase and a poison was circled for each total magnesium ion concentration, to extraoplate a calculated value for the concentration of free metal ions required to reseal DNA.

3.3 Conclusions and future work

The DNA resealing reaction of DNA gyrase was investigated in this chapter. The results conclude that DNA resealing can be stimulated by the removal of metal ions. This can be achieved by the addition of the metal ion chelator EDTA, diluting out the metal ions, the slow removal of metal ions by dialysis or exchanging the reaction buffer with a desalting column.

3.3.1 Limitations in stimulating DNA resealing by lowering the metal ion concentration

The models proposed for the metal ion mechanisms of gyrase to explain the findings from this thesis are somewhat radical, however provide the grounds to warrant further investigations. Many of the conclusions drawn, and the models proposed from the data, are dependent on DNA resealing data using EDTA or other methods to lower the concentration of free metal ions in solution. Elucidating the role of metal ions using these experiments has limitations. Metal ions are implicated in not only catalysis of DNA cleavage and religation, but also may have structural and regulatory roles that influences enzyme activity. Metal ions also bind to and stabilises DNA, with one metal ion potentially binding per DNA phosphate. These experiments cannot distinguish between the effect of removing these metal ions, from the metal ions which bind at the DNA cleavage and resealing sites. Additionally, these experiments were performed on timescales down to 15 seconds. Using more sophisticated techniques, such as stopped-flow, would capture kinetic data on the millisecond timescale. This would be particularly interesting for studying the nicked intermediate formed during DNA resealing, which appears very quickly and the magnitude of this intermediate has likely not been captured in these experiments. The metal ions at are likely too dynamic for more specific techniques, such as Electron Nuclear Double Resonance/Electron Paramagnetic Resonance (EPR/ENDOR), which can look at specific, stable protein-metal ion interactions, or Inductively Coupled Plasma-Mass Spectrometry (ICP-MS), which can determine the number of metal ions per enzyme complex. Studies using EPR/ENDOR and ICP-MS were investigated as part of this project, however the initial findings concluded that these experiments would not be fruitful or feasible.

3.3.2 Studying the stability of gyrase-DNA cleavage complexes stabilised by compounds

Previous literature studies suggested that the resealing of DNA cleavage complexes that were stabilised by fluoroquinolones were due to disruption of the water-metal ion bridge required for compound binding, driving the compound to dissociate and releasing the inhibition on DNA resealing by the fluoroquinolone [121]. By comparing the rate of DNA resealing with an IPY, which does not require metal ions to bind, the rate of DNA resealing was unchanged [fig. 3.5]. Additionally, diluting DNA cleavage complexes with dilution buffer which contained either drug or no drug, showed the difference between compound dissociation, which resulted in slow DNA resealing, or DNA resealing stimulated by the removal of metal ions, triggering fast DNA resealing [fig. 3.9]. These data suggest that when comparing the persistence of drug-stabilised DNA cleavage complexes, dilution experiments with metal ions in the dilution buffer should be used. Therefore, the only trigger to push the position of equilibrium towards DNA resealing would be compound dissociation. Resealing assays in the presence of EDTA would be measuring both compound dissociation, and DNA resealing as a result of the removal of the catalytic metal ion.

3.3.3 Metal ion dynamics during DNA cleavage and resealing

Both strands of the DNA require metal ions to reseal since the rate of resealing of the nicked and linear DNA was dependent on the concentration of free metal ions in solution. Moreover, it is likely that the metal ions leave the enzyme after each stage of DNA cleavage and resealing, as each stage was affected by the metal ion concentration.

Why the DNA resealing reaction can still proceed at a lower metal ion concentration remains unanswered. Both DNA cleavage and resealing depend on the concentration of free metal ions, but the dependency is different, meaning that the DNA cleavage-resealing equilibrium is pushed towards DNA resealing at low concentrations of free metal ions in solution. DNA cleavage could be more affected by the lowering of metal ion concentrations as the metal ion concentration can affect other elements in the topoisomerase reaction cycle. For example, in human topoisomerase IIα, the bending of the gate-DNA has been found to be regulated with structural magnesium ions [179]. Since DNA bending is a key aspect for efficient DNA cleavage, the priming of the topoisomerase to be in a cleavage competent conformation may influence the DNA cleavage kinetics when metal ions are limiting. For DNA cleavage to occur, the

enzyme must be in a cleavage-competent state, including the correct binding and positioning of DNA, whereas for DNA resealing, the correct conformation is much more likely, as DNA is covalently attached to the enzyme. Since DNA reseals immediately following lowering the concentration of free metal ions in solution, the metal ion bound to te enzyme must be very dynamic, rapidly exchanging with the enzyme and solution. Structural metal ions would be more likely to be stably bound to the enzyme, therefore it is more likely that the catalytic metal ions are responsible for pushing the equilibrium towards DNA resealing. An additional factor is that DNA cleavage is much slower than DNA resealing.

An alternative solution to why the equilibrium is pushed towards resealing on lowering the free metal ion concentration could be the affinity for the metal ions to the catalytic metal ion binding site could be different during DNA cleavage and resealing. Whilst the metal ion binding sites are physically at the same location on the enzyme during DNA cleavage and resealing, the DNA is in a different state [fig. 3.28]. The K_d for metal ion binding may be lower for DNA resealing, therefore withstanding the low metal ion concentrations. This may be due to an extra oxygen at the resealing site (from the $3'$ -OH and the phosphodiester bond).

A third solution may be because the number of metal ions required for DNA cleavage and DNA resealing may be different. There are two models for metal ion binding, the two-metal model where two metal ions must be simultaneously present for catalysis, or one metal ion which can bind at both the A- or the B-site [88], [39], [92]. DNA cleavage may require two catalytic metal ions, whereas DNA resealing may be fulfilled with one catalytic metal ion.

DNA cleavage is inhibited at high concentrations of metal ions >15-20 mM [88], DNA cleavage is optimal in the low millimolar range of metal ions. This chapter suggests that DNA resealing can occur in the low micromolar range, however, it remains unclear whether DNA resealing, like with DNA cleavage, is inhibited at high concentrations of metal ions.

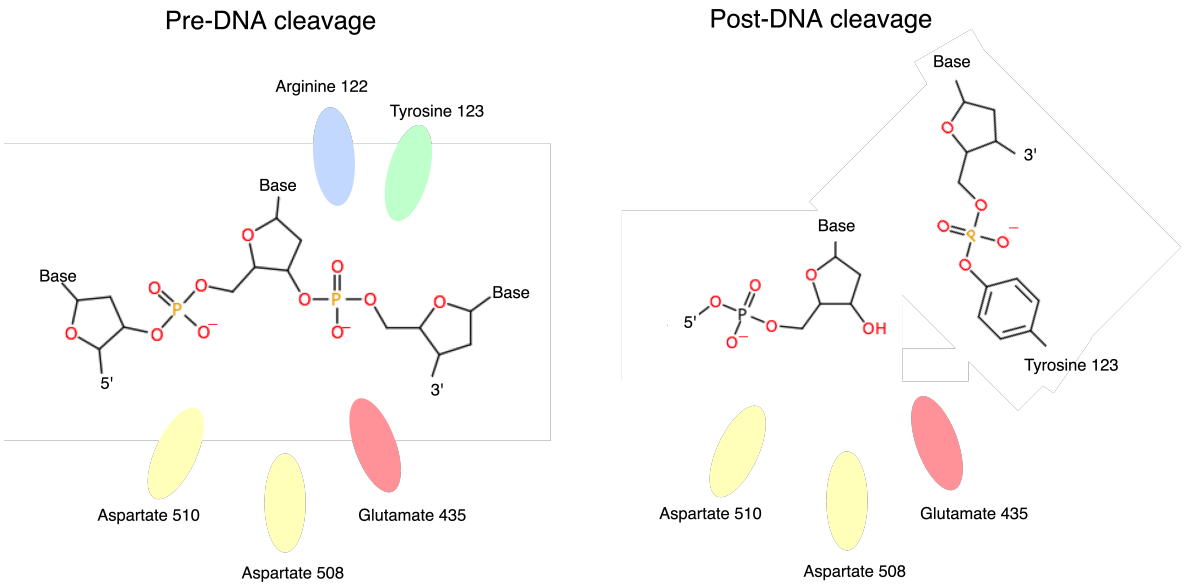

Figure 3.28: The DNA cleavage site of *S. aureus* gyrase. The pre- and post-DNA cleavage site of *S. aureus* gyrase with DNA, showing the acidic metal-ion binding residues and the catalytic tyrosine. The cleaved state is based from crystal structures with the fluoroquinolone moxifloxacin. Since moxifloxacin physically distorts the DNA into a resealing-incompetent state, this form would not be seen natively.

3.3.4 Application of metal ion dynamics to the catalytic metal ion model for DNA gyrase DNA cleavage and resealing

There are currently two models for the roles of the catalytic metal ions during DNA catalysis. The two-metal ion model was first suggested in 2002 by Nobel and Maxwell, because DNA relaxation was enhanced with two different metal ions - magnesium and calcium, when using a *E. coli* gyrase acidic residue mutant GyrB D500H. Further crystallographic evidence of the DNA cleavage site led to the proposal of a catalytic mechanism involving one metal ion, due to the presence of 1 metal ion in the majority of crystal structures. This model's hypothesis is that one metal ion is sufficient to catalyse DNA cleavage, and that the B-site acts to store the metal ion until it is required at the catalytic site (A-site) [39], [92] [fig. 3.29a]. These models have been considered as static, and for the models to fit with the conclusions drawn from the DNA resealing experiments, the models were adapted to form dynamic metal ion models, which can fit with both a 1- or two-metal mechanism [fig. 3.29b]. The DNA resealing data may preferably fit with a one-metal mechanism, since at such low metal ion concentrations, the occupation of both metal ion binding sites would be less probable. Alternatively, for the two-metal ion mechanism, the metal situated at the B-site may not be dynamic.

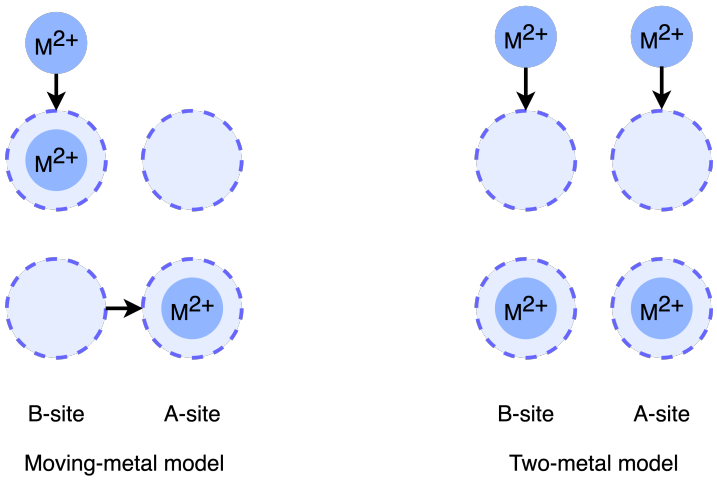

(a)

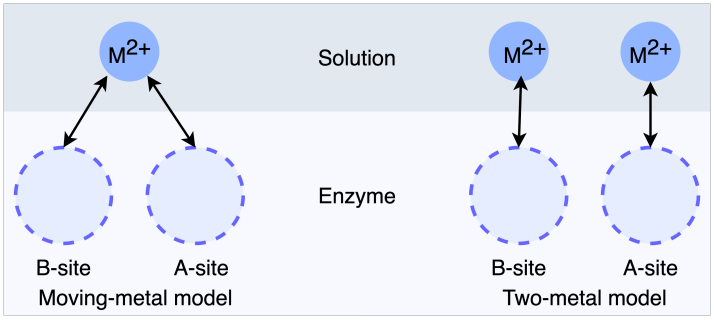

(b)

Figure 3.29: Models for the catalytic metal ion mechanism for DNA cleavage and DNA resealing. The current models for the roles of the catalytic metal ions during DNA cleavage and DNA resealing **(a)** were adapted to form models where the metal ions are dynamic with the free metal ions in solution **(b)**.

3.3.5 Enzyme asymmetry during the DNA cleavage and resealing reaction

When DNA cleavage complexes were resealed by *E. coli* gyrase stimulated by EDTA to remove metal ions from solution, in the presence of a fluoroquinolone, the linear DNA resealed via a nicked intermediate [fig. 3.14a]. The position of equilibrium shifted towards DNA resealing [fig. 3.30].

In absence of compound, the linear DNA did not completely reseal, the supercoiled DNA initially decreased and the nicked DNA had a corresponding increase, which then partially resealed [fig. 3.14b]. A new equilibrium was reached, where both the second stage in DNA cleavage and resealing, nicked to linear, and nicked to sealed respectively, are unfavoured with respect to the other DNA cleavage and resealing events (sealed to nicked, and linear to nicked). The position of equilibrium shifts towards gyrase covalently attached to one strand of the DNA

helix [fig. 3.30]. Therefore, the enzyme demonstrated asymmetry during the DNA cleavage and resealing process, since the cleavage and resealing of the second DNA strands were affected differently in response to the concentration of free metal ions. There may be different metal ion binding affinities for each stage in the DNA cleavage and resealing cycle. Whilst the resealing of nicked to sealed was affected by the concentration of free metal ions [fig. 3.16b], the increase in the nicked intermediate on addition of EDTA was independent of the concentration of free metal ions. A possible explanation could be that this stage of the DNA cleavage cycle could occur via a metal-independent mechanism. The generation of nicked DNA is unlikely to be only from the resealing of double-stranded DNA cleavage, because the linear DNA was 7.5% before EDTA addition, and the nicked DNA increased by 22%.

DNA cleavage may require a higher concentration of free metal ions in solution, because the role of the B-site metal ion may be more critical for DNA cleavage than DNA resealing. If the B-site metal ion were less important during DNA resealing, at low concentrations of free metal ions in solution, DNA resealing would be more resistant to changes in the metal ion concentration. The B-site metal ion may anchor and orientate the DNA during DNA cleavage. During DNA resealing, the DNA is anchored by a covalent bond, therefore the B-site metal ion would be less important.

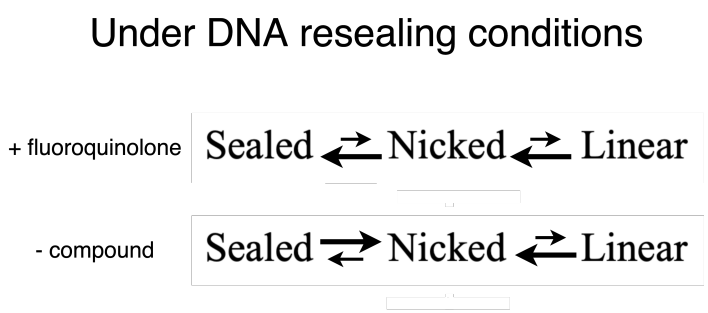

Figure 3.30: The effect of EDTA addition to the position of the DNA cleavage and resealing equilibrium, in the presence or absence of a fluoroquinolone.

3.3.6 Differences in the DNA cleavage and resealing cycle with *S. aureus* gyrase compared with *E. coli* gyrase

S. aureus gyrase reseals DNA on addition of EDTA in the presence of fluoroquinolones [fig. 3.18]. The linear DNA completely resealed, however, unlike with *E. coli* gyrase, the nicked DNA did not completely reseal. The equilibrium may have shifted to disfavour the nicked to sealed stage, or, the fast chelation of metal ions by EDTA may have not given enough time to reseal the second DNA strand, since EDTA will not reach an equilibrium between chelated and

free metal ions instantaneously.

In the absence of a fluoroquinolone in the presence of EDTA, the effect on the position of equilibrium is similar to what was observed with *E. coli* gyrase, however to a greater extent. The nicked DNA increases on addition of EDTA to much higher levels than with *E. coli* gyrase. Like with *E. coli* gyrase, the increase in nicked DNA was independent of the EDTA concentration used [fig. 3.18d]. Possible explanations between the differences in resealing between the enzymes could be that the reaction buffers are very different. The *S. aureus* assay buffer contains the salt potassium glutamate, which is not present in the *E. coli* gyrase buffer. Structurally, *E. coli* gyrase gene contains a 174 bp insert in the TOPRIM domain, which may influence how the enzyme cleaves and reseals DNA.

This work studied the effects of DNA resealing by *E. coli* and *S. aureus* gyrase. Whether the other bacterial type II topoisomerase, topo IV, also follows the DNA resealing trends on addition of EDTA would be a natural progression of the work. DNA resealing assays are used for compound persistence with the human enzymes for the development of drugs for chemotherapy. Performing the DNA resealing assays with human topoIIα and β would be interesting to see if the DNA resealing differences between resealing in the presence or absence of compound are bacterial specific. Another enzyme which would be interesting to study would be topo VI, which lacks the C-terminal domain. There is coordination between closing the DNA gate and resealing DNA, and the opening of the exit gate. Therefore, the control of DNA resealing may be different for this enzyme.

3.3.7 The effect of different metal ions on the DNA resealing reaction of *E. coli* gyrase

The DNA cleavage and resealing reactions are catalysed by divalent metal ions. The effect of DNA resealing assays with magnesium, manganese and calcium ions were compared, which showed that the DNA resealing reaction was much slower for manganese and calcium ions, compared with manganese ions [fig. 3.24]. However, the metal ions could not be accurately compared when using EDTA to lower the metal ions, due to the different affinities for EDTA and the different metal ions. Therefore, dilution was used to compare magnesium ions and calcium ions to reseal *E. coli* gyrase DNA cleavage complexes [fig. 3.24b]. DNA resealing with calcium ions by the dilution method was not only faster than with magnesium ions, calcium ions also completely resealed the DNA, whereas with magnesium ions lowered the level of DNA cleavage. Magnesium ions are harder metal ions than calcium, and therefore may have greater

preference for the catalytic metal ion coordinating acidic residues. A tighter interaction may therefore allow for DNA cleavage to persist.

Whilst the DNA resealing rates cannot be directly compared with different metal ions due to different stability constants for EDTA and the metal ions, the resealing profiled with no compound were compared with calcium, manganese and magnesium ions. On addition of EDTA, the nicked DNA increased significantly when the cleavage and resealing equilibrium was formed with magnesium or manganese ions. However, with calcium ions, the nicked DNA did not increase above what is expected from a nicked intermediate during the resealing of linear DNA. This is due to a difference in enzyme concentration. 12.5-25 - fold more enzyme was used for the magnesium and manganese ion experiments than the calcium ion experiments. Calcium ions have been known to alter the DNA cleavage and resealing equilibrium to favour DNA cleavage. Therefore, at the enzyme concentration used in the calcium ion experiments, the nicked intermediate may not be observed due to the lower enzyme concentration, minimising the effect.

3.3.8 Biological significance of the metal ions influencing DNA resealing

The concentration of magnesium ions in *E. coli* is estimated between 20-100 mM [180]. Magnesium ions in the cell will not all be free, for example, magnesium ions stabilise the negative charges on the phosphate groups on DNA and RNA. Bacteria have magnesium ion transporters, such as MgtA, which maintain the intracellular magnesium ion concentration [181]. The concentration of free magnesium in *E. coli* is estimated between 1-2 mM. From the biochemical data, the millimolar range for magnesium ions is sufficient to support DNA cleavage. Type II topoisomerases can also use other divalent metal ions to fulfil the role of the catalytic metal ion. In *E. coli*, the total concentration of manganese ions is <2 μM, and for cobalt ions, <0.5 μM [182]. Therefore, bacterial cells are unlikely to ever reach the metal ion concentrations estimated for DNA resealing from this work (1-250 μM). However, if metal ions did become limiting in the cell, it would be unlikely that gyrase would become trapped to the DNA during the catalytic cycle due to DNA resealing operating at a greater range of metal ion concentrations. This would prevent the accumulation of lethal double-stranded DNA breaks.

3.3.9 Future experiments to study the DNA cleavage and resealing equilibrium

This chapter summarises DNA resealing experiments where DNA cleavage complexes are stimulated to reseal by lowering the concentration of metal ions. Type II topoisomerase double-stranded DNA breaks can also be ligated by altering the temperature. Human topo IIα changes the position of equilibrium towards resealing at high temperatures (+55°C) and low temperatures >4°C [183]. At high temperatures, the shift towards religation is thought to be due to a decrease in the forward rate (strand scission), as opposed to an increase in the rate of DNA ligation. This result mirrors the finding in this chapter, where the forward reaction (DNA cleavage) is reduced with respect to DNA resealing on removal of metal ions. What is not known about DNA resealing is why DNA resealing is more resistant at high temperatures compared to DNA cleavage, and therefore would be an interesting avenue to explore. Type II topoisomerase-DNA cleavage complexes can also be stimulated to reseal with high concentrations of salt, such as NaCl. It is not known why salt can stimulate DNA resealing, however the effect of high salt, pH or charge may provide interesting insights into the DNA resealing reaction. Additionally, there are thought to be differences in the mechanism of DNA resealing by EDTA and salt. High salt concentrations can reseal DNA cleavage complexes formed at abasic sites, whereas the abasic sites are resistant to DNA resealing stimulated by EDTA [184].

Chapter 4

The importance of gyrase residues to the DNA cleavage and resealing reaction

4.1 Introduction

4.1.1 The roles of lysine residues and the Greek Key domain in DNA gyrase to the resealing of gyrase-DNA cleavage complexes

The DNA cleavage and resealing equilibrium by type II topoisomerases is catalysed by divalent metal ions, which are coordinated by three acidic residues. When the DNA gate is opened to allow passage of the transported DNA segment (T-segment), the enzyme must coordinate the resealing of the broken gate DNA (G-segment) once the T-segment has passed through the DNA break. If the opening and closing of the DNA gates were uncoordinated, the topoisomerase's efficiency would be decreased, and it would be metabolically expensive. Chan and colleagues suggest that in part, coordination is achieved by the motion of the T-segment through the DNA gate, which reorientates the Greek Key domain to control G-segment religation [46]. The Greek Key domain is located within the TOPRIM domain of GyrB and lies below the WHD and TOPRIM and above the DNA exit gate. The repositioning of the Greek Key domain was suggested to move a highly conserved YKGLG motif, which is located two amino acids after the Greek Key domain, in order to destabilise the cleaved state to trigger DNA religation. The YKGLG motif consists of two glycine residues that makes the motif highly flexible. The tyrosine anchors in a hydrophobic pocket so the motif can act as a hinge to orientate the Greek Key domain in proximity of the TOPRIM domain [185].

The lysine residue from the conserved YKGLG motif, which is thought to have a role in the control of the DNA cleavage and resealing cycle, adopts different conformations in crystal and cryo-EM structures. In a structure of *S. aureus* gyrase core fusion with DNA in the uncleaved conformation, and without metal ions bound at the DNA cleavage site (PDB 2XCR) [39], a lysine residue, GyrB K581 points directly at the DNA cleavage catalytic site [fig. 4.1].

The lysine residue is 4.1 Å away from the catalytic tyrosine (mutated to phenylalanine in the structure), 3.4 Å from the non-scissile phosphate, and 4.1 Å away from the scissile phosphate. The lysine is also between 4-5 Å from all three of the metal ion-coordinating acidic residues. In the majority of *S. aureus* gyrase core fusion structures, the Greek Key domain is deleted. The 37-residue Greek Key domain is very flexible, therefore, the deletion has been shown to significantly improve the structure's resolution [39]. This domain is 2 residues from the lysine residue, therefore, when the domain is deleted, the flexibility of the conserved YKGLG loop where the lysine is located is likely to be impacted. In structures where the Greek Key domain is deleted, the lysine residue points away from the catalytic site, as shown in figure 4.1 in yellow (PDB 5CDR [46]). In an *E. coli* gyrase cryo-EM structure (6RKU, [36]), which contains the Greek-Key domain, the lysine (K740) is spatially positioned in between the equivalent lysines from 5CDR and 2XCR, highlighting the flexibility of this region.

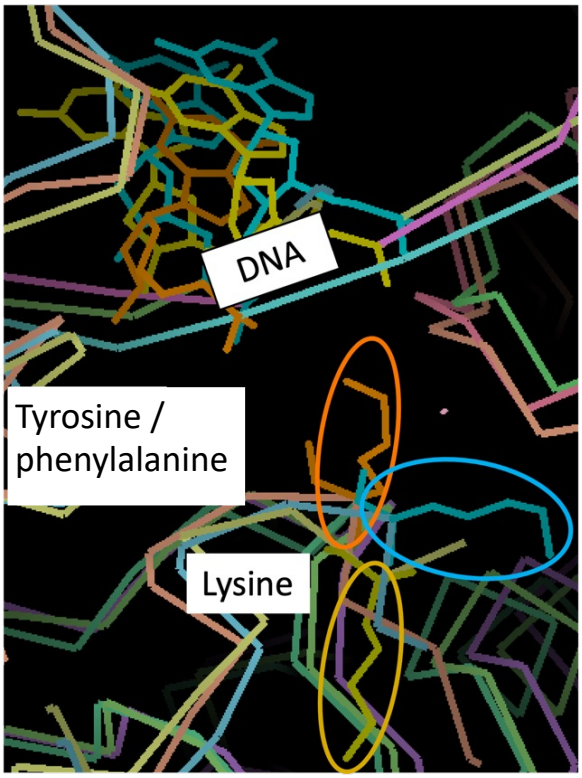

Figure 4.1: The position of a lysine residue from the conserved YKGLG motif in superimposed gyrase structures. Orange: *S. aureus* gyrase core fusion crystal structure with uncleaved DNA and no metal ions bound (PDB 2XCR). The Greek Key domain is not deleted in this construct [39]. Yellow: *S. aureus* gyrase core fusion with the Greek Key domain deleted crystal structure, with artificially nicked DNA and manganese ions bound at the DNA cleavage sites [46]. The lysine residue from the conserved YKGLG motif has been circled. Blue: *E. coli* gyrase cryo-EM structure, with the Greek Key domain. The structure is with artificially nicked DNA, no catalytic metal ions observed at the DNA cleavage site, and the compound gepotidacin was used.

The lysine residue has also been suggested to be able to replace the role of the catalytic metal ions to catalyse the first stage in DNA resealing by occupying the A-site, and to prevent the re-cleavage of the G-segment before the T-segment has left through the exit-gate [46]. This was proposed because on addition of increasing concentrations of EDTA to DNA cleavage complexes, single-strand DNA cleavage complexes accumulated in the presence of the DNA cleavage-stabilising drug quinazoline dione [121]. The conclusion from the results were that the first-stage of DNA resealing (double-stranded DNA break to a single-stranded break) occurring via a metal-independent mechanism, due to the accumulation of nicked DNA when metal ions were removed from solution, and the inhibition of DNA resealing of the second-stage of DNA resealing (single-stranded DNA break to sealed DNA), which would be dependent on metal ions [46]. This phenomenon was investigated in chapter 3, which contradicted this conclusion, proposing that both strands during resealing DNA cleavage complexes stabilised by a drug were dependent on the concentration of free metal ions in solution.

In the literature, mutation of the lysine from the conserved YKGLG motif affected the observed DNA cleavage. When the lysine was mutated in yeast type II topoisomerase to an alanine (K603A), there was a high proportion of DNA cleavage in a DNA cleavage assay, particularly of nicked DNA [45]. Although type I topoisomerases do not have a homologous lysine from the conserved YKGKG motif, lysines have been shown to be very important to the DNA cleavage and resealing reaction in type I topoisomerases. Type I topoisomerases are mechanistically and functionally similar to the type II topoisomerases. Both enzymes have a TOPRIM domain and alter DNA topology by cleaving DNA. Type I topoisomerases cleave DNA via a single-stranded mechanism; type IA topoisomerases form a phosphotyrosine linkage with the $5'$ phosphate, whereas type 1B form the covalent attachment with the $3'$ phosphate. Mutating lysine 532 to an alanine in human topo IB shifted the DNA cleavage-resealing equilibrium towards DNA cleavage; lysine can act as a general acid, donating a proton to the leaving $5'$ OH group during DNA cleavage [186]. In a *Leishmania donovani* topo IB crystal structure, which represents a transition state during DNA cleavage, achieved by replacing the scissile phosphate with vanadate, lysine 352 coordinates the vanadate [103]. Mutation of lysine 13 in *E. coli* topoisomerase IA prevented metal-independent DNA cleavage, suggesting that either lysine or a metal ion can support catalysis for DNA cleavage [170], [94]. Since lysine residues have the chemical properties which could aid DNA cleavage and resealing in type II topoisomerase, and their important role with the similar type I topoisomerases for DNA cleavage and resealing, lysine residues close to the DNA cleavage site in DNA gyrase were

investigated in this chapter.

There are numerous lysines close to the DNA cleavage and resealing active site in type II topoisomerases, other than the lysine present on the conserved YKGLG motif. Mutation of lysine 720 to an asparagine in yeast topoisomerase II led to high levels of double-stranded and single-stranded DNA cleavage in a DNA cleavage assay, compared to the wild-type protein. Mutation of the equivalent residue in human topoisomerase IIα, K743N has been found in human cancer cells [187]. In *E. coli* gyrase, the homologous lysine is located on GyrA, lysine 65, which in crystal structures forms a salt bridge with GyrB E744.

4.1.2 Chapter aims

This chapter aims to explore the effect of mutating lysines close to the DNA cleavage and resealing active site, and deleting the Greek Key domain located within the TOPRIM domain, to the DNA cleavage and resealing reactions of *S. aureus* and *E. coli* gyrase. In particular, the lysines from the YKGLG motif from *E. coli* and *S. aureus* gyrase, K740 and K581 respectively, were mutated to alanine. *E. coli* and *S. aureus* were chosen as Gram-negative and Gram-positive examples, and because both species are used as model species to study emerging antibiotics. Both enzymes also have some different amino acids close to the DNA cleavage and resealing site. Structurally, the enzymes have striking differences in the Greek Key domain. The *S. aureus* gyrase Greek Key domain is 37 amino acids, whereas the *E. coli* gyrase Greek Key domain is 32 amino acids. Further, the *E. coli* gyrase Greek Key domain has a 58 amino acid insert in the middle, which does not form part of the Greek Key structural fold. This insert is known to greatly affect DNA supercoiling, binding, and ATPase activity [47], [48].

The results in chapter 3 observed an accumulation of a nicked intermediate during the resealing of DNA cleavage complexes with *E. coli* gyrase and *S. aureus* gyrase in the absence of a cleavage-stabilising compound [fig. 4.2]. This appearance of the nicked intermediate during DNA resealing did not correlate with the disappearance in the linear DNA, and the quantity of the nicked DNA accumulation was independent of the concentration of free metal ions in solution. The effect of mutating the lysine from the conserved YKGLG motif, and the deletion of the Greek Key domain was studied to see if these mutations affected the DNA resealing of this nicked intermediate in the absence of drugs. Additionally, the high levels of nicked intermediate which does not completely reseal could have resulted from a nicking enzyme in the enzyme preparation. Therefore, the DNA cleavage and resealing samples were phenol extracted, to separate protein-linked DNA cleavage complexes from the aqueous plasmid DNA substrate

and free DNA breaks formed from contamination. Additionally, the role of *E. coli* gyrase GyrA K65, which is located close to the DNA cleavage and resealing site was investigated.

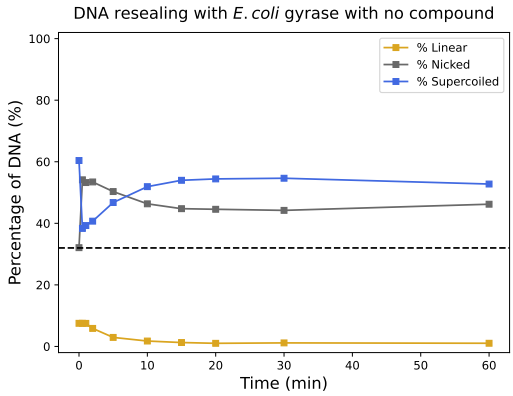

Figure 4.2: The *E. coli* gyrase DNA resealing assay timecourse in the absence of a cleavage-stabilising drug from chapter 3. The nicked intermediate during DNA resealing significantly increases in comparison with the resealing of the double-stranded DNA. DNA cleavage complexes were formed by incubating negatively supercoiled pBR322 DNA with *E. coli* gyrase. Cleavage complexes were resealed by the addition of EDTA. 1 μM of *E. coli* gyrase cleavage complexes formed at 0.5 mM $MgCl_2$ with no drug present. DNA was stimulated to reseal with 10 mM EDTA. A dotted line indicates the starting percentage in nicked DNA, to indicate that the single-stranded DNA cleavage complexes did not return to the base line following resealing stimulating conditions.

4.2 Results

4.2.1 The activity of *E. coli* gyrase △ Greek Key domain

The *E. coli* gyrase Greek Key domain, located within the GyrB TOPRIM domain has been thought to have important roles in the coordination of DNA resealing. The Greek Key domain was proposed to undergo a conformational change when the T-segment DNA passes through the DNA gate. The domain is also thought to coordinate the position of the conserved YKGLG motif, which may have a role in the DNA resealing reaction [46]. Therefore, the Greek Key domain was deleted from *E. coli* GyrB. There is a 174 bp insert within the Greek Key domain sequence, which when deleted, negatively affects gyrase activity [47], [48]. Since this sequence does not form part of the Greek Key protein fold, only the Greek Key domain residues (534-559, and 735-739) were deleted, and replaced by a glycine residue. Therefore, only the effects of the Greek Key domain was investigated.

The *E. coli* GyrB △ Greek Key domain mutant (△GK) was successfully cloned, expressed and purified. The DNA cleavage activity of the △GK GyrB mutant was compared to the wild-type gyrase. The mutant had significantly lower DNA cleavage activity than the wild-type

enzyme. To try to enhance the activity of the mutant, magnesium, manganese or calcium ions were titrated against 200 nM *E. coli* gyrase GyrB △GK [fig. 4.3]. The bands were very faint for the mutant enzyme, due to low activity. The optimal concentration of magnesium ions was 20 mM, 10 mM for calcium ions, and 5 mM for manganese ions. In comparison, the literature value for optimal magnesium concentrations for DNA cleavage for the wild-type *E. coli* gyrase was between 2.5 and 5 mM $MgCl_2$ [91], 4-8 - fold lower than the mutant. The literature values were in agreement with the optimal metal ion concentrations for the wild-type enzyme presented here [fig. 4.3b].

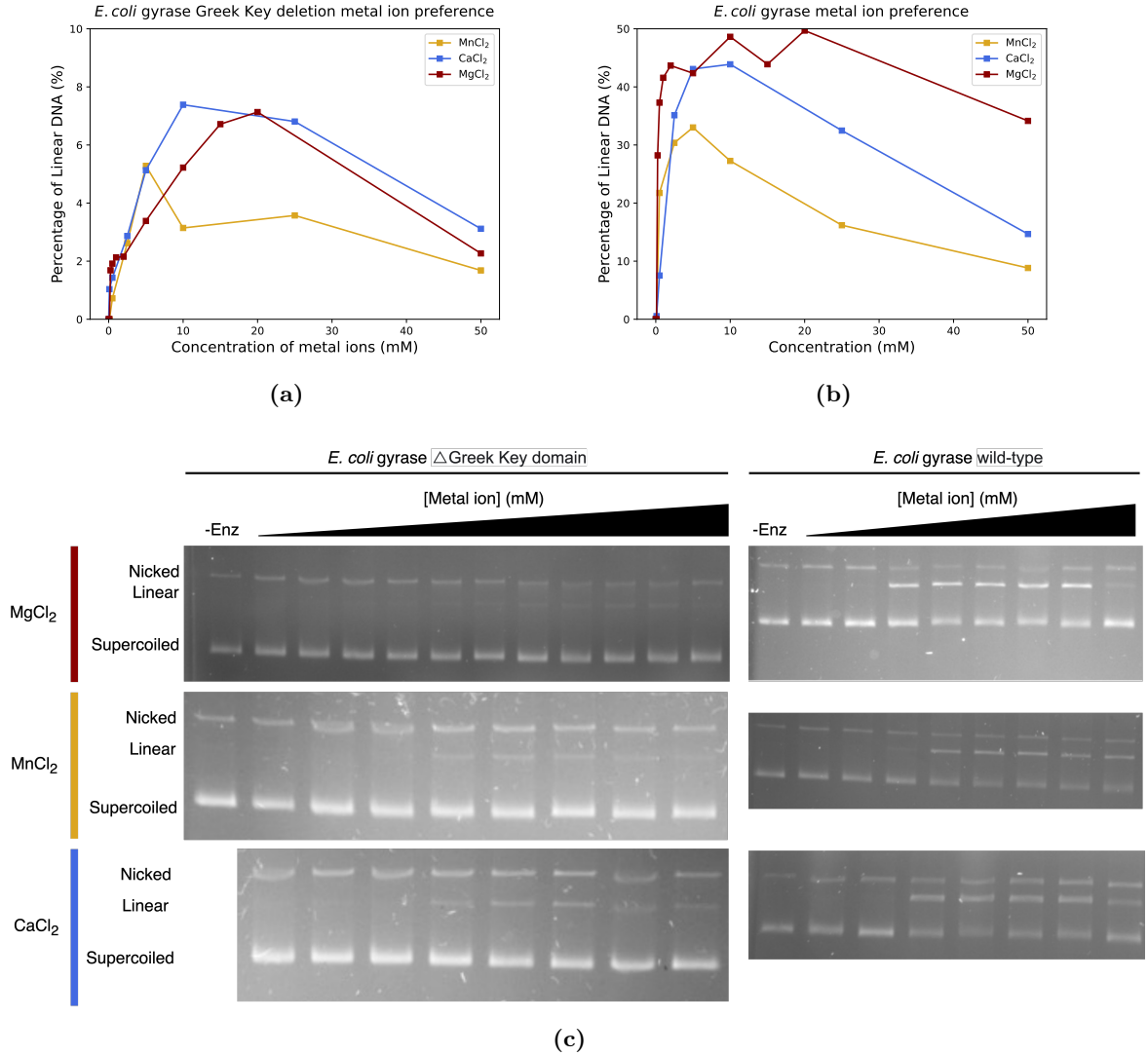

Figure 4.3: The divalent ion preference for the *E. coli* gyrase mutant with the Greek Key domain deleted with accompanying gels. A DNA cleavage reaction was set up with 10 nM of wild-type, or 200 nM of the mutant gyrase and 20 μM ciprofloxacin. Magnesium, manganese and calcium ions were titrated against the enzyme, from 0.1 - 50 mM of metal ions to observe DNA cleavage. **(a)** The metal ion preference for *E. coli* gyrase △Greek Key mutant, and **(b)**, the metal ion preference for *E. coli* gyrase wild-type. **(c)** The accompanying gels for **(a-b)**.

The Greek Key domain on GyrB has been suggested to control the position of the conserved YKGLG motif. The lysine residue has been proposed to be able to replace the role of catalytic metal ions to catalyse the first stage in DNA resealing, and also to prevent the re-cleavage of DNA before the T-segment has left via the exit-gate [46]. This lysine residue in some crystal structures points towards the DNA cleavage catalytic site [fig. 4.1]. The mutation of this lysine in yeast, (K603A) has also been shown to have high levels of DNA cleavage (particularly single-stranded) *in vitro* [45]. Another lysine in yeast, GyrA K720, when mutated to an alanine, showed the same phenotype as K603A - high levels of single-stranded DNA cleavage *in vitro* in comparison to the wild-type enzyme [187]. Therefore, these equivalent mutants in *E. coli* gyrase were investigated. K740A, which lies on the conserved GyrB YKGLG motif was tested. The corresponding lysine to yeast K603 in *E. coli*, GyrA K65, was difficult to clone and thought to be toxic (Cloning tried by the Ghilarov lab), therefore, GyrB E744 was tested, which forms a salt bridge with GyrA K65. The clones for *E. coli* GyrB K740A and GyrB E744A were gifted from the Ghilarov lab. Both mutants were successfully expressed and purified.

The DNA resealing activity of *E. coli* GyrB K740A and GyrB E744A were compared to the wild-type enzyme, by forming an equilibrium between cleaved and sealed gyrase-DNA complexes, and stimulating the DNA to reseal by the addition of the metal ion chelator EDTA [fig. 4.4]. In the absence of a compound with 50 nM of wild-type or gyrase GyrB K740A mutant, a similar percentage of DNA cleavage complexes formed. On addition of EDTA, the double-stranded DNA cleavage products resealed much slower with the gyrase GyrB K740A mutant compared to the wild-type enzyme. To achieve observable levels of DNA cleavage complexes with the gyrase GyrB E744A mutant, a 5-fold higher enzyme concentration was used. The cleavage complexes resealed for this mutant faster than the GyB K740A mutant, but slower than the wild-type enzyme [fig. 4.4a].

In chapter 3, there was a large increase in the nicked DNA on addition of EDTA to DNA cleavage complexes formed in the absence of compound, which did not correlate with the disappearance of double-stranded DNA cleavage. The nicked DNA was analysed on addition of EDTA to DNA cleavage complexes formed in the absence of drug for the *E. coli* gyrase GyrB K740A and GyrB E744A mutants [fig. 4.4b]. The wild-type enzyme had a large increase in the nicked DNA on addition of EDTA, whereas the nicked DNA did not change significantly throughout the DNA resealing assay for both of the mutants.

The DNA resealing activity was tested for the gyrase GyrB K740A and E744A mutants

in the presence of ciprofloxacin [fig. 4.4c]. For the GyrB K740A mutant, the DNA cleavage activity was lower than the wild-type, therefore, 50 nM was used for the wild-type enzyme, and 100 nM of gyrase GyrB K740A was used. On addition of EDTA to the DNA cleavage complexes, the GyrB K740A mutant resealed over 30 minutes, compared to the wild-type gyrase, where the linear DNA resealed after 5 minutes. Since the DNA cleavage activity of gyrase GyrB K744A was low, 250 nM of enzyme was used; the linear DNA resealed in 5 minutes. Looking at the nicked DNA during the DNA resealing assay, on addition of EDTA, nicked DNA accumulated and did not reseal after 30 minutes for the GyrB K740A mutant. Although the nicked intermediate increased during the assay, there is evidence of some single-stranded DNA resealing. Over 30 minutes, 35% of the double-strand DNA cleavage disapeared, and the nicked intermediate accumulated by 17% (proportions are for total DNA). Since the disappearance of linear DNA for the GyrB K740A mutant was slower than for the wild-type, and the resealing of the nicked intermediate was slow, the resealing of both DNA strands are affected by the GyrB K740A mutation [fig. 4.4d]. For the wild-type gyrase, and gyrase GyrB E744A, the nicked DNA resealed back to the no enzyme control base-line.

To conclude, the *E. coli* gyrase GyrB E744A mutant was significantly affected in cleaving DNA in the presence and absence of drug. The DNA resealing activity of *E. coli* gyrase GyrB K740A was significantly slower in comparison to the wild-type enzyme, with and without ciprofloxacin present.

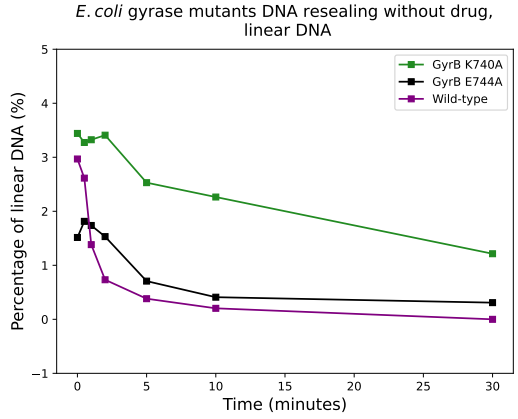

(a)

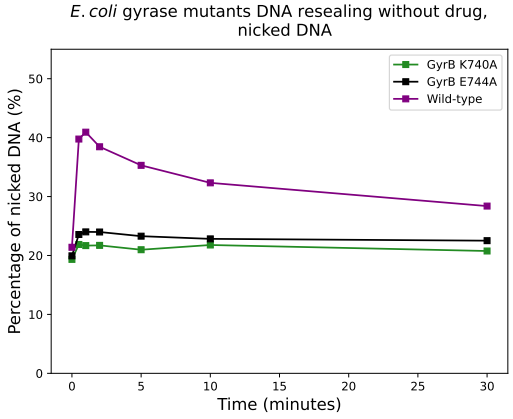

(b)

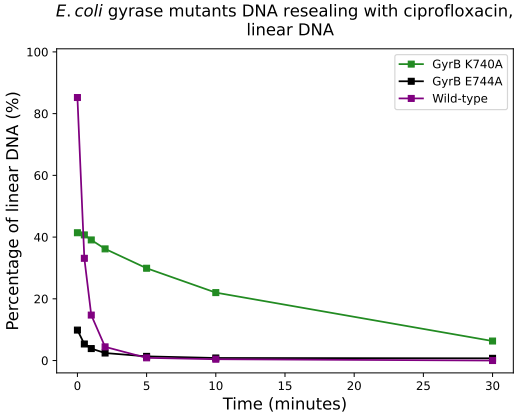

(c)

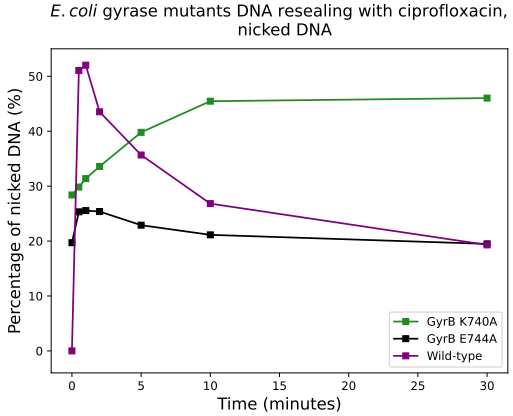

(d)

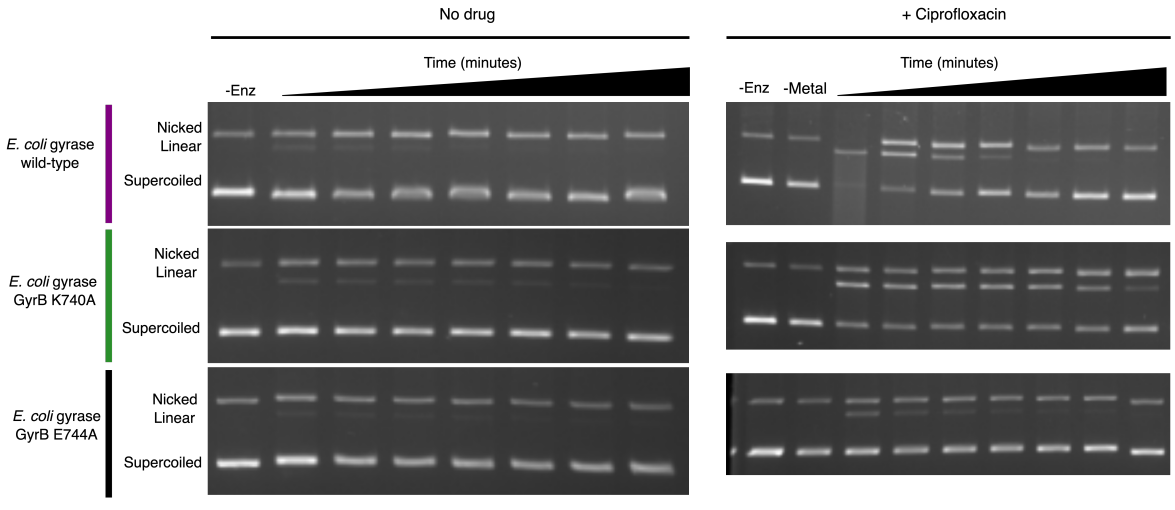

(e)

Figure 4.4: The DNA resealing activity of *E. coli* gyrase wild-type, gyrase GyrB K740A and GyrB E744A and accompanying gels. The DNA cleavage-resealing equilibrium was preformed in the presence of 1 mM $MgCl_2$, before addition of 5 mM EDTA. Time points were taken over 30 minutes, followed by trapping with SDS and digestion with proteinase K.

4.2.2 *S. aureus* gyrase mutants in the DNA cleavage and resealing reaction

The deletion of the Greek Key domain from *E. coli* gyrase resulted in a reduction of the DNA cleavage activity compared to the wild-type enzyme. The reduction in the DNA cleavage activity could either result from the importance of the Greek Key domain to the emzyme's activity, a misfolded protein, or a combination of both. *E. coli* gyrase has an insert of 58 amino acids in the middle of the Greek Key domain. *S. aureus* gyrase does not have this insert, and therefore deletion of this domain is more likely to result in correctly folded enzyme. Additionally, the Greek Key domain is commonly deleted from *S. aureus* gyrase core fusion constructs (GyrB fused to GyrA, with deletion of the N-termanal ATPase domain an C-terminal domain) to improve crystallographic resolution [39], which results in cleavage-competant enzyme. Therefore, the Greek Key domain was deleted in the full length *S. aureus* gyrase, to assess the role of the Greek Key domain to the DNA cleavage and DNA resealing reaction. Additionally, the lysine from the conserved YKGLG motif, located adjacent to the Greek Key domain was mutated (GyrB K581A). Since the Greek Key domain has been proposed to position the YKGLG motif, the DNA cleavage and resealing activities of these mutants were compared, to see if they had the same phenotypes.

The rate of DNA cleavage was compared for the *S. aureus* gyrase wild-type, gyrase △GK and gyrase GyrB K581A mutant in the presence of the DNA cleavage-stabilising drug ciprofloxacin during a timecourse assay [fig. 4.5, 4.6]. The double-stranded DNA cleavage with 5 nM of wild-type enzyme, and 15 nM of the two mutant enzymes were compared [fig. 4.5a-4.5b]. When the linear DNA was scaled to 100%, the wild-type reached equilibrium between cleaved and sealed DNA the fastest, dispite having the lowest concentration, followed by gyrase K581A, and then gyrase GyrB △GK.

During the DNA cleavage timecourse assay, the nicked DNA was compared [fig. 4.5c]. For the wild-type enzyme, the nicked intermediate was visible, increasing to 20% of the total DNA, which was then converted to double-stranded DNA cleavage. The nicked intermediate was significantly more apparent for the gyrase GyrB △GK mutant, increasing to 40%, which was then also converted to double-stranded DNA cleavage products. The nicked intermediate for gyrase GyrB K581A accumulated to the highest levels, rising to 55%. The accumulated nicked intermediate did not return to the baseline level like with the wild-type and gyrase △GK mutant. The gyrase GyrB K581A was able to convert single-stranded cleaved DNA into double-stranded DNA cleavage products, due to the accumulation of linear DNA [fig. 4.5a]. The

high accumulation of nicked DNA could be because the mutant enzyme is inefficient at either cleaving the gyrase-nicked DNA intermediate, or at resealing the gyrase-nicked intermediate, both of which suggest the enzyme may cleave and reseal DNA in a less coordinated fashion when K581 is mutated. Since the Greek Key domain was proposed to position the lysine from the YKGLG motif, it was expected that △GK and GyrB K581A would exhibit the same phenotypes for DNA cleavage. Therefore, the Greek Key domain is likely to have other roles than controlling the position of the lysine. The high levels of nicked DNA observed with *S. aureus* gyrase GyrB K581A was not observed with the equivalent mutant, *E. coli* gyrase GyrB K740A, highlighting the differences between the enzyme.

The ability for the *S. aureus* gyrase GyrB K581A mutant, and △GK mutant to reseal DNA cleavage complexes formed in the presence of the cleavage stabilising compound ciprofloxacin were compared to the wild-type enzyme [fig. 4.7, 4.6]. The wild-type gyrase resealed the linear DNA (double-stranded DNA cleavage complexes) within 5 minutes. There was no significant resealing observed with the gyrase △GK mutant, and a low rate of DNA resealing observed for the gyrase GyrB K581A mutant. The equivalent lysine mutant in *E. coli* gyrase, K740A, also had a slow rate of DNA resealing [fig. 4.4].

The high levels of the nicked intermediate which accumulated during the DNA cleavage timecourse reaction with *S. aureus* gyrase GyrB K581A [fig. 4.5] did not reseal on addition of EDTA [fig. 4.7b]. This suggests that the single-stranded break to sealed stage is impacted for this mutant. There was no nicked intermediate observed for the gyrase △GK mutant, because there was no disappearance in linear DNA [fig. 4.7a]. Since the rate of DNA cleavage and DNA resealing was affected by the gyrase △GK mutant and the GyrB K581A mutant, these mutants must have a role in both DNA cleavage and DNA resealing.

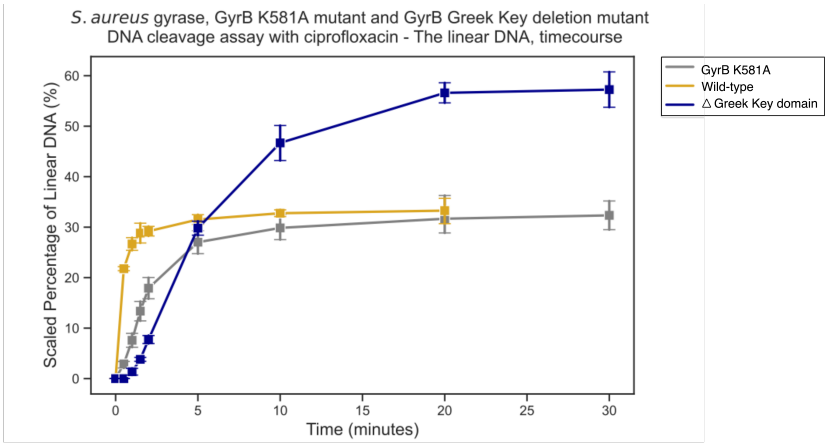

(a)

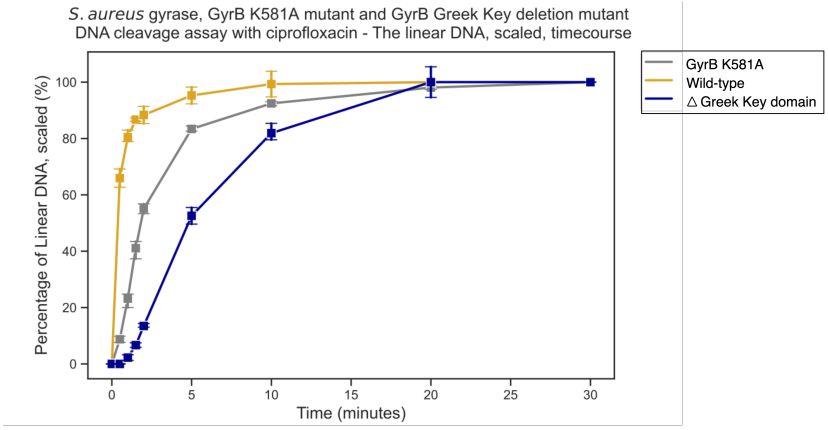

(b)

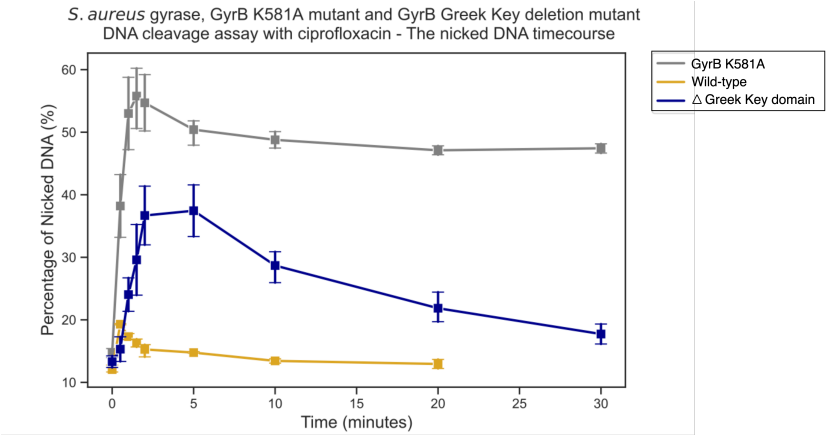

(c)

Figure 4.5: A comparison of the DNA cleavage reaction by *S. aureus* gyrase wild-type, GyrB K581A and GyrB △ Greek Key domain. 5 nM of wild-type *S. aureus* gyrase, and 15 nM of *S. aureus* gyrase GyrB K581A or △ Greek Key domain were assessed in a DNA cleavage assay in the presence of 20 μM ciprofloxacin and 4 mM $MgCl_2$. **(a)** The double-stranded DNA cleavage. **(b)** The double-stranded DNA cleavage, scaled. **(c)** The single-stranded DNA cleavage (nicked) DNA. The DNA cleavage assay samples were analysed on an agarose gel, and the bands quantified. The average from 3 data sets were plotted with error bars (confidence interval - 68%).

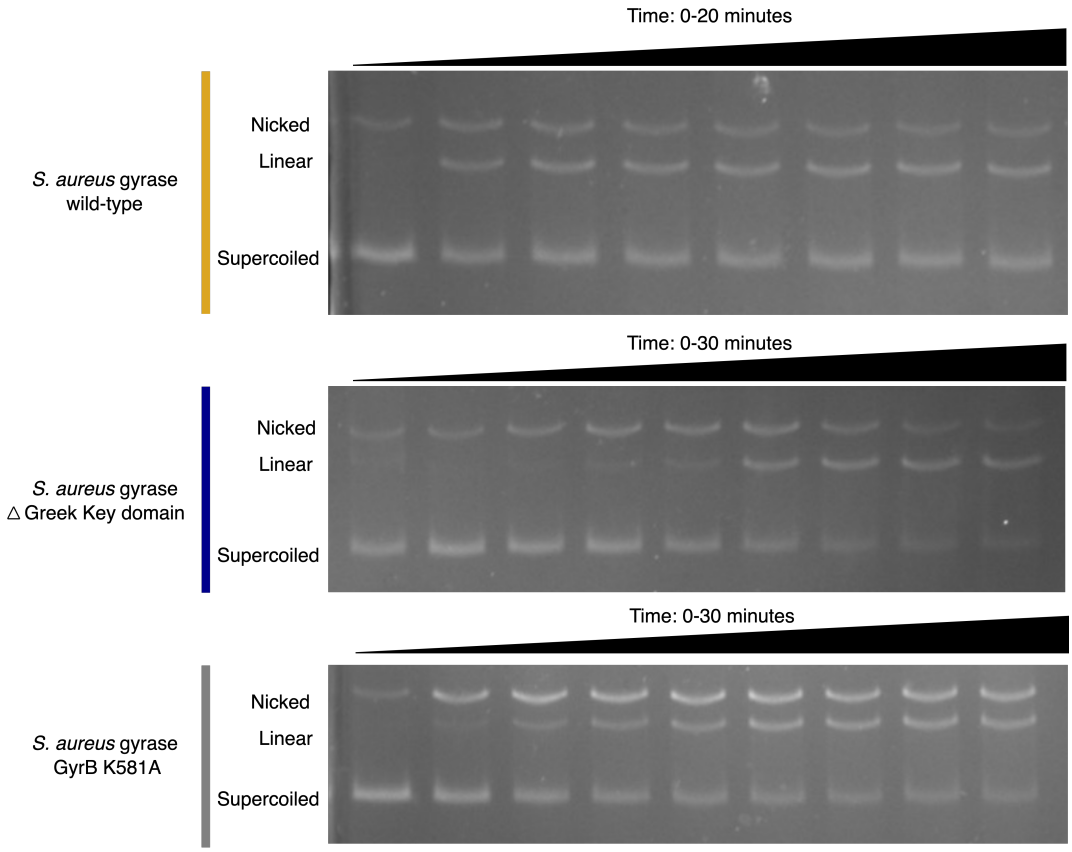

Figure 4.6: A comparison of the DNA cleavage reaction by *S. aureus* gyrase wild-type, GyrB K581A and GyrB △ Greek Key domain, accompanying gels. 5 nM of wild-type *S. aureus* gyrase, and 15 nM of *S. aureus* gyrase GyrB K581A or △ Greek Key domain were assessed in a DNA cleavage assay in the presence of 20 μM ciprofloxacin and 4 mM $MgCl_2$. The average from 3 data sets were plotted with error bars (confidence interval - 68%).

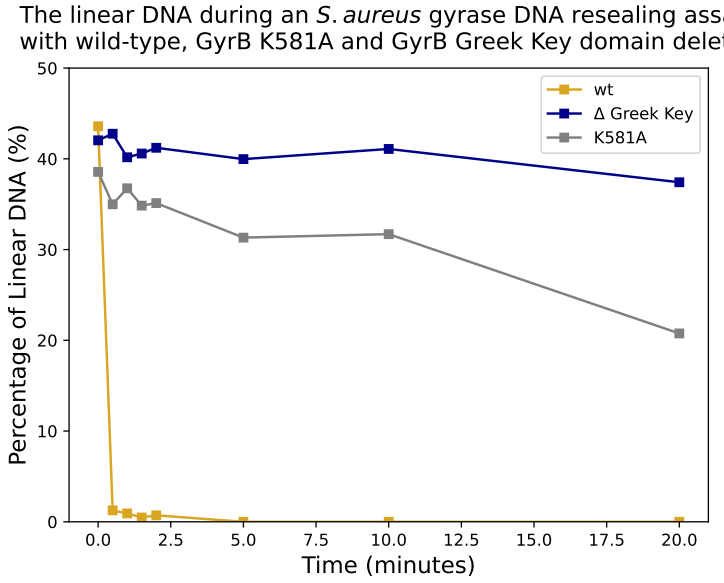

(a)

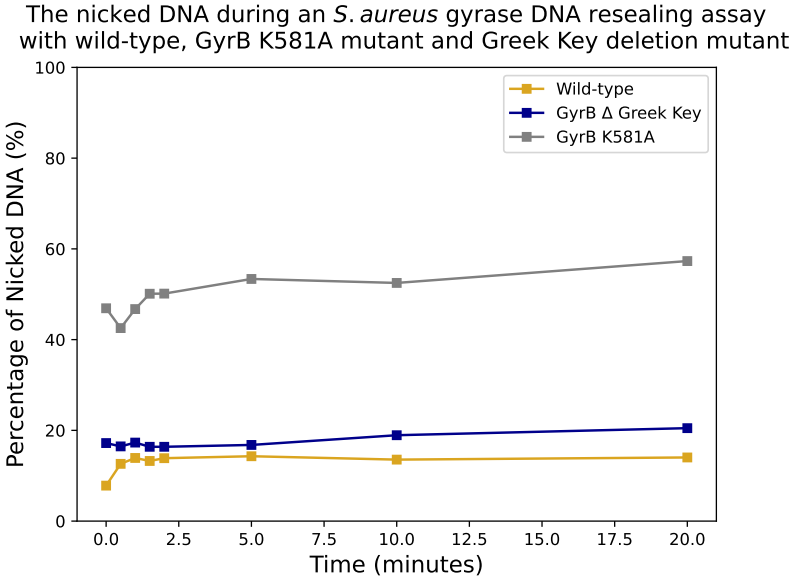

(b)

Figure 4.7: A comparison of the DNA resealing reaction by *S. aureus* gyrase wild-type, GyrB K581A and GyrB △ Greek Key domain. 10 nM of wild-type *S. aureus* gyrase, and 15 nM of *S. aureus* gyrase GyrB K581A or △ Greek Key domain were tested for their ability to reseal DNA in the presence of 20 μM of ciprofloxacin and 1 mM $MgCl_2$. DNA cleavage complexes were stimulated to reseal DNA by the addition of 5 mM EDTA, time points were trapped with SDS and digested with proteinase K. **(a)** The double-stranded DNA resealing. **(b)** The resealing of the nicked intermediate.

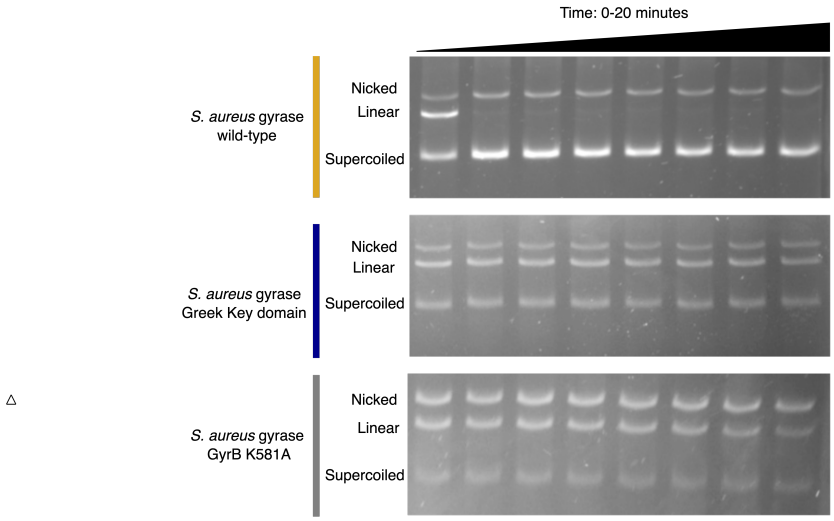

Figure 4.8: A comparison of the DNA resealing reaction by *S. aureus* gyrase wild-type, GyrB K581A and GyrB △ Greek Key domain, accompanying gels. 10 nM of wild-type *S. aureus* gyrase, and 15 nM of *S. aureus* gyrase GyrB K581A or △ Greek Key domain were tested for their ability to reseal DNA in the presence of 20 μM of ciprofloxacin and 1 mM $MgCl_2$. DNA cleavage complexes were stimulated to reseal DNA by the addition of 5 mM EDTA, time points were trapped with SDS and digested with proteinase K.

4.2.3 Extracting *E. coli* gyrase-associated DNA cleavage products from contaminating DNA cleavage products

During DNA resealing time course assays, where EDTA was added to DNA cleavage complexes formed in the absence of a compound, the nicked intermediate accumulated to higher levels than the associated decrease in linear DNA [fig. 4.2]. This result could be due to contamination in the sample. Therefore, to test to see whether the samples were contaminated with a nicking enzyme, the wild-type *E. coli* GyrA and GyrB subunits were tested individually for DNA cleavage activity, along with GyrB K740A and GyrB E744A. The DNA cleavage assay was performed in the absence of metal ions, and the samples were phenol extracted. Any DNA cleavage products in the phenol phase would be DNA cleavage products covalently attached to protein. DNA in the aqueous phase would be unlinked to proteins. When the subunits were assessed separately, there was no DNA cleavage activity which was topoisomerase associated [fig. 4.9].

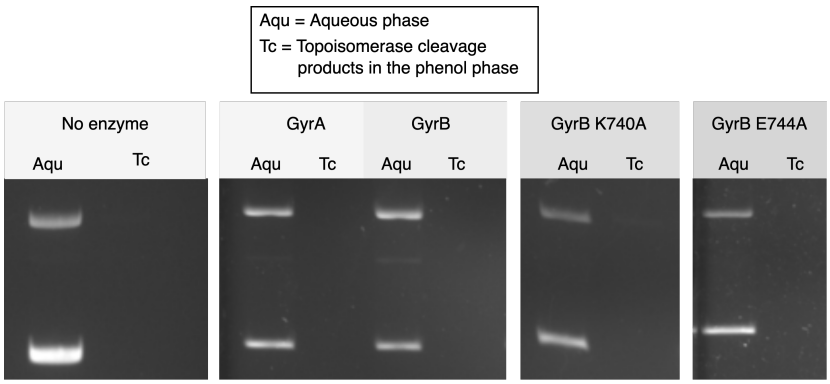

Figure 4.9: The activity of the individual *E. coli* gyrase subunit DNA cleavage activity. A DNA cleavage assay was performed with the individual *E. coli* gyrase subunits (GyrA or GyrB), and mutant subunits (GyrB K740A or GyrB E744A). 200 nM of enzyme was used. The DNA cleavage reaction was trapped with SDS, and the protein-linked DNA cleavage products were separated from aqueous DNA using phenol extractions. Samples were then digested with proteinase K and analysed on an agarose gel. Aqu = aqueous phase, containing non-protein linked DNA. Tc = topoisomerase cleavage products in the phenol phase.

The wild-type *E. coli* gyrase DNA cleavage activity was assessed in the presence and absence of 4 mM $MgCl_2$, to assess whether there was a nicking enzyme contamination in the sample [fig. 4.10]. In the presence of magnesium ions, there was a nicked and linear band in the phenol phase, showing gyrase-associated DNA cleavage. In the absence of magnesium ions, a faint band was present in the phenol phase, representing nicked DNA. This may represent metal-independent DNA cleavage, since this nicking was not observed when the individual GyrA and GyrB subunits were assessed for DNA cleavage activity [fig. 4.9]. Only when GyrA and GyrB were combined was this nicking activity observed in the absence of metal ions. Additionally, this no metal-ion DNA cleavage was not observed with gyrase GyrB K740A or gyrase GyrB E744A. This observed low levels of DNA nicking could also be due to the presence of low levels of contaminating metal ions in the enzyme or assay buffer samples. This could also suggest that GyrB K740A and E744A could be involved in DNA cleavage in the absence of metal ions.

Since the high levels of nicked DNA were observed on addition of EDTA [fig. 4.2], EDTA was added to the DNA cleavage complexes in the presence and absence of metal ions. The DNA cleavage complexes were incubated with EDTA for 0.5 and 10 minutes, to see whether the nicked DNA is covalently protein-linked (phenol phase), or in the aqueous phase (non-topoisomerase associated). In the phenol phase for the wild-type gyrase, on addition of EDTA and in the presence of metal ions, the significant levels of nicked DNA were present in the phenol phase, suggesting they are topoisomerase associated and not due to nicking enzyme contamination.

When the gyrase GyrB K740A and GyrB E744A mutants were assessed, high levels of nicked DNA was not observed on addition of EDTA, suggesting this high nicking activity, if it is coming from gyrase, may involve these residues.

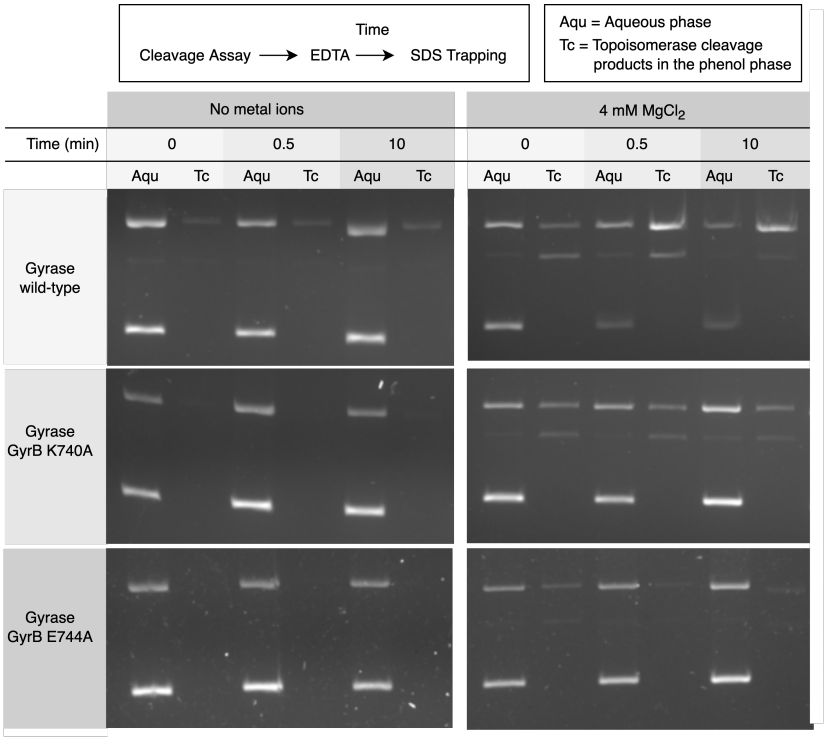

Figure 4.10: The DNA cleavage activity of *E. coli* gyrase, gyrase GyrB K740A and gyrase GyrB E744A mutant on addition of EDTA in the absence of compound. The DNA cleavage-resealing equilibrium was formed between the gyrase and the DNA in the presence or absence of 4 mM $MgCl_2$, followed by the addition of EDTA. 100 nM of *E. coli* gyrase wild-type, or gyrase E744A was used. 25 nM of *E. coli* gyrase GyrB K740A was usedSamples were trapped with SDS following a 0-minute, 0.5-minute, or 10-minute incubation with EDTA. The protein-linked DNA cleavage products were separated from aqueous DNA using phenol extractions. Samples were then digested with proteinase K and analysed on an agarose gel. Aqu = aqueous phase, containing non-protein linked DNA. Tc = topoisomerase cleavage products in the phenol phase.

To highlight the significant increase in nicked DNA on addition of EDTA to DNA cleavage complexes formed by *E. coli* gyrase in the presence of metal ions and in the absence of drugs, a DNA resealing timecourse was phenol extracted. This experiment was performed with *E. coli* gyrase enzyme purified from a different batch and different purification method from the experiment performed in [fig. 4.10], in order to rule out a faulty enzyme batch [fig. 4.11]. The DNA cleavage products were present in the phenol phase (topoisomerase-associated), and the DNA did not reseal following an incubation with EDTA for 4 hours.

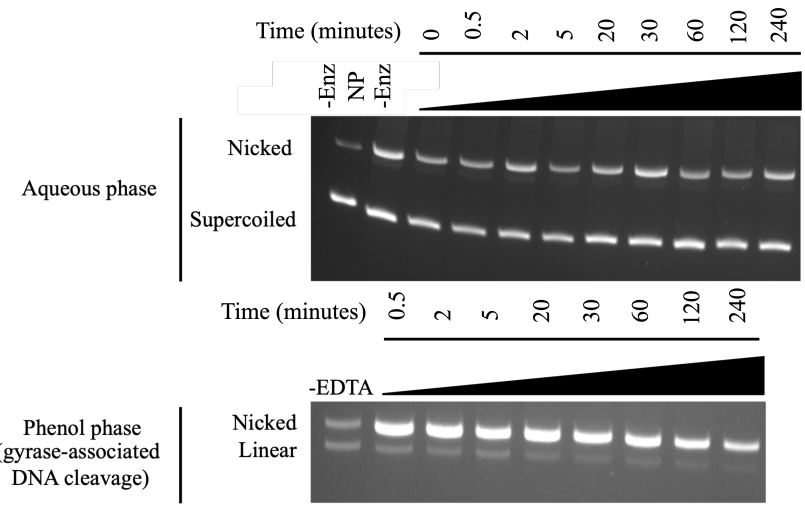

Figure 4.11: The DNA resealing activity of *E. coli* gyrase, without drug present. A DNA cleavage-resealing equilibrium was formed between 250 nM enzyme with 2 mM $MgCl_2$. 10 mM EDTA was used to stimulate DNA resealing. The DNA cleavage complexes were incubated with EDTA for 4 hours. The protein-linked DNA cleavage products were separated from aqueous DNA using phenol extractions. Samples were then digested with proteinase K and analysed on an agarose gel. The aqueous phase contains non-protein linked DNA. The phenol phase contains protein-linked (or, topoisomerase-linked) DNA cleavage products. -Enz = no enzyne control non phenol extracted. -Enz NP = no enzyme control aqueous phase.

4.2.4 Performing phenol extractions on DNA cleavage and resealing assay samples generated from *S. aureus* gyrase

The high levels of nicked DNA observed on addition of EDTA to a DNA cleavage reaction in the absence of a drug was also observed with *S. aureus* gyrase in chapter 3 [fig. 3.18]. Therefore, the DNA cleavage complexes formed by *S. aureus* gyrase in the addition and absence of metal ions and EDTA were phenol extracted, to help separate the samples away from the background nicked contamination from the plasmid substrate, and to see if there was any nicking enzyme contamination [fig. 4.12]. In the sample of the DNA cleavage complexes formed in the presence of metal ions, a strong band representing the double-stranded DNA cleavage, and a slightly fainter band representing the nicked DNA was observed in the phenol phase. On addition of EDTA to the sample, the ratio of nicked and linear DNA was altered; an intense band was observed for the nicked DNA, which was brighter than the linear DNA band before the addition of EDTA.

In the phenol extraction experiments with *E. coli* gyrase, there was a faint nicked band present in the phenol phase when no metal ions were added to the DNA cleavage assay. This experiment was repeated with *S. aureus* gyrase. When no metal ions were added to the DNA cleavage reaction, there was a strong nicked and faint linear band present in the phenol phase,

suggesting this DNA cleavage is gyrase-associated. The intensity of the nicked and linear bands were comparable to when EDTA was added to *S. aureus* gyrase DNA cleavage complexes in addition of metal ions. This suggests that there are differences between the *S. aureus* and *E. coli* gyrase enzymes when cleaving DNA at no, or low metal ion concentrations. It is noted that this cleavage is observed only at very high enzyme concentrations.

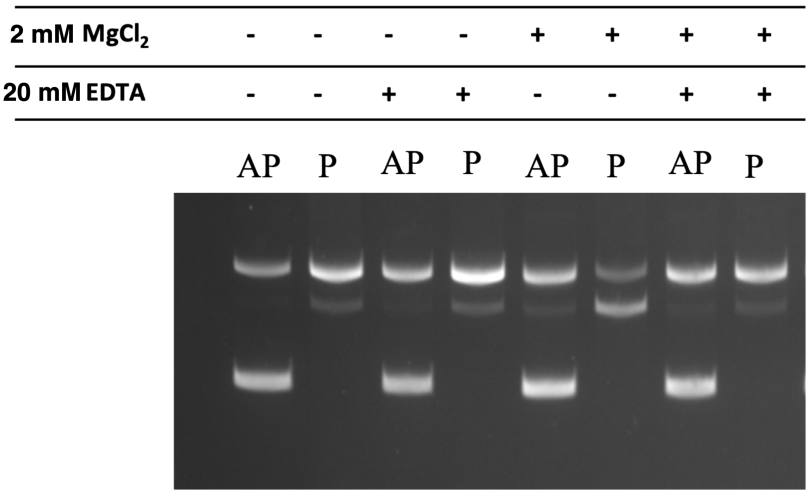

Figure 4.12: The DNA cleavage activity of the wild-type *S. aureus* gyrase in the presence and absence of magnesium ions and EDTA. The DNA cleavage assay with 250 nM enzyme were run in the presence or absence of 2 mM $MgCl_2$, and the presence or absence of 20 mM EDTA. For samples where EDTA was added, the samples were trapped with SDS after a 30-second incubation period. The protein-linked DNA cleavage products were separated from aqueous DNA using phenol extractions. Samples were then digested with proteinase K and analysed on an agarose gel. AP = aqueous phase, containing non-protein linked DNA. P = topoisomerase cleavage products in the phenol phase.

The *S. aureus* gyrase GyrB K581A mutant DNA cleavage and resealing samples were phenol extracted [fig. 4.13]. In the presence of metal ions, because *S. aureus* gyrase GyrB K581A is deficient in DNA resealing, the observed DNA cleavage activity is very high, therefore, for phenol extractions with metal ions, 15 nM of enzyme was used, in comparison to 250 nM with the wild-type enzyme. On addition of EDTA to DNA cleavage complexes formed in the presence of metal ions, the nicked DNA did not increase to very high levels, as was observed with the wild-type *S. aureus* gyrase enzyme. *E. coli* gyrase GyrB K740A also did not have high increases in nicked DNA on addition of EDTA to DNA cleavage complexes formed with magnesium ions with no compound [fig. 4.10]. *S. aureus* gyrase GyrB K581A also had high levels of DNA nicking in absence of metal ions, which was also observed with the wild-type *S. aureus* gyrase, but not with the *E. coli* gyrase K740A mutant. This suggests that the *S. aureus* and *E. coli* gyrase lysine residue from the YKGLG motif may contribute differently to the DNA cleavage and resealing reaction.

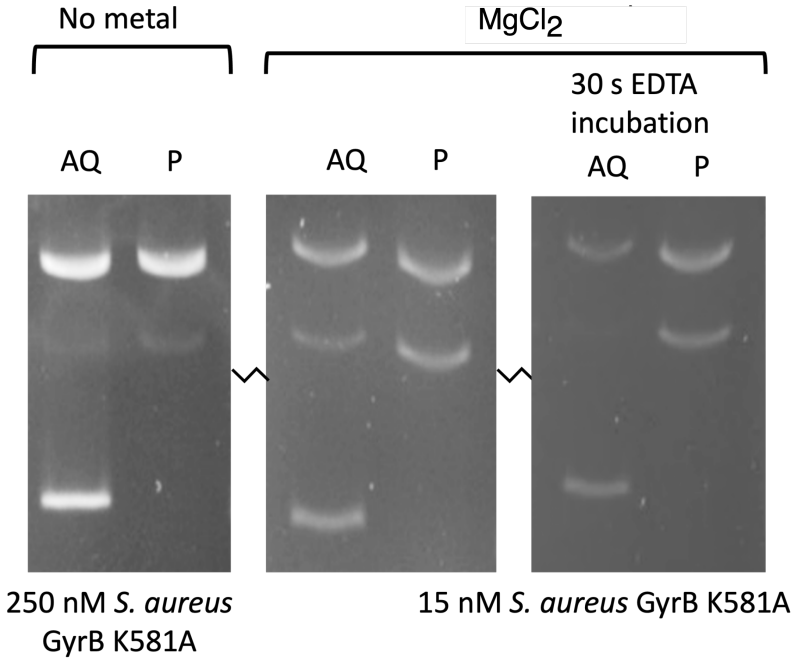

Figure 4.13: The DNA cleavage activity of the *S. aureus* gyrase mutant GyrB K581A in the presence and absence of magnesium ions and EDTA. The DNA cleavage assay was run in the presence or absence of 2 mM $MgCl_2$, and the presence or absence of 10 mM EDTA. For samples where EDTA was added, the samples were trapped with SDS after a 30-second incubation period. For samples which contained metal ions, 15 nM of gyrase was used. For samples which did not contain metal ions, 250 nM of enzyme was used. The protein-linked DNA cleavage products were separated from aqueous DNA using phenol extractions. Samples were then digested with proteinase K and analysed on an agarose gel. AP = aqueous phase, containing non-protein linked DNA. P = topoisomerase cleavage products in the phenol phase.

4.3 Conclusions and future work

4.3.1 The role of the Greek Key domain and the lysine residue from the YKGLG motif

The Greek Key domain is a disordered domain which lies below the TOPRIM and WHD domains which bind the gate DNA and make up the DNA cleavage and resealing sites. When the T-segment has passed through the DNA-gate, the Greek Key domain has been proposed to undergo a conformational change to orientate a conserved motif, YKGLG located a few amino acids after the Greek Key domain. The lysine residue from this motif when mutated in yeast led to high levels of single- and double-stranded DNA cleavage [45]. The lysine residue was also proposed to be able to replace the role of catalytic metal ions [46], (which contradicts the findings from chapter 3) and also prevent the recleavage of DNA before the T-segment has left gyrase [46].

The results in this chapter suggests that the mutation of the lysine residue from the YKGLG motif from *E. coli* and *S. aureus* gyrase leads to high levels of single- and double-stranded DNA cleavage, which agrees with the literature findings with yeast topoisomerase II. To build on the results found in the literature, these results suggest that mutation of the lysine negatively affects both the rate of DNA cleavage and DNA resealing. Previously, the lysine had only been proposed to affect the ability of type II topoisomerases to reseal DNA. This lysine residue affects the DNA cleavage and resealing of both strands of the DNA, however the enzyme is particularly inefficient at cleaving and resealing the nicked intermediate substrate. The lysine residue may be involved in coordination between the two DNA cleavage and resealing active sites. Due to the lysine's proximity to the active site, the lysine may have a role in coordinating the DNA, metal ions, DNA or metal coordinating amino acids.

The *E. coli* gyrase Greek Key domain mutant may be misfolded due to low DNA cleavage activity. The Greek Key domain in *E. coli* gyrase has a 58-amino acid insert within the Greek Key domain, which was not deleted for experiments in this chapter. If the Greek Key domain mutant was to be redesigned, a longer linker could be used, since each region of the Greek Key domain was replaced with a single glycine.

The Greek Key deletion mutant in *S. aureus* gyrase affected the rate of DNA cleavage and resealing. Both the cleavage of the first and second DNA strands were affected by this mutation. The Greek Key domain deletion mutant was slower at accumulating double-stranded DNA cleavage products than the gyrase GyrB K581A mutant. Although the gyrase Greek Key domain mutation was slower at generating double-stranded DNA cleavage, the cleavage of both DNA strands was more coordinated than the GyrB K581A mutant, since once the DNA cleavage and resealing reaction reached equilibrium, the nicked DNA returned to the baseline level. It is interesting how the lysine mutant and Greek Key domain deletion mutations did not negatively affect DNA cleavage and resealing equally. The Greek Key domain may have additional roles towards DNA cleavage and resealing. To investigate whether deleting the Greek Key domain deletion inhibited the action of the lysine residue, a double mutation of the Greek Key domain deletion, and K581A could be made.

4.3.2 The effect of *E. coli* GyrB E744A to the DNA cleavage and resealing reaction

A lysine mutation in human topoisomerase IIα, K743N was found in human tumour cells, the mutation aids genomic duplications, making the cell predisposed to oncogenic mutations

[187]. The equivalent mutation in yeast topo II led to high levels of single-stranded DNA cleavage *in vitro*. The cloning for this mutation in human topo IIα [187] and *E. coli* gyrase was challenging and thought to be toxic (cloning was tried by the Ghilarov lab). Therefore, this chapter assesses the activity of *E. coli* gyrase GyrB E744A, which forms a salt-bridge with the GyrA lysine 65 in structures, and therefore thought to control the position of the lysine. The *E. coli* gyrase GyrB E744A mutant did not exhibit the high levels of nicked DNA like observed with yeast topo II K720N. The mutant could be misfolded, or, the salt bridge between the lysine may not be as important as evidenced from structures.

In a cryo-EM structure with human topo IIα, DNA and the cleavage-stabilising drug gepotidacin (6RKU) [36], the lysine residue (K743) points at the conserved and essential arginine, which is located adjacent to the catalytic tyrosine. In other structures, such as the *S. aureus* gyrase crystal structure with uncleaved DNA (2XCR) [46], the lysine residue forms a salt-bridge with a glutamate residue. The lysine residue may be involved in the coordinated control of DNA cleavage, since single-stranded DNA cleavage was a phenotype with the lysine mutant [187]. In structures where the DNA is uncleaved, the salt-bridge was intact, and in structures with cleaved DNA, the lysine points closer towards the arginine.

4.3.3 Metal-independent activity of *E. coli* and *S. aureus* gyrase

When DNA cleavage assays by *S. aureus* gyrase in the absence of metal ions were phenol extracted, high levels of nicked DNA were observed, and low levels of nicking were observed with *E. coli* gyrase. Additionally, high levels of nicking was observed on addition of EDTA to the DNA cleavage complexes formed in the presence of metal ions for *E. coli* or *S. aureus* gyrase. This activity could be due to metal-independent DNA cleavage activity by the enzyme. Metal-independent DNA cleavage activity has not been identified in the literature for type II topoisomerases. This could be because the majority of DNA cleavage experiments with these enzymes are performed at a lower enzyme concentration with cleavage-stabilising drugs. The high levels of nicking were only observed at high concentrations of gyrase. Additionally, the low levels of nicking activity with *E. coli* gyrase with no metal is only apparent when the samples were phenol extracted, since the nicking would not be observed above the background nicked band from the original plasmid substrate. The *S. aureus* gyrase no metal activity was much more significant than with *E. coli* gyrase, which could be due to the differences in the sequence, structure, or assay buffer conditions. Since metal ions catalyse DNA cleavage and resealing, metal ions could significantly enhance the enzyme activity by increasing the probability of DNA

cleavage and resealing, but not be strictly required. The premise for no-metal activity with gyrase may achievable, since some type I topoisomerases do not require metal ions to cleave and reseal DNA, and catalyse DNA cleavage and resealing using amino acids [170], [94].

The nicking activity in the absence of metal ions to DNA cleavage assays could be due to low levels of contaminating metal ions from the enzyme prep or assay buffers, which could support DNA cleavage. This metal ion concentration is likely to be very low, since no metal ions are added during the protein purification process. For future experiments, the chances for contaminating metal ions in the DNA cleavage reaction which could catalyse DNA cleavage should be minimised. The levels of DNA nicking in the absence of metal ions, and a DNA cleavage assay in the presence of metal ions on addition of EDTA were the same for *S. aureus* gyrase. Since EDTA forms an equilibrium with solution to bind metal ions, there would be a low level of metal ions in solution. Contaminating metal ions could be removed by adding metal chelating beads such as Chelex 100 resin. Alternatively, this apparent no metal activity could be achieved with other metal ions/salts in the buffer, such as potassium ions, which is not a divalent metal ion.

4.3.4 Similarities and conclusions drawn from the metal ion mechanisms between the type I and type II topoisomerases

The conclusions drawn from these first two results chapters were applied to design models for the metal ion catalysis of DNA cleavage and resealing by type II topoisomerases, and similarities with the type I topoisomerases were considered. For example, the metal ions have been considered to fulfil the same role during strand scission and strand ligation in type II topoisomerases. However, some type I topoisomerases, such as human top3B, have different mechanisms for catalysing the strand scission and ligation reactions. This may hold true for gyrase, because this thesis concluded that the DNA cleavage and resealing reactions of gyrase have different metal ion requirements with respect to the concentration of free metal ions in solution.

Top3B cleaves DNA which is catalysed either by a divalent metal ion, or a conserved lysine residue. The reverse reaction, DNA ligation, requires the presence of the lysine residue and a catalytic metal ion [17]. Topo3B was proposed to need both the charge from lysine and a metal ion for DNA ligation to bring the two broken strands need into proximity. The $3'$ hydroxyl needs to be moved into position to attack the phosphotyrosyl bond. During DNA cleavage by top3B, the DNA backbone is intact and therefore there are less components that require

positioning.

The position of the lysine and metal ion in topo 3B does not align with the position of the A- and B-site metal ion in type II topoisomerases. The lysine and metal ion in top3B has similarities to the canonical two-metal ion mechanism during DNA resealing, where two metal ions coordinate with the same phosphate. Type II topoisomerases do not use the canonical two-metal ion mechanism, because only one metal ion coordinates the scissile phosphate.

The type II topoisomerases have a conserved lysine residue (which is not homologous to the top3B lysine) located on the YKGLG motif on the TOPRIM domain. Due to the flexibility of the lysine residue, and the close proximity to the DNA cleavage site, the type II topoisomerase lysine may play a similar role to the conserved lysine in top3B. In a *S. aureus* gyrase crystal structure [39], this lysine residue points between the scissile and non-scissile phosphate [fig. 4.1]. The lysine residue is not visualised in this position in the cleaved or pre-cleavage conformations in other crystal structures, because the domain adjacent to the YKGLG motif in these structures is deleted to improve resolution. The flexible loop on which the lysine residue resides is likely in an artificial conformation in these structures. Additionally, the lysine is not pictured coordinating DNA in the full-length *E. coli* gyrase cryo-EM structures [36].

Although the position of the conserved lysine residue from the YKGLG motif is relatively unknown during the type II topoisomerase catalytic cycle, the lysine residue may be implicated in a similar role during DNA cleavage or resealing to the lysine from the top3B enzyme. The lysine residue in type II topoisomerases, along with the A-site catalytic metal ion may both be required to position the $3'$ hydroxyl group on the cleaved DNA strand during DNA resealing. The $3'$ hydroxyl group must be in the proximity of the phosphotyrosyl linkage for ligation. The lysine and A-site metal ion may also both aid stabilisation of the negative charge in the pentavalent transition state formed during DNA religation. For top3B, either a metal ion or a lysine residue is required to catalyse DNA cleavage. This may also be the case with the type II topoisomerases during catalysis of DNA cleavage. Prior to DNA cleavage, the DNA backbone is intact, and therefore there would be no need to bring DNA strands together.

4.3.5 The role of a conserved lysine in the DNA cleavage and resealing equilibrium of DNA gyrase

In order to investigate the role of the conserved lysine residue in the DNA cleavage and ligation reaction of gyrase, the lysine was mutated to alanine. This thesis finds that mutation of the lysine residue from the YKGLG motif in both *E. coli* and *S. aureus* gyrase inhibits the rate of DNA resealing, leading to the accumulation of DNA-cleavage complexes. Mutation of the lysine residue on gyrase disproportionately affected DNA resealing compared with DNA cleavage. Therefore, these findings fit the topo 3B model, where a lysine residue and metal ion are both required for DNA resealing, but not DNA cleavage. Further, deletion of the Greek Key domain in *S. aureus* gyrase also led to inhibition of DNA resealing. Deletion of the Greek Key domain in gyrase may be unable to orientate the lysine from the YKGLG motif, which directly proceeds the domain.

Both double-stranded and single-strand DNA breaks accumulated on mutation of the lysine residue or deletion of the Greek Key domain in gyrase, which was skewed towards single-strand DNA cleavage intermediates. For the wild-type enzyme, on cleavage of the first strand of DNA, the DNA is more flexible, which increases the propensity for cleavage of the second strand. When the lysine residue is mutated, the lysine would be unable to position the DNA broken ends with respect to the catalytic tyrosine. Therefore, this work proposes a model where the first DNA cleavage event may occur in absence of a lysine residue, since the DNA has low flexibility. The second strand scission event is more efficient with the lysine residue present, which may be due to the lysine coordinating the DNA phosphate (either the scissile or non-scissile phosphate). Following the first strand scission event, the DNA is more flexible and therefore requires additional coordination for the second strand scission event.

4.3.6 Gyrase asymmetry during the DNA cleavage reaction

The idea of DNA flexibility altering the DNA cleavage and resealing properties of singularly nicked DNA can also be applied to the findings in chapter 3. On addition of the metal ion chelator EDTA to stimulate DNA resealing of gyrase-DNA cleavage complexes in the absence of a DNA cleavage-stabilising compound, nicked DNA cleavage complexes accumulated. This nicked DNA did not correlate with the decrease in the double-stranded DNA cleavage complexes. The single-strand DNA product instead accumulated due to the first stage of strand scission, but not the second stage, proceeding at low concentrations of metal ions. These findings can be

applied to a possible metal ion model, where the role of the B-site metal ion during anchoring and positioning of the DNA for cleavage via coordination of the non-scissile phosphate is more critical for the second DNA cleavage, due to increased DNA fexibility. The DNA would be more flexible following cleavage of one DNA strand, which influences the DNA cleavage at the other site. This model would favour a one metal ion model for the first strand scission event, since the model proposes that the B-site metal ion would not be essential for strand-scission. The model would fit a one metal ion, or a two metal ion model for the scission of the second strand, since the role of the B-site metal ion may be critical for this cleavage.

4.3.7 Future mutational analysis of type II topoisomerases

The residues around the DNA cleavage and resealing sites have been investigated in this chapter. The roles of other domains in type II topoisomerases to the DNA cleavage and resealing reaction have not been fully investigated. DNA gyrase must coordinate the opening and closing of three gates with the cleavage and resealing of DNA. Gyrase is able to perform DNA cleavage and resealing in absence of ATP, however, DNA cleavage is enhanced in the presence of ATP. Therefore, the enzyme must have conformational changes to translate the binding, hydrolysis and dissociation of ATP from the enzyme to the DNA gate. In *E. coli* topo IV, three ParE mutations, G110S, S123L and T201A all inhibited the DNA religation of DNA cleavage complexes [188]. These mutations were all located on the ATPase domain. For future mutational investigations of the DNA resealing reaction, it would be interesting whether equivalent mutations in gyrase also affect DNA religation, since ATP is essential for DNA cleavage in Topo IV, but not for DNA gyrase.

Chapter 5

The roles of gyrase residues in coordinating the catalytic divalent metal ions during DNA cleavage and DNA resealing

5.1 Introduction

5.1.1 Biochemical evidence for the metal ion mechanism for DNA cleavage by type II topoisomerases

Type II topoisomerases require divalent metal ions to catalyse the nucleophilic attack of the catalytic tyrosine on the scissile phosphate to cleave DNA. The type II topoisomerases have two DNA cleavage-religation sites per enzyme complex - one for each strand scission event. At the DNA cleavage site, there are two metal ion binding sites, the A-site, or catalytic metal-binding site, and a non-catalytic B-site [88], [39]. Based on biochemical evidence, two metal ions were proposed to catalyse the DNA cleavage and resealing reaction, where both the A- and B-site would be occupied during catalysis [88]. DNA cleavage levels by the *E. coli* gyrase GyrB D498A mutant, which is a metal-binding residue that coordinates the B- and A-site metal ions, were slightly enhanced in the presence of calcium and magnesium, compared to the sum of the DNA cleavage from the individual metal ions. Additionally, DNA relaxation was significantly enhanced for the *E. coli* gyrase GyrB D500H mutant in the presence of magnesium and calcium, compared with the sum of the relaxation catalysed with either magnesium or calcium. GyrB D500 is a residue which cooridinates the B-site metal ion. Since two metal ions were contributing synergistically to the enzyme's activity, a two-metal ion model was proposed. Both the GyrB D500H and D498A mutants had altered the enzyme's metal ion preferences and the effects of activity enhancement were not observed with the wild-type gyrase.

Further biochemical data have supported the enhancement of enzyme activity in the presence of two different metal ions from other type II topoisomerases - topo IV and human topoisomerase II α, using short radio-labeled DNA strands [98], [89]. Additionally, titration of metal ions

in a DNA cleavage assay resulted in a sigmoidal curve, suggesting a biphasic concentration dependence for metal ions [98]. The shape of the curve represented the binding of each metal ion to the A-site and the B-site. Together, this provided strong evidence that type II topoisomerases require two simultaneously-present metal ions to cleave and reseal DNA.

An additional metal ion model was proposed, where only one metal ion would be sufficient to support the DNA cleavage and resealing reaction. Crystallographic structures of type II topoisomerases suggested only one divalent metal ion would be required to catalyse the DNA cleavage and resealing reaction [39]. The authors suggest that the biochemical data supporting the two-metal ion model can be explained by an alternative hypothesis. To explain the enhancement of activity when two different divalent metal ions are present, asymmetrical metal ion binding at the DNA cleavage sites was proposed, where only one metal ion is present at the catalytic metal ion binding site (A-site) per enzyme. When a metal ion is present at the A-site on one side of the enzyme, on the other side of the enzyme, the B-site is occupied, and a different divalent metal ion occupies the A-site and the B-site [fig. 5.1]. This may be required to switch the enzyme from a state which can efficiently bind DNA, to a conformation which can cleave DNA, since calcium ions have been shown to enhance DNA binding, and magnesium/manganese ions are more sufficient to support DNA cleavage [175]. Bax and colleagues suggest an additional explanation, where metal ions have a 'ping-pong' mechanism. One type of metal ion, such as calcium ions may be required to assist orientating and binding the DNA, followed by dissociation. A different metal ion may then associate and perform the catalysis of DNA cleavage. A third solution could be that metal ions may bind elsewhere on the enzyme, providing a structural or regulatory role, which could contribute towards the enhancement of the enzyme's activity.

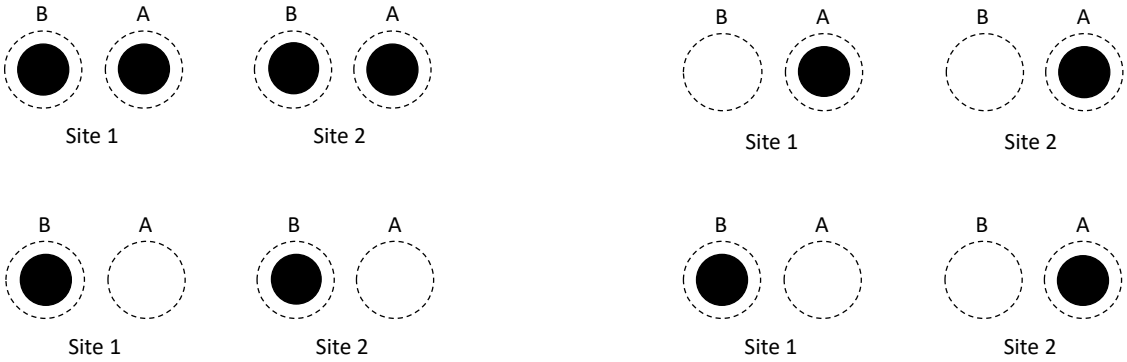

Figure 5.1: Possible positions of the catalytic metal ions during catalyis of type II topoisomerases. There are two metal-ion binding sites per active site, and two active sites on a type II topoisomerases complex. The metal-binding A-site is the catalytic site, and the B-site is the non-catalytic site. Both metal binding sites could be simultaneously occupied by metal ion, or there could be zero/one metal ion at each DNA cleavage site. Metal ion binding at each catalytic site may not be symmetrical.

5.1.2 Asymmetric *E. coli* gyrase mutants

The hypothesis proposed by Bax and colleagues, where metal ions may bind asymmetrically with respect to the two gyrase cleavage sites [39], was explored. Asymmetric *E. coli* gyrase mutants were investigated here, where mutations were introduced on only one side of the gyrase complex, and the other side of the gyrase was wild-type [fig. 5.2]. The asymmetric DNA gyrase complex was first developed by Gubeav and colleagues [189]. The gyrase complex consists of a GyrB-GyrA fusion co-purified with GyrA (BA·A) by tandem affinity purification. The gyrase complex can then reconstituted by the addition of GyrB (BA·A + GyrB), forming a heterodimeric enzyme

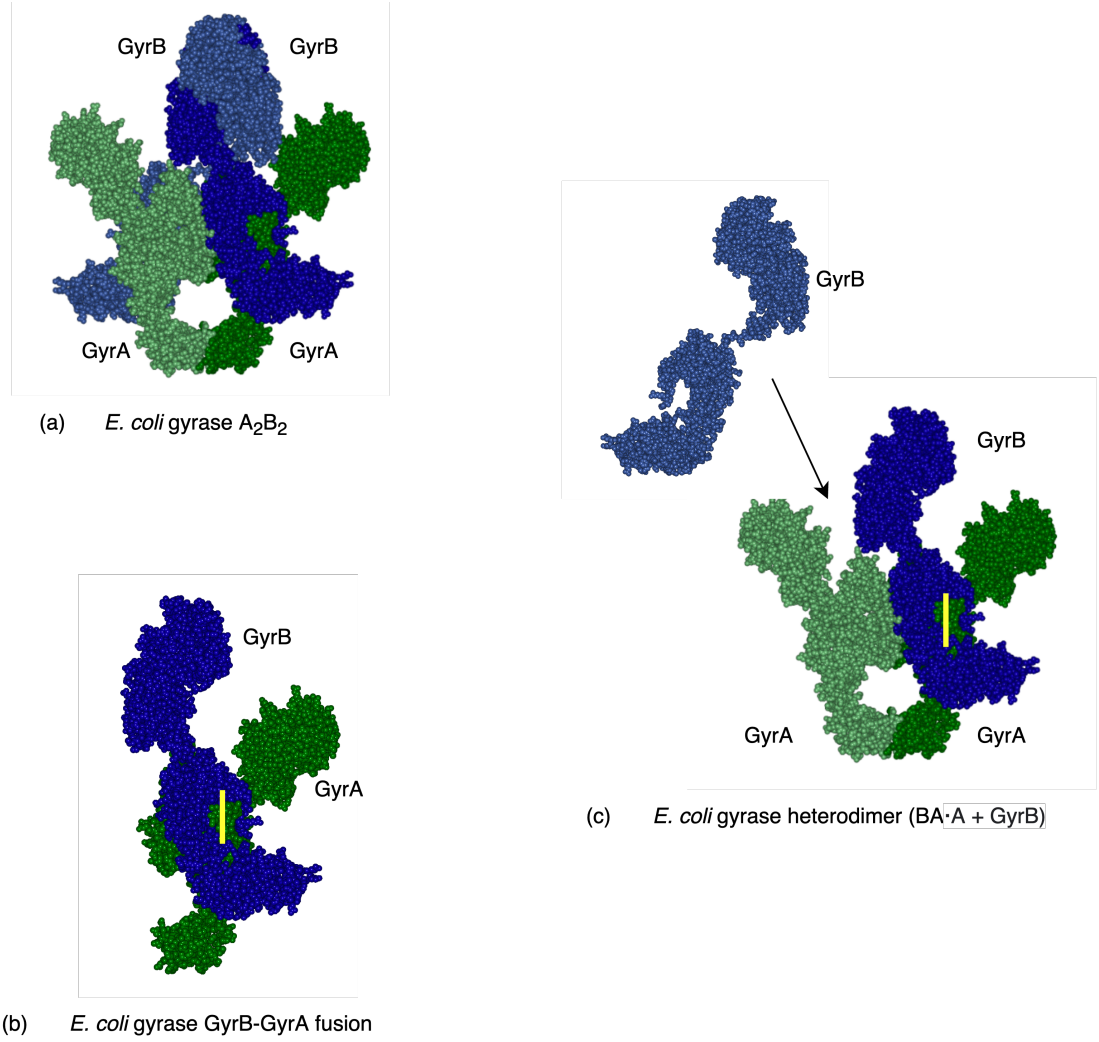

Figure 5.2: The *E. coli* gyrase A_2B_2 construct, the GyrB-GyrA fusion and the heterodimer constructs. (a) The *E. coli* gyrase native form (A_2B_2). **(b)** The *E. coli* gyrase GyrB-GyrA fusion. Once in solution, a homodimeric complex would form between two BA fusions $(BA)_2$. **(c)** The *E. coli* gyrase heterodimer, formed of a GyrB-GyrA fusion co-purified with GyrA. Following purification, GyrB can be added back to form the complete gyrase construct (GyrB-GyrA·GyrA + GyrB). The *E. coli* gyrase structures were recreated from 6RKW [36] using qtmg software. The yellow line in **(b-c)** represents the fusion between GyrB and GyrA.

5.1.3 Chapter aims

The *E. coli* gyrase GyrB D500H DNA relaxation activity was enhanced with two different divalent metal ions (calcium ions and magnesium ions), compared with the sum of the DNA relaxation activity in the presence of the calcium and magnesium ions individually. This enhancement was not observed with the wild-type enzyme [88]. The plan for this chapter was to apply the metal-ion enhancement experiment to the heterodimer system, to investigate the hypothesis of asymmetric metal ion binding at the DNA cleavage and resealing site. If GyrB D500H at only one of the DNA cleavage site was introduced in gyrase complex, and

the other DNA cleavage site was mutated to be unable to coordinate metal ions, then activity enhancement by two different metal ions due to asymmetric metal ion binding could be studied. If metal ions cannot bind on one side of the gyrase complex, the metal ions at that DNA cleavage site would not be able to influence the DNA cleavage or resealing activity at the other site.

To knock out metal ion binding, a triple mutation of the metal-coordinating acidic residues mutated to alanine was planned. Additionally, on the same side as the triple acidic metal ion mutant, the catalytic tyrosine was planned to be mutated to prevent DNA cleavage. Therefore, any DNA cleavage observed would be a result of activity from the opposite side of the enzyme. If these mutations were introduced, then no metal ion binding would occur at one of DNA cleavage sites, and therefore would not be influencing DNA cleavage at the DNA cleavage site mutated to GyrB D500H.

There are limitations of using the heterodimer system to study the effect of asymmetric gyrase mutations. In the presence of one catalytic tyrosine per gyrase complex ($GyrBA_{y122X}$·A + GyrB, or, GyrBA·A_{y122X} + GyrB), ie, one tyrosine mutated to either a phenylalanine or leucine, gyrase was able to perform double-stranded DNA cleavage, and supercoil and relax DNA, albeit at a reduced rate [189]. Despite that type II topoisomerases alter DNA topology via a double-stranded DNA break to achieve strand-passage, which requires two catalytic tyrosines, gyrase was proposed to be able to alter topology with only one single-stranded DNA break via a swivel mechanism, a radical departure from the cononical mechanism [189], [190]. Later, the one-tyrosine activity was also proposed to be achieved by subunit exchange, where the GyrA protein with the tyrosine mutation could be exchanged with a different GyrA subunit with a catalytic tyrosine [191].

This chapter aimed to express and purify *E. coli* GyrB D500H, and a triple mutant in the three acidic metal-coordinating residues (GyrB E424A, D498A and D500A). These mutants were introduced into the GyrB protein, and the GyrBA fusion. Therefore, the mutations could be assessed on the heterodimer (BA·A + GyrB), homodimer $(BA)_2$, and the native heterotetramer (A_2B_2) enzymes. Exploring the mutations on the heterodimer, homodimer and heterotetramer controlled for the effect of fusing GyrB to GyrA. Additionally, the catalytic tyrosine and adjacent residues were mutated (GyrA R121L, Y122L, T123L) as a control to observe the extent of one tyrosine activity, and to avoid any metal binding coordination properties of these residues, which are very close to the metal-ion binding site. The plan for

these mutants once constructed were to tested to see if there was DNA relaxation enhancement in the presence of two different divalent metal ions, like observed by Nobel and Maxwell [88], and to see if this enhancement was also observed with the DNA cleavage reaction. Additionally, the prospects of using the heterodimer system to study the effect of a mutation on one side of the enzyme will be assessed. The heterodimer system is an exciting development to the topoisomerase field, with applications including mechanistic studies and aiding antibiotic development studies.

5.2 Results

5.2.1 Designing experiments to test *E. coli* gyrase heterodimer mutants to measure enzyme activity enhancement with two different metal ions

The DNA relaxation activity of *E. coli* gyrase can be enhanced when catalysed by magnesium and calcium ions, and when GyrB is mutated to D500H [88]. The enzyme relaxation activity enhancement with two different metal ions was greater than the sum of the individual activities only when one type of metal ion was used for the GyrB D500H mutant only. These experiments initiated important biochemical evidence to support the two-metal ion model for the catalysis of DNA cleavage [88], [89], [90], [94]. An alternative explanation was later proposed for the enhancement of activity with two different metal ions. One metal ion could be binding on one side of the enzyme to aid DNA binding or priming for DNA cleavage, and a second, different metal ion could be catalysing DNA cleavage on the opposite side of the gyrase complex [39]. Additionally, different metal ions may have structural or regulatory roles in gyrase.

To address the hypothesis of asymmetric metal ion binding to the DNA cleavage site, the plan was to make a series of heterodimer mutants, such that the effect of the D500H mutant on one side only could be assessed independently of effects from the opposite DNA cleavage site [fig. 5.3].

The experimental design was to test a series of GyrB mutations. Not all of these mutations could be made, due to cloning difficulties. If all the mutations could have been made, the plan was as follows: GyrB D500H would be mutated on both sides of the enzyme, and the effect of the fusion on one and both sides of the enzyme was tested **(a)**. The double GyrB D500H mutant would be compared to the activity of a single GyrB D500H mutation with wild-type

GyrB on the opposite side of the enzyme complex **(a-b)**. Since the cleavage of one DNA strand enhances the DNA cleavage of the second DNA strand, GyrA would be mutated to be unable to cleave DNA on one side of the enzyme complex (GyrA R121L. Y122L, T123L). Therefore, only DNA cleavage from D500H would be measured. Additionally, on the same side as the GyrA mutations, the metal ion residues would be knocked out (D498A, D500A, E424A), so that metal ions cannot bind to the DNA cleavage site. Metal ions on one side of the DNA cleavage complex would hopefully have no cooperative effects on the DNA cleavage complex on the opposite side. The triple acidic metal ion binding residues mutant proved difficult to clone, and therefore a single mutant of one of the metal ion binding residues, GyrB E424A was substituted in place of the triple mutant.

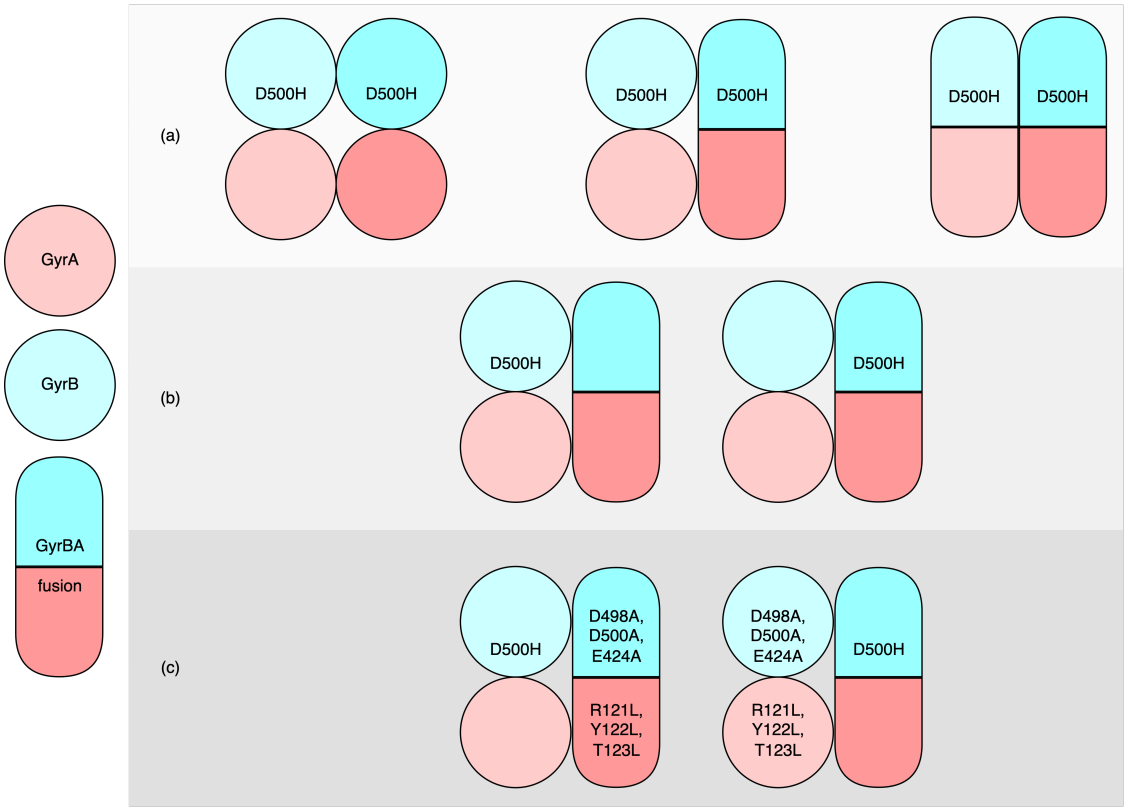

Figure 5.3: *E. coli* gyrase A_2B_2, heterodimer (BA·A + GyrB) and homodimer $((BA)_2)$ mutants. (a) *E. coli* A_2B_2, heterodimer and homodimer mutants with GyrB mutated to D500H on both sides. **(b)** *E. coli* gyrase heterodimer mutants with GyrB mutated to D500H on one side of the gyrase complex. **(c)** *E. coli* gyrase heterodimer mutants with GyrB D500H mutated on one side of the enzyme, and on the opposite side, GyrB mutated to knock out the metal binding residues (D498A, D500A, E424A), and on the same side, GyrA mutated to be unable to cleave DNA (R121L, Y122L, T123L).

Following the purification of the *E. coli* gyrase heterodimer mutants, the activity of the mutants was tested in DNA relaxation and DNA cleavage assays. Since the original experiments

by Nobel and Maxwell [88] tested the DNA relaxation enhancement with GyrB D500H, calcium and magnesium, these experiments will test to see if activity enhancement with two metal ions is also observed for DNA cleavage. During a DNA cleavage assay, the double-stranded DNA cleavage band or single-stranded DNA cleavage band (nicked) would measure DNA cleavage from both DNA cleavage sites on the enzyme. Therefore, a DNA cleavage assays with a modified protocol was planned, such that DNA cleavage by the BA fusion from the heterodimer, and the non-fusion side can be separated. Therefore, DNA cleavage by the side with the GyrB D500H mutation can be isolated. Although ultimatly there was not time to complete this experiment, figure 5.4 details the experimental plan. The protocol uses radiolabelled pBR322 via nicked translation, where ATP with the alpha phosphate labelled with ^{32}P is incorporated into the plasmid. Following a DNA cleavage assay with the heterodimeric gyrase, the trapped DNA cleavage complexes are processed with micrococcal nuclease to digest the plasmid, such that only gyrase covalently attached to short radiolabelled oligo remains. The protein samples can be analysed on an acrylamide gel, dried, exposed to a phosphor screen and imaged. A band at 97 kDA for GyrA, and 187 kDa for the fusion would be expected on the gel, representing gyrase which has cleaved DNA [fig. 5.4].

5.2.2 Expression and purification of *E. coli* gyrase metal-coordinating mutants

E. coli GyrB, *E. coli* GyrB D500H, *E. coli* GyrB E424A, *E. coli* BA·A, *E. coli* BA_{LLL}·A (R121L, Y122L, Y123L), $B_{D500H}A$·A, B_{E424A}·A, $(BA)_2$ and $(B_{D500H}A)_2$ were purified [fig. 5.6]. The designed protein constructs were successfully cloned, expressed and purified for all proteins except *E. coli* GyrB D500H, and the triple acidic residue GyrB mutant GyrB E424A, D498A and D500A.

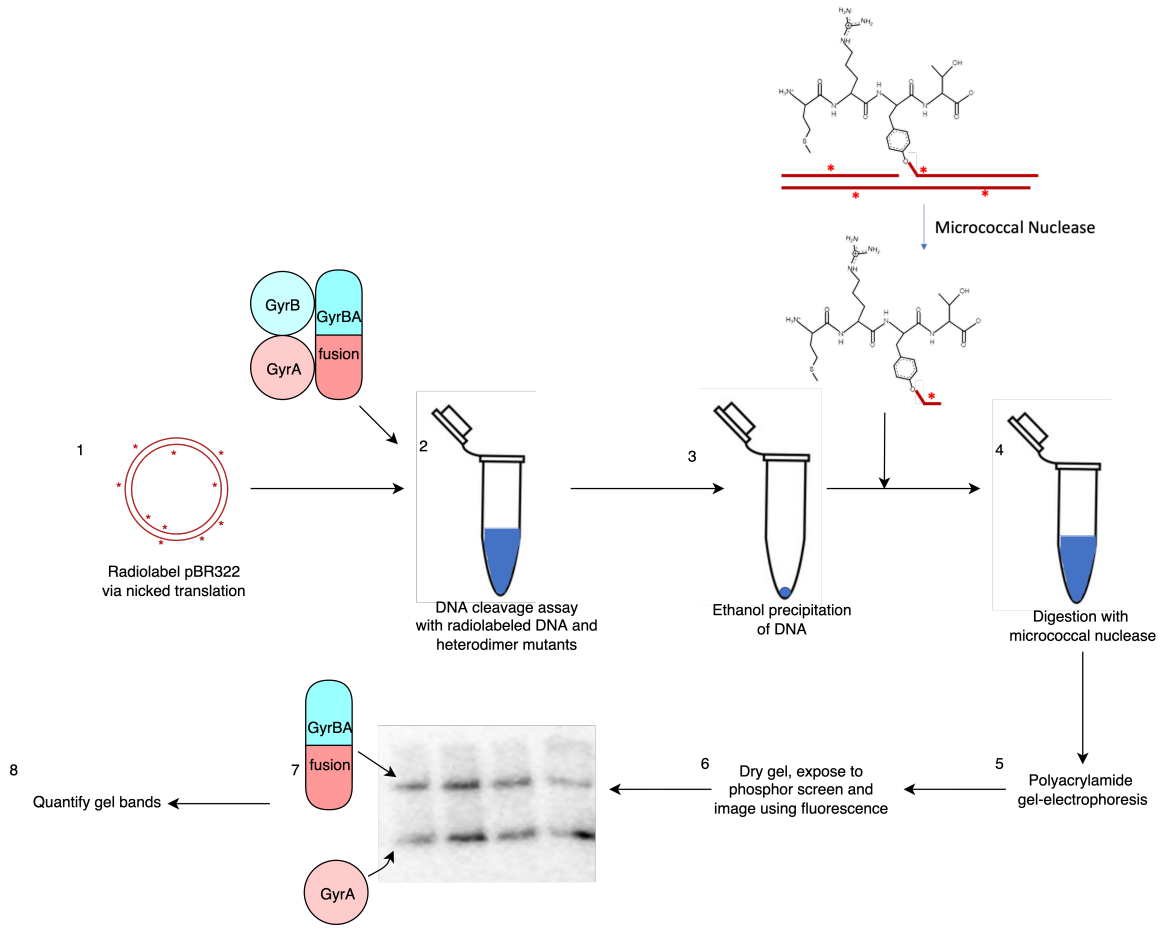

Figure 5.4: *E. coli* gyrase heterodimer (BA·A + GyrB) experimental design to measure DNA cleavage on one side of the gyrase complex. 1. DNA is radiolabelled via nicked translation with ^{32}P-ATP on the alpha phosphate. 2. A DNA cleavage assay with the heterodimer enzyme and radiolabelled DNA followed by trapping with SDS. 3. DNA is ethanol precipitated. 4. The DNA is digested with micrococcal nuclease to leave gyrase-short radiolabeled DNA oligos (image for micrococcal nuclease digestion taken from [191]), followed by a further ethanol precipitation clean-up step. 5. Samples ran on a polyacrylamide gel. 6. The polyacrylamide gel is dried, exposed to a phosphor screen and imaged using fluorescence. 7. Viewing the gel image. 8. Quantify gel bands.

Initially, mutagenesis of *E. coli* GyrB D500H was attempted on pAG111, which was the same plasmid used for wild-type GyrB. The cloning proved challenging; when the correct mutation was identified by sequencing, there were undesired additional deletions or mutations elsewhere on the plasmid. Therefore, the cloning construct was changed to mutate another plasmid carrying GyrB (pET28b). In this construct, GyrB had an N-terminal His-tag and a C-terminal strep-tag. Cloning was successful with this construct, and therefore the protein was expressed and purified [fig. 5.6]. The purified product was degrading during purification, and therefore the expression was optimised from expressing in 2x-YT media to LB, inducing the cells at OD=0.6 to OD=0.35, overnight expression at 18°C was changed to 2.5 hours at

37°C, and the cells used to express the protein was changed from *E. coli* BL21(DE3) to *E. coli* JM109. Expressing the protein at a lower concentration for less time helped the stability of the protein, because less degradation was observed during purification. The wild-type GyrB protein from other experiments in this thesis was not tagged, and was expressed in pAG111 rather than pET28b. Therefore, the proteins expressed from pAG111 and pET28b were compared to assess the impact of the different expression and protein purification protocols. The DNA cleavage levels were not affected between the two GyrB proteins, however, the supercoiling levels from the pET28b were 10-fold lower than from pAG111. Therefore, for experiments in this chapter, the GyrB protein expressed from the pET28b plasmid was used in wild-type comparisons.

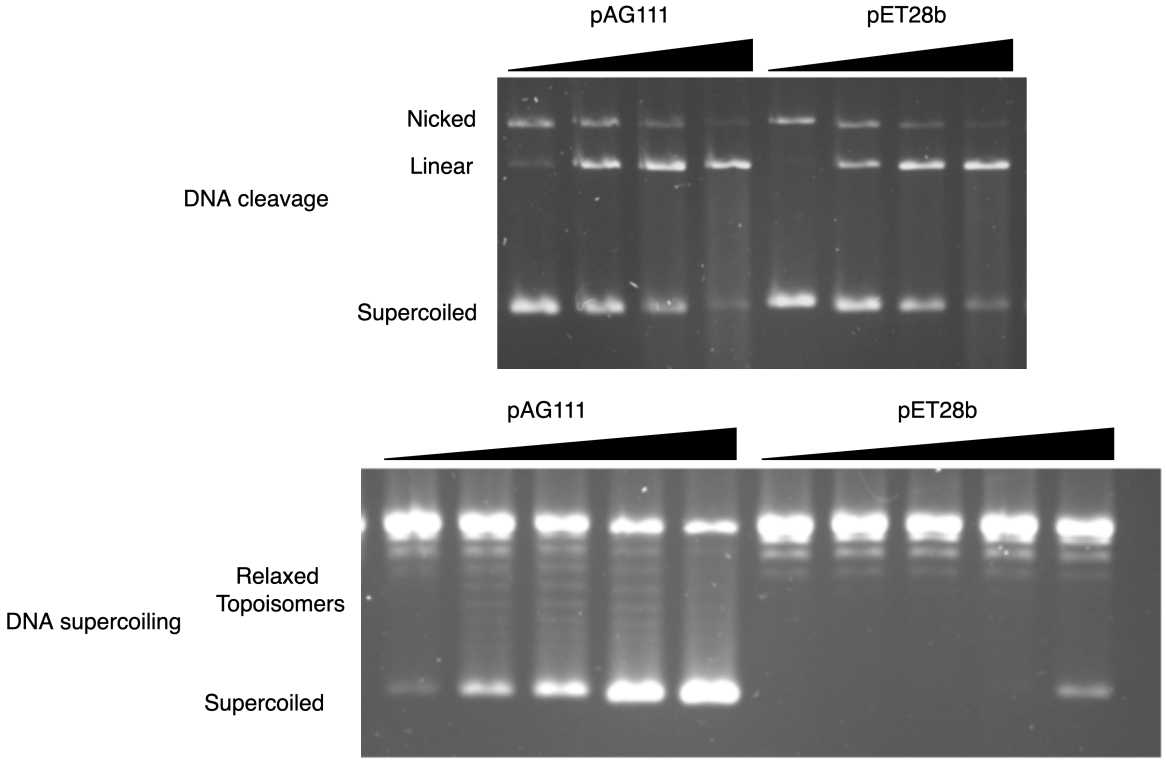

Figure 5.5: Activity comparisons of *E. coli* gyrase with GyrB expressed from pET28b or pAG111. To test the DNA cleavage activity between the two enzyme preps, the enzyme concentration was titrated against the DNA in a 2-fold dilution series, from 25 to 1.25 nM enzyme. To test the DNA supercoiling activity, the enzyme concentration was titrated in 4-fold dilution series from 0.15 to 6.25 nM enzyme.

The triple acidic residue mutant (GyrB E424A, D498A and D500A) which would be used as a mutant which cannot bind metal ions, could not be observed following protein expression trials. Therefore, a single mutant, GyrB E424A, which corresponds to the acidic residue which

coordinates the A-site, or, catalytic site metal was expressed and purified for A_2B_2, homodimer and heterodimer experiments.

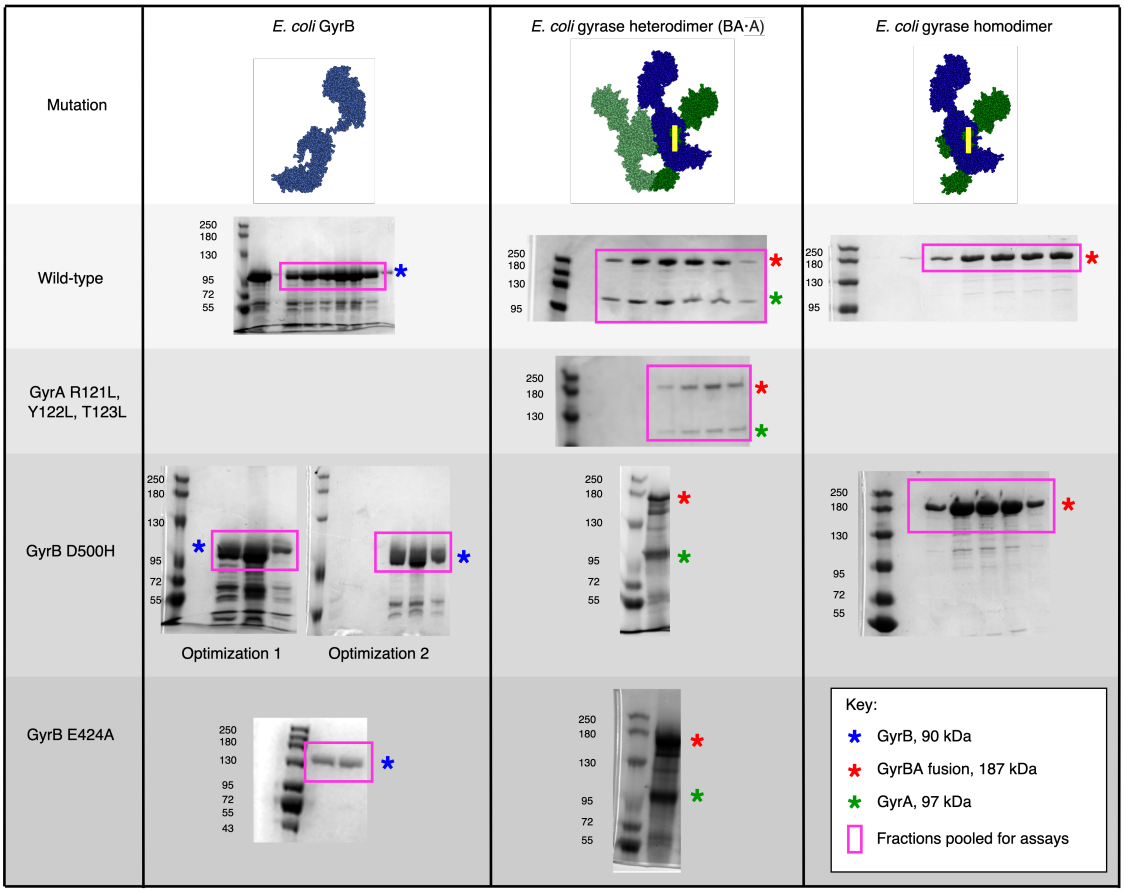

Figure 5.6: The purified protein products of *E. coli* GyrB mutants, heterodimer mutants (BA·A) and homodimer mutants $(BA)_2$. The purification of wild-type and mutant GyrB proteins. Genes for wild-type and D500H GyrB (tagged with His and Strep tags) were both subsequently removed, were cloned into plasmid pET28b. The purification of D500H GyrB was purified twice, with optimisation. The gene for GyrB E424A was cloned into pAG111 (no tag). The GyrBA fusion on pPTQ18 plasmid and GyrA from pACYC plasmid were co-expressed to form part of the heterodimer protein (BA·A). The heterodimer wild-type and mutants ($GyrB_{D500H}A$·A, $GyrB_{E424A}$·A and $GyrBA_{R121L,Y122L,T123L}$·A) genes were cloned into plasmid pPTQ18 for the fusion, and plasmid pACYC-duet for GyrA. The homodimer ($(BA)_2$ and $(B_{D500H}A)_2$) genes were cloned in pTTQ18. The fusion was double tagged (His and strep) which were cleaved during purification.

5.2.3 The impact on enzyme activity of fusing *E. coli* GyrB to GyrA

The *E. coli* gyrase heterodimer system consists of a fusion between GyrB and GyrA on one side of the enzyme, and free subunits on the other. The effect of constraining the GyrB and GyrA subunit on the DNA cleavage and supercoiling activity were assessed using an enzyme titration [fig. 5.7]. The A_2B_2 enzyme had the highest DNA cleavage activity, followed by the heterodimer (BA·A + B) and the homodimer $(BA)_2$ [fig. 5.7a]. For DNA supercoiling activity, the same trend was followed. The C_{50} values were calculated for the supercoiling

reaction. From the C_{50} values, which is defined as the concentration required to supercoil 50% of the DNA, the heterodimer had an order of magnetude less activity than the A_2B_2 enzyme. The homodimer had an order of magnitude less activity than the heterodimer. The C_{50} values for the A_2B_2 enzyme, heterodimer and homodimer were 0.36, 4.0 and 36.7 nM respectively. Therefore, the fusion constrained the enzyme, and reduced the DNA cleavage and supercoiling activity. The C_{50} values were not calculated for DNA cleavage because the DNA cleavage activity did not plateau in the concentration range tested. The concentration range was not increased further because this would be enzyme expensive and band quantification would be difficult as multiple DNA cleavage events would occur per plasmid. For clarity, the individual data points have not been added to the DNA cleavage graph, because one of the repeats included a different selection of enzyme concentrations.

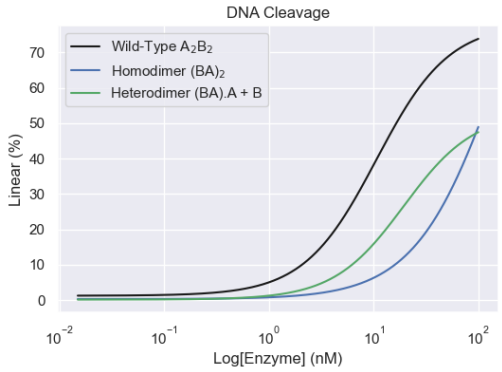

(a)

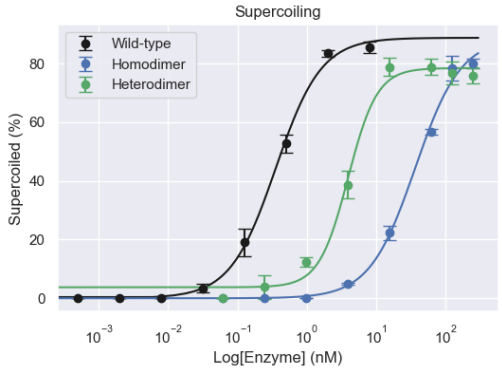

(b)

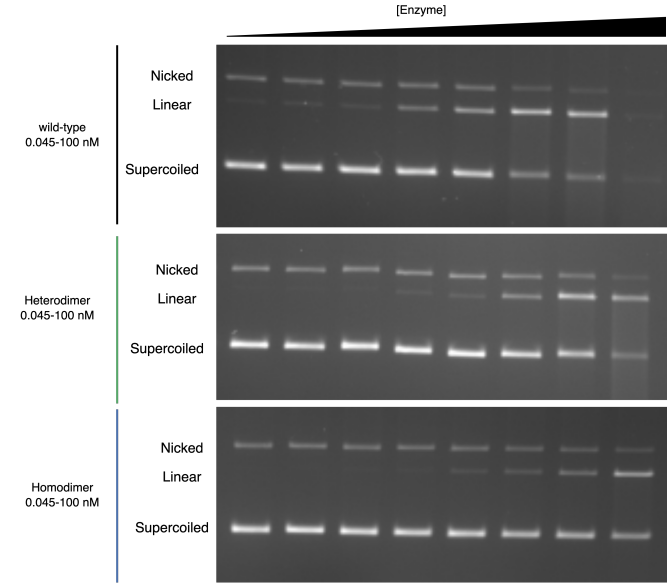

(c)

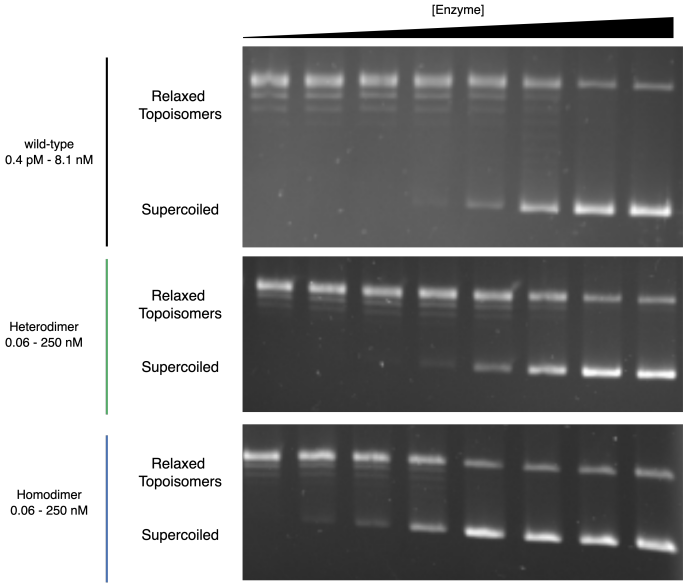

(d)

Figure 5.7: A comparison of the activity of *E. coli* gyrase wild-type, heterodimer (BA.B + A) and homodimer $(BA)_2$ in DNA cleavage and supercoiling assays. The enzyme concentration was varied whilst the DNA concentration was kept constant. The reactions were incubated for 30 minutes at 37°C. **(a)** Double-stranded DNA cleavage stabilisation by the enzymes in the presence of 20 μM ciprofloxacin and negatively supercoiled pBR322. The average from three data sets were plotted and fitted to a four-parameter curve. **(b)** DNA supercoiling activity with relaxed pBR322. **(c-d)** Accompanying gels, DNA cleavage and DNA supercoiling respectively. The average from three data sets were potted and fitted to a four-parameter curve to calculate the C_{50} (The enzyme concentration at which the enzyme activity is 50%). The C_{50} values were determined to be 0.36 nM, 4.0 nM and 36.7 nM for the wild-type, heterodimer and homodimer respectively. Standard deviation was calculated for the error bars for the supercoiling assay data sets. The DNA cleavage and supercoiling assays were analysed using agarose gels, bands quantified using ImageJ and curves plotted in python.

5.2.4 The DNA cleavage, relaxation and supercoiling activity of the *E. coli* gyrase A_2B_2, heterodimer and homodimer D500H

Nobel and Maxwell [88] observed the greatest enhancement in activity with the *E. coli* gyrase GyrB D500H mutant with two different metal ions during DNA relaxation. To recreate this experiment, the DNA relaxation activity was assessed for the *E. coli* GyrB D500H A_2B_2 mutant, homodimer $(BA)_2$ and heterodimer (BA·A + B). No DNA relaxation activity was observed for either of these mutants. Figure 5.8 shows no significant observable DNA relaxation activity from the A_2B_2 D500H mutant when using either magnesium, manganese or calcium ions, although a very high enzyme concentration was used (500 nM), and a long incubation time (75 minutes). It could be that the protein purified is misfolded, or less active than the GyrB D500H purified in the literature [88]. Therefore, GyrB D500H was re-expressed and purified under optimised protein expression conditions [fig. 5.6]. The re-purified GyrB D500H had less contamination/degradation than the first purification, however, did not result in observable DNA relaxation (data not shown).

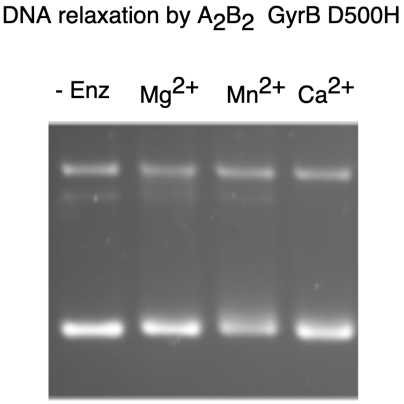

Figure 5.8: The DNA relaxation activity of *E. coli* gyrase GyrB D500H A_2B_2 mutant. 500 nM of enzyme was used in a DNA relaxation assay, in the presence of either 4 mM $MgCl_2$, $MnCl_2$ or $CaCl_2$. The relaxation assay was performed at 37°C for 75 minutes.

Since there was no DNA relaxation activity observed with GyrB D500H A_2B_2 enzyme, the DNA supercoiling and cleavage activity was assessed for the A_2B_2 enzyme, and the heterodimeric GyrB D500H (BA·A + $GyrB_{D500H}$) enzyme [fig. 5.9]. No supercoiling activity was observed with the A_2B_2 mutant up to 50 nM enzyme. Supercoiling activity was observed with the BA·A + $GyrB_{D500H}$ heterodimer. This supercoiling activity was observed because BA·A (incomplete gyrase complex, no added GyrB) had DNA supercoiling activity [fig. 5.10. This activity could be observed because one of the DNA cleavage sites is wild-type, which

was sufficient to support catalysis. The enzyme could be using subunit exchange of the GyrB subunit to a wild-type, or the enzyme could be performing strand-passage with only one active DNA cleavage site, as suggested in the literature [189], [190], [191].

Low DNA cleavage activity were observed with the A_2B_2 GyrB D500H enzyme in the absence of a DNA cleavage stabilising drug (data not shown), therefore, ciprofloxacin was used to try to enhance DNA cleavage. Low levels of DNA cleavage activity were observed with the A_2B_2 mutant at 50 nM, which had comparable activity to 1 nM of the BA·A + $GyrB_{D500H}$. The GyrB D500H homodimer $(B_{D500H}A)_2$ was also tested for DNA cleavage activity, however, no DNA cleavage activity was observed in the presence or absence of drug. The low activity of the D500H mutants was surprising, since the experiments by Nobel and Maxwell [88] used the GyrB D500H mutant in DNA relaxation experiments to show the enhancement with two different metal ions. The proteins purified in these experiments may be less stable or unfolded. This may be because the GyrB D500H was purified from a different plasmid under different purification conditions. Introducing the double-affinity tags during protein expression may have affected the stability of the protein. It is also noted that significant degradation was found during the two protein purifications of the GyrB D500H enzyme.

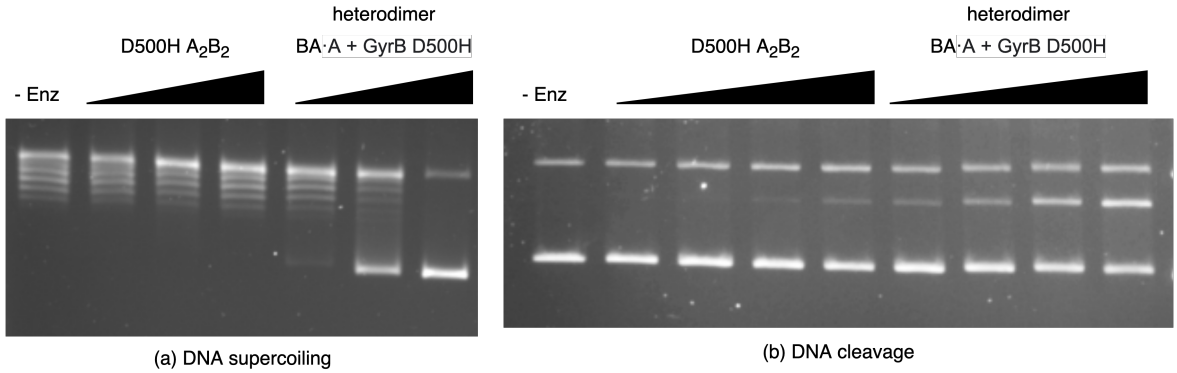

Figure 5.9: The DNA supercoiling and cleavage activity of *E. coli* gyrase A_2B_2 GyrB D500H, and BA·A + GyrB D500H. (a) The DNA supercoiling activity was compared of 1, 5, and 50 nM of the A_2B_2 and heterodimer enzymes. **(b)** The DNA cleavage activity in the presence of 20 μM ciprofloxacin and at 5, 10, 25 and 50 nM of the A_2B_2 enzyme, and heterodimer.

5.2.5 The impact of knocking out the catalytic tyrosine activity on one side of *E. coli* gyrase

In the literature, the heterodimer construct had activity when the catalytic tyrosine was mutated on one side of the gyrase enzyme (BA_{Y122F}·A + GyrB), and even had activity when

the heterodimer construct (BA·A) was assayed without the GyrB addition, ie. incomplete gyrase complex formation. This activity was thought to either be due to a strand passage mechanism involving single-stranded DNA cleavage [189] or subunit exchange [191]. Since heterodimer constructs with GyrA R121L, Y122L, T123L (LLL) will be used in the experiments with two different metal ions, the activity of this mutant was tested compared to the wild-type heterodimer enzyme [fig. 5.10]. In the absence of GyrB, the activity of the wild-type and LLL mutant GyrBA·A were tested (lanes 2 and 3, respectively). The wild-type enzyme had significant DNA cleavage at 50 nM of enzyme, and there was a low quantity of double-stranded DNA cleavage for the LLL mutant. On addition of GyrB, the wild-type and LLL mutant heterodimer had more DNA cleavage than in the absence of GyrB. Since the GyrBA·A was active in absence of GyrB, this will provide limitations and challenges to further heterodimer experiments. It would be useful for further heterodimer experiments to design a mutant which does not have BA·A activity, and only gains activity on completion of the gyrase complex with GyrB.

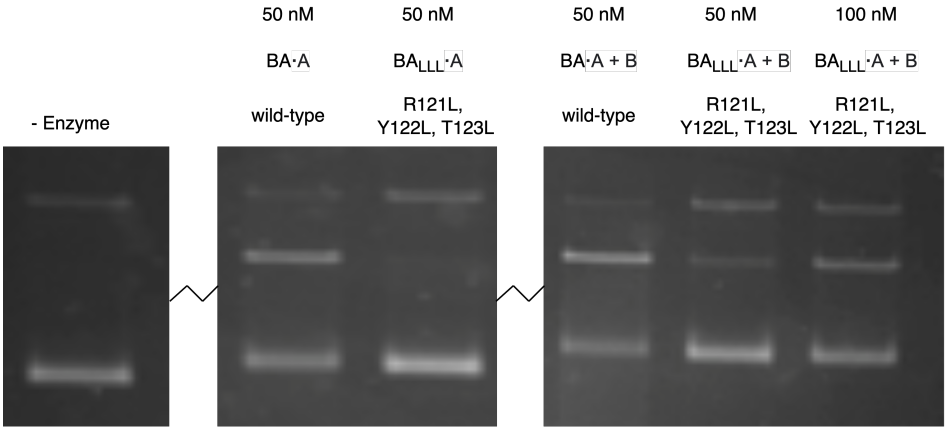

Figure 5.10: The DNA cleavage activity of *E. coli* BA·A, BA·A + GyrB, BA$_{LLL}$·A and BA$_{LLL}$·A + GyrB. The DNA cleavage activity of 50 nM of *E. coli* gyrase heterodimer BA·A and BA$_{LLL}$·A were compared. The LLL mutant is GyrA R121L, Y122L and T123L on the fusion side. The activity of *E. coli* gyrase heterodimer BA·A + GyrB and BA$_{LLL}$· + GyrB (the complete gyrase complex) was also tested at 50 nM for the wild-type, and 50 and 100 nM for the mutant.

5.2.6 Metal ion preferences for *E. coli* gyrase GyrB D500H and E424A

The original experimental design, was to test a heterodimeric enzyme with GyrB D500H on one side of the *E. coli* gyrase complex, and a triple metal ion binding residue mutant on the opposite side of the complex. The enhancement of DNA cleavage with two different metal ions would only take into account the metal ion binding sites on one side of the gyrase complex. Since the triple mutant was unable to be expressed, the activity of a single mutant, GyrB E424A was

compared to GyrB D500H, to see if the GyrB E424A mutation, which coordinates the catalytic metal ion, was significant enough to affect DNA cleavage compared with GyrB D500H [fig. 5.11]. In the literature, the enhancement of activity with the gyrase GyrB D500H enzyme was observed with DNA relaxation. Therefore, this mutant was tested to see if enhancement with two different metal ions during DNA cleavage was also observed.

The DNA cleavage activity and metal ion preferences of GyrB D500H, E424A and the wild-type were compared for magnesium, manganese and calcium ions [fig. 5.11a-5.11b]. In order to achieve reasonable levels of DNA cleavage, a significantly higher enzyme concentration for the mutants (150 nM) was used compared to the wild-type (25 nM), therefore, the levels of DNA cleavage cannot be compared between the wild-type and mutant enzymes. For both the wild-type and GyrB D500H mutant, calcium was the preferred metal ion for double-stranded DNA cleavage without a drug present. This is in agreement with the literature, that calcium enhances DNA cleavage in absence of a compound by inhibiting the reverse reaction, DNA resealing [176]. Calcium ions also promoted significant nicking of DNA for the gyrase GyrB D500H mutant. For the wild-type enzyme, manganese ions promoted the most DNA nicking. For the gyrase D500H mutant, the nicking was proportional to the amount of linear DNA cleavage, where the linear DNA cleavage was roughly a third of the levels of the nicked DNA for each divalent metal ion. For the gyrase GyrB E424A mutant, manganese ions were the preferred metal ion for both double- and single-stranded DNA cleavage. Since gyrase GyrB D500H and E424A had similar enough levels of DNA cleavage, the GyrB E424A mutant was not significant enough to knock out the enzyme's activity, and therefore it is likely that metal ions were still able to bind to the GyrB E424A mutant. Since GyrB D498 and D500 coordinate the B-site metal ion, and D500 and E424 coordinate the A-site metal, it is likely that the contributions from the non-mutated acidic residues could support DNA cleavage. Although a triple mutant could not be expressed, a double mutant (GyrB E424A + D500A, or E424A + D408A) could be explored in the future.

Due to low levels of DNA cleavage achieved by the gyrase GyrB mutants, DNA cleavage with different metal ions were compared in the presence of ciprofloxacin [fig. 5.11c-5.11d]. The gyrase GyrB D500H mutant had the greatest preference for manganese ions to catalyse double-stranded DNA cleavage. This supports literature findings that this mutant prefers manganese ions [88]. Additionally, the DNA cleavage levels in the presence of magnesium and calcium ions for the gyrase D500H mutant was tested, since DNA relaxation activity was enhanced with these metal ions in the literature [88]. The sum of the individual metal ions (at 4

mM each) DNA cleavage was similar to the DNA cleavage levels with 2 mM of magnesium and calcium ions together. Since the total metal ion concentrations were kept constant, it would be useful to repeat the experiment with 2 mM calcium and 2 mM magnesium individually to properly calculate the sum of the individual metal ions.

The metal ion preference for gyrase GyrB E424A was manganese ions, however the DNA cleavage levels were significantly lower than the gyrase D500H mutant. For the wild-type enzyme, there was no clear preference in metal ions, and the DNA cleavage levels for the wild-type enzyme in the presence of both magnesium and calcium ions were similar to the DNA cleavage for the individual metal ions, highlighting the wild-type enzyme's non-preference for metal ions in the presence of compounds. For the two gyrase mutants, nicking levels were very high. For the wild-type enzyme, there was no increase in nicked DNA from the control plasmid. In some cases, the nicked DNA decreased, which resulted from subtracting the nicking levels from the background nicking from the plasmid substrate.

The enhancement in the DNA cleavage activity with *E. coli* gyrase GyrB D500H in the presence of magnesium and calcium ions was unclear. Since the total metal ion concentration was kept constant, the proper sum of the individual metal ions could not be calculated to see if enhancement in DNA cleavage activity with magnesium and calcium ions would be observed [fig. 5.12]. The experiment was repeated with two concentrations for the individual metal ions, 2 mM and 4 mM. Additionally, since the fluoroquinolone ciprofloxacin was used, which requires metal ions to bind to the enzyme, an IPY was also used for the gyrase GyrB D500H mutant, since IPYs do not require metal ions to stabilise DNA cleavage [fig. 3.5].

The sum of the individual metal ions for linear DNA cleavage for the gyrase GyrB D500H mutant in the presence of 2 mM of magnesium and calcium was 18.4%. The DNA cleavage levels in the presence of 2 mM of calcium and magnesium ions was 19.7%, which was not significantly higher than the sum of the individual metal ions. However, the DNA double-stranded DNA cleavage activity with 2 mM magnesium and calcium ions (19.7%) were higher than the DNA cleavage activity with 4 mM magnesium ions (14.0%) or 4 mM of calcium ions (10.5%). In the presence of an IPY, the sum of the individual metal ions was greater than the DNA cleavage activity in the presence of both magnesium and calcium ions, suggesting that the higher DNA cleavage levels in the presence of two different metal could be due to metal ion preferences for the binding of fluoroquinolones due to the water-metal ion bridge. For the wild-type enzyme, the sum of the DNA cleavage activity in the presence of 2 mM Mg^{2+} or Ca^{2+} was 106% and

much higher, compared to the activity with 2 mM each (40%). There was no enhancement in DNA cleavage with two different metal ions for the wild-type enzyme in the presence of ciprofloxacin. These results are inconclusive as to whether DNA cleavage with the gyrase GyrB D500H mutant are enhanced in the presence of two different metal ions.

5.3 Conclusions and future work

5.3.1 The cloning, expression and purification *E. coli* gyrase GyrB D500H mutant is important for stability and activity

The cloning of *E. coli* GyrB D500H genes into pAG111 was challenging; following mutagenesis using PCR and sequencing, either the mutation would not be present on the plasmid, or the correct mutation would be introduced with additional mutations elsewhere on the plasmid. Although the primers were changed, PCR conditions varied and the mutagenesis technique changed (Infusion vs overlapping primers), and cloning in different cell lines, mutagenesis was not successful. When mutagenesis is unsuccessful after significant optimisation, the mutation introduced may be unstable or toxic to the cells expressing the plasmid. *E. coli* GyrB D500H had previously successfully been cloned in the literature [88], which was also cloned in pAG111, however, it was unclear to why mutagenesis was not successful in this instance. Another plasmid with the GyrB gene was available in the lab in pET28b, and the GyrB protein had double affinity tags for purification (N-terminal His-tag and C-terminal strep-tag). Site directed mutagenesis of GyrB D500H was successful on this plasmid. pAG111 is a high-copy number plasmid, whereas pET28b is a low copy number plasmid. Therefore, pET28b is more likely to express less protein when the PCR products are cloned into bacteria, which may be less toxic.

The expression of *E. coli* GyrB D500H was more stable when expression was optimised to shorter induction times, and inducing at an early OD_{600} (induction at OD=0.3 at 37°C for 2.5 hours vs induction at OD=0.6 at 18°C overnight). During the protein purification stage, there was less protein degradation when the protein was induced to express at a lower OD and for a shorter period of time. The protein expression and purification could be optimised for future experiments, since there was still substantial degradation. The protein was continually being degraded during the protein purification, and therefore the protein expression could be optimised further, such as expression in different media or cell lines. The protein could be less stable due to the double-affinity tags, and therefore GyrB D500H could be re-cloned to remove

the tags.

When comparing the purification and activity of *E. coli* GyrB in pAG111 and pET28b, the GyrB from pET28 was less pure than when expressed and purified from pAG111. The supercoiling activity for wild type GyrB was 10-fold less active when purified from pET28b, than pAG111. The DNA cleavage activities for GyrB from both plasmid were comparable. The differences in activity between GyrB expressed from two different plasmids could be because the GyrB on pET28b has two affinity tags, which may affect the folding of the protein. Additionally, pET28b has higher expression levels of proteins compared with pAG111. High protein expression levels may affect the protein folding or lead to aggregation. The DNA supercoiling may be affected more than the DNA cleavage activity, because DNA supercoiling is more intensive, requiring the coordination from all the gyrase domains. This may be more affected from misfolded enzyme. Alternatively, the DNA resealing reaction may be inhibited, resulting in higher levels of observable DNA cleavage.

5.3.2 The DNA cleavage activities of *E. coli* GyrB E424A

Since a triple metal ion binding mutant could not be purified, a single mutant in one of the three residues coordinating metal ion binding at the DNA cleavage site was mutated, GyrB E424A. GyrB E424A corresponds to the metal binding at the catalytic metal ion binding site (A-site). GyrB E424A had DNA cleavage activity in the presence and absence of the fluoroquinolone ciprofloxacin. Therefore, the mutant was not successful at preventing the catalytic metal ion binding to the enzyme. D498 is adjacent to E424 in crystal structures, and also contributes towards coordinating the A-site metal ion and B-site metal ion, whereas D500 coordinates only the B-site metal ion. Therefore, a double mutant of GyrB D498A and E424A would hopefully prevent A-site binding, compared to mutating D500 and one of either E424 or D498.

5.3.3 The enhancement of *E. coli* gyrase activity on addition of two different metal ions

In the presence of calcium and magnesium ions for the *E. coli* GyrB D500H enzyme in the presence of ciprofloxacin, the sum of the DNA cleavage activity at 2 mM $MgCl_2$ and 2 mM $CaCl_2$ was similar to the level of DNA cleavage when 2 mM of each metal ion were combined. Therefore, enhancement with two different metal ions was not observed compared to the sum of the individual activities. However, the DNA cleavage activity with 2 mM of each metal ion (4 mM metal total) in the same DNA cleavage reaction was greater than the activity of 4 mM

of $MgCl_2$ or 4 mM $CaCl_2$. This result suggests that there was some enhancement affects with two different metal ions. Since this result was not observed during a DNA cleavage activity with an IPY, this enhancement effect could be due to ciprofloxacin binding preferring one type of metal ion.

The DNA cleavage activities of *E. coli* GyrB D500H may not have been significantly enhanced compared to the enhancement observed in the literature with DNA relaxation [88], because two metal ions could be enhancing the rate of DNA resealing. If DNA resealing was also enhanced by two different metal ions, the enhancement of the DNA cleavage product may not be observed. The DNA cleavage and resealing reaction, and the relaxation reaction may have different requirements for metal ions, such as structural and regulatory metal ions.

5.3.4 Future considerations to use the *E. coli* gyrase heterodimer system to test asymmetric mutants

The *E. coli* heterodimer system is a promising system to study the effect of mutating DNA gyrase on one side of the enzyme complex. As described in the literature, the BA·A heterodimer without the completion of the gyrase complex by the addition of GyrB, has DNA cleavage, supercoiling and relaxation activity [189], [190], [191]. This activity was thought to be either from gyrase being able to perform strand passage by a nicking mechanism, where ATP binding releases wrapped DNA, allowing DNA to rotate around the non-cleaved DNA strand [189]. Or, the activity could result from subunit exchange, where the strong GyrA dimer interface can be broken and exchanged when in proximity to other gyrase complexes [191].

It is important to not have activity from BA·A because the activity may be resulting from a wild-type enzyme, as opposed to a heterodimer. For future heterodimer experiments, BA·A activity (without the addition of GyrB to complete the gyrase complex), must not have activity. If the subunit exchange model was correct, there may be mutations or conditions which inhibit subunit exchange. Possible mutation areas to explore could be to design a fusion construct with both GyrA and B subunits, which may limit subunit exchange. There may be buffer conditions to reduce subunit exchange effects. If the polarity of the buffer was altered, this may prevent association of gyrase complexes to allow subunit exchange, or strengthen the gyrase subunit interfaces. If the heterodimer system could be re-designed to prevent activity of the *E. coli* gyrase BA·A protein, the heterodimer system could be applied to gyrases from other species, or topo IV, which is also a heterotetramer.

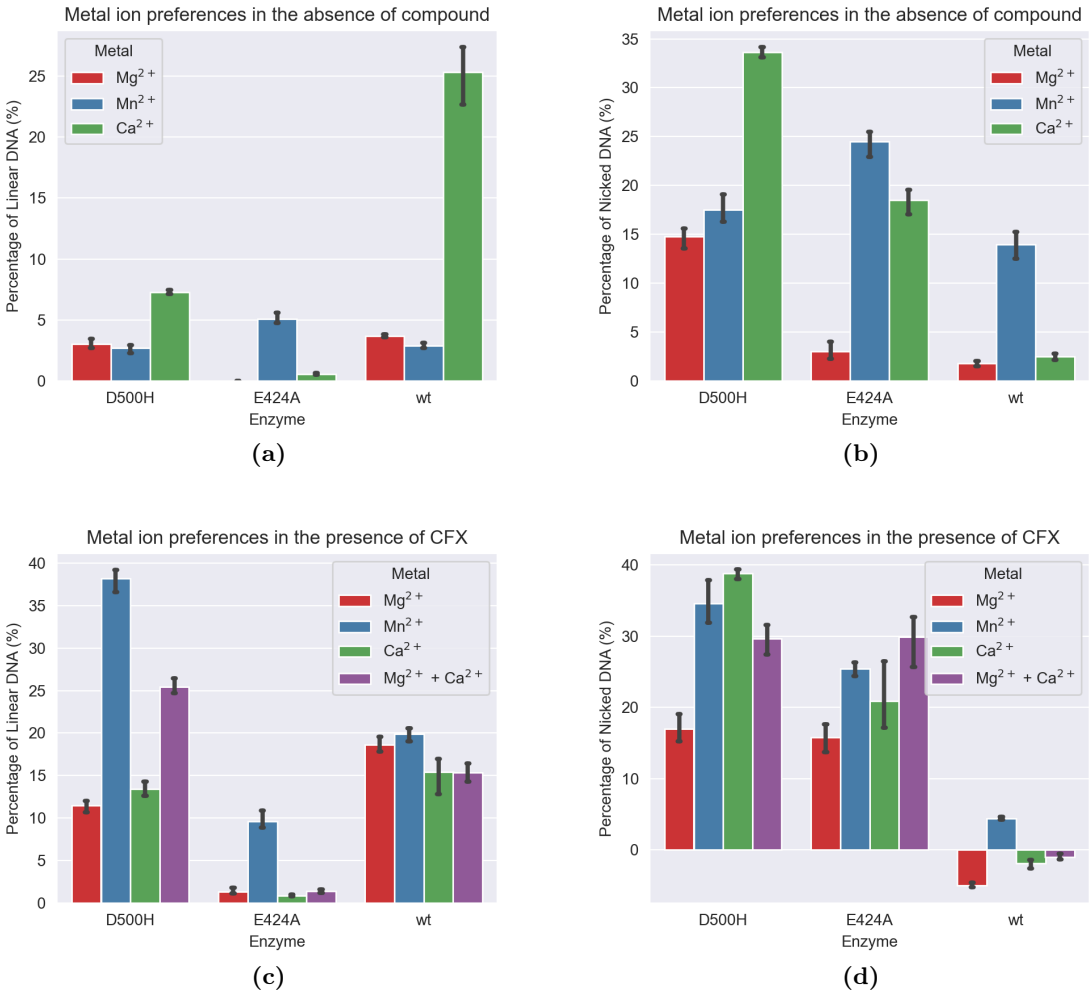

Figure 5.11: A comparison of the metal ion preferences for *E. coli* gyrase wild-type, GyrB D500H, and GyrB E424A to cleave DNA. The preference for *E. coli* gyrase A_2B_2 wild-type enzyme (25 nM), or mutants (150 nM) to cleave DNA in the presence of 4 mM of $MgCl_2$, $MnCl_2$ or $CaCl_2$ were measured. The double-stranded DNA cleavage **(a)** or single-stranded DNA cleavage **(b)** were measured. The wild-type (10 nM) and mutant (150 nM) *E. coli* gyrase enzymes were tested for their preference in metal ions to cleave DNA in the presence of 20 μM ciprofloxacin. 4 mM total metal ion concentration was used - when DNA cleavage levels were measured in the presence of magnesium and calcium, 2 mM of each metal ion was used. The levels of double-stranded DNA cleavage **(c)** and single-stranded DNA cleavage **(d)** were measured.

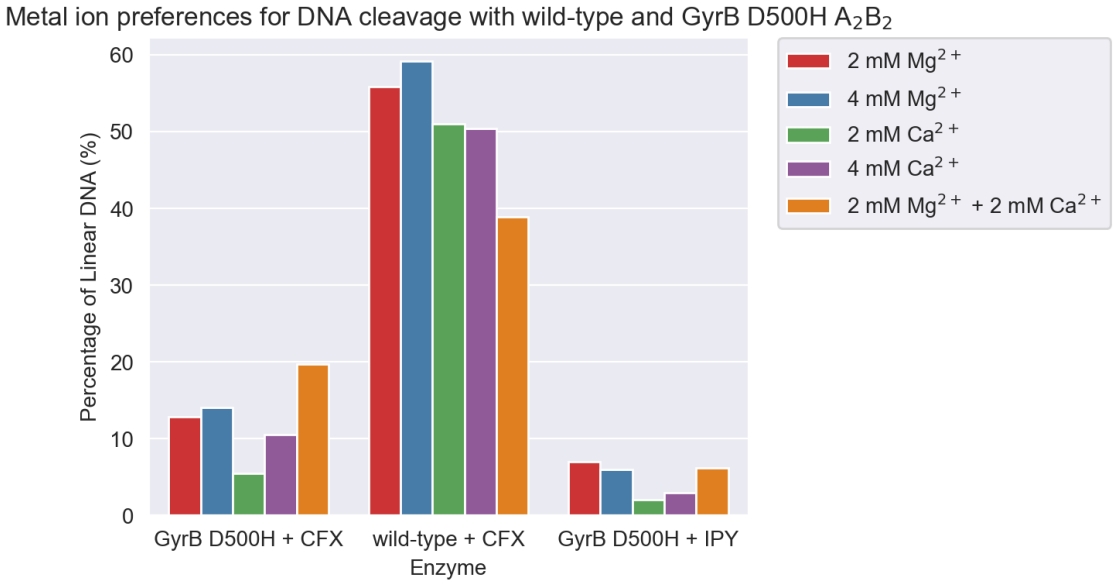

(a)

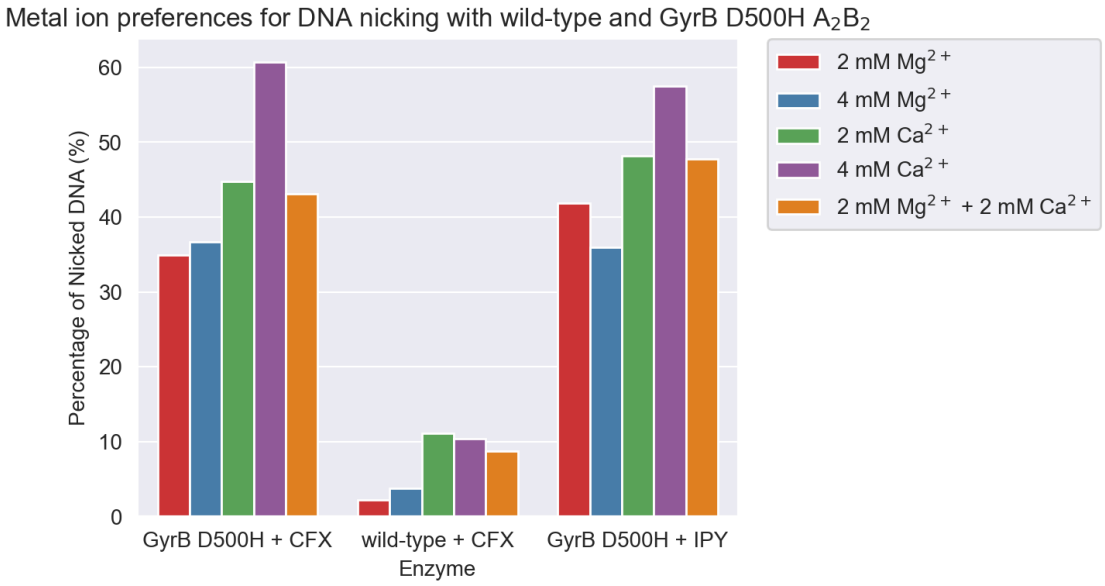

(b)

Figure 5.12: The metal ion preferences for DNA cleavage of A_2B_2 *E. coli* gyrase wild-type and GyrB D500H in the presence of ciprofloxacin or an imidazopyrazinone. The preference for *E. coli* gyrase A_2B_2 wild-type enzyme (12.5 nM), or GyrB D500H (200 nM) to cleave DNA in the presence of 2 - 4 mM of $MgCl_2$ or $CaCl_2$, or 2 mM $MgCl_2$ + 2 mM $CaCl_2$ were measured. The double-stranded DNA cleavage **(a)** or single-stranded DNA cleavage **(b)** were measured. The mutant gyrase GyrB D500H DNA cleavage was measured in the presence of either 50 μM ciprofloxacin or 50 μM of the IPY t1. For the wild-type gyrase, DNA cleavage was measured in the presence of 50 μM ciprofloxacin.

Chapter 6

Characterisation of the Quinazoliniums: a novel synthetic antibiotic series targeting topoisomerases

6.1 Introduction

The pharmaceutical industry have faced challenges in the search and development for new antibiotics, including entry and efflux from bacteria, toxicity to humans and unpromising profits, resulting in abandoning vital drug discovery projects [192]. To combat the lack of support for antibiotic development from industry, consortiums have been created to support academic antibiotic research in collaboration with industry to accelerate the drug discovery pipeline. The European Gram Negative AntiBacterial Engine (ENABLE) project was initiated in 2014 to target key Gram-negative pathogens by providing funding support, initiating collaborations and bring together a hub of experts. The work presented in this chapter is supported by the ENABLE consortium, which investigates the biochemical characterisation of a novel series of synthetic antibiotics, developed by chemists from Uppsala University named the Quinazoliniums (QZMs) [fig. 6.1].

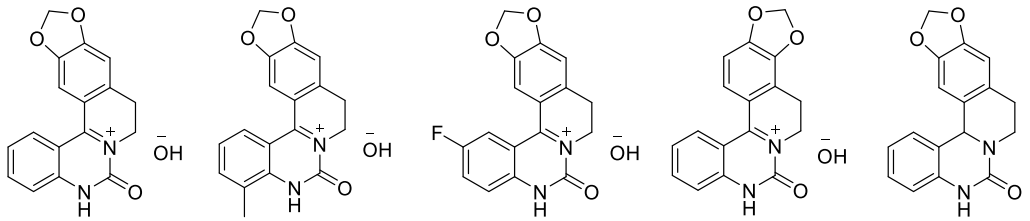

Figure 6.1: The structures of the quinazoliniums: 1488, 1529, 1532, 2086 and BT9701.

The QZMs are synthetic compounds and consist of a quinoline moiety, which is a benzene ring fused to a pyrimidine ring. Additionally, there is a carbonyl group in the 2 position, between the two nitrogens on the pyrimidine ring, thereby forming a quinazolin-2(1H)-one.

Quinazolinones are derivatives of biologically active heterocyclic compounds in different areas of medicine, and have also been used in gyrase-targeting compounds, such as the fluoroquinolone-like 8-methoxyl 2,4-dione and 8-methyl 2,4-diones [193]. These quinazoline diones have striking clinical potential due to their activity against fluoroquinolone-resistant gyrase and topo IV mutants which disrupt the water-metal ion bridge required for fluoroquinolone binding [121]. Inhibitors of gyrase are commonly made of heterocycles with at least 2 rings. Ciprofloxacin has a quinolone moiety, and the imidazopyrazinones contain a benzene ring fused to a pyrazinone ring (fig. 6.2). The heterocycles allow for intercalation into DNA at the DNA cleavage site through π-π stacking interactions, particularly with nitrogen-containing heteroaromatic heterocycles.

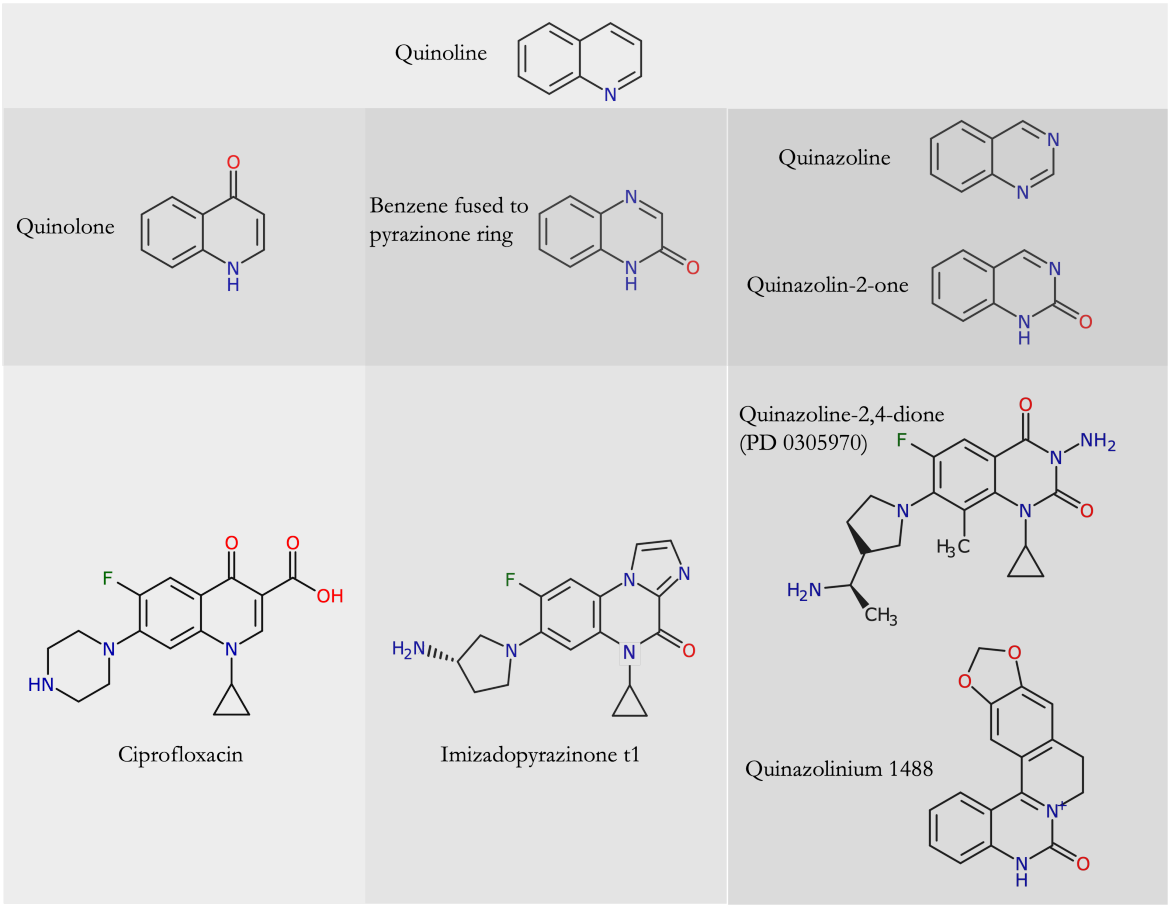

Figure 6.2: The structures of heterocycle-based gyrase inhibitors which stabilise DNA cleavage, and the compound building blocks. The compound structures of quinoline, quinolone, ciprofloxacin, a pyrazinone fused to a benzene ring, imidazopyrazinone, quinazoline, quinazolino-2-one, quinazoline-2,4-dione (PD 0305970), and the quinazolinium 1488.

Condensed to the quinazolinone moiety is 5,6,7,8-tetrahydro-[1,3]dioxolo[4,5-g]isoquinoline, which consists of a piperidine ring, followed by a benzene ring and a 1,3-dioxolane, thereby

forming 5 fused rings. Compounds consisting of 5 rings have been found to inhibit other topoisomerases, such as the topoisomerase I inhibitor camptothecin, a plant alkaloid first isolated from *Camptotheca acuminata* which intercalates into DNA at the DNA cleavage site, and interacts with topoisomerase I [194]. Another strikingly similar compound to the QZMs is berberrubine, a plant alkaloid isolated from *Berberis vulgaris*. Berberrubine also has an isoquinoline moiety which consists of 5 fused rings and stabilises single- and double-stranded DNA cleavage by human topo II, and displays antitumor activity [195] (fig. 6.3).

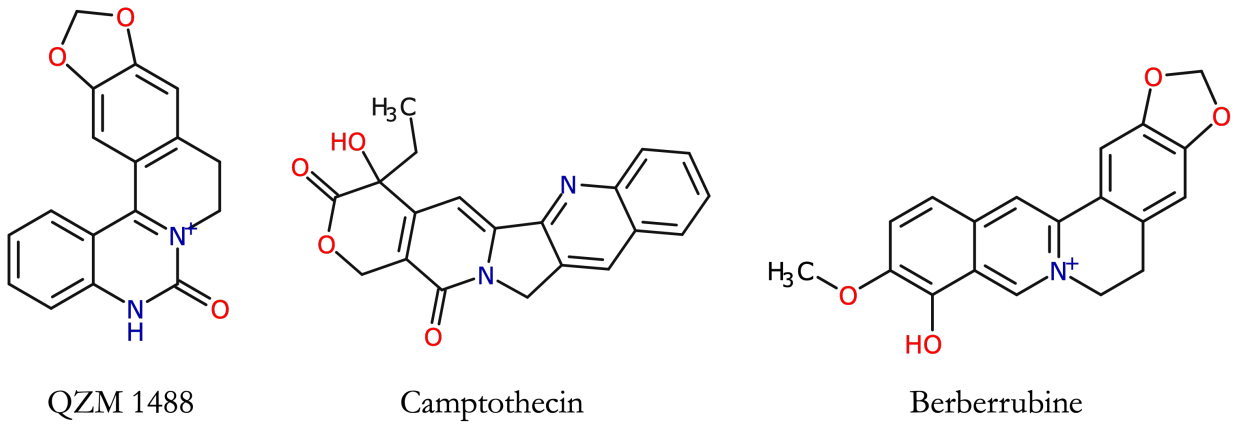

Figure 6.3: The structures of compounds with similar scaffolds to the QZMs that are also topoisomerase inhibitors. The compound structure of camptothecin, from *Camptotheca acuminata*, a human topoisomerase II inhibitor which stabilises topoisomerase-DNA cleavage complexes. The structure of berberrubine from *Berberis vulgaris*, consisting of an isoquinoline moiety, like with the QZMs.

The QZMs originated from the diversification of 3,4-dihydroquinazolinones to generate a series of N-polyheterocycles [196]. One of these compounds, after storage in DMSO, was found to exhibit antibacterial activity against *E. coli* of 32 mg/L. Oxidation of the neutral nitrogen formed a quaternary, positively charged nitrogen between the piperidine ring and the pyrimidine ring, and also resulted in a colour change of the compound from colourless to yellow. Replacement of the methoxy functional groups with 1,3-dioxolane formed the lead compound 1488, and BT9701 is the neutral form of 1488. Further modifications of the benzene ring on QZM 1488 led to compounds 1529 and 1532 by the addition of a methyl group and fluoro group respectively, and movement of the position of the dioxolane group formed compound 2086.

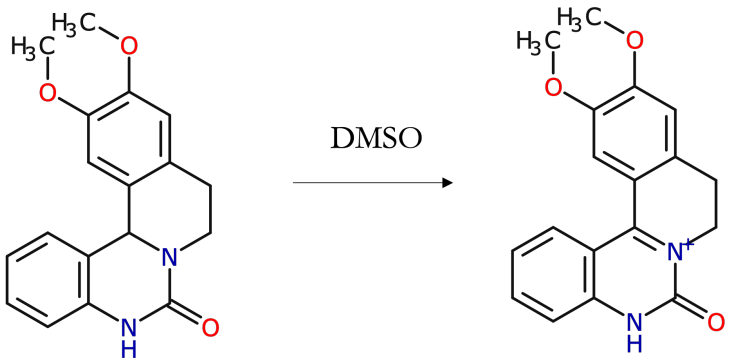

Figure 6.4: The oxidation reaction of a precursor to QZM 1488, which gave the compound series antibacterial properties.

The QZMs were found to have antibacterial activity against key Gram-negative pathogens by Uppsala University, as demonstrated by their minimum inhibitory concentration data (tbl. 6.1). The QZMs had activity against the Gram-negative pathogens *E. coli*, *Pseudomonas. aeruginosa* (*P. aeruginosa*), *Klebsiella. pneumonaie* (*K. pneumonaie*) and *Acinetobacter. baumannii* (*A. baumannii*), and no activity against the Gram-positive *S. aureus*. QZM 1488 was the most active compound against *E. coli*, followed by 2086, 1532, 1529 and BT9701. This trend in potency is generally followed with the other Gram-negative pathogens. The compounds were tested against sensitive strains, to see how import and export of the compounds affected potency. The *E. coli* strain with ΔTolC, deficient in a channel which exports small molecules, the *E. coli* strain with an LPS mutation which increases permeability of the outer cell membrane to compounds, and the *P. aeruginosa* strain deficient in compound efflux were tested. Each of the QZMs were found to be more effective, suggesting possible barriers for compound entry and compound retention in the bacteria. Interestingly, QZM 2086 was more active than 1488 in *E. coli* and *P. aeruginosa* efflux strains, suggesting the compound may be more susceptible to removal from the bacteria, and potentially could be more active against the compounds' target.

	Compound (mg/L)				
Species	BT9701	1488	1529	1532	2086
E. coli wt	>64	4	32	16	4
E. coli ΔtolC	8	≤2	1	8	≤ 0.125
E. coli lps mutant	32	≤2	4	8	2
P. aeruginosa wt	>64	64	>64	>64	64
P. aeruginosa efflux defective	32	≤2	64	1	0.5
K. pneumoniae wt	>64	16	>64	>64	32
A. baumannii wt	>64	32	>64	64	32
S. aureus wt	>64	64	>64	>64	>64

Table 6.1: The MIC values for different bacterial species treated with QZMs. The QZM antibacterial activity against *E. coli* wild-type, *E. coli* with tolC deleted and isogenic to ATCC 25922, *E. coli* D22 (lps mutant, hypersensitive), *P. aeruginosa* wild-type, *P. aeruginosa* efflux deficient (isogenic to PAO1), *K. pneumonaie* wild-type, *A. baumanii* wild-type, and *S. aureus* as a Gram-positive control. Data is from Uppsala University.

Resistant mutants of *E. coli* against QZM 1488 occur at a frequency of $<1*10^{-9}$ at 4 times the MIC. QZM-resistant *E. coli* mutants mapped to the quinolone-resistance-determining region (QRDR) on DNA gyrase. The QRDR is a location on the type II topoisomerases where point mutations are located which result in resistance to compounds such as the fluoroquinolones by reducing the compound's binding affinity, and therefore clinically important to find drugs which bypass resistance in this region. Uppsala University found when testing QZM 1488 against *E. coli* with mutations in the QRDR on DNA gyrase, they found the QZMs had less antibacterial activity (tbl. 6.2). Interestingly, the compounds were less affected by the GyrA S83L and D87N mutations compared with ciprofloxacin. The residues are involved in coordinating the water-metal ion bridge in fluoroquinolones, which is essential for the potent binding of the compounds. Therefore, the QZMs were predicted to have a distinct binding mechanism from the fluoroquinolones by bypassing the requirement for the water-metal ion bridge.

Genotype	Liquid MIC (mg/L)			
	CFX		1488	
	MIC	mutant/wt	MIC	mutant/wt
ΔtolC	0.002	1	0.06	1
GyrA G81D ΔtolC	0.016	8	8.00	125
GyrA D82G ΔtolC	0.016	8	2.00	31
GyrA A84P ΔtolC	0.016	8	2.00	31
GyrB K447E ΔtolC	0.0005	0.25	4.00	63
GyrB S464Y ΔtolC	0.032	16	1.00	16
GyrA S83L, ΔtolC	0.064	32	0.13	2
GyrA D87N ΔtolC	0.032	16	0.25	4
GyrA S83L, D87N, ΔtolC	0.063	31.5	0.13	2

Table 6.2: The MIC values for *E. coli* fluoroquinolone-resistant strains treated with QZM 1488. MIC values were determined for common fluoroquinolone-resistant *E. coli* with mutations on DNA gyrase against QZM 1488, and ciprofloxacin. The magnitude in the MIC shift from the wild-type and the mutant *E. coli* was calculated.

This chapter aims to biochemically characterise the QZMs to confirm the target of the compound series, and to assess whether DNA gyrase was the main target, since most bacteria have both DNA gyrase and topo IV. There is a high degree of homology between gyrase and topo IV, and therefore by targeting both enzymes, the antibiotics are highly effective and can kill a wide spectrum of bacteria [197]. The type II topoisomerases have different activities which contribute to the enzyme's overall function. By assaying the DNA supercoiling, relaxation and cleavage stabilisation activity of the topoisomerases, how the QZMs specifically affected each of these activities was assessed to better understand the mechanism of action. Different classes of topoisomerase inhibitors bind to distinct sites on gyrase, for example, the quinolone-binding pocket, the ATP-binding pocket, the NBTIs site, and other sites, which all modulate the activities of gyrase uniquely [198]. The fluoroquinolones trap the topoisomerase on DNA by stabilising the enzyme-DNA complex in the cleaved state. The drugs will therefore prevent DNA supercoiling and DNA relaxation from proceeding, and accumulation of cleaved DNA is observed in DNA cleavage assays. NBTIs act by stabilising single-strand DNA cleavage complexes, which can be distinguished from double-stranded DNA cleavage in DNA cleavage assays. Aminocoumarins inhibit the ATPase activity by competing with ATP; since DNA relaxation by gyrase does not require ATP to relax DNA, the drugs inhibit the supercoiling activity, but not the relaxation activity of DNA gyrase. These experiments will give an indication to the mechanism of action, and the binding site from assaying the compounds

against the different gyrase activities, and be able to compare the efficacy of the QZMs to other common gyrase inhibitors to assess their antibiotic potential.

From the MIC data, the compounds were more active against Gram-negative bacteria, and therefore testing the QZMs against the Gram-positive *S. aureus* gyrase was investigated, to understand whether the topoisomerase target, or the accumulation in the cell resulted no antibacterial activity. Additionally, whether the compounds would be toxic in humans by testing the compounds against human topoisomerase II, and in the model organism *Galleria mellonella* (*G. mellonella*) was tested. Human type II topoisomerases are only inhibited by fluoroquinolone antibiotics at very high concentrations, which are not achieved in an antibiotic dose [199], the QZMs must not significantly inhibit the human enzymes to be successful antibiotics. *G. mellonella* has a similar innate immune system to humans, and toxicity of drugs to the larvae correlates to the toxicity in mice and rats [158]. Numerous gyrase inhibitors, including fluoroquinolones and thiophenes, have been discontinued due to toxicity [199],[138], and therefore early toxicity data from *G. mellonella* is an important guide to whether the QZM series is worth pursuing.

X-ray crystallography was performed, because the binding site of the QZMs was important to characterise, not only to confirm the mechanism of action, but to aid the development of the QZM series to develop the next generation of the quinazoliniums. To confirm the binding site of the compounds in the crystal structure, and validate the MIC data, the QZMs against *E. coli* gyrase mutants was assayed, to see the contribution of individual residues to the potency. The gyrase mutants selected included clinically important mutants which contribute to fluoroquinolone-resistant bacterial strains. The activity of the QZMs and fluoroquinolones with these mutants was compared, to see if the QZMs could be used against fluoroquinolone resistant bacteria.

6.2 Results and Discussions

6.2.1 The novel antibiotic compounds target *E. coli* gyrase in *in vitro* assays

The MIC data from Uppsala University showed that the QZMs had antibacterial activity against a number of bacteria, and were overall most effective at killing *E. coli*, compared with *A. baumanii*, *K. pneumoniae*, *P. aeruginosa* and *S. aureus* [tbl. 6.1]. DNA gyrase was identified as a likely target at Uppsala University from generating resistance mutants and sequencing,

followed by testing the antibacterial activity of the lead compound QZM 1488 with common fluoroquinolone resistance mutations in *E. coli* [tbl. 6.2].

The QZMs had the best antibacterial activity against *E. coli*, compared with the other pathogens tested. Therefore the compounds were tested against *E. coli* gyrase to confirm *in vitro* inhibition activity. The QZMs were titrated against *E. coli* gyrase in *in vitro* gel-based biochemical assays: DNA supercoiling, cleavage and relaxation assays. Densitometric analysis of agarose gels calculated the proportions of supercoiled, relaxed, nicked or linear DNA. The data were fitted to a four-parameter curve to determine the IC_{50} and CC_{50} values to quantify compound potency and to compare the QZM activity to other antibiotics [fig. 6.5][tbl. 6.3]. In the case of DNA supercoiling and relaxation inhibition assays, the IC_{50} values were calculated, which were defined to be the concentration of the drug at which the activity of the enzyme was inhibited by 50% (eqn. 6.1-6.2). When assaying the QZMs in DNA cleavage stabilisation assays, the CC_{50} values were calculated, defined by the concentration of the drug which the DNA cleavage complexes were stabilised by 50% (eqn. 6.3) [tbl. 6.3].

The IC_{50} values can be theoretically linked to binding affinities through the Cheng-Prusoff equation. This relationship relates the K_i value, which is the inhibitory constant to the IC_{50} for a competitive inhibitor [200]. This link holds true for competitive inhibitors with no cooperativity. Common DNA gyrase inhibitors include the fluoroquinolones, which do are not simple competitive inhibitors, and cooperativity exists in the enzyme - the cleavage of one DNA strand enhances the DNA cleavage of the second strand. If the QZMs acted similarly to the fluoroquinolones, the IC_{50} values calculated can not be approximated to the K_i to provide information on QZM affinity for the enzyme.

$$\text{Supercoiled DNA (\%)} = \text{Min} + \frac{\text{Max - Min}}{1 + \frac{[\text{Compound}]}{IC_{50}}} \tag{6.1}$$

$$\text{Relaxed DNA (\%)} = \text{Min} + \frac{\text{Max - Min}}{1 + \frac{[\text{Compound}]}{IC_{50}}} \tag{6.2}$$

$$\text{Cleaved DNA (\%)} = \text{Min} + \frac{\text{Max - Min}}{1 + \frac{CC_{50}}{[\text{Compound}]}} \tag{6.3}$$

The most potent compound against *E. coli* gyrase was QZM 1488, followed by 2086, 1532 and then 1529. The trend was consistent across the DNA supercoiling, relaxation and cleavage

stabilisation assays, and additionally the same order of QZM potency held true from the MIC values against the *E. coli* bacteria. For DNA supercoiling, the IC_{50} ranged from 3.6 - 11.7 μM, the DNA relaxation IC_{50} values ranged from 15.4 - 107.5 μM and the DNA cleavage CC_{50} values ranged from 9.6 - 33 μM.

Across the different types of assays, the IC_{50} and CC_{50} values for each QZM were not consistent for each assay. The compounds were most efficient at DNA supercoiling inhibition, followed by DNA cleavage stabilisation and DNA relaxation inhibition. For QZM 1488, the DNA cleavage CC_{50} and the DNA relaxation IC_{50} was increased by 2.7-fold and 4.3-fold respectively, compared with the DNA supercoiling IC_{50}. The difference between potency of the QZMs in the DNA supercoiling and DNA cleavage assay was the greatest for QZM 1488, and 1529 had the greatest difference in potency between DNA supercoiling and DNA relaxation.

The variation in compound potency across DNA supercoiling, cleavage and relaxation assays was consistent with the literature, which observe type II topoisomerase inhibitors, including ciprofloxacin, are most affective at inhibiting the DNA supercoiling activity [201]. In part, this compound potency variation is because different stages of the gyrase reaction cycle were measured. Additionally, gyrase concentration was not consistent across the assays - gyrase is much more efficient at DNA supercoiling compared to DNA relaxation.

6.2.2 The quinazoliniums stabilise double-stranded DNA cleavage by *E. coli* gyrase

The QZMs were inhibitory to DNA relaxation and stabilised DNA cleavage. Both assays were performed in the absence of ATP, suggesting the QZMs were unlikely to be inhibitors of the ATPase domain like other gyrase inhibitors, such as the aminocoumarin novobiocin [202]. Inhibition of DNA supercoiling and relaxation indicated the compounds prevent successive DNA strand passage rounds. The compounds were likely to have a mechanism of action similar to the fluoroquinolones due to the cleavage stabilisation activity, and from the *E. coli* strains with resistance to QZM 1488 with mutations in the quinolone resistance determining region [tbl. 6.2]. The compounds stabilised double-stranded DNA cleavage, which is also observed with compounds including the fluoroquinolones, IPYs, and etoposide. Single-strand DNA cleavage did not accumulate, indicating that the compounds do not act similarly to the NBTIs, which stabilise single-stranded DNA cleavage [123].

The QZM activity against *E. coli* gyrase was compared with ciprofloxacin to assess the potential for the antibiotic series. The DNA supercoiling IC_{50} for ciprofloxacin was determined to be 1.2 μM, which was in good agreement with other literature values [120]. The lead compound, 1488 IC_{50} value was 3-fold less potent than ciprofloxacin, whereas the least active compound, 1529, was 12.2-fold less potent than ciprofloxacin.

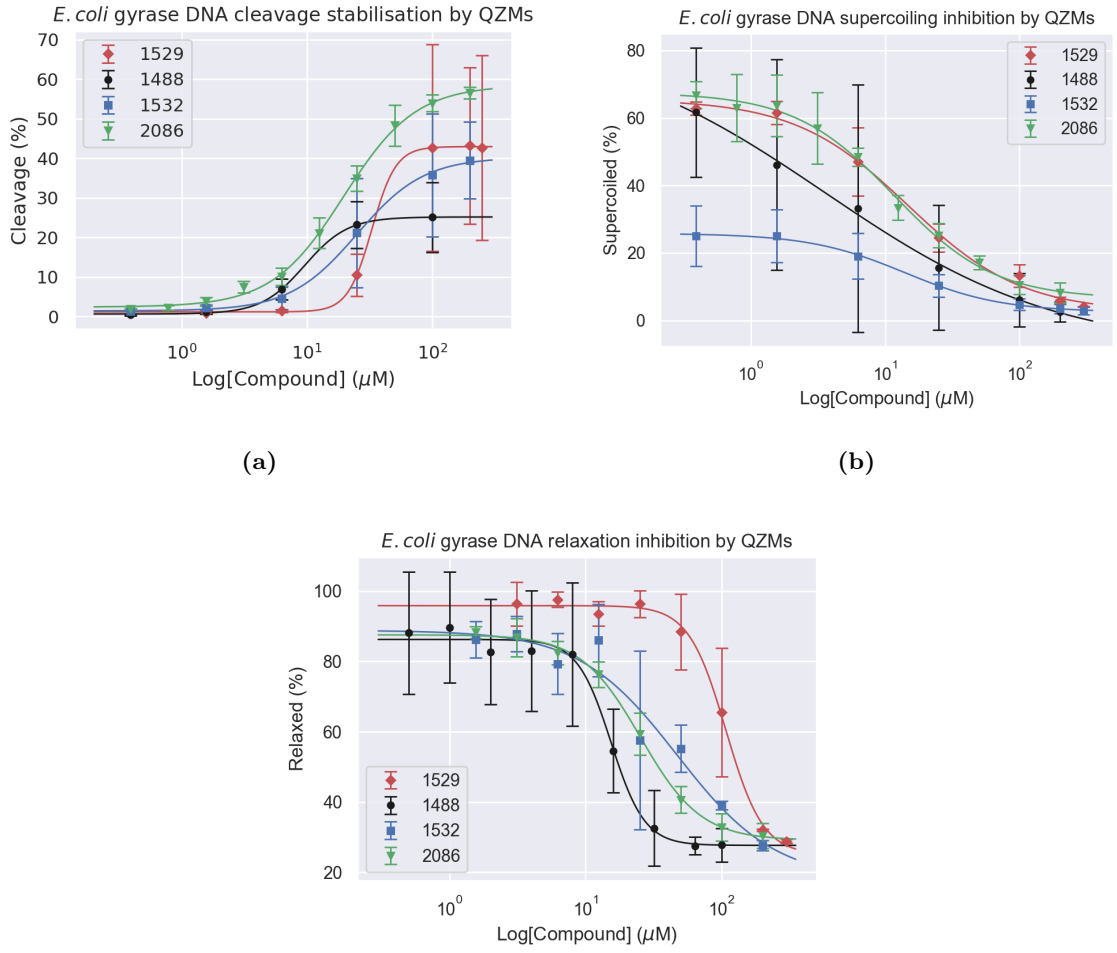

Figure 6.5: Potency of QZMs 1488, 1529, 1532 and 2086 against *E. coli* gyrase in *in vitro* assays. (a) DNA cleavage stabilisation CC_{50} curves. 15 nM of gyrase, negatively supercoiled pBR322 DNA, 0.39-100 μM 1488 at 2% DMSO, 1.56-250 μM 1529 at 1.7% DMSO, 0.39 - 200 μM 1532 at 4% DMSO and 0.39 - 200 μM 2086 at 3.6% DMSO were assayed in DNA cleavage assays. **(b) DNA supercoiling inhibition IC_{50} curves.** 5 nM of gyrase, relaxed pBR322 DNA and 0.39-200 μM of each QZM was assayed at 4% DMSO for compounds 1488 and 1532, 1.7% DMSO for compound 1532 and 3.6% DMSO for compound 2086. For QZM 1532, 2,5 nM of gyrase was used. **(c) DNA relaxation inhibition IC_{50} curves.** 50 nM of gyrase was assayed against 0.5 - 100 μM of 1488 at 2% DMSO, 3.1-300 μM 1529 at 1.7% DMSO, 1.6-200 μM 1532 at 4% DMSO and 0.5-100 μM 2086 at 2% DMSO using negatively supercoiled pBR322 DNA. The QZMs were titrated against *E. coli* gyrase. The DNA cleavage, supercoiling and relaxation assays were imaged using agarose gels and bands quantified using ImageJ. Curves were generated in python by fitting to a 4-parameter CC_{50}/IC_{50} curve using repeat 3 datasets. Standard deviation was calculated for the error bars.

Compound	Relaxation IC_{50} (μM)	Supercoiling IC_{50} (μM)	Cleavage CC_{50} (μM)
1488	15.4	3.6	9.6
1529	107.5	14.6	33.0
1532	47.1	14.0	25.1
2086	25.4	11.7	19.7
CFX	ND	1.2	ND

Table 6.3: IC_{50} and CC_{50} values for *E. coli* gyrase with QZMs. The IC_{50} and CC_{50} values from DNA cleavage, supercoiling and relaxation assays were calculated from 3 repeat datasets fitted to a 4-parameter curve in python.

6.2.3 Quinazolinium BT9701 is not active against *E. coli* gyrase and is highly unstable

When QZM BT9701 was dissolved into 100% DMSO, a colour change of the solution was observed, from colourless to yellow. The colourless and yellow samples of BT9701 were tested for DNA cleavage stabilisation activity against *E. coli* gyrase [fig. 6.6]. BT9701 incubated in 100% DMSO for 5 hours had DNA cleavage stabilisation activity, whereas BT9701 incubated into DMSO for no longer than 2 minutes did not have cleavage stabilisation activity above the control. The QZM series were developed from a precursor which gained activity after storage in DMSO due to oxidation of the isoquinoline ring system [196]. Oxidation of BT9701 would also lead to the formation of the positively charged quaternary nitrogen and therefore forming 1488. BT9701, which had a prior incubation in 100% DMSO, was sent for analysis by high-resolution mass spectrometry, which confirmed the conversion of BT9701 to 1488. 1488 had good DNA cleavage stabilisation activity, providing an explanation for the gain of activity of BT9701 after DMSO incubation. Due to the stability of BT9701, and no observable DNA cleavage stabilisation against *E. coli* gyrase, BT9701 was not included in further biochemical assays against topoisomerases. The positive charge on the quaternary nitrogen in the QZM series could therefore be essential for DNA cleavage stabilisation activity.

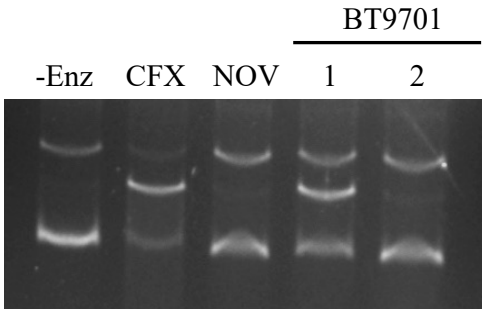

1. BT9701 incubated with DMSO for 5 hours
2. BT9701 incubated with DMSO < 2 minutes

Figure 6.6: The DNA cleavage activity of QZM BT9701 with *E. coli* gyrase. BT9701 was priorly incubated in 100% DMSO for 5 hours (1) or < 2 minutes (2) before use in the DNA cleavage assay. 20 μM novobiocin and ciprofloxacin were used as controls.

6.2.4 The main target of the quinazoliniums in *E. coli* was DNA gyrase, as opposed to topoisomerase IV

Whether the compounds dual targeted gyrase and topo IV, or primarily acted through inhibition of one of the bacterial type II topoisomerase enzymes was assessed. DNA gyrase and topo IV are both targets of the quinolone antibiotics and in most cases, DNA gyrase is the primary target for quinolones in Gram-negative bacteria, and topo IV is the primary target in Gram-positive bacteria. The QZMs were more effective against Gram-negative bacteria than Gram-positive bacteria, pointing us towards gyrase as the primary target for the QZMs [tbl. 6.1]. To confirm, the QZMs were tested against *E. coli* topo IV *in vitro* in DNA cleavage and relaxation assays to compare with the results of the QZMs against *E. coli* gyrase in [section 6.2.3].

The QZMs were assayed against *E. coli* topo IV for DNA cleavage activity at 40 and 200 μM for each QZM, the compounds had activity [fig. 6.7]. The DNA cleavage levels were not high enough to produce reliable CC_{50} curves, however 1488 and 1529 were more active compared with 1532 and 2086. The higher activity of 1529 compared to 1532 and 2086 against topo IV was not in agreement with the *in vitro* assays against *E. coli* gyrase or the MIC data.

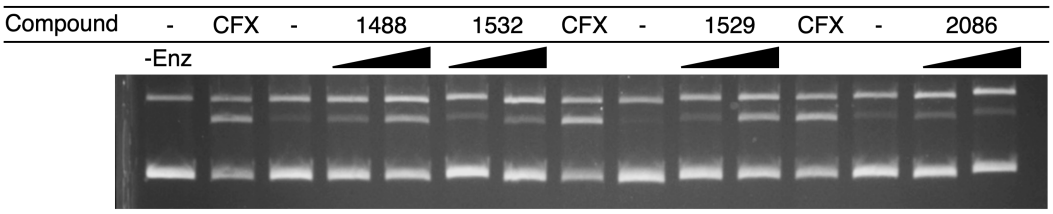

Figure 6.7: *E. coli* topo IV DNA cleavage stabilisation with CFX and QZMs. 40 and 200 μM of QZM was tested at DMSO concentrations of 4.0% for 1488 and 1532, 3.6% for 2086 and 1.7% for 1529 against 1 activity unit of topo IV with negatively supercoiled pBR322 DNA. No compound controls and CFX controls (20 μM) were performed at each DMSO concentration.

To confirm whether successive strand-passage was blocked by QZMs with topo IV, like with gyrase, the QZMs were tested for inhibition of DNA relaxation activity against *E. coli* topo IV [fig. 6.8]. The supercoiled band was not present in samples with QZMs, indicating that the QZMs did not inhibit DNA relaxation. The relaxed DNA bands on the agarose gel were closer to the nicked DNA band for samples with compound present compared to the DMSO control [fig. 6.8a]. The change in band migration could be due to intercalation of the compounds into DNA.

The samples from the topo IV relaxation assay were ran on a chloroquine gel to separate the nicked and relaxed topoisomers on the gel due to the subtle differences in band migration observed previously [fig. 6.8b]. An additional control of the QZMs with relaxed DNA was included. Particularly with QZMs 1529 and 2086, the DNA had slower migration on the agarose gel compared to the no compound DMSO control. A possible explanation would be that the QZMs are weak intercalators. If the compounds were intercalating into the DNA, the DNA would unwind the negatively supercoiled DNA and add compensatory positive supercoils. Decreasing the twist in DNA increases the writhe because the linking number cannot change without breakage of the DNA backbone. The DNA would be less negatively supercoiled in the presence of compound, therefore changing the equilibrium of the relaxed topoisomers produced by topo IV.

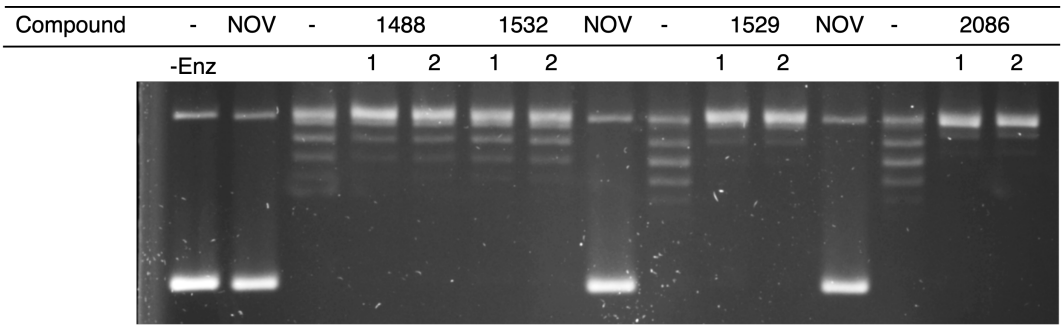

(a) No intercalator

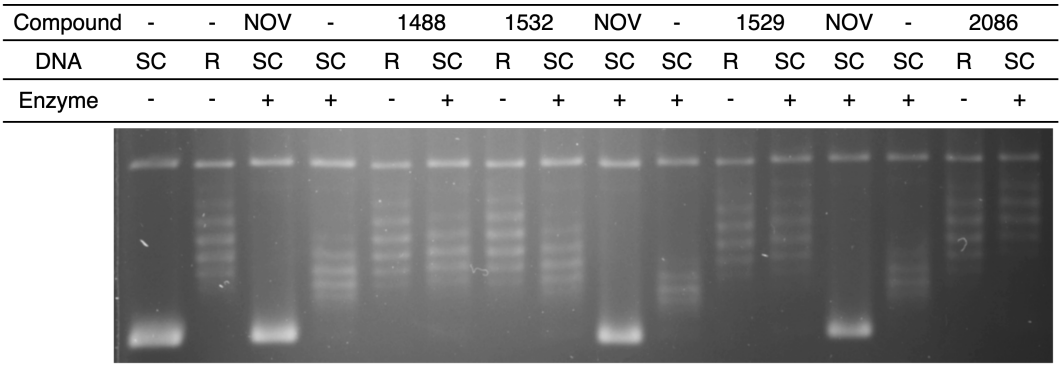

(b) 1.5 μg/mL chloroquine

Figure 6.8: *E. coli* topo IV DNA relaxation inhibition with the QZMs. (a) Relaxation inhibition was tested using 200 μM QZM, repeated twice using negatively supercoiled pBR322 DNA. Samples were analysed on an agarose gel with no intercalator present. **(b)** 200 μM of QZM was tested for inhibition of topo IV relaxation. The starting DNA material used was relaxed (R) or negatively supercoiling (SC) pBR322 DNA. Samples were analysed on an agarose gel in the presence of 1.5 μg/mL chloroquine. DMSO concentrations of 4.0% for 1488 and 1532, 3.6% for 2086 and 1.7% for 1529 were used. No compound controls and 20 μM novobiocin were run at the corresponding DMSO percentage.

6.2.5 The quinazolinium antibiotics do not target human topoisomerase IIα

For the QZMs to be successful as an antibiotic in treating bacterial infections in humans, the compounds must selectively target the bacterial topoisomerases and have no off target effect on the human type II topoisomerase enzymes. The QZMs against human topo IIα was assayed in a DNA cleavage assay [fig. 6.9] and a DNA relaxation assay [fig. 6.10], which may link to toxicity of the QZMs in humans. There was no observable stabilisation of nicked or linear DNA, suggesting that the compounds do not target the human enzyme.

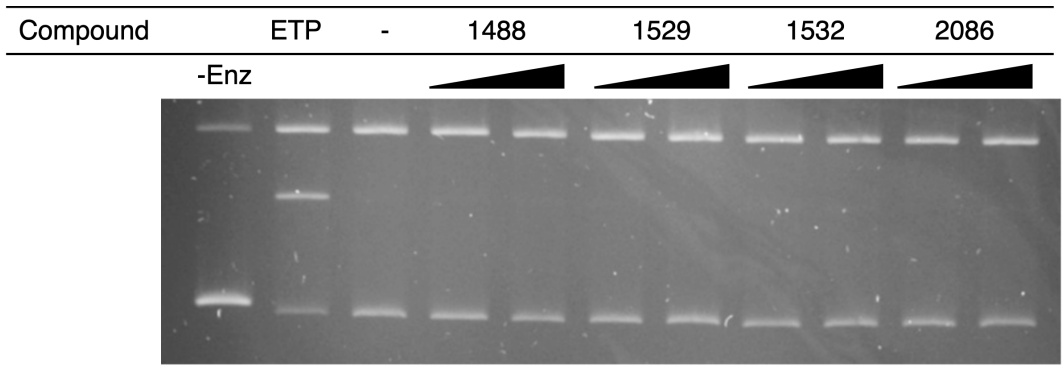

Figure 6.9: Human topo IIα DNA cleavage stabilisation with QZMs. 50 and 100 μM of each QZM, 1488, 1529, 1532 and 2086, was tested at 2.0% DMSO in a DNA cleavage assay against 1 activity unit of human topo IIα. No compound and etoposide (500 μM) controls were performed. The assay was carried out using negatively supercoiled DNA.

In the DNA relaxation inhibition assay with human topo IIα, faint supercoiled bands were visible, particularly for the 1529 and 2086 samples, indicating low levels of DNA relaxation inhibition (fig. 6.10). To see if there was evidence for QZM intercalation affecting human topo IIα relaxation, samples were run on a chloroquine gel. The result was not clear to whether the observed inhibition was due to QZM intercalation, or from topoisomerase inhibition. For both human topo IIα and *E. coli* topo IV, 1529 and 2086 gave the most inhibition of relaxation.

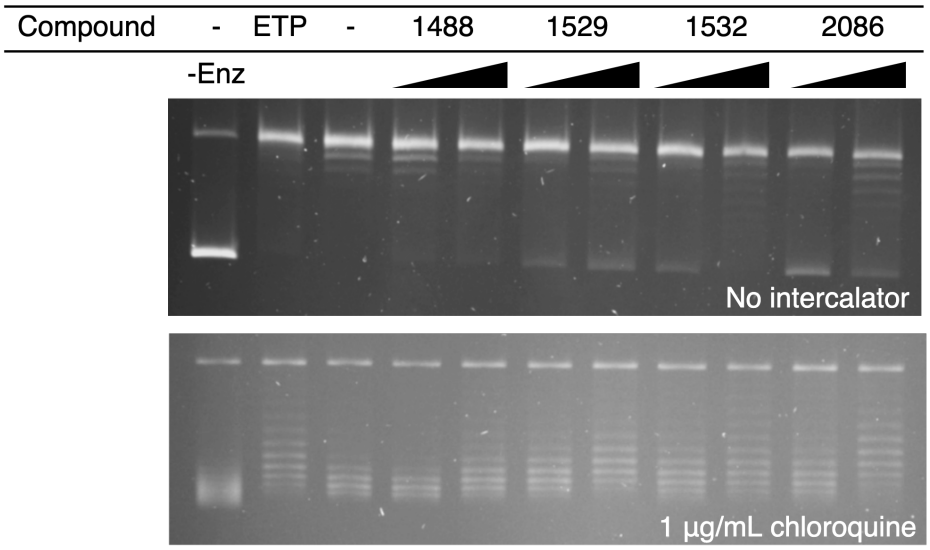

Figure 6.10: Human topo IIα DNA relaxation inhibition assay with QZMs. 50 and 100 μM of QZM was tested at 2.0% DMSO against 1 activity unit of human topoisomerase IIα. No compound and etoposide controls (500 μM) were performed. Negatively supercoiled pBR322 DNA was the substrate for the assay.

6.2.5.1 Assesment of the toxicity of the QZMs in *G. mellonella*

The QZMs were tested for toxicity in a model organism. Toxcitiy of antibiotics to *G. mellonella* larvae have been found to correlate with toxcitity in rodents [158]; the toxicity of the QZMs will determine the antibiotic potential of the series. In collaboration with Harriet Gooch (John Innes Centre), who raised and injected 5 larvae with 1 mg/mL QZM at 20% DMSO, which corresponded to 80 mg/kg of compound in the larvae and equivalent to 20x the MIC for *E. coli* with QZM 1488 (4 mg/L). A mortality rate of over 2 larvae per 5 larvae considers the compounds to be toxic. The mortality of the larvae was assesed. There were no dead larvae for QZM 1488, 1 larvae died in one of the replicates for QZM 1529 and 2086, and for QZM 1532, one larvae died in each of the replicates (tbl. 6.4). The compounds were therefore not toxic at 80 mg/kg for *G. mellonella* larvae.

Compound	Mortality per 5 larvae		
	1	2	3
PBS control	0	0	0
1488	0	0	0
1529	0	0	1
1532	1	1	1
2086	0	0	1

Table 6.4: The toxicity of the QZMs on *G. mellonella* larvae at 20x the MIC for QZM 1488. The QZMs at 1 mg/mL and solubalised into 20% DMSO were injected into 5 *G. mellonella* larvae and incubated for 24 hours at 30°C. The results were replicated 5 times and PBS at 20% DMSO was used as a control. Up to 2 dead larvae indicates the compounds are not toxic.

6.2.6 The quinazoliniums have weak intercalation activity with DNA

To confirm whether the QZMs were inhibiting the DNA relaxation by *E. coli* topo IV and human topo IIα, or the observed inhibition was a result of QZM intercalation into the DNA, an intercalation assay was run using wheat germ topo I [fig. 6.11]. The QZMs were incubated with negatively supercoiled DNA to allow the compounds to intercalate into the DNA. Topo I was then added to relax the negatively supercoiled DNA. If the compounds were intercalators, the DNA will be unwound and less negatively supercoiled, like with the positive control m-AMSA. Therefore, on addition of topo I, the enzyme would raise the linking number less in the presence of an intercalator.

The samples were run on agarose gels with and without chloroquine. There was no clear result to whether the QZMs were intercalators from the gel run in absence of chloroquine. Chloroquine addition to the gel resulted in better separation between the relaxed topoisomers and therefore the QZMs 1529 and 2086 migrated slightly slower compared with the DMSO control, indicating low levels of intercalation. Since 1529 and 2086 also gave the most inhibition of DNA relaxation by human topo IIα [fig. 6.10], it is likely that the low levels of inhibition were the effect of QZM intercalation in the DNA substrate. The QZMs were also tested with relaxed DNA as a substrate, to ensure the QZMs were not targeting wheat germ topo I, which was particularly important to run, due to the scaffold similarity between the QZMs, and the topoisomerase I inhibitor camptothecin. From the chloroquine gel, 1529 and 2086 migrated slower than the control, indicating that the QZMs were not affecting the topo I activity.

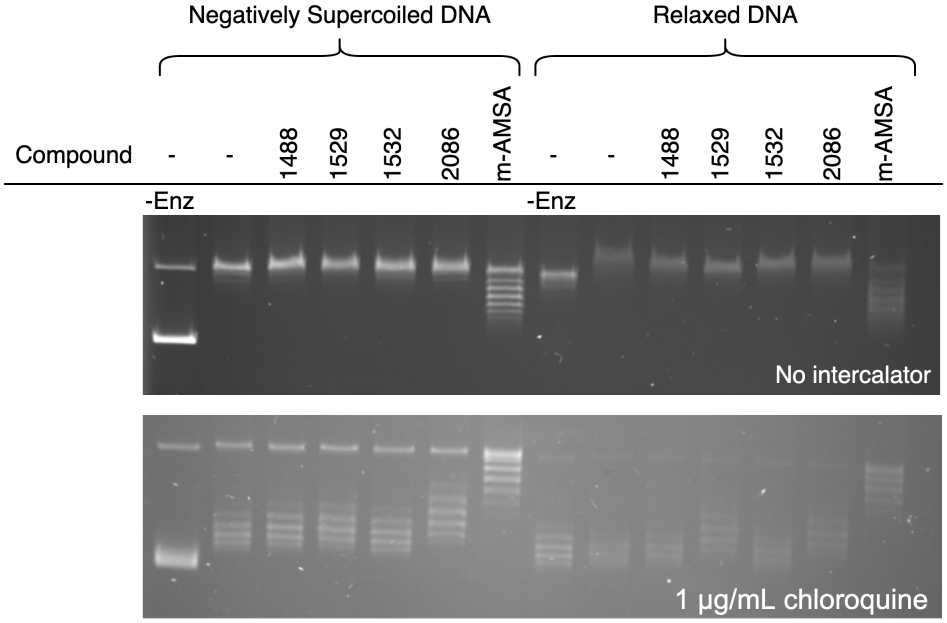

Figure 6.11: Intercalation assay with the QZMs using wheat germ topo I. 200 μM of each QZM were tested in a DNA intercalation assay with negatively supercoiled and relaxed pBR322 DNA substrates. 50 μM of m-AMSA as the positive controls, and the DMSO negative controls were run. The samples were analysed on an agarose gel without chloroquine (top), and at 1 μg/mL of chloroquine (bottom).

6.2.7 The quinazoliniums do not stabilise DNA cleavage by *M. mazei* topoisomerase VI

Topo VI is primarily an archeal enzyme, but is also found in some bacteria, plants and algae. Topo VI is an attractive drug target for herbicides due to the enzyme's key role in endoreduplication in plants, and for antimalarials by targeting *Plasmodium falciparum* topo VI

[203]. *M. mazei* topo VI was readily avaliable, and therefore the enzyme was assayed against the QZMs in a DNA cleavage assay [fig. 6.12]. No DNA cleavage stabilisation of nicked or linear DNA above the DMSO control was observed in the pesence of the QZMs. Previously, the QZMs have been predicted to have a similar mechanism of action as the fluoroquinolones. The fluoroquinolones are not affective against *M. mazei* topo VI [203], therefore, no cleavage stabilisation from the QZMs against *M. mazei* topo VI was not surprising.

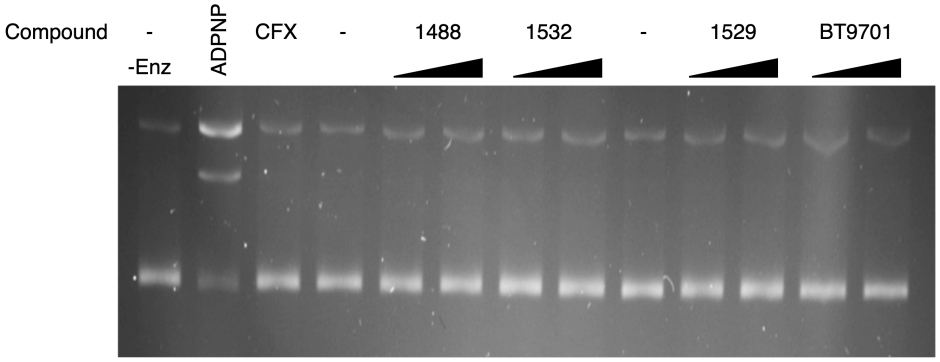

Figure 6.12: DNA cleavage stabilisation activity by QZMs against *M. mazei* topoisomerase VI. 40 nM of *M. mazei* topo VI was assayed against 100 and 200 μM of each QZM in a DNA cleavage assay, at 4.0% (1488 and 1532), and 1.7% (1529 and BT9701) DMSO using negatively supercoiled DNA. No compound, 1 mM ADPNP, and 20 μM CFX were used as controls.

6.2.8 *S. aureus* gyrase *in vitro* can be targeted by the quinazoliniums

From the biochemical analysis of the QZMs, the results suggested the QZMs primarily target bacterial DNA gyrase via stabilisation of double-stranded DNA breaks. The next step was to have a crystal structure of the QZMs and gyrase to characterise the compound binding site, to inform structure-based drug design. The *S. aureus* gyrase crystallography system is well established, compared with *E. coli* gyrase. From the MIC data, the compounds showed little to no antibacterial activity towards wild-type *S. aureus*, and it was therefore unclear whether the QZMs could bind to this enzyme. Sensitive strains weren't tested in *S. aureus*, meaning the QZMs could have difficulty with entry or be exported from the bacteria, before inhibiting gyrase. Therefore, QZMs 1488, 1529, 1532 and 2086 were tested against *S. aureus* gyrase in *in vitro* DNA cleavage assays [fig. 6.13]. The compounds stabilised DNA cleavage, QZMs 1529 and 1488 had the best activity. The QZMs were titrated against *S. aureus* gyrase and the data for QZM 1529 was fitted to a CC_{50} curve. The CC_{50} value was calculated to be 109.2 μM [fig. 6.14]. The DNA cleavage stabilisation by 1488, 1532 and 2086 was too low to produce reliable CC_{50} curves.

Although compound 1529 was the most active compound against *S. aureus* gyrase, the

CC_{50} value was 3.3-fold higher than with *E. coli* gyrase. 1488 was the most active compound against *E. coli* gyrase and therefore it was an interesting as to why the *S. aureus* gyrase was more resistant to QZM 1488, compared with 1529. The result was not unexpected, since some fluoroquinolones, including ciprofloxacin are significantly more potent against *E. coli* gyrase than *S. aureus* gyrase. The results point towards the high MICs of the QZMs against *S. aureus* are likely due to poor inhibition of the topoisomerases, rather than entry into the bacteria. It must also be noted that in *S. aureus* gyrase, the main target for ciprofloxacin is topo IV as opposed to gyrase, which could hold true for the QZMs [204]. The QZMs have not been tested against *S. aureus* topo IV and would be an important experiment for the future.

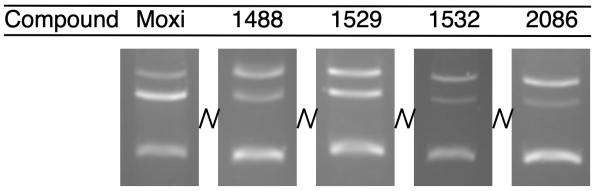

Figure 6.13: *S. aureus* gyrase DNA cleavage with QZMs. The cleavage stabilisation activity assay by 300 μM of QZM 1488, 1529, 1532 and 2086 against 15 nM of *S. aureus* gyrase. 100 μM of moxifloxacin was used as a control.

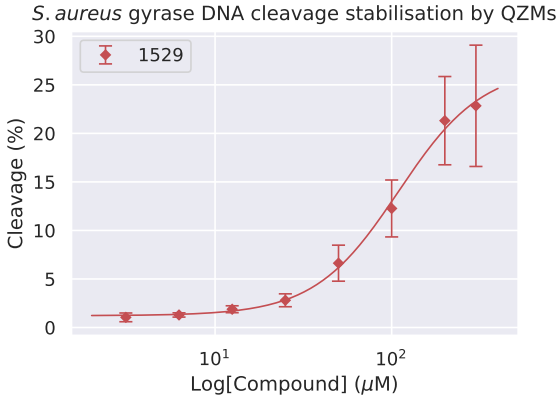

Figure 6.14: *S. aureus* gyrase DNA cleavage stabilisation with QZM 1529. The cleavage stabilisation activity of QZM 1529 was tested against *S. aureus* gyrase. The data was fitted to a CC_{50} curve with standard deviation calculated from 3 data sets in python. The CC_{50} was calculated to be 109.3 μM.

The QZMs were tested for inhibition against *S. aureus* gyrase supercoiling activity, however, no supercoiling inhibition was observed when the maximum concentrations that the compounds were soluble was used. Since the compounds have DNA cleavage stabilisation activity, there was some confidence the compounds were specifically binding to the enzyme, and had the

potential to have low inhibition on gyrase supercoiling. A time course assay was performed to track potential slowing of the DNA supercoiling reaction caused by the QZMs [fig. 6.15] The experiment is similar to that performed with microcin B17 to show microcin slows down supercoiling by *E. coli* gyrase [205]. The time course assay was performed with 1488 and no inhibition or slowing of DNA supercoiling was observed. There was little to no inhibition of supercoiling by the QZMs on *S. aureus* gyrase. Since the compounds were active in stabilising DNA cleavage, the *S. aureus* gyrase core fusion crystallography system route was chosen to obtain crystal structures. The QZMs were able to target the DNA cleavage reaction as opposed to the DNA supercoiling reaction, potentially because the DNA cleavage step may not be the rate limiting step in the supercoiling cycle. Despite the DNA cleavage stabilisation by the QZMs, the compounds were ineffective at DNA supercoiling inhibition.

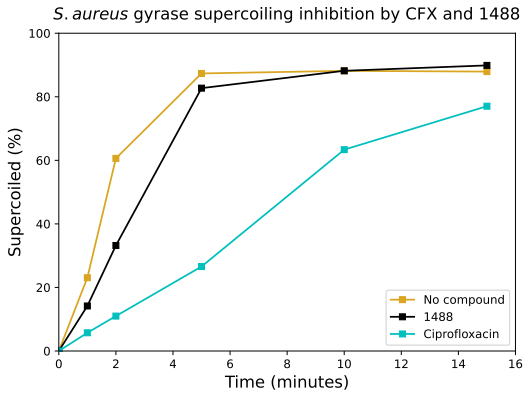

Figure 6.15: *S. aureus* gyrase DNA supercoiling timecourse with CFX and QZM 1488. The supercoiling inhibition activity of 20 μM CFX, 200 μM QZM 1488 and no compound at 4% DMSO with relaxed pBR322 DNA was performed. Time points up to 15 minutes were taken by trapping with SDS.

6.2.9 Crystallisation trials with *S. aureus* gyrase and the Quinazoliniums

After the QZM's DNA cleavage activity against *S. aureus* gyrase was confirmed, crystallisation trials with 1488, 1529, 1532 and 2086 were set up. The *S. aureus* gyrase core fusion has been successfully used in crystal structures with fluoroquinolones such as moxifloxacin [52], and imidazopyrazinones [120], both of which act to inhibit topoisomerases by stabilising DNA cleavage, similar to the QZMs. The protein construct for the *S. aureus* gyrase core fusion was a fusion of the C-terminal region of GyrB and the N-terminal region of GyrA, with the flexible Greek Key domain deleted to improve the resolution [39]. The core fusion construct is able to perform the breakage-reunion activity on DNA, however, since there is no ATPase domain or wrapping domain, the enzyme cannot supercoil or relax DNA.

Crystallisation trials used the commercial screen MIDASplus™ and the sitting drop method. *S. aureus* gyrase core fusion wild-type and also a mutant in the catalytic tyrosine which forms the phosphotyrosine linkage (Y123F) to break DNA was used. A 20-bp oligo with artificial nicked staggered by 4-bp to mimic DNA in the cleaved state was used with the catalytic tyrosine mutant (Y123F). A 20-bp uncleaved oligo was used with the wild-type, which would then be cleaved by the enzyme, forming a covalent phosphotyrosine linkage [fig. 6.16]. Using the wild-type and the phosphotyrosine mutant with different DNA oligos has been used previously to capture different conformational states of the enzyme [52].

Three small crystals of *S. aureus* gyrase core fusion wild-type with 1488 in G9 from the MIDASplus™ screen appeared after 4-6 weeks of incubation [fig. 6.16d]. For compound 1529, medium-sized crystals which took 1-2 weeks to grow were observed with wild-type in the condition C11 [fig. 6.16a], and Y123F mutant in conditions C2 [fig. 6.16b] and H2 [fig. 6.16c] from the MIDASplus™ screen. The crystals were fished with the help of Dr. Clare Stevenson, and sent to the Diamond Light Source synchrotron.

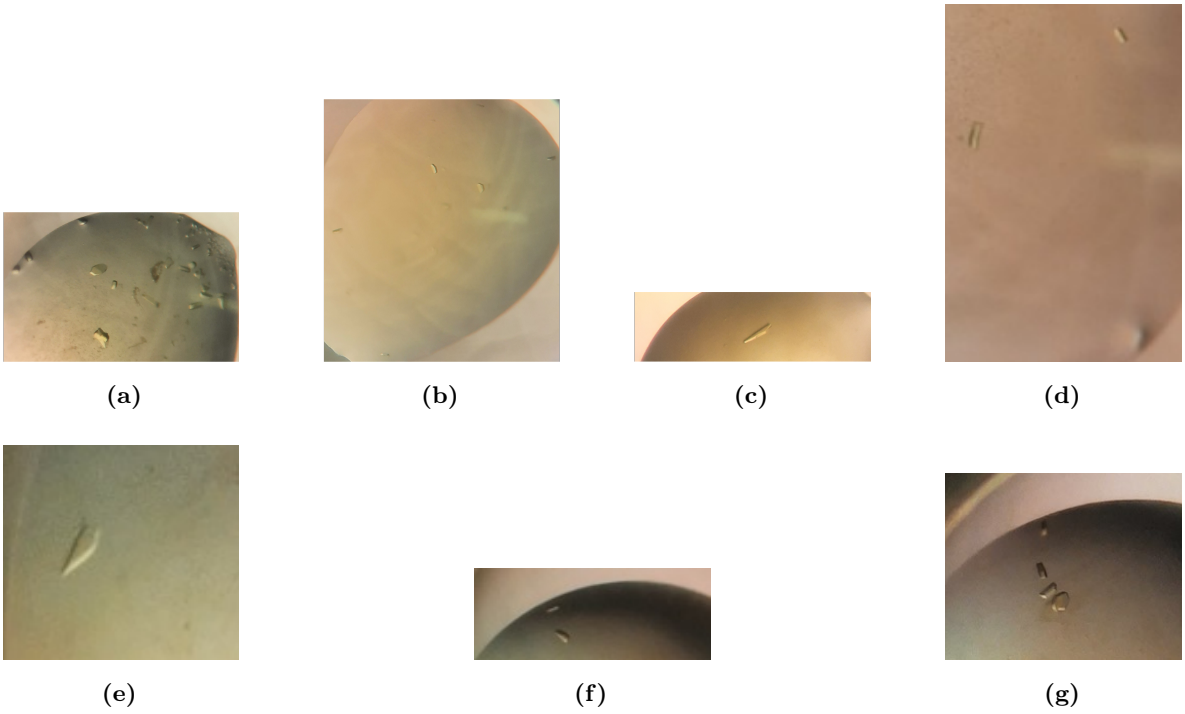

Figure 6.16: Crystals of *S. aureus* gyrase core fusion with QZM 1529 and 1488 crystallised from the commercial screen MIDASplus™. *S. aureus* gyrase core fusion wild-type **(a)** from C2, and Y123F mutant **(b)** and **(c)** from C11 and H1 respectively crystallised from the commercial screen MIDASplus™ with QZM 1529. **(d)** *S. aureus* gyrase core fusion wild-type with 1488 crystallised with the commercial screen MIDASplus™ G9. **(e-g)** Crystals of 1529 with *S. aureus* gyrase core fusion Y123F mutant from an optimisation plate based around C11 from the commercial screen MIDASplus™. The wild-type protein was crystallised with 1448-T 20-mer intact DNA and for gyrase Y123F mutant, the pre-nicked 20-12p-8 DNA was used.

The crystals of *S. aureus* gyrase core fusion with QZM 1488 and 1529 did not diffract to high resolution [fig. 6.16a - 6.16d]. The crystal from [fig. 6.16c] diffracted to the highest resolution and a dataset was collected at 3.5-4.0-Å resolution. The structure was not solved because the dataset was contaminated with multiple lattices. Based around the condition which gave the best diffraction (H1 from MIDASplus™) and the crystals which were visually more 3-D (C11 from MIDASplus™), two optimisation plates were designed using the *S. aureus* gyrase core fusion wild-type and Y123F mutant with QZM 1529. The concentration of the precipitant, (SOKERLAN CP-42 or pentaerythritol ethoxylate 15/4 EO/OH), pH and the type of metal ions in the conditions were screened. No crystals were observed in the SOKERLAN CP-42 plate (optimised from H1 from MIDASplus™). Three conditions grew promising crystals with the *S. aureus* gyrase Y123F mutant in the pentaerythritol ethoxylate plate (optimised from C11 from MIDASplus™). The conditions were 25% pentaerythritol ethoxylate 15/4 EO/OH at pH 8 - 8.75 with either 50 mM $MnCl_2$ or a mix of 50 mM $MgCl_2$ and 50 mM $MnCl_2$ [fig. 6.16e - 6.16g]. The crystal which gave the best diffraction [fig. 6.16f] was solved to 2.98-Å resolution in collaboration with Prof. Dave Lawson (John Innes Centre crystallography platform).

6.2.10 The 2.98-Å resolution structure of *S. aureus* gyrase with quinazolinium 1529

In the 2.98-Å resolution structure of *S. aureus* gyrase core fusion Y123F mutant with QZM 1529, two gyrase complexes were present in the asymmetric unit. The structure was solved in the P1 2_1 1 space group, which belongs to the monoclinic point group and has a 2_1 screw axis. The statistics for the crystal structure are given in table 6.5.

Space group	P 1 2_1 1
Unit cell	monoclinic
Unit cell dimensions	
a (Å)	88.57
b (Å)	168.98
c (Å)	122.08
α (°)	90.00
β (°)	100.79
γ (°)	90.00
Wavelength (Å)	0.9795
Resolution range (Å)	60.69-2.99
No. reflections	483539
Unique reflections/free	70526, 3535
Completeness (%)	99.4
Multiplicity	6.9
Wilson B-factor ($Å^2$)	69.9
R_{merge} (%)	0.17
Average B-value, all atoms ($Å^2$)	88.0
$I/\sigma(I)$	1.30
CC(1/2)	0.995
R, R_{free} (%)	0.272, 0.301
RMS deviations	
Bond (Å)	0.0026
Angle (°)	0.817
Ramachandran plot	
Favoured (%)	95
Allowed (%)	3
Outliers (%)	0

Table 6.5: The parameters and statistics from the data collection and refinment of the *S. aureus* gyrase core fusion Y123F mutant structure with quinazolinium 1529.

Viewing gyrase down the two-fold axis pictures two molecules of 1529 per gyrase complex hemi-intercalating into the DNA at the DNA cleavage site [fig. 6.17]. The compounds were modelled in the same orientation in each site, which was their most likely conformation. For a low resolution structure, the density could allow for the compound to flip along the y-axis and have two binding modes at the DNA cleavage site, which has been reported in gyrase-fluoroquinolone crystal structures [162]. QZM 1529 binds to gyrase similarly to fluoroquinolones, but without the requirement for the water-metal ion bridge - the binding is therefore more similar to the imizadopyrazinones. This result was unsurprising, since the MIC data demonstrated that the amino acid residues required to form the water-metal ion bridge for fluoroquinolones do not

give rise to significant QZM 1488 resistance in *E. coli* [tbl. 6.2]. Additionally, the water-metal ion bridge is formed from the ketone and carboxylic acid moiety on the fluoroquinolone and QZMs lacks the carboxylic acid group.

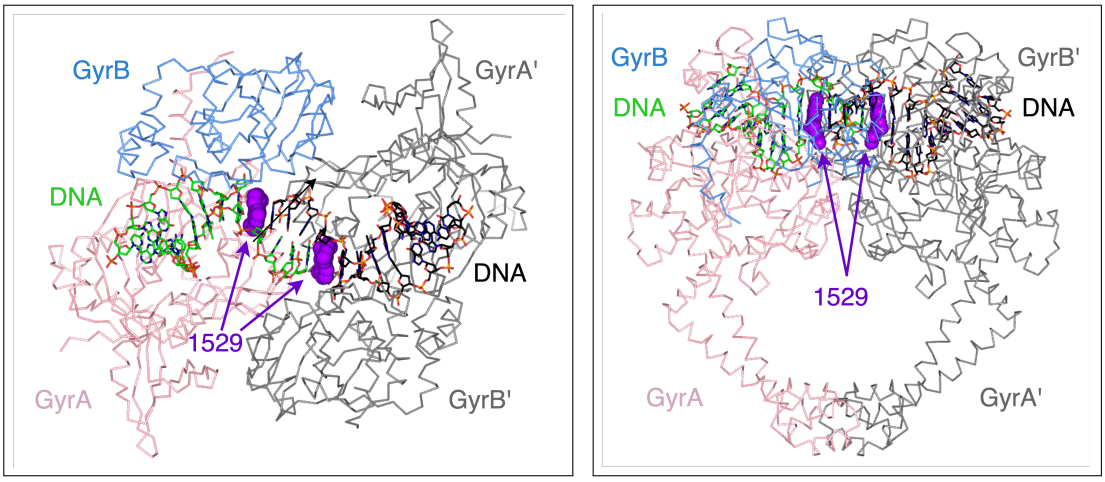

(a) **(b)**

Figure 6.17: The 2.98-Å resolution structure of *S. aureus* gyrase core fusion Y123F mutant with QZM 1529. (a) Gyrase viewed down the diagonal two-fold rotational axis at the GyrA dimer interface. Two 1529 molecules (purple) are present per gyrase complex (2 gyrase complexes and 4 1529 molecules in the asymmetric unit). 1529 is visualised intercalating into the DNA at the site of the artificial nick in the DNA. **(b)** The two-fold axis orientated vertically, giving an orthogonal view of gyrase. GyrA and GyrB are coloured pink and blue respectively on one half of the complex, the remaining half is coloured grey.

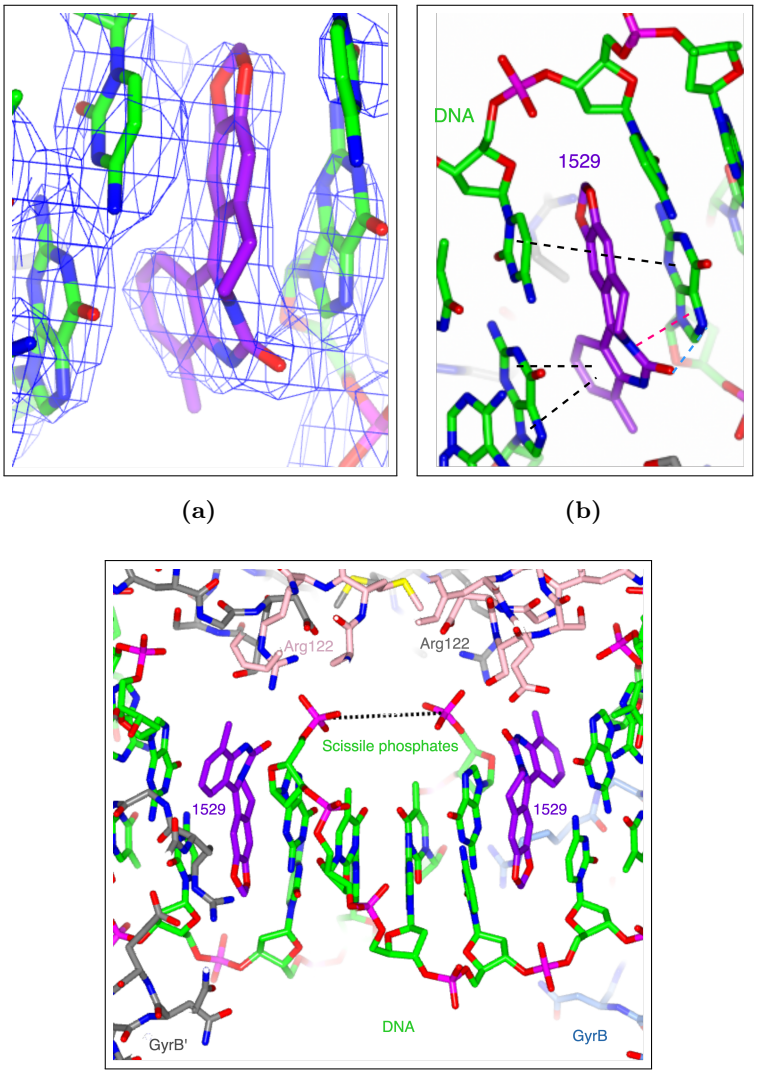

Figure 6.18: QZM 1529 with *S. aureus* gyrase core fusion Y123F mutant 2.98-Å resolution crystal structure. (a) The electron density surrounding QZM 1529. The sigma factor for scaling of electron density was not recorded. **(b)** QZM 1529 intercalating into the DNA and interacting by pi-pi stacking (black), hydrogen bonds (blue) and cation-pi interactions (magenta). The hydrogen bond between the carbonyl oxygen on the pyrimidine ring from 1529, and the nitrogen from gyanine was 3.12 Å. **(c)** Two molecules of QZM 1529 intercalating into the DNA at the DNA cleavage site. The scissile phosphates (pink) were 9.37 Å apart.

QZM 1529 intercalated with DNA and made contacts through pi-pi stacking interactions via the B and E rings of 1529, and the DNA bases. Additionally, there was a cation-pi interaction between the positively charged quaternary nitrogen on the 6-membered B-ring of 1529, and the 5-membered ring of guanine. The cation-pi interaction validates the importance of the charged nitrogen to form the hydrogen bond and for QZM activity, since the neutrally charged BT9701 QZM had poor antibacterial activity and no gyrase inhibition. There was also a direct

hydrogen bond between the carbonyl oxygen from the pyrimidine ring on 1529, and a nitrogen from guanine of 3.1 Å [fig. 6.18b]. The equivalent amino acid residues which gave rise to resistance in *E. coli* to QZM 1488 were investigated [fig. 6.19]. The closest residue to QZM 1529 on the GyrA alpha-helix was serine 84, which was 3.5 Å away, which could be too long for a direct hydrogen bond, however, the bond cannot be ruled out due to low resolution.

The scissile phosphates were coordinated by arginine 122 by direct hydrogen bonds ranging from 2.6 - 3.1 Å from the arginine nitrogen and the phosphate oxygens across the 4 arginines in the asymmetric unit. Arginine 122 was 3.56 Å from the 1529 methyl group. Equivalent residues which gave QZM resistance in *E. coli* included GyrA aspartate 83, serine 85 and glutamate 88, and GyrB asparagine 475, which were all >4 Å from 1529. The density of GyrB arginine 458 was poor and thus was deleted in 2 out of the 4 positions in the asymmetric unit. The remaining two arginines were in different conformations, suggesting the arginine was very flexible. Only one of the arginine conformations formed a direct hydrogen bond of 2.76 Å from the arginine terminal nitrogen to the 1529 oxygen from ring A [fig. 6.19c].

6.2.11 A comparison of the *S. aureus* gyrase QZM 1529 2.98-Å resolution structure with structures of functionally similar drugs, and of *E. coli* gyrase.

The QZMs are a novel series of synthetic antibiotics, however the heterocycle series have structural elements in common with other type II topoisomerase DNA cleavage stabilisers (fig. 6.2). Gyrase antibiotics commonly contain a condensed benzene ring and a nitrogenous heteroaromatic 6-membered ring, as with the fluoroquinolones, imidazopyrazinones and the quinazoline diones. When these compounds are superimposed in crystal structures of the compound and a type II topoisomerase, the condensed two rings align in the same orientation, despite the antibiotic's diverse scaffold. The position of the quinazolin-2-one from 1529 differed from other gyrase antibiotics. The 1529 *S. aureus* gyrase structure was compared with the quinazoline-2,3-dione (PD 0305970) and *S. pneumoniae* topo IV crystal structure, because the QZMs also have a quinazoline ring (fig. 6.20). The two structures were superimposed based on secondary structure, and the quinazoline rings were in different orientations. The benzene ring was rotated by 90°, such that the benzene ring from 1529 aligns with the cyclopropane group from the quinazoline-2,4-dione. The pyrimidine rings occupy the same structural space, however due to the rotation, the nitrogens and carbons do not align.

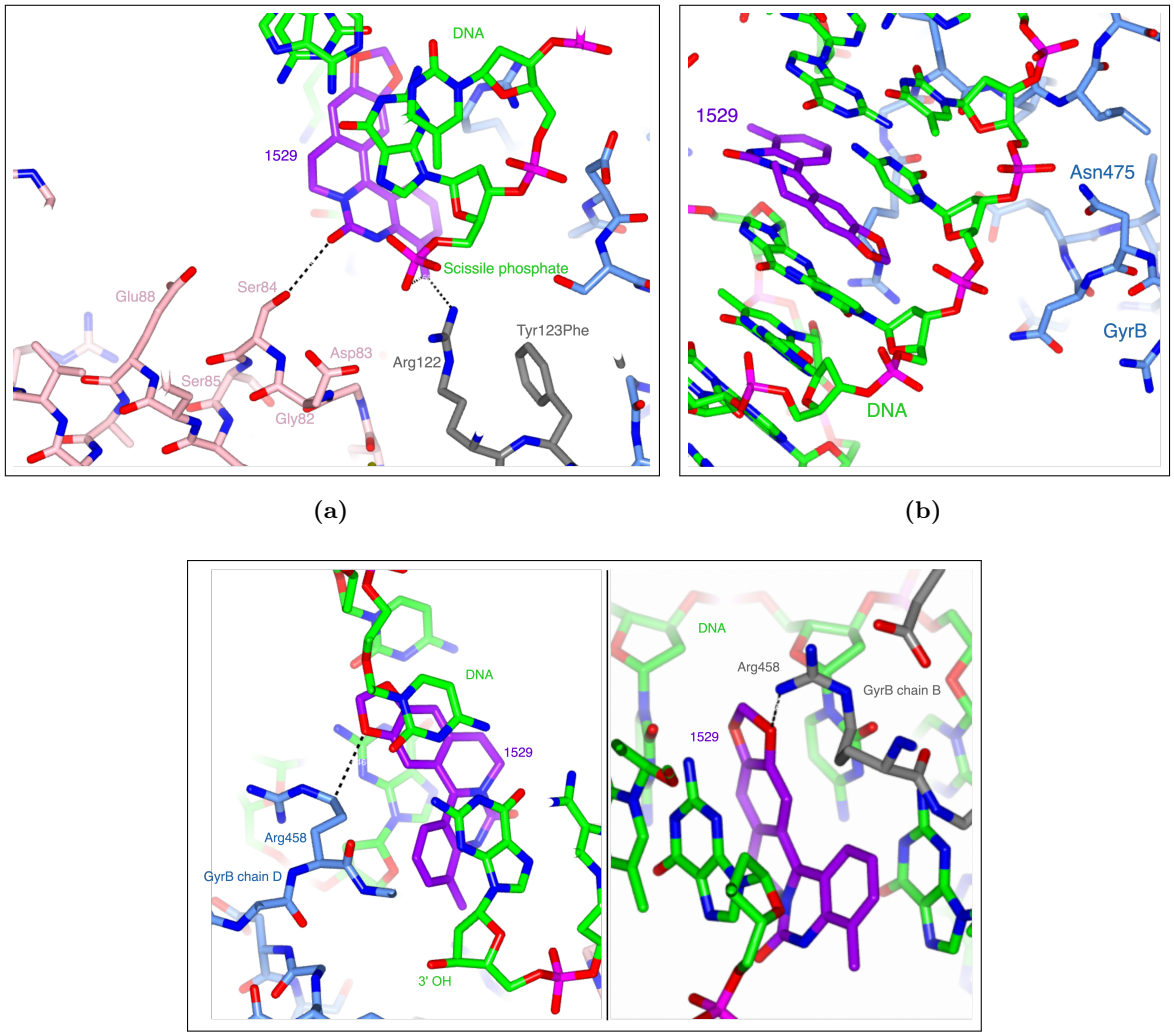

Figure 6.19: The amino acid residue interactions with QZM 1529 in the 2.98-Å resolution *S. aureus* gyrase core fusion Y123F crystal structure. (a) QZM 1529 interacting with GyrA residues equivalent to those identified from *E. coli* MIC data which gave resistance to QZM 1488: glycine 82, aspartate 83, serine 84, serine 85 and glutamate 88. Arginine 122 hydrogen bonds with the scissile phosphate. **(b)** GyrB Asparagine 475 interacting with the DNA near the DNA cleavage site and the 1529 intercalation site. In *E. coli*, mutation of the equivalent residue gave rise to resistance to QZM 1488. **(c)** The GyrB arginine 458 side chain interacting with the side of QZM 1529 on each half of the gyrase complex. The arginines are in different conformations. Left - shortest distance between arginine and 1529 is 3.56 Å. Right - hydrogen bond between N-terminal nitrogen on arginine, and oxygen from 1529 ring A. The equivalent residue in *E. coli* gyrase gave rise to resistance to QZM 1488. QZM 1529 (purple), GyrA (pink), GyrB (blue), the opposite GyrBA fusion (grey) and DNA (green).

To understand why the quinazoline ring from the 1529 structure was in a new position compared to other common gyrase antibiotic DNA cleavage stabilisers, QZM 1529 was overlayed into the topo IV quinazoline dione structure and the quinazoline rings were aligned from the two compounds (fig. 6.20). QZM 1529 extended parallel to the GyrA alpha-helix, however no steric clashes were observed. Steric clashes were therefore not the reason for the new

position of the quinazoline ring on the QZMs in the structure. It is unlikely that QZM 1529 adopts this conformation natively, because the MIC data suggested GyrB residues were implicated in QZM resistance, which would not interact with QZM 1529 in the quinazoline ring alignment conformation. The differential positions of the quinazoline rings should be taken into consideration when improving on the QZM scaffold to mimic structures of successful antibiotics such as the fluoroquinolones. For example, if the C7 position of the benzene ring was modified with a 1,4-diazinane ring like with ciprofloxacin, the diazinane ring would not point into the DNA cleavage site towards GyrB, but instead be positioned close to the GyrA phosphotyrosine.

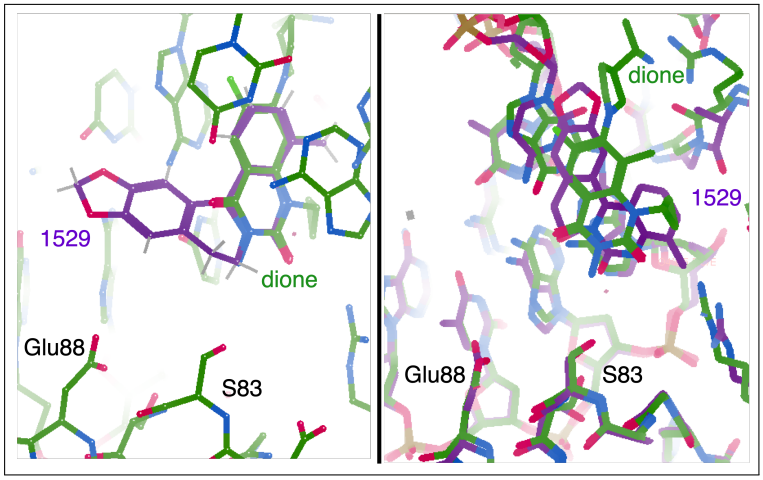

Figure 6.20: Predicting the binding site of QZM 1529, based on a structually similar fluoroquinolone-like quinazoline2,4-dione and alignment on the quinazolinedione ring, and the superimposition of the QZM crystal structure with the quinazoline-2,4-dione structure. QZM was modelled into the crystal structure *S. pneumoniae* topo IV based on alignment of the quinazoline-2,4-dione ring of 3-amino-7-((3R)-3-[(1S)-1-aminoethyl]pyrrolidin-1-yl)-1-cyclopropyl-6-fluoro-8-methylquinazoline-2,4(1H,3H)-dione. The *S. aureus* gyrase crystal structure with 1529 was superimposed against the quinazoline-2,4-dione structure, to reveal a new position of the quinazolinone ring by QZM 1529. The model structure used was from pdb 4z4q. The quinazoline-2,4-dione structure is coloured green, and 1529 structure in purple.

The 1529 structure was compared to the successful fluoroquinolone antibiotics structures to see if structural differences were resulting in the difference in activity between fluoroquinolones and QZMs. The crystal structure of 1529 was compared with the 2.95-Å resolution crystal structure of *S. aureus* gyrase core fusion wild-type and moxifloxacin by superimposing the secondary structure [fig. 6.21] [46]. The structures had highly similar secondary structure conformations [fig. 6.21a - 6.21b]. The GyrA alpha-helix loops were in the same position and the amino acids had similar conformations, accept glutamate 88, whose orientation varied throughout the asymmetric unit in the 1529 structure due to poor resolution. The GyrB

arginine 458 in the moxifloxacin structure was pushed away from the DNA compared to the 1529 structure, on account of the larger size of moxifloxacin [fig. 6.21c]. Another significant difference was the position of the scissile phosphates; in the 1529 structure, the phosphates were much closer together at 9.37 Å, compared to 23.15 Å in the moxifloxacin structure. The phosphate positioning was a result of the scissile phosphates in the 1529 structure flipping away from the phenylalanine and towards the 1529 compound.

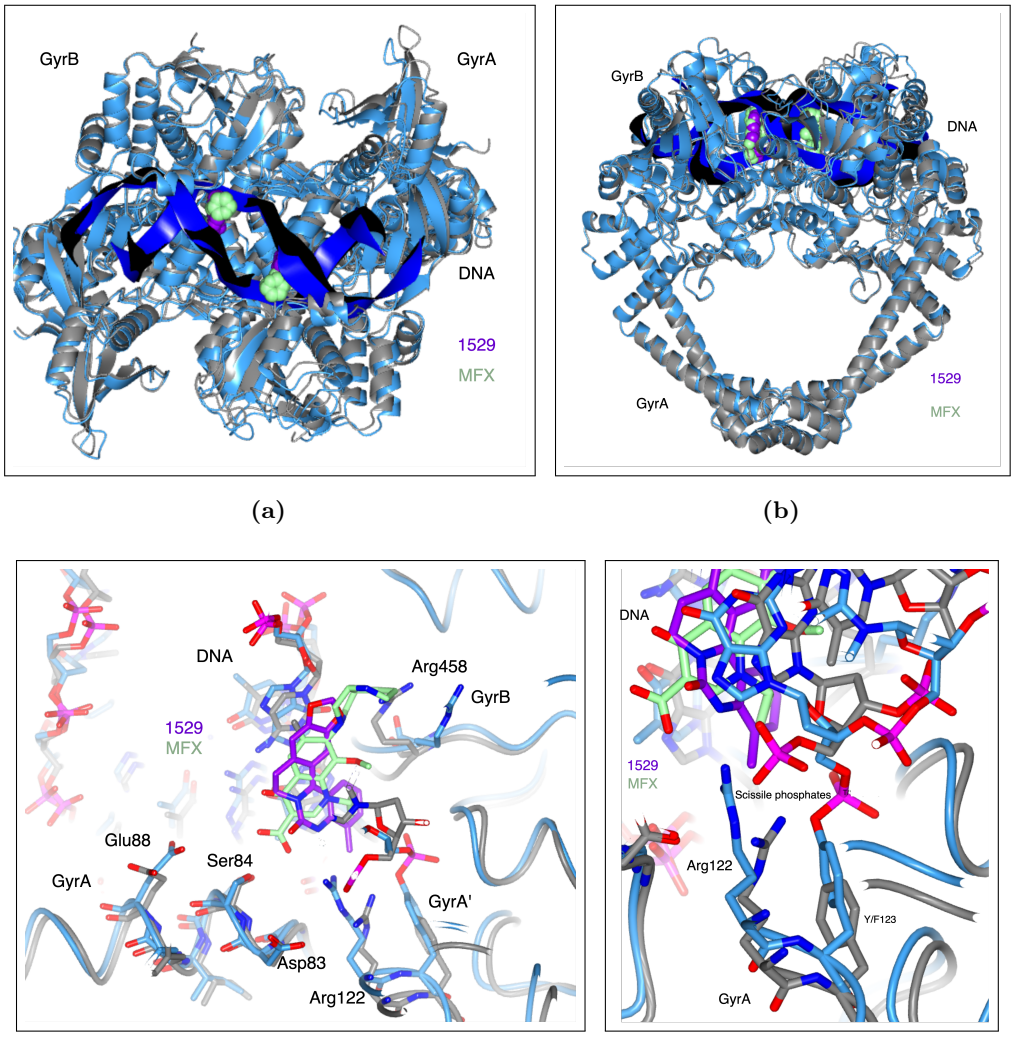

Figure 6.21: The 2.98-Å *S. aureus* gyrase core fusion Y123F with QZM 1529 superimposed using secondary structure (SSM) with the 2.95-Å *S. aureus* gyrase core fusion wild-type with moxifloxacin structure - pdb 5cdq. **(a)** The top view of the superimposed 1529 and moxifloxacin structures at the GyrA dimer down the 2-fold axis. **(b)** The orthogonal side view with the two-fold axis vertical of the 1529 and moxifloxacin structures. **(c)** The superimposed 1529 and moxifloxacin structures showing the amino acid residues interacting with 1529 or moxifloxacin on the GyrA loop, the GyrB arginine 458 and the GyrA tyrosine/phenylalanine. **(d)** The positions of the scissile phosphates in the 1529 and moxifloxacin superimposed structures. The scissile phosphate were shifted towards the compound in the 1529 structure. Grey - 1529 structure. Blue - 5cdq moxifloxacin structure. Purple - 1529. Pale green - moxifloxacin. Pink - phosphates.

The 1529 structure was superimposed with the *S. aureus* gyrase core fusion wild-type 3.08-Å structure with the imidazopyrazinone (IPY) t1 to compare the 1529 structure to a compound which also does not require a water-metal ion bridge to bind [fig. 6.22] [120]. The GyrA alpha-helix amino acids were in a similar conformation. The IPY is larger than 1529 and therefore the nitrogen from the 5-membered double nitrogen-containing ring on the IPY was able to form a direct hydrogen bond with GyrA serine 84. Serine 84 in the 1529 structure was too far away to act similarly on 1529. In line with the moxifloxacin structure, the position of the scissile phosphates are much further apart than the 1529 structure at 23.26 Å.

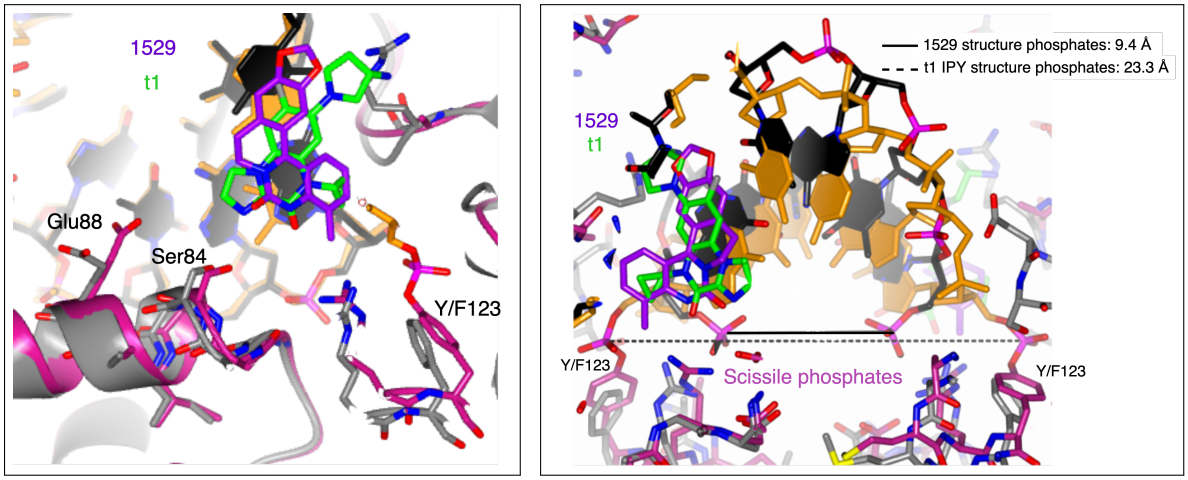

(a) **(b)**

Figure 6.22: Superimposing the 3.08-Å *S. aureus* gyrase core fusion Y123F 1529 structure with the structure of *S. aureus* gyrase wild-type core fusion with the imidazopyrazinone t1. **(a)** A view of the GyrA loop showing overlay agreement of GyrA serine 84, and the catalytic tyrosine/phenylalanine. **(b)** The positions of the scissile phosphates between the IPY t1 and 1529 structures. The scissile phosphates were 9.4-Å apart (solid-line) in the 1529 structure, and 23.3-Å in the IPY structure (dashed line). Grey - 1529 structure, magenta - 6fqm IPY t1 structure, purple - 1529, green - IPY t1.

From the MIC data and biochemical data, the lead QZM compound 1488 was significantly more active against *E. coli* gyrase than *S. aureus* gyrase. The crystal structure was compared to the cryo-EM 4.0-Å *E. coli* gyrase structure with gepotidacin. Gepotidacin is a DNA cleavage stabiliser, however, intercalates into the DNA in the center of the 4-bp stagger [fig. 6.23] [36]. The position of the GyrA alpha-helix in the structures were similar and the residues on the helix were identical except for *S. aureus* gyrase serine 85 which is an alanine in *E. coli* gyrase, which interacts with DNA [fig. 6.23a].

The positions of the homologous basic amino acids lysine 447 in *E. coli* gyrase and arginine 458 in *S. aureus* gyrase were superimposed to see whether they would affect QZM activity [fig.

6.23b]. The lysine residue was shifted backwards, further away from 1529 than arginine 458. The lysine was closest to the region on 1529 which is identical across all the QZM compound series, and therefore the lysine/arginine amino acid difference cannot cause the difference in activity of 1529 and 1488, but could be why the compounds were more active against *E. coli* gyrase compared with *S. aureus* gyrase. Mutation of serine 464 in *E. coli* gave rise to QZM 1488 resistance. Comparing the position of the alpha-helix the residue resides on in *S. aureus* gyrase, the helix was pushed slightly closer towards the DNA. Similarly, with the lysine/arginine amino acid difference, the helix was closest to the A ring of 1529, which is identical in the QZM series, and therefore could cause the activity difference of the QZMs between *E. coli* gyrase and *S. aureus* gyrase [fig. 6.23c]. The position of the scissile phosphates in the 1529 structure significantly differed in the fluoroquinolone and IPY structure, however in the 4.6-Å *E. coli* gyrase structure without drug present, the phosphates were in a similar conformation to the 1529 structure, and close together - 12.25 Å apart. The *E. coli* gyrase conformational state was described as an intermediate to DNA opening and corresponds with the shortening of the distance of the catalytic tyrosines, which was not observed in the 1529 structure.

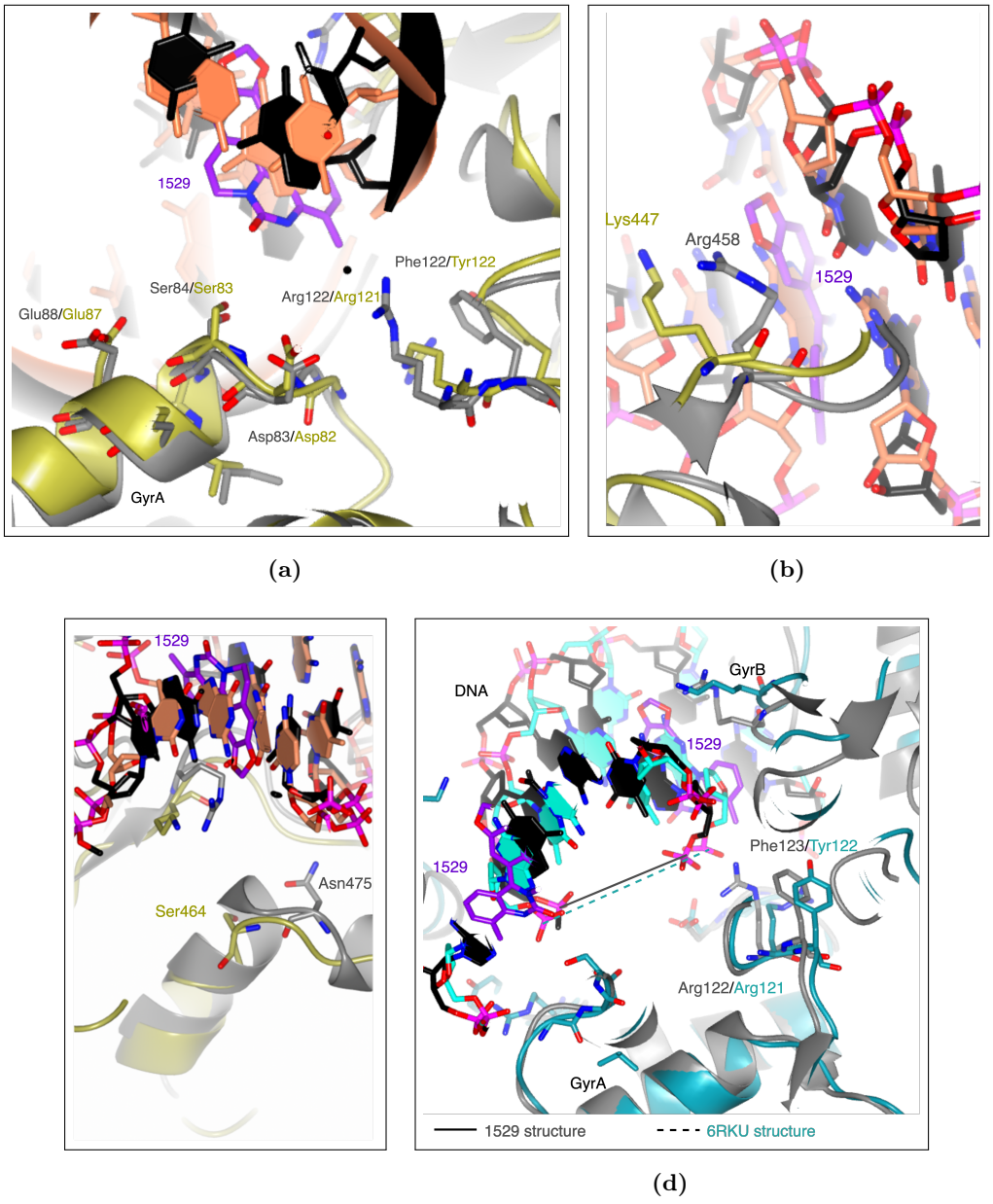

Figure 6.23: The superimposition of the *E. coli* gyrase cryo-EM structures. The gepotidacin structure - 6rku, at 4.0-Å and the structure without compound present - 6rkv 4.6-Å with the *S. aureus* gyrase core fusion Y123F mutant with QZM 1529. **(a)** A view of the superimposed GyrA alpha-helix residues from the gepotidacin *E. coli* gyrase structure. **(b)** The superimposed GyrB arginine 458 from *S. aureus* gyrase, and the homologous residue lysine 447 from *E. coli* gyrase from the gepotidacin *E. coli* gyrase structure. **(c)** A view of the GyrB residues asparagine 475 from *S. aureus* gyrase and the equivalent *E. coli* residue Ser464 from the *E. coli* gyrase gepotidacin structure. The GyrA and B amino acids (**(a-c)**) gave rise to resistant *E. coli* bacteria to the lead compound QZM 1488. **(d)** The superimposed *E. coli* gyrase structure from 6rkv (no compound present) showing the positions of the scissile phosphates.

6.2.12 *E. coli* gyrase mutants with predicted resistance to QZMs

The crystal structure of *S. aureus* gyrase with QZM 1529 identified the binding site and amino acid interactions for QZM 1529 to *S. aureus* gyrase. The QZMs were more effective at killing *E. coli*, and therefore more clinically important to characterise the binding site of the QZMs against the QZM target *E. coli* gyrase. Understanding the individual contributions of each amino acid residue of gyrase to the QZM binding site will aid the compound series development. From the crystal structure, the distance between the amino acids at the QZM binding site and the compound were often too long to characterise as a bond. Additionally, the crystal structure was with QZM 1529, which was the least potent against *E. coli* gyrase. Therefore, clinically relevant gyrase mutants were designed, informed by the crystal structure and from the MIC data of *E. coli* with gyrase mutations, to give further insights into the QZM binding site. Each mutant was tested in a supercoiling inhibition assay with QZMs 1488, 1529, 1532 and 2086, and ciprofloxacin. If significant inhibition was observed, IC_{50} values were calculated, to compare differences in potency to the wild-type enzyme.

A total of 7 *E. coli* gyrase mutants were tested against the QZMs [fig. 6.23, 6.24]. From the MIC data of *E. coli* mutant strains tested against QZM 1488, *E. coli* gyrase GyrA G81D was the most resistant to QZM 1488, increasing the MIC value by 125-fold. Interestingly, the equivalent residue in the *S. aureus* gyrase, G82, was 6.5 Å from the methyl group on QZM 1529 which QZM 1488 lacks, or 7 Å away from the nitrogen from the pyrimidine ring. The contribution of the residue towards binding the QZMs was not clear, and therefore the QZMs were tested against *E. coli* gyrase GyrA G81D [fig. 6.24a]. At 400 μM of each QZM, no significant gyrase supercoiling inhibition was observed. The mutant significantly affected the supercoiling inhibition of ciprofloxacin, raising the IC_{50} value to an estimated 1.85 mM [fig. 6.24a], 1542-fold higher than with the wild-type enzyme. *E. coli* GyrA G81D is a clinically relevent mutant which confers resistance to the fluoroquinolones [206]. The change from a neutral to negatively charged amino acid may disrupt conformation or binding of the GyrA alpha-helix amino acids in the QRDR.

E. coli with a mutation of gyrase GyrA D82G also affected the potency of QZM 1488, increasing the MIC value 31-fold. In the crystal structure, the equivalent residue lies at the GyrA-GyrA interface, close to the catalytic tyrosine and over 6 Å from the QZM. *E. coli* gyrase GyrA D82N, which is a clinically significant mutant [120], was tested against the QZMs and ciprofloxacin [fig. 6.24b]. No supercoiling inhibition was observed with QZMs 1529, 1532 and

2086, up to 400 μM compound. Minimal inhibition by QZM 1488 was observed with 100 μM compound, however the inhibition was not potent enough to calculate or estimate reliable IC_{50} values. Inhibition of the mutant enzyme by ciprofloxacin was decreased, the IC_{50} value was calculated to be 579.8 μM, 483-fold higher than for the wild-type enzyme. GyrA D82 does not make direct contact with QZM 1529 or ciprofloxacin in crystal structures. GyrA D82N has been hypothesised to impair the function of the enzyme by reducing the enzyme's DNA cleavage function [120], therefore QZM resistance to this residue may be achieved by an allosteric mechanism.

E. coli gyrase S83L is frequently found in clinical isolates resistant to fluoroqinolones due to the residue's importance in forming the water-metal ion bridge. The equivalent residue in *S. aureus* gyrase, S84, makes direct contact with fluoroquinolones and similar compounds, such as IPYs [207], [120]. GyrA S84 was 3.5 Å from QZM 1529, which may be too far for a direct hydrogen bond. From the MIC data, this residue affected the MIC value from 1488 with *E. coli* gyrase GyrA S83L minimally, increasing the MIC 2-fold, compared with 32-fold for ciprofloxacin. The *E. coli* GyrA S83L mutant was tested in a supercoiling inhibition assay against QZMs and ciprofloxacin [fig. 6.24c]. QZM 1488 had a lower IC_{50} value than ciprofloxacin, at 12.8 and 21.5 μM respectively, which corresponds with a 3.6- and 17.9-fold increase from the wild-type IC_{50} values respectively. Since the MIC for QZM 1488 was lower than ciprofloxacin for this mutant, the data are in good agreement. IC_{50} values of 66.8 and 39.8 μM were calculated for QZMs 1532 and 2086 respectively, and minimal supercoiling inhibition was observed by QZM 1529, starting at 100 μM.

There are differences in the amino acids at the quinazolinium binding site between *E. coli* and *S. aureus* gyrase, which may contribute towards the substantial difference in potency of the quinazoliniums for each enzyme. *E. coli* gyrase GyrA A84 corresponds to a serine in *S. aureus* GyrA. Additionally, *E. coli* gyrase GyrA A84P conferred significant resistance to the QZMs, increasing the MIC value 31-fold. Clinical isolates of *E. coli* resistant to fluoroquinolones have been found with GyrA A84V or A84P, which are both thought to disrupt the GyrA alpha-helix and perturb compound binding [208]. Mutating GyrA A84P would be a structurally disruptive mutation and therefore a conservative neutral mutation, GyrA A84S was chosen to mimic the *S. aureus* GyrA S85 [fig. 6.24d]. The QZMs were able to inhibit the supercoiling activity of the GyrA A84S mutant, and the IC_{50} values were estimated due to incomplete inhibition. QZM 1488, 1532 and 2086 had estimated IC_{50} values of 300 μM, and QZM 1529 had an estimated IC_{50} of 200 μM. QZM 1529 was the least active QZM against wild-type *E. coli* gyrase, and the

most active QZM against *S. aureus* gyrase. The *E. coli* gyrase A84S was therefore less resistant to QZM 1529 due to the compound's methyl group, however still increased the IC_{50} value by 13.7-fold. A84S was significantly less resistant to ciprofloxacin than the QZMs, increasing the IC_{50} value by 2.4-fold.

Like with *E. coli* gyrase GyrA S83, GyrA D87 coordinates the water-metal ion bridge with fluoroquinolones and is often mutated in resistant *E. coli*, particularly in combination with an S83 mutation [209]. GyrA D87 has been mutated to numerous amino acids to gain resistance, including histidine, glycine and asparagine. *E. coli* gyrase GyrA D87N did not significantly affect the MIC value for QZM 1488 compared with ciprofloxacin, and therefore an interesting mutant to test biochemically [fig. 6.24e]. Ciprofloxacin potency was significantly effected, increasing the IC_{50} value 120.3-fold due to the disruption of the water-metal ion bridge. The QZMs were not effective against *E. coli* gyrase D87N, 1488 and 1532 had an estimated IC_{50} of 400, and QZM 1529 and 2086 had an IC_{50} of >400 μM. This does not agree with the MIC data and unexpected, since the QZMs do not bind with a water-metal ion bridge, suggesting D87 has an important contribution towards the QZM binding directly, or binding pocket structure. The disagreement between the MIC and biochemical data could be because the mutant protein is unfolded, or DNA cleavage may not be rate-limiting for the mutant. Testing this mutant for resistance against the QZMs in a DNA cleavage stabilisation assay would assess whether DNA cleavage would be equally as affected as supercoiling.

Clinical isolates are known for quinolone resistance from *E. coli* gyrase GyrB, such as K447E [210]. From the MIC data with *E. coli* gyrase GyrB K447E and QZM 1488, the mutant significantly affected compound potency, and the equivelant residue in the *S. aureus* gyrase crystal structure formed direct hydrogen bonds with QZM 1529. To confirm the crystal interaction since the residue resolution was poor, and to investigate biochemically the residue importance, the QZMs were tested against *E. coli* gyrase GyrB K447E for supercoiling inhibition [fig. 6.24]. Up to 200 μM of QZM, no supercoiling inhibition was observed, highlighting the essential nature of the residue for QZM potency.

E. coli gyrase GyrB S464 mutants resistant to fluoroquinolones have been clinically isolated and include S464Y and S464F [211]. The residue interacts with the DNA close to the quinolone and QZM binding pocket, however does not make a direct interaction. From the MIC data, S464Y moderately increased the MIC value for QZM 1488 and due to no direct QZM interaction with the amino acid, S464Y was an interesting residue to characterise biochemically [fig. 6.24f].

QZM 1488 was the most potent, followed by 1532, 1529 and 2086, increasing the IC_{50} by 9.4-, 3-, 4- and 8.5-fold respectively. QZMs 1488 and 2086 were the most affected by the mutations. QZMs 1529 and 1532 have additional side groups, a methyl and a fluorine respectively, whereas 1488 and 2086 do not. The importance of S464 may therefore may be more critical for QZMs 1488 and 2086.

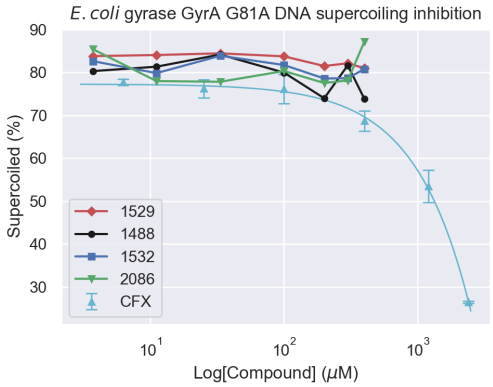

(a)

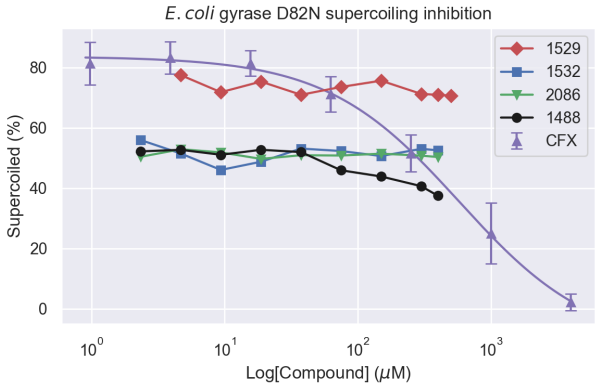

(b)

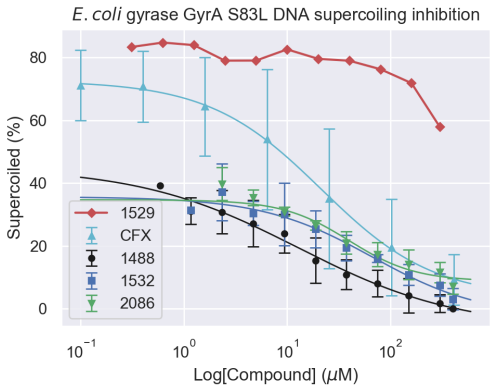

(c)

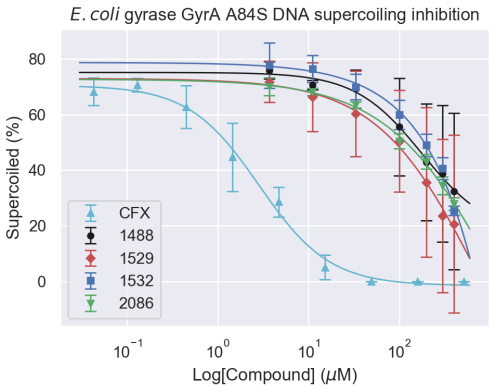

(d)

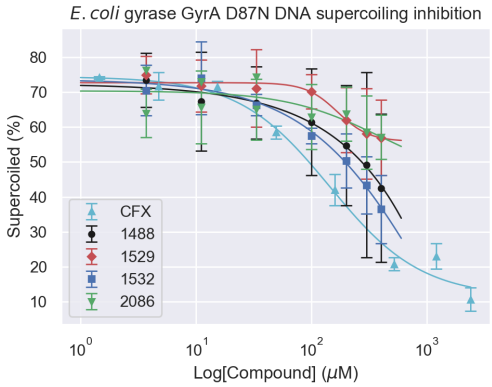

(e)

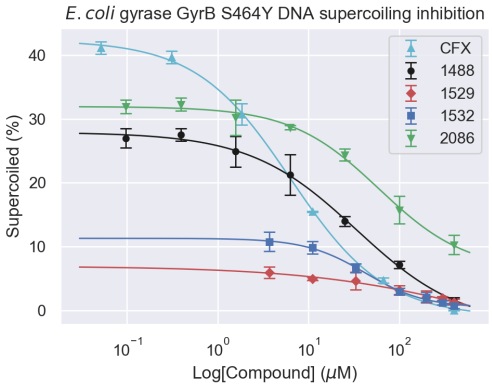

(f)

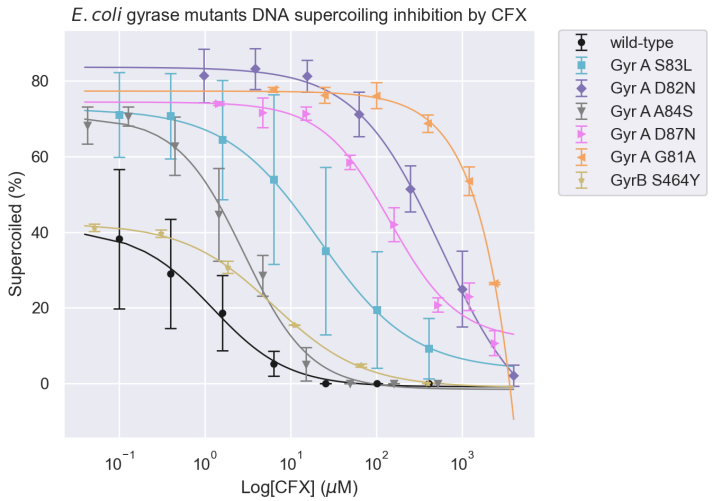

(g)

Figure 6.23: IC_{50} values for *E. coli* gyrase and mutants with the QZMs and CFX. The IC_{50} values from DNA supercoiling assays were calculated for *E. coli* gyrase GyrA G81A, GyrA D82N, GyrA S83L, GyrA A84S, GyrA D87N and GyrB S464Y for the QZMs and CFX. **(a)** QZM and CFX inhibition of *E. coli* gyrase GyrA G81A. 20 nM enzyme was used. **(b)** QZM and CFX inhibition of 25 nM *E. coli* gyrase GyrA D82N. **(c)** QZM and CFX inhibition of 25 nM *E. coli* gyrase GyrA S83L. **(d)** QZM and CFX inhibition of 20 nM *E. coli* gyrase GyrA A84S. **(e)** QZM and CFX inhibition of 20 nM *E. coli* gyrase GyrA D87N. **(f)** QZM and CFX inhibition of 1 or 3 nM *E. coli* gyrase GyrB S464Y.**(g)** CFX inhibition of wild-type, GyrA G81A, GyrA D82N, GyrA S83L, GyrA A84S, GyrA D87N and GyrB S464Y *E. coli* gyrase. The QZMs were tested up to 400 μM and the assays were run at 4-8% DMSO. Data were generated from 3 repeat datasets fitted to a 4-parameter curve in python with standard deviation if full inhibition was reached. Otherwise, data was plotted as a line graph.

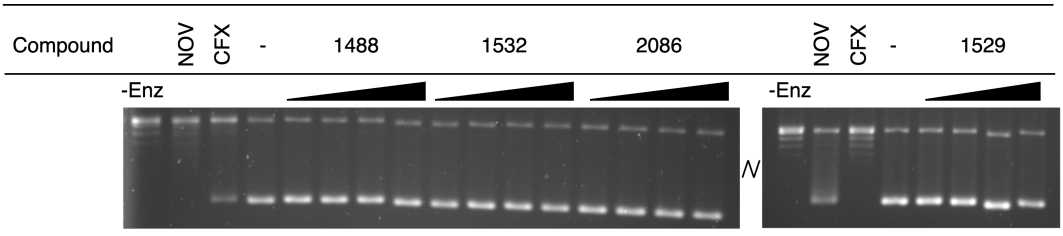

Figure 6.24: QZMs DNA supercoiling inhibition activity against the *E. coli* gyrase mutant GyrB K447E. 25-200 μM of each QZM, in a 4-fold dilution series, were tested at 4.0% (1488 and 1532 and 2086), and 1.7% (1529) DMSO. No compound, 20 μM NOV and 20 μM CFX were used as controls.

Compound	wt	GyrA G81A	GyrA D82N	GyrA S83L	GyrA A84S	GyrA D87N	GyrB K447E	GyrB S464Y
	IC_{50} (μM)							
1488	3.6	>400	>400	12.8	300*	400*	>200	33.7
1532	14.0	>400	>400	66.8	300*	400*	>200	42.5
2086	11.7	>400	>400	39.7	300*	>400	>200	100*
1529	14.6	>400	>400	>300	200*	>400	>200	59.8
CFX	1.2	1850*	579.8	21.5	2.9	144.4	ND	6.33

Table 6.6: IC_{50} values for *E. coli* gyrase and mutants with the QZMs and CFX. The IC_{50} values from DNA supercoiling assays were calculated for *E. coli* gyrase wild-type, GyrA G81D, GyrA D82N, GyrA S83L, GyrA A84S, GyrA D87N, GyrB K447E and GyrB S464Y for QZMs and CFX. Where appropriate, IC_{50}s were generated from 3 repeat datasets fitted to a 4 parameter curve in python. Data sets if incomplete but sufficient inhibition was observed, IC_{50} values were estimated by eye from the IC_{50} curves, indicated with an asterix (*). If insufficient inhibition was observed, IC_{50} values were not calculated or estimated.

6.3 Discussion and future work

The work in this chapter assesses the antibiotic potential of the novel, synthetic antibiotic series - the quinazoliniums, and their mode of action against the type II topoisomerases. These compounds are of potential clinical interest for their ability to bypass the water-metal ion bridge, which is required for the successful fluoroquinolone antibiotics to bind, and therefore resistant bacteria are commonly mutated in the region. Currently, the quinazoliniums are not potent enough to be considered for clinical trials. This work confirms the quinazolinium's cellular targets, elucidates the mechanism of action and drug potency biochemically, identifies the quinazolinium binding site, and characterises clinically important resistant mutants against the QZMs. The studies have assesed the compound's antibiotic potential and aided optimisation of the compound series, with the hopes of generating highly active antibiotics for the future.

6.3.1 Assessment of the quinazoliniums as antibiotics against *E. coli*

Antibiotic resistance is inevitable; new antibiotics must be potent and have different targets or mechanisms of action to avoid cross resistance with current drug-resistant bacterial species. The QZMs would be attractive to take forward as antibiotic candidates if they were more potent than current alternatives. Compared to the fluoroquinolone ciprofloxacin, the lead compound 1488 did not have greater bactericidal activity on wild-type *E. coli*, or the quinolone resistance mutants GyrA A81D, GyrA D82G, GyrA A84P, GyrB K447E and GyrB S464Y. Biochemically, the QZMs had higher IC_{50} and CC_{50} values than ciprofloxacin for wild-type *E. coli* gyrase supercoiling inhibition, relaxation inhibition, and cleavage stabilisation activity.

Futhermore, the QZMs were less active than ciprofloxacin at supercoiling inhibition by GyrA G81A, GyrA D82N, GyrA A84S, GyrA D87N, GyrB K447E and GyrB S464Y. Therefore, the QZMs would not be an improved antibiotic for *E. coli* wild-type, or against the quinolone resistance mutants discussed.

Where the QZMs differ from the fluoroquinolones is their ability to bypass the water-metal ion bridge. QZM 1488 was more effective at killing the quinolone-resistant mutant *E. coli* GyrA S83L and D87N than ciprofloxacin. The supercoiling inhibition activity of QZM 1488 by *E. coli* gyrase GyrA S83L had an IC_{50} value lower than ciprofloxacin. When the QZMs were tested biochemically against *E. coli* gyrase GyrA D87N, the QZMs were not active enough to estimate an IC_{50} value, however likely have potency similar to ciprofloxacin. The QZMs should be exploited for their potential against the GyrA S83L and D87N mutants. In a study of clinical isolates of *E. coli* resistant to fluoroquinolones, the GyrA S83L mutation was the most prevalent at 98.9%, followed by the GyrA D87N mutation at 59.8%; these figures include double mutants [212]. Whilst the QZMs are promising against the GyrA S83L mutant, the compounds should be directly compared against the IPYs, which also bypass the water-metal ion bridge. The most active IPY had an IC_{50} value 8.7 times lower for the GyrA S83L mutant compared with ciprofloxacin [120].

6.3.2 The importance of the quinazolinium activity against other topoisomerase targets

There is a high degree of sequence and structural homology between DNA gyrase and topo IV. Antibiotics including the fluoroqiunolones, NBTIs, coumarins and IPYs dual target both enzymes, although the compounds often have a preference for DNA gyrase or topo IV. The primary target of ciprofloxacin is DNA gyrase, whereas for gemifloxacin, the primary target is topo IV [213]. If a compound was equally sensitive to DNA gyrase and topo IV, since both enzymes are essential in the majority of bacteria, two spontaneous evolutionally-beneficial mutations would be required to gain antibiotic resistance. Double mutations are rare for fluoroquinolones and occur at a frequency of 10^{-14} - 10^{-16}, which has been predicted to reduce the rate of resistant bacteria [214]. When the QZMs were tested against *E. coli* topo IV, the QZMs stabilised the DNA cleavage levels, however exhibited little to no inhibition of DNA relaxation. DNA cleavage is unlikely to be the rate-limiting step in the DNA relaxation cycle. In *E. coli* cells, whether the QZMs stabilise persistent DNA cleavage complexes with topo IV which can be converted into lethal double-stranded DNA breaks will determine whether topo

IV is a target for the QZMs. The main target of the QZMs in *E. coli* is DNA gyrase.

Cytotoxicity in human cells is a major barrier to advancing potent and promising antibiotics to clinical trials, which could be due to interactions with mammalian topoisomerases. Topoisomerase poisons can induce genotoxicity to human cells through the accumulation of lethal double-stranded breaks, and catalytic inhibitors affect the essential functions of the human topoisomerases, such as DNA replication. The coumarins are ATPase inhibitors and are very potent gyrase inhibitors. Some coumarins have IC_{50} values lower than fluoroquinolones, and have good MIC values against *S. aureus* [215]. The coumarins are cytotoxic to human cells and therefore were withdrawn clinically due to toxicity. The coumarins target gyrase by a different mechanism to quinolones, and therefore would be an attractive target to combat resistant bacterial strains if the drugs were non-toxic.

For antibiotics targeting gyrase or topo IV, the toxicity in humans is often due to the dual targeting of the antibiotic directly to the human topoisomerase II [216]. The QZMs exhibited no DNA cleavage stabilisation activity on human topo IIα, and little to no inhibition of the enzyme's DNA relaxation activity. Further, the compounds did not show toxicity in *G. mellonella* larvae. Toxicity to *G. mellonella* correlates with toxicity of fluoroquinolone antibiotics in rodents and rats [158]. Early indications of toxicity will inform rational drug development for the chemical series. Whilst the QZM toxicity remains optimistic, additional toxicity tests could include *in vivo* assays in mammalian cell lines, such as mammalian L5178Y mouse lymphoma cells, which can rank the genotoxicity of compounds [217].

Following *E. coli* topo IV and human topo IIα relaxation assays, there were indications that the quinazoliniums were weak DNA intercalators, which was confirmed in intercalation assays with wheat germ topo I. The DNA intercalation activity can indicate how drugs will function in the cell. Anthracyclines such has doxorubacin inhibit human topo II through DNA intercalation, leading to changes in chromatin [137], whereas drugs such as m-amsacrine is both a topoisomerase poison and DNA intercalator, primarily acting through poisoning [218]. If the quinazoliniums were strong intercalators, intercalation properties could be selected for, or against, during chemical optimisation of the series.

6.3.3 The mechanism of action of the quinazoliniums

Topoisomerases can be inhibited catalytically through ATPase activity inhibition, converted into poisons to induce lethal single- or double-stranded DNA breaks, inhibited catalyticially, or

allosterically modulated. The quinazoliniums were shown to stabilise double-stranded DNA cleavage, pointing towards 2 compounds binding per gyrase complex. The ATP-independent reaction, DNA relaxation by *E. coli* gyrase was inhibited by the QZMs, suggesting the compounds are not affecting ATP binding or utilisation by gyrase. The crystal structure confirms 2 compounds at the DNA cleavage site. The binding site is in good agreement with the MIC data, where the quinazoliniums generate resistant mutants in the QRDR.

The QZMs have been confirmed as DNA cleavage stabilisers. In terms of how a compound can stabilise DNA cleavage, quinolones block the DNA resealing reaction. To determine how stable the gyrase-DNA-QZM cleavage complexes are, DNA resealing kinetics experiments could be performed, and compared to other DNA cleavage stabilisers. The rate of DNA resealing may give indications as to how long the cleavage complexes will persist in bacteria, as DNA resealing will increase pathogen survival [121]. DNA resealing assays will show if the QZMs block DNA resealing at both of the DNA cleavage sites equally [120]. DNA resealing assays could be performed with the metal chelator EDTA, or through dilution to stimulate the reverse reaction.

6.3.4 The significance of the crystal structure of a quinazolinium with *S. aureus* gyrase

The rationale behind determining the crystal structure of *S. aureus* gyrase and the quinazoliniums was to confirm the compound binding site, define the protien-drug interactions and predict the increase in QZM potency from *S. aureus* to *E. coli* gyrase. Of the amino acids surrounding QZM 1529 in the *S. aureus* gyrase crystal structure, one amino acid, R458, was close enough to form hydrogen bonds with the compound. The other direct bonds are formed by pi-pi stacking interactions with the DNA, indicating an importance in DNA-QZM interactions. The initial aim was to obtain crystal structures with all the quinazoliniums, particularly 1488, to investigate the properties of 1488 which result in the greatest potency against *E. coli*. From the 1529 crystal structure, it is unclear why QZM 1488 is the most active, since 1488 does not have additional functional groups which the other QZMs in the series lack.

There are 61 structures of *S. aureus* gyrase depositied in the protein data bank [219]. The QZM structure with *S. aureus* gyrase is in good overall structural agreement with relevent *S. aureus* gyrase structures, determined by superimposition of the secondary structure. The GyrA alpha-helix and residues were in similar positions in a fluoroquinolone, IPY and quinazoline dione structure. For compound coordination, the largest variation came from GyrB R458,

which is closer to the DNA cleavage site due to the small size of the QZMs. A notable difference between the current *S. aureus* gyrase structures and the QZM structure, was the position of the scissile phosphates. The scissile phosphates lie much closer together in the QZM structure, at under 10 Å, half the distance recorded in existing *S. aureus* gyrase structures. This distance has only been noted in an *E. coli* gyrase structure. The significance of the position of the phosphates could be in part due to the scissile phosphate contribution to QZM binding, flipping the phosphates away from the catalytic tyrosine. In other fluoroquinolone structures with the GyrA Y123F catalytic tyrosine mutation, the phosphates do not form a phosphotyrosine bond, however the phosphates do not mimic the positions of the phosphates in the QZM 1529 structure.

6.3.5 The potential for quinazoliniums as antibiotic agents against Gram-positive bacteria

To be considered an attractive broad-spectrum antibiotic, antibiotics often target both Gram-positive and Gram-negative bacteria, such as the fluoroquinolones, ampicillin and chloramphenicol. The quinazoliniums had little to no activity on the Gram-positive bacterium *S. aureus*, however no other examples of Gram-positive bacteria were tested against the QZMs. *Mycobacterium tuberculosis* and *Mycobacterium smegmatis* GyrA lack the serine involved in the water-metal ion bridge, and therefore the QZMs may be more effective than fluoroquinolones, which require the serine for a strong water-metal ion bridge to form [220]. *M. tuberculosis* is a significant threats towards antibiotic resistance, as well as other Gram-positive bacteria. Understanding the QZM's preference for Gram-negative bacteria will aid medicinal chemistry to develop the compound series to target both Gram-positive and Gram-negative bacteria.

Since the QZMs had no activity against *S. aureus*, and reduced activity against *S. aureus* gyrase compared with *E. coli* gyrase, it still remains unclear whether the QZMs have reduced entry or increased export from *S. aureus*. Biochemically, the amino acid differences between *E. coli* and *S. aureus* gyrase (GyrA A84 vs S85, and GyrB K447 vs R458) at the QZM binding pocket do not form a complete explanation to the differences in QZM potency. Characterising the binding of the most active compound QZM 1488, or determining the structure of *E. coli* gyrase would help characterise the differences in QZM potency across the species. There are numerous structures of *E. coli* gyrase achieved by cryo-EM in the presence of compounds, such as the NBTI gepotidacin [36]. With recent advances in cryo-EM and examples of *E. coli* gyrase structures, a structure with a QZM appears achievable. The QZMs may have a preference

for topo IV in Gram-positive bacteria, since some fluoroquinolones, such as moxifloxacin and gemifloxacin are more active against topo IV than DNA gyrase in *S. aureus* [213].

6.3.6 Considerations for optimisation of the quinazolinium design based on structural and biochemical data

The quinazoliniums have been structurally characterised against *S. aureus* gyrase, from a Gram-positive bacteria which the QZMs had no activity against. The amino acid differences between *E. coli* gyrase and *S. aureus* gyrase should be considered during chemical optimisation of the QZMs.

The biochemical characterisation of the QZMs against the wild-type and mutant enzymes were carried out using *E. coli* gyrase. In 2019, the leading cause of death as a result of antimicrobial resistance was from *E. coli* [131]. Although *E. coli* is a major public health threat, the bacterium were not placed on the 2019 Centres of Disease Control and Preventions list of bacteria which are either urgent, serious or concerning threats due to antimicrobial resistance. The Gram-negative bacteria categorised as urgent threats include *A. baumannii*, *Enterobacteriaceae* and *Neisseria gonorrhoeae*. Deciding on the right species to target should be considered when modifying the current QZMs. Testing for bactericidal and bacteriostatic activity, and biochemically characterising the potency of the QZMs against additional species, may help with a targeted approach towards critical pathogenic threats.

When designing novel gyrase antibiotics, commonly, compounds have been modified with functional groups to mimic the structure of the successful fluoroquinolone antibiotics. For example, the quinazoline diones have functional groups in identical positions to fluoroquinolones in crystal structures [193]. With considerations to the crystal structure of *S. aureus* gyrase, the quinazoliniums could improve potency by mimicking the positions of the fluoroquinolone functional groups [fig. 6.25]. The QZMs could be modified with a cyclopropane group at the R_1 or R_2 position, an ether group at the R_3 position, or a fluorine at the R_4 or R_5 position. Additionally, the quinazoliniums are much smaller than fluoroquinolones, and based on the crystal structure, there is space to expand the chemical space above the 1,3-dioxolane ring.

In addition to improving the potency of the quinazoliniums, modifications to improve the pharmacokinetic properties of the compounds should be considered. For the quinazoliniums, the method of entry into the cell is unknown and any further modifications to the compounds

should be tested to ensure uptake into bacterial cells is unaffected. Additionally, QZMs 1488, 1532 and 2086 had poor solubility, at ∼5 mM in 100% DMSO. Improving the water solubility of the compounds will increase the compound series attractiveness for development as antibiotics.

The density around the QZM in the crystal structure could allow for there to be more than one binding orientation for the QZM, such as rotating the compound 180° around the longest axis. The potential for the compound to bind in multiple orientations expands the chemical space for modifications to the compound series. Similar compounds, such as the fluoroquinolones have alternative, but less favoured binding orientations to gyrase, evidence of which comes from crystal structures and crosslinking experiments [162].

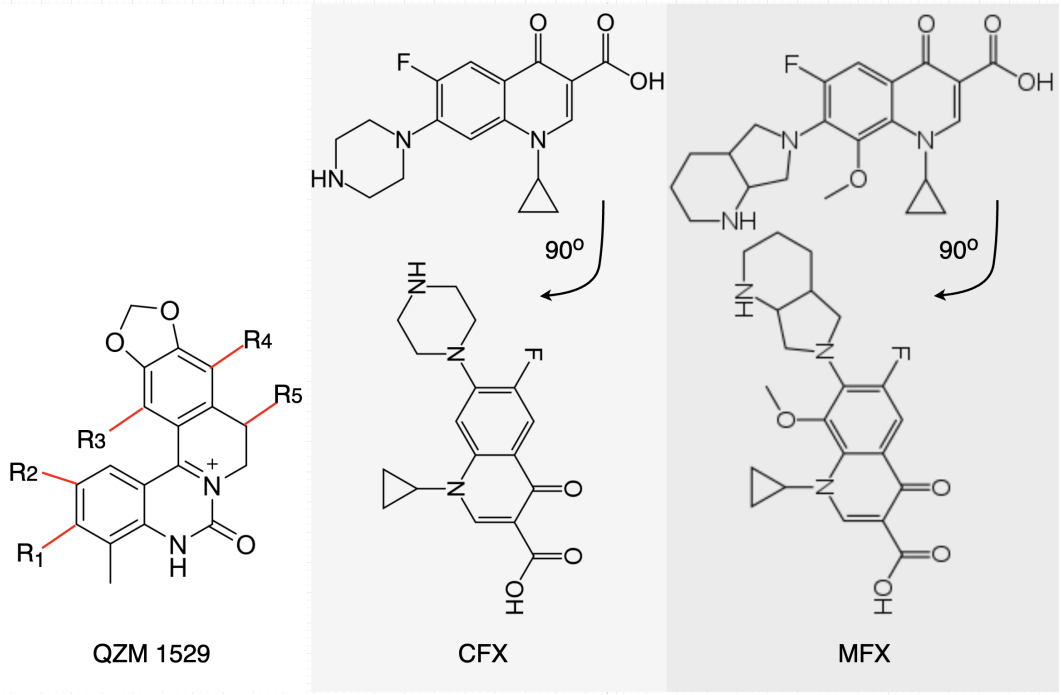

Figure 6.25: Considerations for modifications of the quinazolinium structures. Approximate orientation of the fluoroquinolones ciprofloxacin and moxifloxacin to the quinazolinium 1529 according to the positions in the *S. aureus* gyrase crystal structure.

Chapter 7

General Discussion

This thesis explores the DNA cleavage and resealing reactions of type II topoisomerases by two approaches. The first being the mechanism by which the DNA breakage and reunion reaction proceeds, focusing on the role of metal ions and amino acids at the DNA cleavage site of bacterial DNA gyrase. The second approach is investigating novel synthetic compounds with antibiotic potential, which were found here to disrupt the DNA cleavage and resealing equilibrium.

The first results chapter addresses the question to why the DNA cleavage and resealing reactions have different metal ion requirements, considering both require divalent metal ions for catalysis. It was found that the DNA resealing reaction could proceed at a lower concentration of free metal ions than DNA cleavage. Further, each stage of strand ligation was affected by the concentration of free metal ions, and therefore both strand ligation events require metal ions to proceed. The DNA resealing reaction was instantaneously affected by lowering the concentration of free metal ions. From this evidence, the metal ions must leave the enzyme following DNA cleavage, and rebind for each strand ligation event. These results do not fit with a static or moving metal ion model, and so a dynamic metal ion model was proposed, where the metal ions are in a dynamic equilibrium with the enzyme and solution, which could fit a one or two metal ion model. The chapter also found that the two strand scission/ligation events are affected differenty by the free metal ion concentration, suggesting enzyme asymmetry during the reactions. Models were proposed which incorporated the cleavage status of DNA to why assymetry may occur. The chapter also found that DNA resealing is driven by the free concentration of metal ions, as opposed to any dissociation effects from drug-stabilised DNA cleavage complexes.

In the second results chapter, the role of a conserved lysine residue with potential proximity to the DNA cleavage site, and the Greek Key domain which has been implicated in the DNA resealing reaction were investigated by mutagenesis. The chapter found that both mutants were deficient in the speed of DNA cleavage and DNA resealing, and that DNA resealing was the

most affected. Further, nicked DNA accumulated in DNA cleavage assays, implicating the lysine residue in coordinating the DNA cleavage reaction. Models were suggested to explain a possible role for the lysine in the DNA cleavage and resealing reactions which fit with the data found. The lysine may be involved bringing the broken DNA strands together for DNA resealing, thereby the lysine having a very important role in DNA resealing. During DNA cleavage, the lysine was suggested to coordinate the DNA during the second strand cleavage event, since the DNA would have increased flexibility. This chapter also investigated the potential for a metal-independent DNA cleavage mechanism, since high levels of nicked DNA accumulated without metal ion addition to DNA cleavage reactions only when DNA gyrase subunits were combined. The results concluded either a metal-independent cleavage was occuring, or that low levels of contaminating metal ions supported DNA nicking.

The third results chapter aimed to explore the number of metal ions during DNA cleavage and resealing, by constructing a series of asymmetric gyrase mutants using the heterodimer system. Due to technical reasons, these experiments were incomplete, however, these results provide the preliminary work for further study into asymmetric mutants, and experimental design into desiphering the metal ion mechanism during DNA cleavage. The two metal ion model was first proposed based on biochemical data where the DNA cleavage and relaxation activity of *E. coli* gyrase was enhanced in the presence of magnesium and calcium ions, using GyrB metal ion coordinating residue mutants [88]. Chapter 5 aimed to replicate these experiments, and to build upon the work by generating the acidic residue mutants on one side of the enzyme complex, using heterodimeric enzymes (GyrBA·A + GyrB) [189][191]. The experiments were designed around a hypothesis suggested by Bax and colleagues [39], where this biochemical evidence for the two metal ion mechanism for DNA cleavage catalysis could be explained by asymmetric binding of metal ions between the two DNA cleavage sites on the enzyme complex. Designing a mutant incapable of binding metal ions on one side of the gyrase complex would remove metal ions influencing the DNA cleavage at the opposite site. Since the gyrase activity enhancement with two metal ions could not be replicated in these experiments, and there were difficulties with using the heterodimeric gyrase system, this hypothesis could not be tested. Further studies could instead use end-labelled radioactive nucleotides to measure gyrase cleavage activity, which is more sensitive [90].

7.1 The antibiotic potential of the quinazoliniums

A novel, synthetic compound series developed by Uppsala University called the quinazoliniums which have antibacterial activity against Gram-negative bacteria were characterised here. Using biochemical assays, the main bacterial protein target of the drugs was determined to be DNA gyrase, with low activity against the secondary target topo IV. The compounds were found to be more active against *E. coli* gyrase, as opposed to the *S. aureus* gyrase. These results were in agreement with the MIC data performed by Uppsala University, which found the quinazoliniums were more active against Gram-negative bacteria. The biochemical experiments therefore show that the quinazoliniums are more active against Gram-negative bacteria due to a differences in the protein target, as opposed to differences the properties of Gram-negative or Gram-positive bacteria.

The quinazoliniums were determined to be less active than the fluoroquinolone ciprofloxacin against wild-type *E. coli* gyrase; therefore the quinazoliniums require further chemical optimisation to increase their antibacterial potential. Low DNA cleavage-stabilisation activity was observed with *S. aureus* gyrase, showing the compounds can interact with the enzyme, even if the rate of strand-passage is unaffected. This data provides a starting point for the quinazoliniums to be optimised in parallel to specifically target either Gram-negative and Gram-positive bacterial DNA gyrase. The compounds were not active against the human topoisomerase IIα, or *M. mazei* topo VI and therefore the quinazoliniums are not promising scaffolds to be developed into anti-cancer agents or herbicides, respectively.

Using biochemical and structural analysis, the quinazoliniums were identified to stabilise double-stranded DNA cleavage products, and bind at the quinolone binding pocket. The quinazoliniums and fluoroquinolones bind at the same location to gyrase, and therefore, when the QZMs were tested in a series of *E. coli* gyrase mutants, there was cross resistance between the quinazoliniums and the fluoroquinolones. Despite cross resistance, there were some differences in the gyrase interactions between the compounds. The quinazoliniums do not require a water-metal ion bridge to bind to gyrase, whereas the fluoroquinolones do. The fluoroquinolone ciprofloxacin was less active than the quinazoliniums at targeting the *E. coli* gyrase GyrA S83L mutant. This residue coordinates the water-metal ion bridge in fluoroquinolones. Therefore, the quinazoliniums have the greatest potential to target bacterial strains with the quinolone-resistance mutations which disrupt the fluoroquinolone's water-metal ion bridge.

This thesis presents the *S. aureus* gyrase crystal structure with the quinazolinium 1529, which was solved to 2.98-Å resolution. The structure provides an important tool for structure-informed optimisation of the quinazoliniums. The structure is of *S. aureus* gyrase, which is not the primary target *E. coli* gyrase, and of quinazolinium 1529, the least active quinazolinium against *E. coli* gyrase. Therefore, *E. coli* gyrase mutants in the QRDR were made, to unravel two questions: why the QZMs are more active against *E. coli* as opposed to *S. aureus*, and why QZM 1488 is the most active compound.

List of Abbreviations

3D – 3-dimensinal

ADP – adenosine-5′-diphosphate

ADPNP – 5′-adenylyl β,γ-imidodiphosphate

AMR – antimicrobial resistance

AP/Aqu – aqueous phase

ATP – adenosine-5′-triphosphate

bp – base pair

C_{50} – The enzyme concentration at which the enzyme activity is 50%

Ca^{2+}/$CaCl_2$ – calcium ions/calcium chloride

CC_{50} – the concentration of the drug which the DNA cleavage complexes were stabilized by 50%

CFX – ciprofloxacin

cryo-EM – 3D cryo-electron microscopy

DMSO – dimethyl sulfoxide

DNA – deoxyribose nucleic acid

EDTA – ethylenediaminetetraacetic acid

EPR/ENDOR – electron paramagnetic resonance/electron-nuclear double resonance

Enz – enzyme

ETP – etoposide

GHKL – Gyrase, Hsp90, Histidine Kinase, MutL

GK – Greek Key domain

G-segment – gate segment

GyrA – DNA gyrase A-subunit

GyrB – DNA gyrase B-subunit

Gyrase – DNA gyrase

H2TH – helix-two-turns-helix

IC_{50} – the concentration of the drug at which the activity of the enzyme was inhibited by 50%

ICP-MS – inductively coupled plasma mass spectrometry

IPY – imidazopyrazinone

Lk – linking number

m-AMSA – Amsacrine

MFX/moxi – moxifloxacin

$Mg^{2+}/MgCl_2$ – magnesium ions/magnesium chloride

MIC – minimum inhibitory concentration

$Mn^{2+}/MnCl_2$ – manganese ions/manganese chloride

NBTI – novel bacterial topoisomerase inhibitors

NOV – novobiocin

P – phenol phase

PAGE – polyacrylamide gel electrophoresis

ParC – Topo IV A-subunit

ParE – Topo IV B-subunit

PBS – phosphate buffered saline

PCR – polymerase chain reaction

QRDR – Quinolone resistance-determining region

QZM – quinazolinium

R – relaxed

SC – supercoiled

SDS – sodium dodecylsulphate

Tc – topoisomerase cleavage products in the phenol phase

topo I – topoisomerase I

Topo II – topoisomerase II

topo III – topoisomerase III

top3B – topoisomerase IIIβ

topo IV – topoisomerase IV

topo VI – topoisomerase VI

topo VII – topoisomerase VIII

T-segment – transported segment

TOPRIM – topoisomerase-primase

Tw – twist

WHD – winged-helix-domain

Wr – writhe

WT/wt – wild-type

Bibliography

[1] J. D. Watson and F. H. C. Crick, "Molecular Structure of Nucleic Acids: A Structure for Deoxyribose Nucleic Acid," *Nature*, vol. 171, pp. 737–738, Apr. 1953.

[2] J. C. Wang, "Interaction between DNA and an Escherichia Coli Protein ømega," *Journal of Molecular Biology*, vol. 55, pp. 523–533, Feb. 1971.

[3] J. H. White and W. R. Bauer, "Calculation of the twist and the writhe for representative models of DNA," *Journal of Molecular Biology*, vol. 189, pp. 329–341, May 1986.

[4] A. D. Bates and Anthony. Maxwell, *DNA Topology*. Oxford University Press, 2005.

[5] W. G. Nelson, K. J. Pienta, E. R. Barrack, and D. S. Coffey, "The Role of the Nuclear Matrix in the Organization and Function of DNA," *Annual Review of Biophysics and Biophysical Chemistry*, vol. 15, pp. 457–475, June 1986.

[6] J. Vinograd and J. Lebowitz', "Physical and Topological Properties of Circular DNA," *The Journal of General Physiology*, vol. 49, pp. 103–125, July 1966.

[7] L. Postow, N. J. Crisona, B. J. Peter, C. D. Hardy, and N. R. Cozzarelli, "Topological challenges to DNA replication: Conformations at the fork," *Proceedings of the National Academy of Sciences*, vol. 98, pp. 8219–8226, July 2001.

[8] L. F. Liu and J. C. Wang, "Supercoiling of the DNA template during transcription.," *Proceedings of the National Academy of Sciences*, vol. 84, pp. 7024–7027, Oct. 1987.

[9] H. Peng and K. J. Marians, "Decatenation activity of topoisomerase IV during oriC and pBR322 DNA replication in vitro.," *Proceedings of the National Academy of Sciences of the United States of America*, vol. 90, pp. 8571–8575, Sept. 1993.

[10] P. Forterre, S. Gribaldo, D. Gadelle, and M.-C. Serre, "Origin and Evolution of DNA Topoisomerases," *Biochimie*, vol. 89, pp. 427–446, Apr. 2007.

[11] J. E. Deweese, M. A. Osheroff, and N. Osheroff, "DNA Topology and Topoisomerases: Teaching a "Knotty" Subject," *Biochemistry and molecular biology education : a bimonthly publication of the International Union of Biochemistry and Molecular Biology*, vol. 37, no. 1, pp. 2–10, 2008.

[12] Y. Seol and K. C. Neuman, "The dynamic interplay between DNA topoisomerases and DNA topology," *Biophysical Reviews*, vol. 8, pp. 101–111, Nov. 2016.

[13] J. C. Wang, "DNA topoisomerases: Why so many?," *Journal of Biological Chemistry*, vol. 266, pp. 6659–6662, Apr. 1991.

[14] W. K. McCoubrey and J. J. Champoux, "The role of single-strand breaks in the catenation reaction catalyzed by the rat type I topoisomerase.," *Journal of Biological Chemistry*, vol. 261, pp. 5130–5137, Apr. 1986.

[15] A. Maxwell and M. Gellert, "Mechanistic Aspects of DNA Topoisomerases," in *Advances in Protein Chemistry* (C. B. Anfinsen, J. T. Edsall, and F. M. Richards, eds.), vol. 38, pp. 69–107, Academic Press, Jan. 1986.

[16] T. Viard and C. B. de la Tour, "Type IA topoisomerases: A simple puzzle?," *Biochimie*, vol. 89, pp. 456–467, Apr. 2007.

[17] X. Yang, S. Saha, W. Yang, K. C. Neuman, and Y. Pommier, "Structural and biochemical basis for DNA and RNA catalysis by human Topoisomerase 3β," *Nature Communications*, vol. 13, p. 4656, Aug. 2022.

[18] J. W. Wallis, G. Chrebet, G. Brodsky, M. Rolfe, and R. Rothstein, "A hyper-recombination mutation in S. cerevisiae identifies a novel eukaryotic topoisomerase," *Cell*, vol. 58, pp. 409–419, July 1989.

[19] T. Dasgupta, S. Ferdous, and Y.-C. Tse-Dinh, "Mechanism of Type IA Topoisomerases," *Molecules*, vol. 25, p. 4769, Oct. 2020.

[20] B. C. Soren, J. B. Dasari, A. Ottaviani, F. Iacovelli, and P. Fiorani, "Topoisomerase IB: A relaxing enzyme for stressed DNA," *Cancer Drug Resistance*, vol. 3, pp. 18–25, Mar. 2020.

[21] A. I. Slesarev, K. O. Stetter, J. A. Lake, M. Gellert, R. Krah, and S. A. Kozyavkin, "DNA topoisomerase V is a relative of eukaryotic topoisomerase I from a hyperthermophilic prokaryote," *Nature*, vol. 364, pp. 735–737, Aug. 1993.

[22] A. Osterman and A. Mondragón, "Structures of topoisomerase V in complex with DNA reveal unusual DNA-binding mode and novel relaxation mechanism," *eLife*, vol. 11, p. e72702, Aug. 2022.

[23] D. A. Sutormin, A. K. Galivondzhyan, A. V. Polkhovskiy, S. O. Kamalyan, K. V. Severinov, and S. A. Dubiley, "Diversity and Functions of Type II Topoisomerases," *Acta Naturae*, vol. 13, no. 1, pp. 59–75, 2021.

[24] P. Forterre and D. Gadelle, "Phylogenomics of DNA Topoisomerases: Their Origin and Putative Roles in the Emergence of Modern Organisms.," *Nucleic acids research*, vol. 37, pp. 679–92, Feb. 2009.

[25] P. Villain, R. Catchpole, P. Forterre, J. Oberto, V. da Cunha, and T. Basta, "Expanded Dataset Reveals the Emergence and Evolution of DNA Gyrase in Archaea," *Molecular Biology and Evolution*, vol. 39, p. msac155, Aug. 2022.

[26] M. K. Wall, L. A. Mitchenall, and A. Maxwell, "Arabidopsis thaliana DNA gyrase is targeted to chloroplasts and mitochondria," *Proceedings of the National Academy of Sciences*, vol. 101, pp. 7821–7826, May 2004.

[27] K. C. Dong and J. M. Berger, "Structural Basis for Gate-DNA Recognition and Bending by Type IIA Topoisomerases," *Nature*, vol. 450, pp. 1201–1205, Dec. 2007.

[28] N. H. Thomson, S. Santos, L. A. Mitchenall, T. Stuchinskaya, J. A. Taylor, and A. Maxwell, "DNA G-segment bending is not the sole determinant of topology simplification by type II DNA topoisomerases," *Scientific Reports*, vol. 4, p. 6158, Aug. 2014.

[29] S. C. Kampranis, A. D. Bates, and A. Maxwell, "A model for the mechanism of strand passage by DNA gyrase," *Proceedings of the National Academy of Sciences of the United States of America*, vol. 96, pp. 8414–8419, July 1999.

[30] K. M. Soczek, T. Grant, P. B. Rosenthal, and A. Mondragón, "CryoEM structures of open dimers of gyrase A in complex with DNA illuminate mechanism of strand passage," *eLife*, vol. 7, p. e41215, Nov. 2018.

[31] D. B. Wigley, G. J. Davies, E. J. Dodson, A. Maxwell, and G. Dodson, "Crystal structure of an N-terminal fragment of the DNA gyrase B protein," *Nature*, vol. 351, pp. 624–629, June 1991.

[32] D. C. Hooper, "Bacterial topoisomerases, anti-topoisomerases, and anti-topoisomerase resistance," *Clinical Infectious Diseases: An Official Publication of the Infectious Diseases Society of America*, vol. 27 Suppl 1, pp. S54–63, Aug. 1998.

[33] R. J. Reece and A. Maxwell, "DNA gyrase: Structure and function," *Critical Reviews in Biochemistry and Molecular Biology*, vol. 26, no. 3-4, pp. 335–375, 1991.

[34] E. L. Zechiedrich, A. B. Khodursky, and N. R. Cozzarelli, "Topoisomerase IV, not gyrase, decatenates products of site-specific recombination in Escherichia coli," *Genes & Development*, vol. 11, pp. 2580–2592, Jan. 1997.

[35] C. J. Dorman and M. J. Dorman, "DNA supercoiling is a fundamental regulatory principle in the control of bacterial gene expression," *Biophysical Reviews*, vol. 8, pp. 89–100, Nov. 2016.

[36] A. Vanden Broeck, C. Lotz, J. Ortiz, and V. Lamour, "Cryo-EM Structure of the Complete E. Coli DNA Gyrase Nucleoprotein Complex," *Nature Communications*, vol. 10, p. 4935, Oct. 2019.

[37] L. Costenaro, J. G. Grossmann, C. Ebel, and A. Maxwell, "Small-Angle X-Ray Scattering Reveals the Solution Structure of the Full-Length DNA Gyrase A Subunit," *Structure*, vol. 13, pp. 287–296, Feb. 2005.

[38] L. Costenaro, J. G. Grossmann, C. Ebel, and A. Maxwell, "Modular Structure of the Full-Length DNA Gyrase B Subunit Revealed by Small-Angle X-Ray Scattering," *Structure*, vol. 15, pp. 329–339, Mar. 2007.

[39] B. D. Bax, P. F. Chan, D. S. Eggleston, A. Fosberry, D. R. Gentry, F. Gorrec, I. Giordano, M. M. Hann, A. Hennessy, M. Hibbs, J. Huang, E. Jones, J. Jones, K. K. Brown, C. J. Lewis, E. W. May, M. R. Saunders, O. Singh, C. E. Spitzfaden, C. Shen, A. Shillings, A. J. Theobald, A. Wohlkonig, N. D. Pearson, and M. N. Gwynn, "Type IIA Topoisomerase Inhibition by a New Class of Antibacterial Agents," *Nature*, vol. 466, pp. 935–940, Aug. 2010.

[40] S. Petrella, E. Capton, B. Raynal, C. Giffard, A. Thureau, F. Bonneté, P. M. Alzari, A. Aubry, and C. Mayer, "Overall Structures of Mycobacterium tuberculosis DNA Gyrase Reveal the Role of a Corynebacteriales GyrB-Specific Insert in ATPase Activity," *Structure*, vol. 27, pp. 579–589.e5, Apr. 2019.

[41] J. Papillon, J.-F. Ménétret, C. Batisse, R. Hélye, P. Schultz, N. Potier, and V. Lamour, "Structural insight into negative DNA supercoiling by DNA gyrase, a bacterial type 2A DNA topoisomerase," *Nucleic Acids Research*, vol. 41, pp. 7815–7827, Sept. 2013.

[42] L. Aravind, D. D. Leipe, and E. V. Koonin, "Toprim– a Conserved Catalytic Domain in Type IA and II Topoisomerases, DnaG-type Primases, OLD Family Nucleases and RecR Proteins," *Nucleic Acids Research*, vol. 26, pp. 4205–4213, Sept. 1998.

[43] R. U. Rymer, F. A. Solorio, A. Tehranchi, C. Chu, J. E. Corn, J. L. Keck, J. D. Wang, and J. M. Berger, "Nucleotide-bound structures of the DnaG catalytic core reveal how metal-NTP substrates are bound during primer synthesis and blocked by stringent response alarmones," *Structure (London, England : 1993)*, vol. 20, pp. 1478–1489, Sept. 2012.

[44] C. J. Schiltz, A. Lee, E. A. Partlow, C. J. Hosford, and J. S. Chappie, "Structural characterization of Class 2 OLD family nucleases supports a two-metal catalysis mechanism for cleavage," *Nucleic Acids Research*, vol. 47, pp. 9448–9463, Sept. 2019.

[45] Q. Liu and J. C. Wang, "Similarity in the Catalysis of DNA Breakage and Rejoining by Type IA and IIA DNA Topoisomerases," *Proceedings of the National Academy of Sciences of the United States of America*, vol. 96, pp. 881–886, Feb. 1999.

[46] P. F. Chan, V. Srikannathasan, J. Huang, H. Cui, A. P. Fosberry, M. Gu, M. M. Hann, M. Hibbs, P. Homes, K. Ingraham, J. Pizzollo, C. Shen, A. J. Shillings, C. E. Spitzfaden, R. Tanner, A. J. Theobald, R. A. Stavenger, B. D. Bax, and M. N. Gwynn, "Structural Basis of DNA Gyrase Inhibition by Antibacterial QPT-1, Anticancer Drug Etoposide and Moxifloxacin," *Nature Communications*, vol. 6, p. 10048, Dec. 2015.

[47] A. J. Schoeffler, A. P. May, and J. M. Berger, "A domain insertion in Escherichia coli GyrB adopts a novel fold that plays a critical role in gyrase function," *Nucleic Acids Research*, vol. 38, pp. 7830–7844, Nov. 2010.

[48] M. Chatterji, S. Unniraman, A. Maxwell, and V. Nagaraja, "The Additional 165 Amino Acids in the B Protein of Escherichia coli DNA Gyrase Have an Important Role in DNA Binding," *Journal of Biological Chemistry*, vol. 275, pp. 22888–22894, July 2000.

[49] P. R. Caron and J. C. Wang, "Appendix II: Alignment of Primary Sequences of DNA Topoisomerases," in *Advances in Pharmacology* (L. F. Liu, ed.), vol. 29 of *DNA Topoisomerases: Topoisomerase-Targeting Drugs*, pp. 271–297, Academic Press, Jan. 1994.

[50] N. V. Grishin, "Two tricks in one bundle: Helix–turn–helix gains enzymatic activity," *Nucleic Acids Research*, vol. 28, pp. 2229–2233, June 2000.

[51] J. H. M. Cabral, A. P. Jackson, C. V. Smith, N. Shikotra, A. Maxwell, and R. C. Liddington, "Crystal Structure of the Breakage– Reunion Domain of DNA Gyrase," *Nature*, vol. 388, pp. 903–906, Aug. 1997.

[52] V. Srikannathasan, A. Wohlkonig, A. Shillings, O. Singh, P. F. Chan, J. Huang, M. N. Gwynn, A. P. Fosberry, P. Homes, M. Hibbs, A. J. Theobald, C. Spitzfaden, and B. D. Bax, "Crystallization and Initial Crystallographic Analysis of Covalent DNA-cleavage Complexes of Staphyloccocus Aureus DNA Gyrase with QPT-1, Moxifloxacin and Etoposide," *Acta crystallographica. Section F, Structural biology communications*, vol. 71, pp. 1242–6, Oct. 2015.

[53] G. Orphanides and A. Maxwell, "Evidence for a conformational change in the DNA gyrase-DNA complex from hydroxyl radical footprinting," *Nucleic Acids Research*, vol. 22, pp. 1567–1575, May 1994.

[54] K. D. Corbett, R. K. Shultzaberger, and J. M. Berger, "The C-terminal Domain of DNA Gyrase A Adopts a DNA-bending Beta-Pinwheel Fold.," *Proceedings of the National Academy of Sciences of the United States of America*, vol. 101, pp. 7293–8, May 2004.

[55] V. M. Kramlinger and H. Hiasa, "The "GyrA-box" Is Required for the Ability of DNA Gyrase to Wrap DNA and Catalyze the Supercoiling Reaction," *Journal of Biological Chemistry*, vol. 281, pp. 3738–3742, Feb. 2006.

[56] A. J. Ruthenburg, D. M. Graybosch, J. C. Huetsch, and G. L. Verdine, "A Superhelical Spiral in the Escherichia coli DNA Gyrase A C-terminal Domain Imparts Unidirectional Supercoiling Bias," *Journal of Biological Chemistry*, vol. 280, pp. 26177–26184, July 2005.

[57] B. H. Schmidt, N. Osheroff, and J. M. Berger, "Structure of a topoisomerase II-DNA-nucleotide complex reveals a new control mechanism for ATPase activity," *Nature structural & molecular biology*, vol. 19, pp. 1147–1154, Nov. 2012.

[58] L. Brino, A. Urzhumtsev, M. Mousli, C. Bronner, A. Mitschler, P. Oudet, and D. Moras, "Dimerization of Escherichia coli DNA-gyrase B provides a structural mechanism for activating the ATPase catalytic center," *The Journal of Biological Chemistry*, vol. 275, pp. 9468–9475, Mar. 2000.

[59] E. M. Smith and A. Mondragón, "Basic residues at the C-gate of DNA gyrase are involved in DNA supercoiling," *Journal of Biological Chemistry*, vol. 297, Aug. 2021.

[60] J. Roca, J. M. Berger, S. C. Harrison, and J. C. Wang, "DNA transport by a type II topoisomerase: Direct evidence for a two-gate mechanism.," *Proceedings of the National Academy of Sciences*, vol. 93, pp. 4057–4062, Apr. 1996.

[61] R. J. DiGate and K. J. Marians, "Identification of a potent decatenating enzyme from Escherichia coli.," *Journal of Biological Chemistry*, vol. 263, pp. 13366–13373, Sept. 1988.

[62] J. Kato, Y. Nishimura, R. Imamura, H. Niki, S. Hiraga, and H. Suzuki, "New topoisomerase essential for chromosome segregation in E. coli," *Cell*, vol. 63, pp. 393–404, Oct. 1990.

[63] E. L. Zechiedrich, A. B. Khodursky, S. Bachellier, R. Schneider, D. Chen, D. M. J. Lilley, and N. R. Cozzarelli, "Roles of Topoisomerases in Maintaining Steady-state DNA Supercoiling in Escherichia coli," *Journal of Biological Chemistry*, vol. 275, pp. 8103–8113, Mar. 2000.

[64] K. C. Neuman, G. Charvin, D. Bensimon, and V. Croquette, "Mechanisms of chiral discrimination by topoisomerase IV," *Proceedings of the National Academy of Sciences of the United States of America*, vol. 106, pp. 6986–6991, Apr. 2009.

[65] T.-J. Hsieh, L. Farh, W. M. Huang, and N.-L. Chan, "Structure of the Topoisomerase IV C-terminal Domain: A Broken β-Propeller Implied A Role As Geometry Facilitator In Catalysis," *Journal of Biological Chemistry*, vol. 279, pp. 55587–55593, Dec. 2004.

[66] H. Peng and K. J. Marians, "The Interaction of Escherichia coli Topoisomerase IV with DNA," *Journal of Biological Chemistry*, vol. 270, pp. 25286–25290, Oct. 1995.

[67] T. Hsieh and D. Brutlag, "ATP-dependent DNA topoisonmerase from D. melanogaster reversibly catenates duplex DNA rings," *Cell*, vol. 21, pp. 115–125, Aug. 1980.

[68] T. Goto and J. C. Wang, "Yeast DNA topoisomerase II is encoded by a single-copy, essential gene," *Cell*, vol. 36, pp. 1073–1080, Apr. 1984.

[69] B. A. Keller, S. Patel, and L. M. Fisher, "Molecular cloning and expression of the Candida albicans TOP2 gene allows study of fungal DNA topoisomerase II inhibitors in yeast.," *Biochemical Journal*, vol. 324, pp. 329–339, May 1997.

[70] C. A. Austin, J.-H. Sng, S. Patel, and L. M. Fisher, "Novel HeLa topoisomerase II is the IIβ isoform: Complete coding sequence and homology with other type II topoisomerases," *Biochimica et Biophysica Acta (BBA) - Gene Structure and Expression*, vol. 1172, pp. 283–291, Mar. 1993.

[71] F. H. Drake, G. A. Hofmann, S. M. Mong, J. O. Bartus, R. P. Hertzberg, R. K. Johnson, M. R. Mattern, and C. K. Mirabelli, "In vitro and intracellular inhibition of topoisomerase

II by the antitumor agent merbarone," *Cancer Research*, vol. 49, pp. 2578–2583, May 1989.

[72] G. Capranico, S. Tinelli, C. A. Austin, M. L. Fisher, and F. Zunino, "Different patterns of gene expression of topoisomerase II isoforms in differentiated tissues during murine development," *Biochimica Et Biophysica Acta*, vol. 1132, pp. 43–48, Aug. 1992.

[73] A. M. Fry, C. M. Chresta, S. M. Davies, M. C. Walker, A. L. Harris, J. A. Hartley, J. R. Masters, and I. D. Hickson, "Relationship between topoisomerase II level and chemosensitivity in human tumor cell lines," *Cancer Research*, vol. 51, pp. 6592–6595, Dec. 1991.

[74] A. K. McClendon, A. C. Rodriguez, and N. Osheroff, "Human Topoisomerase IIα Rapidly Relaxes Positively Supercoiled DNA: Implications For Enzyme Action Ahead Of Replication Forks," *Journal of Biological Chemistry*, vol. 280, pp. 39337–39345, Nov. 2005.

[75] M. P. Lee, M. Sander, and T. Hsieh, "Nuclease protection by Drosophila DNA topoisomerase II. Enzyme/DNA contacts at the strong topoisomerase II cleavage sites," *The Journal of Biological Chemistry*, vol. 264, pp. 21779–21787, Dec. 1989.

[76] B. Thomsen, C. Bendixen, K. Lund, A. H. Andersen, B. S. Sørensen, and O. Westergaard, "Characterization of the interaction between topoisomerase II and DNA by transcriptional footprinting," *Journal of Molecular Biology*, vol. 215, pp. 237–244, Sept. 1990.

[77] R. M. Linka, A. C. Porter, A. Volkov, C. Mielke, F. Boege, and M. O. Christensen, "C-Terminal regions of topoisomerase II α and II β determine isoform-specific functioning of the enzymes in vivo," *Nucleic Acids Research*, vol. 35, pp. 3810–3822, June 2007.

[78] A. K. McClendon, A. C. Gentry, J. S. Dickey, M. Brinch, S. Bendsen, A. H. Andersen, and N. Osheroff, "Bimodal Recognition of DNA Geometry by Human Topoisomerase IIα," *Biochemistry*, vol. 47, pp. 13169–13178, Dec. 2008.

[79] C. Buhler, D. Gadelle, P. Forterre, J. C. Wang, and A. Bergerat, "Reconstitution of DNA topoisomerase VI of the thermophilic archaeon Sulfolobus shibatae from subunits separately overexpressed in Escherichia coli," *Nucleic Acids Research*, vol. 26, pp. 5157–5162, Nov. 1998.

[80] C. Buhler, J. H. Lebbink, C. Bocs, R. Ladenstein, and P. Forterre, "DNA topoisomerase VI generates ATP-dependent double-strand breaks with two-nucleotide overhangs," *The Journal of Biological Chemistry*, vol. 276, pp. 37215–37222, Oct. 2001.

[81] F. Hartung and H. Puchta, "Molecular characterization of homologues of both subunits A (SPO11) and B of the archaebacterial topoisomerase 6 in plants," *Gene*, vol. 271, pp. 81–86, June 2001.

[82] D. Gadelle, M. Krupovic, K. Raymann, C. Mayer, and P. Forterre, "DNA topoisomerase VIII: A novel subfamily of type IIB topoisomerases encoded by free or integrated plasmids in Archaea and Bacteria," *Nucleic Acids Research*, vol. 42, pp. 8578–8591, Sept. 2014.

[83] T. J. Wendorff and J. M. Berger, "Topoisomerase VI senses and exploits both DNA crossings and bends to facilitate strand passage," *eLife*, vol. 7, p. e31724, Mar. 2018.

[84] S. J. McKie, P. R. Desai, Y. Seol, A. M. Allen, A. Maxwell, and K. C. Neuman, "Topoisomerase VI is a chirally-selective, preferential DNA decatenase," *eLife*, vol. 11, p. e67021, 2022.

[85] E. L. Zechiedrich, K. Christiansen, A. H. Andersen, O. Westergaard, and N. Osheroff, "Double-Stranded DNA Cleavage/Religation Reaction of Eukaryotic Topoisomerase II: Evidence for a Nicked DNA Intermediate," *Biochemistry*, vol. 28, no. 15, pp. 6229–6236, 1989.

[86] S. C. Kampranis and A. Maxwell, "The DNA Gyrase-Quinolone Complex: ATP Hydrolysis And The Mechanism Of DNA Cleavage," *Journal of Biological Chemistry*, vol. 273, pp. 22615–22626, Aug. 1998.

[87] J. E. Deweese and N. Osheroff, "Coordinating the Two Protomer Active Sites of Human Topoisomerase IIalpha: Nicks as Topoisomerase II Poisons.," *Biochemistry*, vol. 48, pp. 1439–41, Feb. 2009.

[88] C. G. Noble and A. Maxwell, "The Role of GyrB in the DNA Cleavage-Religation Reaction of DNA Gyrase: A Proposed Two Metal-Ion Mechanism," *Journal of Molecular Biology*, vol. 318, pp. 361–371, Apr. 2002.

[89] J. E. Deweese, A. B. Burgin, and N. Osheroff, "Human Topoisomerase IIalpha Uses a Two-Metal-Ion Mechanism for DNA Cleavage.," *Nucleic acids research*, vol. 36, pp. 4883–93, Sept. 2008.

[90] J. E. Deweese, A. B. Burgin, and N. Osheroff, "Using 3'-Bridging Phosphorothiolates To Isolate the Forward DNA Cleavage Reaction of Human Topoisomerase IIα," *Biochemistry*, vol. 47, pp. 4129–4140, Apr. 2008.

[91] J. E. Deweese, F. P. Guengerich, A. B. Burgin, and N. Osheroff, "Metal Ion Interactions in the DNA Cleavage/Ligation Active Site of Human Topoisomerase IIα," *Biochemistry*, vol. 48, pp. 8940–8947, Sept. 2009.

[92] B. D. Bax, G. Murshudov, A. Maxwell, and T. Germe, "DNA Topoisomerase Inhibitors: Trapping a DNA-Cleaving Machine in Motion," *Journal of molecular biology*, vol. 431, pp. 3427–3449, Aug. 2019.

[93] G. Magarò, F. Prati, B. Garofalo, G. Corso, G. Furlotti, C. Apicella, G. Mangano, N. D'Atanasio, D. Robinson, F. P. Di Giorgio, and R. Ombrato, "Virtual Screening Approach and Investigation of Structure–Activity Relationships To Discover Novel Bacterial Topoisomerase Inhibitors Targeting Gram-Positive and Gram-Negative Pathogens," *Journal of Medicinal Chemistry*, vol. 62, pp. 7445–7472, Aug. 2019.

[94] B. H. Schmidt, A. B. Burgin, J. E. Deweese, N. Osheroff, and J. M. Berger, "A Novel and Unified Two-Metal Mechanism for DNA Cleavage by Type II and IA Topoisomerases," *Nature*, vol. 465, no. 7298, p. 641, 2010.

[95] Q. Liu and J. C. Wang, "Identification of active site residues in the "GyrA" half of yeast DNA topoisomerase II," *The Journal of Biological Chemistry*, vol. 273, pp. 20252–20260, Aug. 1998.

[96] J. Wang, P. Yu, T. C. Lin, W. H. Konigsberg, and T. A. Steitz, "Crystal structures of an NH2-terminal fragment of T4 DNA polymerase and its complexes with single-stranded DNA and with divalent metal ions," *Biochemistry*, vol. 35, pp. 8110–8119, June 1996.

[97] C. A. Brautigam and T. A. Steitz, "Structural principles for the inhibition of the 3'-5' exonuclease activity of Escherichia coli DNA polymerase I by phosphorothioates," *Journal of Molecular Biology*, vol. 277, pp. 363–377, Mar. 1998.

[98] S. L. Pitts, G. F. Liou, L. A. Mitchenall, A. B. Burgin, A. Maxwell, K. C. Neuman, and

N. Osheroff, "Use of divalent metal ions in the DNA cleavage reaction of topoisomerase IV," *Nucleic Acids Research*, vol. 39, pp. 4808–4817, June 2011.

[99] E. G. Gibson, B. Bax, P. F. Chan, and N. Osheroff, "Mechanistic and Structural Basis for the Actions of the Antibacterial Gepotidacin against Staphylococcus Aureus Gyrase," *ACS Infectious Diseases*, p. acsinfecdis.8b00315, Feb. 2019.

[100] T. J. Wendorff, B. H. Schmidt, P. Heslop, C. A. Austin, and J. M. Berger, "The Structure of DNA-Bound Human Topoisomerase II Alpha: Conformational Mechanisms for Coordinating Inter-Subunit Interactions with DNA Cleavage," *Journal of Molecular Biology*, vol. 424, pp. 109–124, Dec. 2012.

[101] N. Cao, K. Tan, T. Annamalai, A. Joachimiak, and Y.-C. Tse-Dinh, "Investigating Mycobacterial Topoisomerase I Mechanism from the Analysis of Metal and DNA Substrate Interactions at the Active Site," *Nucleic Acids Research*, vol. 46, pp. 7296–7308, Aug. 2018.

[102] G. Narula, T. Annamalai, S. Aedo, B. Cheng, E. Sorokin, A. Wong, and Y.-C. Tse-Dinh, "The strictly conserved Arg-321 residue in the active site of Escherichia coli topoisomerase I plays a critical role in DNA rejoining," *The Journal of Biological Chemistry*, vol. 286, pp. 18673–18680, May 2011.

[103] D. R. Davies, A. Mushtaq, H. Interthal, J. J. Champoux, and W. G. J. Hol, "The Structure of the Transition State of the Heterodimeric Topoisomerase I of Leishmania Donovani as a Vanadate Complex with Nicked DNA," *Journal of Molecular Biology*, 2006.

[104] W. Hwang, J. Yoo, Y. Lee, S. Park, P. L. Hoang, H. Cho, J. Yu, T. M. Hoa Vo, M. Shin, M. S. Jin, D. Park, C. Hyeon, and G. Lee, "Dynamic coordination of two-metal-ions orchestrates λ-exonuclease catalysis," *Nature Communications*, vol. 9, p. 4404, Oct. 2018.

[105] B. Chevalier, D. Sussman, C. Otis, A.-J. Noël, M. Turmel, C. Lemieux, K. Stephens, R. J. Monnat, and B. L. Stoddard, "Metal-Dependent DNA Cleavage Mechanism of the I-CreI LAGLIDADG Homing Endonuclease„" *Biochemistry*, vol. 43, pp. 14015–14026, Nov. 2004.

[106] A. Guasch, M. Lucas, G. Moncalián, M. Cabezas, R. Pérez-Luque, F. X. Gomis-Rüth, F. de la Cruz, and M. Coll, "Recognition and processing of the origin of transfer DNA by conjugative relaxase TrwC," *Nature Structural & Molecular Biology*, vol. 10, pp. 1002–1010, Dec. 2003.

[107] M. Chandler, F. de la Cruz, F. Dyda, A. B. Hickman, G. Moncalian, and B. Ton-Hoang, "Breaking and joining single-stranded DNA: The HUH endonuclease superfamily," *Nature reviews. Microbiology*, vol. 11, pp. 525–538, Aug. 2013.

[108] T. Nakamura, Y. Zhao, Y. Yamagata, Y.-j. Hua, and W. Yang, "Watching DNA polymerase η make a phosphodiester bond," *Nature*, vol. 487, pp. 196–201, July 2012.

[109] B. D. Freudenthal, W. A. Beard, D. D. Shock, and S. H. Wilson, "Observing a DNA polymerase choose right from wrong," *Cell*, vol. 154, pp. 157–168, July 2013.

[110] J. A. Jamsen, W. A. Beard, L. C. Pedersen, D. D. Shock, A. F. Moon, J. M. Krahn, K. Bebenek, T. A. Kunkel, and S. H. Wilson, "Time-lapse crystallography snapshots of a double-strand break repair polymerase in action," *Nature Communications*, vol. 8, p. 253, Aug. 2017.

[111] Y. Gao and W. Yang, "Capture of A Third Mg2+ is Essential for Catalyzing DNA Synthesis," *Science (New York, N.Y.)*, vol. 352, pp. 1334–1337, June 2016.

[112] N. Oezguen, C. H. Schein, S. R. Peddi, T. D. Power, T. Izumi, and W. Braun, "A "Moving Metal Mechanism" for Substrate Cleavage by the DNA Repair Endonuclease APE-1," *Proteins: Structure, Function, and Bioinformatics*, vol. 68, pp. 313–323, Apr. 2007.

[113] Y. Pommier, E. Leo, H. Zhang, and C. Marchand, "DNA Topoisomerases and Their Poisoning by Anticancer and Antibacterial Drugs," *Chemistry & Biology*, vol. 17, pp. 421–433, May 2010.

[114] X. Liang, Q. Wu, S. Luan, Z. Yin, C. He, L. Yin, Y. Zou, Z. Yuan, L. Li, X. Song, M. He, C. Lv, and W. Zhang, "A comprehensive review of topoisomerase inhibitors as anticancer agents in the past decade," *European Journal of Medicinal Chemistry*, vol. 171, pp. 129–168, June 2019.

[115] M. E. Wall, M. C. Wani, C. E. Cook, K. H. Palmer, A. T. McPhail, and G. A. Sim, "Plant Antitumor Agents. I. The Isolation and Structure of Camptothecin, a Novel Alkaloidal Leukemia and Tumor Inhibitor from Camptotheca Acuminata," *Journal of the American Chemical Society*, vol. 88, pp. 3888–3890, Aug. 1966.

[116] Y. H. Hsiang, M. G. Lihou, and L. F. Liu, "Arrest of replication forks by drug-stabilized topoisomerase I-DNA cleavable complexes as a mechanism of cell killing by camptothecin," *Cancer Research*, vol. 49, pp. 5077–5082, Sept. 1989.

[117] B. L. Staker, K. Hjerrild, M. D. Feese, C. A. Behnke, A. B. Burgin, L. Stewart, and L. Stewart, "The Mechanism of Topoisomerase I Poisoning by a Camptothecin Analog.," *Proceedings of the National Academy of Sciences of the United States of America*, vol. 99, pp. 15387–92, Nov. 2002.

[118] R. H. J. Mathijssen, W. J. Loos, J. Verweij, and A. Sparreboom, "Pharmacology of topoisomerase I inhibitors irinotecan (CPT-11) and topotecan," *Current Cancer Drug Targets*, vol. 2, pp. 103–123, June 2002.

[119] S. Sandhaus, P. P. Chapagain, and Y.-C. Tse-Dinh, "Discovery of Novel Bacterial Topoisomerase I Inhibitors by Use of in Silico Docking and in Vitro Assays," *Scientific Reports*, vol. 8, p. 1437, Dec. 2018.

[120] T. Germe, J. Vörös, F. Jeannot, T. Taillier, R. A. Stavenger, E. Bacqué, A. Maxwell, and B. D. Bax, "A New Class of Antibacterials, the Imidazopyrazinones, Reveal Structural Transitions Involved in DNA Gyrase Poisoning and Mechanisms of Resistance," *Nucleic Acids Research*, vol. 46, pp. 4114–4128, May 2018.

[121] K. Drlica, A. Mustaev, T. R. Towle, G. Luan, R. J. Kerns, and J. M. Berger, "Bypassing Fluoroquinolone Resistance with Quinazolinediones: Studies of Drug-Gyrase-DNA Complexes Having Implications for Drug Design," *ACS Chemical Biology*, vol. 9, pp. 2895–2904, Dec. 2014.

[122] "EAGLE-2 and EAGLE-3 phase III trials for gepotidacin stopped early for efficacy following pre-planned interim analysis by Independent Data Monitoring Committee | GSK." https://www.gsk.com/en-gb/media/press-releases/gsk-announces-phase-iii-trials-for-gepotidacin/, Nov. 2022.

[123] T. J. Miles, A. J. Hennessy, B. Bax, G. Brooks, B. S. Brown, P. Brown, N. Cailleau, D. Chen, S. Dabbs, D. T. Davies, J. M. Esken, I. Giordano, J. L. Hoover, G. E. Jones, S. K. Kusalakumari Sukmar, R. E. Markwell, E. A. Minthorn, S. Rittenhouse, M. N.

Gwynn, and N. D. Pearson, "Novel Tricyclics (e.g., GSK945237) as Potent Inhibitors of Bacterial Type IIA Topoisomerases," *Bioorganic & Medicinal Chemistry Letters*, vol. 26, pp. 2464–2469, May 2016.

[124] N. G. Bush, I. Diez-Santos, L. R. Abbott, and A. Maxwell, "Quinolones: Mechanism, Lethality and Their Contributions to Antibiotic Resistance," *Molecules (Basel, Switzerland)*, vol. 25, p. E5662, Dec. 2020.

[125] G. Y. Lesher, E. J. Froelich, M. D. Gruett, J. H. Bailey, and R. Pauline. Brundage, "1,8-Naphthyridine Derivatives. A New Class of Chemotherapeutic Agents," *Journal of Medicinal and Pharmaceutical Chemistry*, vol. 5, pp. 1063–1065, Sept. 1962.

[126] G. G. Zhanel, K. Ennis, L. Vercaigne, A. Walkty, A. S. Gin, J. Embil, H. Smith, and D. J. Hoban, "A Critical Review of the Fluoroquinolones," *Drugs*, vol. 62, pp. 13–59, Jan. 2002.

[127] L. S. Redgrave, S. B. Sutton, M. A. Webber, and L. J. V. Piddock, "Fluoroquinolone Resistance: Mechanisms, Impact on Bacteria, and Role in Evolutionary Success.," *Trends in microbiology*, vol. 22, pp. 438–45, Aug. 2014.

[128] K. J. Aldred, R. J. Kerns, and N. Osheroff, "Mechanism of Quinolone Action and Resistance," *Biochemistry*, vol. 53, pp. 1565–1574, Mar. 2014.

[129] H. Yoshida, M. Bogaki, M. Nakamura, and S. Nakamura, "Quinolone resistance-determining region in the DNA gyrase gyrA gene of Escherichia coli.," *Antimicrobial Agents and Chemotherapy*, vol. 34, pp. 1271–1272, June 1990.

[130] L. J. V. Piddock, "Fluoroquinolone resistance," *BMJ : British Medical Journal*, vol. 317, pp. 1029–1030, Oct. 1998.

[131] C. J. Murray, K. S. Ikuta, F. Sharara, L. Swetschinski, G. R. Aguilar, A. Gray, C. Han, C. Bisignano, P. Rao, E. Wool, S. C. Johnson, A. J. Browne, M. G. Chipeta, F. Fell, S. Hackett, G. Haines-Woodhouse, B. H. K. Hamadani, E. A. P. Kumaran, B. McManigal, R. Agarwal, S. Akech, S. Albertson, J. Amuasi, J. Andrews, A. Aravkin, E. Ashley, F. Bailey, S. Baker, B. Basnyat, A. Bekker, R. Bender, A. Bethou, J. Bielicki, S. Boonkasidecha, J. Bukosia, C. Carvalheiro, C. Castañeda-Orjuela, V. Chansamouth, S. Chaurasia, S. Chiurchiù, F. Chowdhury, A. J. Cook, B. Cooper, T. R. Cressey, E. Criollo-Mora, M. Cunningham, S. Darboe, N. P. J. Day, M. D. Luca, K. Dokova, A. Dramowski, S. J. Dunachie, T. Eckmanns, D. Eibach, A. Emami, N. Feasey, N. Fisher-Pearson, K. Forrest, D. Garrett, P. Gastmeier, A. Z. Giref, R. C. Greer, V. Gupta, S. Haller, A. Haselbeck, S. I. Hay, M. Holm, S. Hopkins, K. C. Iregbu, J. Jacobs, D. Jarovsky, F. Javanmardi, M. Khorana, N. Kissoon, E. Kobeissi, T. Kostyanev, F. Krapp, R. Krumkamp, A. Kumar, H. H. Kyu, C. Lim, D. Limmathurotsakul, M. J. Loftus, M. Lunn, J. Ma, N. Mturi, T. Munera-Huertas, P. Musicha, M. M. Mussi-Pinhata, T. Nakamura, R. Nanavati, S. Nangia, P. Newton, C. Ngoun, A. Novotney, D. Nwakanma, C. W. Obiero, A. Olivas-Martinez, P. Olliaro, E. Ooko, E. Ortiz-Brizuela, A. Y. Peleg, C. Perrone, N. Plakkal, A. Ponce-de-Leon, M. Raad, T. Ramdin, A. Riddell, T. Roberts, J. V. Robotham, A. Roca, K. E. Rudd, N. Russell, J. Schnall, J. A. G. Scott, M. Shivamallappa, J. Sifuentes-Osornio, N. Steenkeste, A. J. Stewardson, T. Stoeva, N. Tasak, A. Thaiprakong, G. Thwaites, C. Turner, P. Turner, H. R. van Doorn, S. Velaphi, A. Vongpradith, H. Vu, T. Walsh, S. Waner, T. Wangrangsimakul, T. Wozniak, P. Zheng, B. Sartorius, A. D. Lopez, A. Stergachis, C. Moore, C. Dolecek, and M. Naghavi, "Global Burden of Bacterial Antimicrobial Resistance in 2019: A Systematic Analysis," *The Lancet*, vol. 399, pp. 629–655, Feb. 2022.

[132] WHO Advisory Group on Integrated Surveillance of Antimicrobial Resistance (AGISAR), *Critically Important Antimicrobials for Human Medicine.* sixth ed., 2018.

[133] J. Desai, S. S, S. Kumar, and R. Sharma, "Novel Bacterial Topoisomerase inhibitors (NBTIs) – A comprehensive review," *European Journal of Medicinal Chemistry Reports*, vol. 3, p. 100017, Dec. 2021.

[134] C. Perry, M. Hossain, M. Powell, A. Raychaudhuri, N. Scangarella-Oman, C. Tiffany, S. Xu, E. Dumont, and S. Janmohamed, "Design of Two Phase III, Randomized, Multicenter Studies Comparing Gepotidacin with Nitrofurantoin for the Treatment of Uncomplicated Urinary Tract Infection in Female Participants," *Infectious Diseases and Therapy*, vol. 11, pp. 2297–2310, Dec. 2022.

[135] E. L. Baldwin and N. Osheroff, "Etoposide, Topoisomerase II and Cancer," *Current Medicinal Chemistry - Anti-Cancer Agents*, vol. 5, no. 4, pp. 363–372.

[136] S. Douedi and M. P. Carson, "Anthracycline Medications (Doxorubicin)," in *StatPearls*, Treasure Island (FL): StatPearls Publishing, 2022.

[137] H. Taymaz-Nikerel, M. E. Karabekmez, S. Eraslan, and B. Kırdar, "Doxorubicin induces an extensive transcriptional and metabolic rewiring in yeast cells," *Scientific Reports*, vol. 8, pp. 1–14, Sept. 2018.

[138] P. F. Chan, T. Germe, B. D. Bax, J. Huang, R. K. Thalji, E. Bacqué, A. Checchia, D. Chen, H. Cui, X. Ding, K. Ingraham, L. McCloskey, K. Raha, V. Srikannathasan, A. Maxwell, and R. A. Stavenger, "Thiophene Antibacterials That Allosterically Stabilize DNA-cleavage Complexes with DNA Gyrase," *Proceedings of the National Academy of Sciences*, vol. 114, pp. E4492–E4500, May 2017.

[139] C. D. Hardy and N. R. Cozzarelli, "Alteration of Escherichia coli Topoisomerase IV to Novobiocin Resistance," *Antimicrobial Agents and Chemotherapy*, vol. 47, pp. 941–947, Mar. 2003.

[140] U. Galm, J. Schimana, H.-P. Fiedler, J. Schmidt, S.-M. Li, and L. Heide, "Cloning and analysis of the simocyclinone biosynthetic gene cluster of Streptomyces antibioticus Tü 6040," *Archives of Microbiology*, vol. 178, pp. 102–114, Aug. 2002.

[141] R. H. Flatman, A. J. Howells, L. Heide, H.-P. Fiedler, and A. Maxwell, "Simocyclinone D8, an Inhibitor of DNA Gyrase with a Novel Mode of Action," *Antimicrobial Agents and Chemotherapy*, vol. 49, pp. 1093–1100, Mar. 2005.

[142] M. J. Edwards, R. H. Flatman, L. A. Mitchenall, C. E. M. Stevenson, T. B. K. Le, T. A. Clarke, A. R. McKay, H.-P. Fiedler, M. J. Buttner, D. M. Lawson, and A. Maxwell, "A crystal structure of the bifunctional antibiotic simocyclinone D8, bound to DNA gyrase," *Science (New York, N.Y.)*, vol. 326, pp. 1415–1418, Dec. 2009.

[143] S. J. Hearnshaw, M. J. Edwards, C. E. Stevenson, D. M. Lawson, and A. Maxwell, "A New Crystal Structure of the Bifunctional Antibiotic Simocyclinone D8 Bound to DNA Gyrase Gives Fresh Insight into the Mechanism of Inhibition," *Journal of Molecular Biology*, vol. 426, pp. 2023–2033, May 2014.

[144] A. Maxwell and A. J. Howells, "Overexpression and Purification of Bacterial DNA Gyrase," in *DNA Topoisomerase Protocols: Volume I: DNA Topology and Enzymes* (M.-A. Bjornsti and N. Osheroff, eds.), Methods in Molecular Biology, pp. 135–144, Totowa, NJ: Humana Press, 1999.

[145] E. Gasteiger, C. Hoogland, A. Gattiker, S. Duvaud, M. R. Wilkins, R. D. Appel, and A. Bairoch, "Protein Identification and Analysis Tools on the ExPASy Server," in *The Proteomics Protocols Handbook* (J. M. Walker, ed.), pp. 571–607, Totowa, NJ: Humana Press, 2005.

[146] C. A. Schneider, W. S. Rasband, and K. W. Eliceiri, "NIH Image to ImageJ: 25 years of image analysis," *Nature Methods*, vol. 9, pp. 671–675, July 2012.

[147] J. Schindelin, I. Arganda-Carreras, E. Frise, V. Kaynig, M. Longair, T. Pietzsch, S. Preibisch, C. Rueden, S. Saalfeld, B. Schmid, J.-Y. Tinevez, D. J. White, V. Hartenstein, K. Eliceiri, P. Tomancak, and A. Cardona, "Fiji: An open-source platform for biological-image analysis," *Nature Methods*, vol. 9, pp. 676–682, July 2012.

[148] P. Virtanen, R. Gommers, T. E. Oliphant, M. Haberland, T. Reddy, D. Cournapeau, E. Burovski, P. Peterson, W. Weckesser, J. Bright, S. J. van der Walt, M. Brett, J. Wilson, K. J. Millman, N. Mayorov, A. R. J. Nelson, E. Jones, R. Kern, E. Larson, C. J. Carey, İ. Polat, Y. Feng, E. W. Moore, J. VanderPlas, D. Laxalde, J. Perktold, R. Cimrman, I. Henriksen, E. A. Quintero, C. R. Harris, A. M. Archibald, A. H. Ribeiro, F. Pedregosa, and P. van Mulbregt, "SciPy 1.0: Fundamental algorithms for scientific computing in Python," *Nature Methods*, vol. 17, pp. 261–272, Mar. 2020.

[149] W. McKinney, "Data Structures for Statistical Computing in Python," in *Python in Science Conference*, (Austin, Texas), pp. 56–61, 2010.

[150] J. D. Hunter, "Matplotlib: A 2D Graphics Environment," *Computing in Science & Engineering*, vol. 9, pp. 90–95, May 2007.

[151] C. R. Harris, K. J. Millman, S. J. van der Walt, R. Gommers, P. Virtanen, D. Cournapeau, E. Wieser, J. Taylor, S. Berg, N. J. Smith, R. Kern, M. Picus, S. Hoyer, M. H. van Kerkwijk, M. Brett, A. Haldane, J. F. del Río, M. Wiebe, P. Peterson, P. Gérard-Marchant, K. Sheppard, T. Reddy, W. Weckesser, H. Abbasi, C. Gohlke, and T. E. Oliphant, "Array programming with NumPy," *Nature*, vol. 585, pp. 357–362, Sept. 2020.

[152] M. L. Waskom, "Seaborn: Statistical data visualization," *Journal of Open Source Software*, vol. 6, p. 3021, Apr. 2021.

[153] C. Vonrhein, C. Flensburg, P. Keller, A. Sharff, O. Smart, W. Paciorek, T. Womack, and G. Bricogne, "Data processing and analysis with the autoPROC toolbox," *Acta Crystallographica. Section D, Biological Crystallography*, vol. 67, pp. 293–302, Apr. 2011.

[154] P. R. Evans and G. N. Murshudov, "How good are my data and what is the resolution?," *Acta Crystallographica Section D: Biological Crystallography*, vol. 69, pp. 1204–1214, July 2013.

[155] A. J. McCoy, R. W. Grosse-Kunstleve, P. D. Adams, M. D. Winn, L. C. Storoni, and R. J. Read, "Phaser crystallographic software," *Journal of Applied Crystallography*, vol. 40, pp. 658–674, Aug. 2007.

[156] G. N. Murshudov, A. A. Vagin, and E. J. Dodson, "Refinement of macromolecular structures by the maximum-likelihood method," *Acta Crystallographica. Section D, Biological Crystallography*, vol. 53, pp. 240–255, May 1997.

[157] L. Potterton, S. McNicholas, E. Krissinel, J. Gruber, K. Cowtan, P. Emsley, G. N. Murshudov, S. Cohen, A. Perrakis, and M. Noble, "Developments in the CCP4 molecular-graphics project," *Acta Crystallographica Section D: Biological Crystallography*, vol. 60, pp. 2288–2294, Dec. 2004.

[158] K. Ignasiak and A. Maxwell, "Galleria Mellonella (Greater Wax Moth) Larvae as a Model for Antibiotic Susceptibility Testing and Acute Toxicity Trials," *BMC Research Notes*, vol. 10, p. 428, Aug. 2017.

[159] L. M. Wentzell and A. Maxwell, "The complex of DNA gyrase and quinolone drugs on DNA forms a barrier to the T7 DNA polymerase replication complex," *Journal of Molecular Biology*, vol. 304, pp. 779–791, Dec. 2000.

[160] W. J. Cannan and D. S. Pederson, "Mechanisms and Consequences of Double-strand DNA Break Formation in Chromatin," *Journal of cellular physiology*, vol. 231, pp. 3–14, Jan. 2016.

[161] A. Sankar, K. M. Swanson, J. Zhou, A. B. Jena, J. S. Ross, N. D. Shah, and P. Karaca-Mandic, "Association of Fluoroquinolone Prescribing Rates With Black Box Warnings from the US Food and Drug Administration," *JAMA Network Open*, vol. 4, p. e2136662, Dec. 2021.

[162] A. Mustaev, M. Malik, X. Zhao, N. Kurepina, G. Luan, L. M. Oppegard, H. Hiasa, K. R. Marks, R. J. Kerns, J. M. Berger, and K. Drlica, "Fluoroquinolone-Gyrase-DNA Complexes: Two Modes of Drug Binding," *The Journal of Biological Chemistry*, vol. 289, pp. 12300–12312, May 2014.

[163] A. Kolarič, T. Germe, M. Hrast, C. E. M. Stevenson, D. M. Lawson, N. P. Burton, J. Vörös, A. Maxwell, N. Minovski, and M. Anderluh, "Potent DNA gyrase inhibitors bind asymmetrically to their target using symmetrical bifurcated halogen bonds," *Nature Communications*, vol. 12, p. 150, Jan. 2021.

[164] A. M. Wilstermann and N. Osheroff, "Positioning the 3′-DNA Terminus for Topoisomerase II-mediated Religation," *Journal of Biological Chemistry*, vol. 276, pp. 17727–17731, May 2001.

[165] S. Soubeyrand, L. Pope, and R. J. Haché, "Topoisomerase IIα-dependent induction of a persistent DNA damage response in response to transient etoposide exposure," *Molecular Oncology*, vol. 4, pp. 38–51, Feb. 2010.

[166] E. Multon, J.-F. Riou, D. LeFevre, J.-C. Ahomadegbe, and G. Riou, "Topoisomerase II-mediated DNA cleavage activity induced by ellipticines on the human tumor cell line N417," *Biochemical Pharmacology*, vol. 38, pp. 2077–2086, July 1989.

[167] J. T. Wilson, X. Jiang, B. C. McGill, E. C. Lisic, and J. E. Deweese, "Examination of the Impact of Copper(II) α-(N)-Heterocyclic Thiosemicarbazone Complexes on DNA Topoisomerase IIα," *Chemical Research in Toxicology*, vol. 29, pp. 649–658, Apr. 2016.

[168] X.-S. Pan, K. A. Gould, and L. M. Fisher, "Probing the Differential Interactions of Quinazolinedione PD 0305970 and Quinolones with Gyrase and Topoisomerase IV," *Antimicrobial Agents and Chemotherapy*, vol. 53, pp. 3822–3831, Sept. 2009.

[169] J. E. Deweese and N. Osheroff, "The DNA cleavage reaction of topoisomerase II: Wolf in sheep's clothing," *Nucleic Acids Research*, vol. 37, pp. 738–748, Feb. 2009.

[170] D. Strahs, C.-X. Zhu, B. Cheng, J. Chen, and Y.-C. Tse-Dinh, "Experimental and computational investigations of Ser10 and Lys13 in the binding and cleavage of DNA substrates by Escherichia coli DNA topoisomerase I," *Nucleic Acids Research*, vol. 34, pp. 1785–1797, Mar. 2006.

[171] C. N. Fredd and H. S. Fogler, "Alternative Stimulation Fluids and Their Impact on Carbonate Acidizing," *SPE Journal*, vol. 3, pp. 34–41, Mar. 1998.

[172] D. J. Janecki and J. P. Reilly, "Denaturation of metalloproteins with EDTA to facilitate enzymatic digestion and mass fingerprinting," *Rapid Communications in Mass Spectrometry*, vol. 19, no. 10, pp. 1268–1272, 2005.

[173] S. Karkare, F. Yousafzai, L. A. Mitchenall, and A. Maxwell, "The Role of Ca 2+ in the Activity of Mycobacterium Tuberculosis DNA Gyrase," *Nucleic Acids Research*, vol. 40, no. 19, pp. 9774–9787, 2012.

[174] H. A. Flaschka, *EDTA Titrations: An Introduction to Theory and Practice*. Elsevier, Oct. 2013.

[175] F. Mueller-Planitz and D. Herschlag, "Coupling between ATP Binding and DNA Cleavage by DNA Topoisomerase II," *The Journal of Biological Chemistry*, vol. 283, pp. 17463–17476, June 2008.

[176] N. Osheroff and E. L. Zechiedrich, "Calcium-Promoted DNA Cleavage by Eukaryotic Topoisomerase II: Trapping the Covalent Enzyme-DNA Complex in an Active Form," *Biochemistry*, vol. 26, pp. 4303–4309, July 1987.

[177] D. C. Harris, *Quantitative Chemical Analysis*. W.H. Freeman, fifth ed., 2015.

[178] M. T. Henzl, J. D. Larson, and S. Agah, "Estimation of parvalbumin Ca(2+)- and Mg(2+)-binding constants by global least-squares analysis of isothermal titration calorimetry data," *Analytical Biochemistry*, vol. 319, pp. 216–233, Aug. 2003.

[179] S. Lee, S.-R. Jung, K. Heo, J. A. W. Byl, J. E. Deweese, N. Osheroff, and S. Hohng, "DNA Cleavage and Opening Reactions of Human Topoisomerase IIα Are Regulated via Mg2+-Mediated Dynamic Bending of Gate-DNA," *Proceedings of the National Academy of Sciences*, vol. 109, pp. 2925–2930, Feb. 2012.

[180] F.-X. Theillet, A. Binolfi, T. Frembgen-Kesner, K. Hingorani, M. Sarkar, C. Kyne, C. Li, P. B. Crowley, L. Gierasch, G. J. Pielak, A. H. Elcock, A. Gershenson, and P. Selenko, "Physicochemical Properties of Cells and Their Effects on Intrinsically Disordered Proteins (IDPs)," *Chemical Reviews*, vol. 114, pp. 6661–6714, July 2014.

[181] S. Subramani, H. Perdreau-Dahl, and J. P. Morth, "The magnesium transporter A is activated by cardiolipin and is highly sensitive to free magnesium in vitro," *eLife*, vol. 5, p. e11407, 2016.

[182] S. A. Loutet, A. C. K. Chan, M. J. Kobylarz, M. M. Verstraete, S. Pfaffen, B. Ye, A. L. Arrieta, and M. E. P. Murphy, "The Fate of Intracellular Metal Ions in Microbes," in *Trace Metals and Infectious Diseases* (J. O. Nriagu and E. P. Skaar, eds.), Cambridge (MA): MIT Press, 2015.

[183] K. D. Bromberg and N. Osheroff, "DNA cleavage and religation by human topoisomerase II alpha at high temperature," *Biochemistry*, vol. 40, pp. 8410–8418, July 2001.

[184] M. E. Shea and H. Hiasa, "Replicative helicases can translocate through abasic site-induced covalent topoisomerase IV-DNA complexes," *Nucleic Acids Research*, vol. 29, pp. 614–621, Feb. 2001.

[185] G. Fu, J. Wu, W. Liu, D. Zhu, Y. Hu, J. Deng, X.-E. Zhang, L. Bi, and D.-C. Wang, "Crystal structure of DNA gyrase B′ domain sheds lights on the mechanism for T-segment navigation," *Nucleic Acids Research*, vol. 37, pp. 5908–5916, Sept. 2009.

[186] H. Interthal, P. M. Quigley, W. G. J. Hol, and J. J. Champoux, "The Role of Lysine 532 in the Catalytic Mechanism of Human Topoisomerase I," *Journal of Biological Chemistry*, vol. 279, pp. 2984–2992, Jan. 2004.

[187] A. Boot, M. Liu, N. Stantial, V. Shah, W. Yu, K. C. Nitiss, J. L. Nitiss, S. Jinks-Robertson, and S. G. Rozen, "Recurrent mutations in topoisomerase IIα cause a previously undescribed mutator phenotype in human cancers," *Proceedings of the National Academy of Sciences*, vol. 119, p. e2114024119, Jan. 2022.

[188] P. Nurse, S. Bahng, E. Mossessova, and K. J. Marians, "Mutational Analysis of Escherichia coliTopoisomerase IV," *Journal of Biological Chemistry*, vol. 275, pp. 4104–4111, Feb. 2000.

[189] A. Gubaev, D. Weidlich, and D. Klostermeier, "DNA Gyrase with a Single Catalytic Tyrosine Can Catalyze DNA Supercoiling by a Nicking-Closing Mechanism," *Nucleic Acids Research*, vol. 44, pp. 10354–10366, Dec. 2016.

[190] D. Klostermeier, "Why Two? On the Role of (A-)Symmetry in Negative Supercoiling of DNA by Gyrase," *International Journal of Molecular Sciences*, vol. 19, p. 1489, May 2018.

[191] T. Germe, B. N. G, B. Victoria, S. Dominik, B. Justin, and M. Anthony, "Rapid, DNA-induced subunit exchange by DNA gyrase," *eLife*, vol. 12, Apr. 2023.

[192] U. Theuretzbacher, K. Outterson, A. Engel, and A. Karlén, "The Global Preclinical Antibacterial Pipeline," *Nature Reviews Microbiology*, vol. 18, pp. 275–285, May 2020.

[193] L. M. Oppegard, K. R. Streck, J. D. Rosen, H. A. Schwanz, K. Drlica, R. J. Kerns, and H. Hiasa, "Comparison of in Vitro Activities of Fluoroquinolone-like 2,4- and 1,3-Diones," *Antimicrobial Agents and Chemotherapy*, vol. 54, pp. 3011–3014, July 2010.

[194] S. Baikar and N. Malpathak, "Secondary Metabolites as DNA Topoisomerase Inhibitors: A New Era towards Designing of Anticancer Drugs," *Pharmacognosy Reviews*, vol. 4, no. 7, pp. 12–26, 2010.

[195] S. A. Kim, Y. Kwon, J. H. Kim, M. T. Muller, and I. K. Chung, "Induction of Topoisomerase II-Mediated DNA Cleavage by a Protoberberine Alkaloid, Berberrubine," *Biochemistry*, vol. 37, pp. 16316–16324, Nov. 1998.

[196] R. T. Sawant, M. Y. Stevens, C. Sköld, and L. R. Odell, "Microwave-Assisted Branching Cascades: A Route to Diverse 3,4-Dihydroquinazolinone-Embedded Polyheterocyclic Scaffolds," *Organic Letters*, vol. 18, pp. 5392–5395, Oct. 2016.

[197] Y. Pommier, "Drugging Topoisomerases: Lessons and Challenges," *ACS chemical biology*, vol. 8, pp. 82–95, Jan. 2013.

[198] M. Salman, P. Sharma, M. Kumar, A. S. Ethayathulla, and P. Kaur, "Targeting Novel Sites in DNA Gyrase for Development of Anti-Microbials," *Briefings in Functional Genomics*, p. elac029, Sept. 2022.

[199] C. A. Fief, K. G. Hoang, S. D. Phipps, J. L. Wallace, and J. E. Deweese, "Examining the Impact of Antimicrobial Fluoroquinolones on Human DNA Topoisomerase IIα and IIβ," *ACS Omega*, vol. 4, pp. 4049–4055, Feb. 2019.

[200] Y. Cheng and W. H. Prusoff, "Relationship between the inhibition constant (K1) and the concentration of inhibitor which causes 50 per cent inhibition (I50) of an enzymatic reaction," *Biochemical Pharmacology*, vol. 22, pp. 3099–3108, Dec. 1973.

[201] J. G. Heddle, T. Lu, X. Zhao, K. Drlica, and A. Maxwell, "gyrB-225, a Mutation of DNA Gyrase That Compensates for Topoisomerase I Deficiency: Investigation of Its Low Activity and Quinolone Hypersensitivity," *Journal of Molecular Biology*, vol. 309, pp. 1219–1231, June 2001.

[202] M. Gellert, M. H. O'Dea, T. Itoh, and J. Tomizawa, "Novobiocin and coumermycin inhibit DNA supercoiling catalyzed by DNA gyrase.," *Proceedings of the National Academy of Sciences*, vol. 73, pp. 4474–4478, Dec. 1976.

[203] J. Taylor, L. Mitchenall, M. Rejzek, R. Field, and A. Maxwell, "Application of a Novel Microtitre Plate-Based Assay for the Discovery of New Inhibitors of DNA Gyrase and DNA Topoisomerase VI," *PloS one*, vol. 8, p. e58010, Feb. 2013.

[204] F. Blanche, B. Cameron, F. X. Bernard, L. Maton, B. Manse, L. Ferrero, N. Ratet, C. Lecoq, A. Goniot, D. Bisch, and J. Crouzet, "Differential Behaviors of Staphylococcus Aureus and Escherichia Coli Type II DNA Topoisomerases," *Antimicrobial Agents and Chemotherapy*, vol. 40, pp. 2714–2720, Dec. 1996.

[205] O. A. Pierrat and A. Maxwell, "The Action of the Bacterial Toxin Microcin B17. Insight into the Cleavage-Religation Reaction of DNA Gyrase," *The Journal of Biological Chemistry*, vol. 278, pp. 35016–35023, Sept. 2003.

[206] E. Cambau, F. Bordon, E. Collatz, and L. Gutmann, "Novel gyrA point mutation in a strain of Escherichia coli resistant to fluoroquinolones but not to nalidixic acid.," *Antimicrobial Agents and Chemotherapy*, vol. 37, pp. 1247–1252, June 1993.

[207] K. Bhatnagar and A. Wong, "The mutational landscape of quinolone resistance in Escherichia coli," *PLOS ONE*, vol. 14, p. e0224650, Nov. 2019.

[208] D. R. Macinga, P. J. Renick, K. M. Makin, D. H. Ellis, A. A. Kreiner, M. Li, K. J. Rupnik, E. M. Kincaid, C. D. Wallace, B. Ledoussal, and T. W. Morris, "Unique Biological Properties and Molecular Mechanism of 5,6-Bridged Quinolones," *Antimicrobial Agents and Chemotherapy*, vol. 47, pp. 2526–2537, Aug. 2003.

[209] P. Heisig and R. Tschorny, "Characterization of fluoroquinolone-resistant mutants of escherichia coli selected in vitro," *Antimicrobial Agents and Chemotherapy*, vol. 38, pp. 1284–1291, June 1994.

[210] J. Heddle and A. Maxwell, "Quinolone-Binding Pocket of DNA Gyrase: Role of GyrB," *Antimicrobial Agents and Chemotherapy*, June 2002.

[211] L. M. Weigel, G. J. Anderson, and F. C. Tenover, "DNA Gyrase and Topoisomerase IV Mutations Associated with Fluoroquinolone Resistance in Proteus mirabilis," *Antimicrobial Agents and Chemotherapy*, vol. 46, pp. 2582–2587, Aug. 2002.

[212] M. Mirzaii, S. Jamshidi, M. Zamanzadeh, M. Marashifard, S. A. A. Malek Hosseini, M. Haeili, F. Jahanbin, F. Mansouri, D. Darban-Sarokhalil, and S. S. Khoramrooz, "Determination of gyrA and parC mutations and prevalence of plasmid-mediated quinolone resistance genes in Escherichia coli and Klebsiella pneumoniae isolated from patients with urinary tract infection in Iran," *Journal of Global Antimicrobial Resistance*, vol. 13, pp. 197–200, June 2018.

[213] D. Ince, X. Zhang, L. C. Silver, and D. C. Hooper, "Topoisomerase Targeting with and Resistance to Gemifloxacin in Staphylococcus aureus," *Antimicrobial Agents and Chemotherapy*, vol. 47, pp. 274–282, Jan. 2003.

[214] J. Strahilevitz and D. C. Hooper, "Dual Targeting of Topoisomerase IV and Gyrase To Reduce Mutant Selection: Direct Testing of the Paradigm by Using WCK-1734, a New Fluoroquinolone, and Ciprofloxacin," *Antimicrobial Agents and Chemotherapy*, vol. 49, pp. 1949–1956, May 2005.

[215] H. Liu, D.-G. Xia, Z.-W. Chu, R. Hu, X. Cheng, and X.-H. Lv, "Novel coumarin-thiazolyl ester derivatives as potential DNA gyrase Inhibitors: Design, synthesis, and antibacterial activity," *Bioorganic Chemistry*, vol. 100, p. 103907, July 2020.

[216] F. Collin, S. Karkare, and A. Maxwell, "Exploiting bacterial DNA gyrase as a drug target: Current state and perspectives," *Applied Microbiology and Biotechnology*, vol. 92, no. 3, pp. 479–497, 2011.

[217] D. J. Smart and A. M. Lynch, "Evaluating the genotoxicity of topoisomerase-targeted antibiotics," *Mutagenesis*, vol. 27, p. 359, May 2012.

[218] A. C. Ketron, W. A. Denny, D. E. Graves, and N. Osheroff, "Amsacrine as a Topoisomerase II Poison: Importance of Drug–DNA Interactions," *ACS Publications*, vol. 58, pp. 1730–1739, Feb. 2012.

[219] wwPDB consortium, "Protein Data Bank: The single global archive for 3D macromolecular structure data," *Nucleic Acids Research*, vol. 47, pp. D520–D528, Jan. 2019.

[220] K. J. Aldred, T. R. Blower, R. J. Kerns, J. M. Berger, and N. Osheroff, "Fluoroquinolone interactions with Mycobacterium tuberculosis gyrase: Enhancing drug activity against wild-type and resistant gyrase," *Proceedings of the National Academy of Sciences of the United States of America*, vol. 113, pp. E839–E846, Feb. 2016.